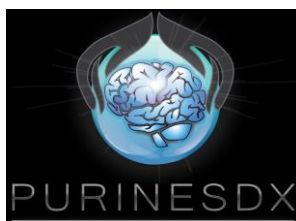


Cover Art by Gaia Balduzzi  
Graphic Editor: Greta Balduzzi



Instituto-Fundación Teófilo Hernando de I+D del Medicamento  
Departamento de Farmacología y Terapéutica  
Facultad de Medicina  
Universidad Autónoma de Madrid

**DESIGN, SYNTHESIS AND PHARMACOLOGICAL  
EVALUATION OF NOVEL BLOOD-BRAIN BARRIER-  
PERMEABLE NON-NUCLEOTIDE PURINE DERIVATIVES  
AS P2X7 ANTAGONISTS FOR THE TREATMENT OF  
NEURODEGENERATIVE DISEASES**

PhD thesis by

**Francesco Calzaferri**

Supervised by

**Prof. Antonio García García**

**Dr. Cristóbal de los Ríos Salgado**

Madrid, 2021



Instituto-Fundación Teófilo Hernando de I+D del Medicamento  
Departamento de Farmacología y Terapéutica  
Facultad de Medicina  
Universidad Autónoma de Madrid

Prof. **Antonio García García** as director and group leader of the Department of Pharmacology and Therapeutics at the University Autónoma of Madrid, and Dr. **Cristóbal de los Ríos Salgado** as co-director and group leader of the Health Research Institute at the University Hospital de la Princesa (Madrid) CERTIFY that

**Francesco Calzaferri** carried out the research of this Doctoral Thesis entitled: “**Design, synthesis and pharmacological evaluation of novel blood-brain barrier-permeable non-nucleotide purine derivatives as P2X7 antagonists for the treatment of neurodegenerative diseases**” under their supervision and the support of the EU Horizon 2020 Research and Innovation Program, Marie Skłodowska-Curie, Grant Agreement N. 766124, to obtain the doctoral degree with international mention at the University Autónoma of Madrid.

Madrid, 25<sup>th</sup> January 2021

Prof. Antonio García García  
Emeritus Professor, UAM  
(director)

Dr. Cristóbal de los Ríos Salgado  
“Miguel Servet II” researcher  
(co-director)

## List of publications

**Calzaferri F**, Narros-Fernández P, de Pascual R, de Diego AMG, Nicke A, Egea J, García AG & de los Ríos C (2021). Synthesis and pharmacological evaluation of novel non-nucleotide purine derivatives as P2X7 antagonists for the treatment of neuroinflammation. J Med Chem (in press)

**Calzaferri F\***, Ruiz-Ruiz C\*, de Diego AMG, de Pascual R, Méndez-López I, Cano-Abad MF, Maneu V, de los Ríos C, Gandía L & García AG (2020). The purinergic P2X7 receptor as a potential drug target to combat neuroinflammation in neurodegenerative diseases. Med Res Rev, 40 (6):2427-2465. DOI: 10.1002/med.21710

Ruiz-Ruiz C\*, **Calzaferri F\*** & García AG (2020). P2X7 receptor antagonism as a potential therapy in amyotrophic lateral sclerosis. Front Mol Neurosci 13:93. DOI: 10.3389/fnmol.2020.00093

*\*equal contribution*

## Acknowledgments

This PhD thesis was accomplished with the work and support of several mates. I thank them a lot for their help and I hope that the good relationship we have created so far will continue in the next years.

Antonio, gracias por haberme seleccionado para este proyecto y por haber siempre confiado en mis ideas y en mis capacidades. He crecido mucho, también gracias a tus indicaciones que me han llevado hasta este punto.

Cristóbal, ¡gracias por ser buen jefe y también compañero! Ha sido un placer aprender de ti los trucos del laboratorio. Probablemente, a veces has pensado que era un poco raro ("¡¡estos italianos!!"), pero sé que en tus palabras hacia mí siempre ha habido mucho cariño y apoyo, y de verdad, ha sido muy importante para mí.

A la Fundación Teófilo Hernando, en particular a María Fagoaga y a sus miles de abrazos por correo, y a María Cieza por su apoyo administrativo, riguroso e impecable. Gracias a la Universidad Autónoma de Madrid, a Luis(i), con quien quizás haya compartido casi más tiempo (comiendo) que con los demás. A Concha por aguantar a los pobres doctorandos que no sabemos cómo subir un informe al SIGMA.

PurinesDX, what a great team! I feel so lucky to be part of this Network! Thanks Tobias for literally making this. Thanks Isabela, because everybody knows that this wouldn't have been possible without you and your perfect organisation. And I couldn't have been a decent representative without your indications 😊 Thanks Prof. Di Virgilio for your wise recommendations and the cells you sent us. ¡Cate, Ivana and Pauliii, qué bonito lo que hemos hecho en estos años! Also thanks to Martina, Giorgia and Monica, it was a pleasure to share time with you! And Lidia, my co-representative. He disfrutado mucho del trabajo contigo y nuestras chats por Whatsapp 😊

Diego, gracias por haber creído en mí en Barcelona y por compartir conmigo ese correo en que se decía que se buscaban 14 estudiantes para investigar sobre el sistema purinérgico. Todo empezó ahí.

Mi amiga zampabollos, nunca dejaré de llamarte así (ya sabes que es cómodo para encontrarte en el móvil). Has vivido conmigo esta experiencia desde el principio hasta el final (¡¡y espero más!!). Sé que en ti siempre podré confiar, también para que no siga diciendo metabolita en un congreso, por ejemplo. Nos entendemos casi sin hablar, pero hablamos mucho, demasiado, y eres la única persona a quién le gusta escuchar mis audios de 20 minutos en Whatsapp. Y aunque siempre haya entrado

en el labo diciendo esa frase que Dani me veta poner en la tesis, que sepas que contigo el día ha sido siempre mejor.

Amoreeee, ¡eres mi descubrimiento del departamento jajaja! Hemos congeniado casi desde el principio y... ¡ya hemos pensado en montar nuestro propio laboratorio juntos! Pues, así haremos. Y seguiremos siendo confidentes, de trabajo, de ideas geniales, de amor, de chicos guapos, o mejor, de sus espaldas (nuestra debilidad). Siempre estaré por si necesitas quejarte. Pero sobretodo tu tienes que estar siempre para cuando necesite YO quejarme, que pasa bastante a menudo, y lo sabes.

¡Penquita! ¡Cuántas risas juntos! Fuiste la primera en hablarme cuando llegué. Era durante la comida. Me has acogido desde el principio y mira ahora, aquí seguimos enviándonos stickers y compartiendo desayunos. Gracias por tu compañía spensierata.

lago, hemos creado una fuerte amistad que me ha hecho disfrutar el doble. Gracias por compartir conmigo tus ideas, consideraciones y confidencias. ¡Recuerda que tengo nuestra bebida mágica! ¡Creo que ha llegado el momento de celebrar!

Raquel, ¡mi compañera de vitrina! Ha sido un placer trabajar y reirme contigo en el labo. Luciiiiia, ¡sin ti no habría descubierto los Manolitos que tanto nos gustan! Gracias por tu compañía.

¡A todos los compañeros del departamento! Primero, Ricardo, ¡compañeeero! Pero también Ana, Peti, Kikesito, Eric, Fer, Carmen, Sheila, Abe, Ander, Almudena, Javier E., Paloma N. y ¡muchos más!

Caro, la mia amica toscana che non mi fa mai mancare un buon jamón italiano! Conosci mi ha fatto sentire bene in questa nuova città. Senza la tua amicizia, i tuoi consigli e il tuo appoggio probabilmente non sarei quello che sono. Non ti toglierai mai di dosso questo nanetto bergamasco. E lo stesso vale per Ricki! Ormai conosco anche le tue speciali canzoncine! Sei stato tutto una scoperta! Grazie per i forti abbracci e per le tue facce ridicole, che non smettono mai di farmi ridere.

To the people from Munich! Annette, you've been a good example of scientist to me. Thanks for taking me in your laboratory and being always available in case I needed support. Anna! Thanks for teaching me everything there, but above all for our great friendship, with many oocytes on our ways, as well as some spying activities at the Honolulu Zoo, deep conversations, and amusing evenings playing the flute together! Yves, I spent some quality time with you in the lab and I've always felt comfortable with you and your wise advices! Thanks! Robin, erinnere ich mich noch so gut daran, wie ich dir im Santiago gesagt habe, dass ich Deutsch lernen wollte. Das erst Wort, das ich dir gesagt habe, war "DAS Zug", und ich kann dein Gesicht nicht vergessen! Vielen Dank für den Spaß! Y ¡¡Antoñiiiiito!! ¡Vamos, uno de los mejores amigos que he conocido durante estos años! Gracias por

dejarte abrazar cada vez que te veo, por guiarme por Munich (aunque yo siempre diga Monaco), compartir tus cotilleos conmigo y por confiar en mí 😊

Jesús, Irini, Lourdes, Sara, Enol, y todos los compañeros en Janssen, me habéis acogido desde el primer día, me habéis mostrado vuestro cariño y vuestra gran profesionalidad. Luego llegó un virus maldito, pero también después de meses, ahí estábais preguntándome qué tal todo. ¡Gracias!

Dora, thanks for helping me so much during these intense months! Now it is time to enjoy our postdoc lives! Y Diana, ¡ha sido un placer compartir estos años contigo también!

A Cecilia, che mi ha fatto crescere in questo periodo di grandi cambiamenti! Christiane, danke für die Deutschen Studen und deine Freundschaft und Gesellschaft 😊

Gli amici in Italia! Franci (un'altra vittima dei miei messaggi audio), Fe, Martina, Simo, Meri, Cate, Alessia, le gemelle. Alla fine, poco ci vediamo, ma sempre siete pronti a riaccogliermi a braccia aperte! Le amicizie della uni non finiscono mai, eh! Gianlu e Davide, che ogni volta che ho bisogno di sushi, un letto, alcohol per distrarmi, o un video sul compleanno di Bambola Star mi siete sempre vicino!

Gli amici italiani a Barcellona, a Parigi, e a Riga! Simo, tra una pandemia e l'altra abbiamo tipo un paio di viaggi in programma che non abbiamo ancora capito quando fare ahaha! Però ci sei sempre, e questo è l'importante. Grazie! Los Cachopos (Rosina, Rossellina, Fabietto e Carlino – non ce n'è uno senza diminutivo)! Siamo la dimostrazione che quando l'amicizia c'è davvero, la distanza non si fa così pesante, e rivedersi è sempre una grande festa.

La Cugi. Distanti da molto tempo, ma sempre presente. Sappiamo bene che il sangue da solo non sempre funziona per rimanere davvero uniti, ma noi ci vogliamo bene e ci saremo sempre, l'uno per l'altro. E grazie per la fantastica copertina! ❤️ Grazie anche a Greta per il suo aiuto!

La mia famiglia, Mamma, Papà e Fratelli. Avete creduto in me, mi avete sempre aiutato. Grazie a tutti voi, che nonostante la distanza non mi avete mai fatto sentire solo, aiutandomi a raggiungere questo traguardo. Ci sarete sempre e per me questo è importante. Grazie anche ai nonni Pepi e Pepina, tutta la super mega family, la nonna Antonietta, Maria e Giacomino, che hanno accompagnato mamma e papà ogni volta che venivano a trovarmi in giro per l'Europa, e Carla, che sempre mi pensa. E un pensiero speciale alla zia Giulia, che mi ha fatto capire tante cose. Ma tante. E da sempre.

Y finalmente mi casa. Una gata boxeadora, y un chico que es mi vida. Nuestro mundo es la cosa más bonita que conozco. Eres presente y futuro, libertad y refugio, muchas risas y apoyo. Ese cartón de pizza fue la cosa más espontanea que te mostré para seguir soñando juntos. Gracias. Te quiero.

そしてその砂嵐が終わったとき、  
どうやってそいつをくぐり抜けて生きのびることができたのか、  
君にはよく理解できないはずだ。

いや本当にそいつが去ってしまったのかもたしかじゃないはずだ。  
でも一つだけはっきりしていることがある。

その嵐から出てきた君は、そこに足を踏み入れた時の君じゃないっていうことだ。  
そう、それが砂嵐というものの意味なんだ。

村上春樹著「海辺のカフカ」より

*And once the storm is over  
You won't remember how you made it through  
How you managed to survive.  
You won't even be sure, in fact, whether the storm is really over.  
But one thing is certain.  
When you come out of the storm you won't be the same person who walked in.  
That's what this storm's all about.*

(From Kafka on the Shore, by Haruki Murakami)

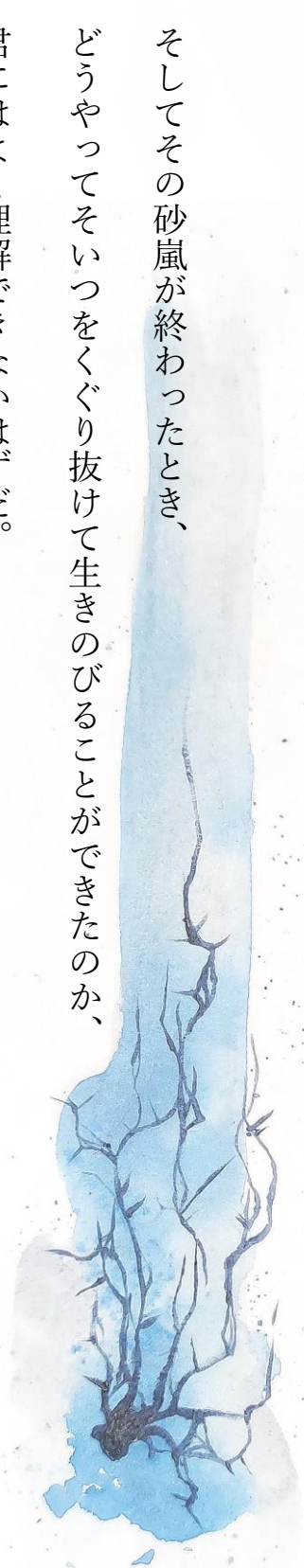




# Table of contents

1. Abstract.....	3
2. Context of the thesis.....	9
3. Introduction.....	13
3.1. The purinergic signalling.....	13
3.1.1. P0 receptors.....	13
3.1.2. P1 receptors and their potential role for the treatment of CNS diseases.....	15
3.1.3. P2Y receptors and their potential role for the treatment of CNS diseases.....	15
3.1.4. P2X receptors and their potential role for the treatment of CNS diseases.....	17
3.1.5. Targeting the enzymes of the purinergic signalling in the CNS.....	21
3.2. The P2X7 receptor.....	23
3.3. The role of P2X7 receptor in neuroinflammation and neurodegenerative diseases.....	31
3.3.1. Alzheimer's disease.....	34
3.3.2. Parkinson's disease.....	35
3.3.3. Huntington's disease.....	36
3.3.4. Multiple sclerosis.....	37
3.3.5. Amyotrophic lateral sclerosis.....	38
3.4. Ligands targeting the P2X7 receptor.....	40
4. Research hypothesis and objectives.....	57
5. Results and discussion.....	61
5.1. Design of novel non-nucleotide purine derivatives as P2X7 antagonists.....	61
5.2. Synthesis and structural characterisation of the non-nucleotide purine derivatives.....	67
5.2.1. 9-(2-chlorobenzoyl)purines <b>1</b> and <b>3</b> .....	67
5.2.2. 9-(2-chlorophenyl)sulfonyl purines <b>4-8</b> .....	69
5.2.3. 1-Aryl-2-purinyloethanones <b>9-12, 16-19, 21, 23, 25, 38, 40</b> .....	70
5.2.4. Xanthine derivatives <b>26-36</b> .....	76

5.2.5.	Partial conclusions.....	80
5.3.	Pharmacological evaluation of purine derivatives as P2X7 antagonists.....	81
5.3.1.	YO-PRO-1 dye uptake assay in hP2X7-overexpressing HEK293 cells.....	81
5.3.2.	ATP currents in human P2X7 cRNA-injected <i>X. laevis</i> oocytes.....	84
5.3.3.	Cytosolic Ca <sup>2+</sup> imaging in hP2X7-overexpressing HEK293 cell populations.....	89
5.3.4.	P2X7-induced interleukin-1 $\beta$ release in rat peritoneal macrophages.....	92
5.3.5.	Selectivity of the non-nucleotide purine derivatives on the P2X subtypes.....	94
5.3.6.	Partial conclusions.....	98
5.4.	Evaluation of blood-brain barrier permeability.....	99
5.4.1.	Blood-brain barrier permeability of the non-nucleotide purine derivatives.....	99
5.4.2.	Evaluation of compounds affinity for the P-glycoprotein efflux pump.....	101
5.4.3.	Partial Conclusions.....	102
5.5.	Docking study of compound <b>9</b> at the allosteric pocket of the P2X7 receptor.....	103
6.	General discussion.....	105
7.	Conclusions.....	113
8.	Experimental section.....	119
8.1.	General procedures and materials.....	119
8.2.	Molecular design.....	119
8.3.	Chemical characterisation.....	119
8.4.	Synthesis.....	120
8.4.1.	Preparation of synthetic precursors <b>2</b> , <b>13–15</b> , <b>20</b> , <b>22</b> , <b>24</b> , <b>37</b> and <b>39</b> .....	120
8.4.2.	General procedure for the synthesis of 2-chlorobenzoyl purines <b>1</b> and <b>3</b> , and 2-chlorobenzoyl theobromine <b>26</b> .....	123
8.4.3.	General procedure for the synthesis of sulfonamides <b>4–8</b> and <b>27–34</b> .....	124
8.4.4.	General procedure for the preparation of purinyl/xanthinyl-2,4-dichlorophenylethanones/propanones <b>9–10</b> , <b>12</b> , <b>16–19</b> , <b>21</b> , <b>23</b> , <b>25</b> , <b>35–36</b> , <b>38</b> .....	130
8.4.5.	Synthesis of 2-[2-chloro-6-(methylamino)-9 <i>H</i> -purin-9-yl]-1-(2,4-dichlorophenyl)ethan-1-one ( <b>11</b> ).....	136

8.4.6.	Synthesis of 2-chloro-1-(2-chlorobenzyl)-9-methyl-1,9-dihydro-6 <i>H</i> -purin-6-one ( <b>40</b> )	
		137
8.5.	Pharmacological methods .....	137
8.5.1.	HEK293-hP2X7 cell culture .....	137
8.5.2.	YO-PRO-1 iodide uptake .....	138
8.5.3.	Fura-2 Ca <sup>2+</sup> measurements.....	138
8.5.4.	Electrophysiological measurements .....	138
8.5.5.	Isolation of murine peritoneal macrophages and IL-1 $\beta$ detection .....	140
8.5.6.	Parallel artificial membrane permeability assay (PAMPA) .....	140
8.5.7.	P-glycoprotein ATPase activity assay .....	141
8.5.8.	Molecular docking.....	142
8.5.9.	Data analysis.....	143
9.	References.....	147
10.	Annexes .....	177
10.1.	Nuclear magnetic resonance spectra of compounds <b>1</b> , <b>7</b> , <b>9</b> , <b>26</b> , <b>27</b> and <b>36</b> .....	177
10.2.	X-ray diffraction data of compounds <b>11</b> and <b>27</b> .....	189
11.	Abbreviations .....	195

A horizontal watercolor brushstroke in shades of light blue and white, with a darker blue blotch on the right side, serving as a background for the text.

**Abstract**

# 1. Abstract

Neuroinflammation is a condition involved in the pathogenesis of several central nervous system (CNS) diseases. The ATP-gated purinergic P2X7 receptor stands out among the druggable biological targets that participate in neuroinflammation. Indeed, P2X7 activation by high concentrations of ATP, which usually occur under damaging conditions, triggers a pro-inflammatory signal in immune cells. Thus, P2X7 is considered a damage signal receptor, and *Big Pharma* and Academia have developed many effective P2X7 antagonists to mitigate the damage signal propagation. Nevertheless, only recently, their focus has shifted to target P2X7 in the CNS for the treatment of CNS disorders.

This PhD dissertation aims at finding out novel P2X7 antagonists with proper brain-blood barrier (BBB) permeability as new pharmacological tools to study P2X7 signalling and potential therapeutic agents against neurodegenerative diseases (NDDs). We designed and synthesised 31 novel non-nucleotide purine derivatives and assessed their pharmacological activity as potential P2X7 antagonists by YO-PRO-1 dye uptake and cytosolic calcium concentration ( $[Ca^{2+}]_c$ ) increase in HEK293 cells stably-expressing human P2X7 (hP2X7). We also tested their blocking effect and selectivity by two-electrode voltage clamp (TEVC) in *Xenopus laevis* hP2X7-expressing oocytes. To prove their physiological relevance, we evaluated whether they could modulate the P2X7-mediated IL-1 $\beta$  release in mouse peritoneal macrophages. In addition, the BBB permeability profile of the compounds was predicted using the parallel artificial membrane permeability assay (PAMPA), and the P-glycoprotein ATPase activity assay. Among all the compounds, we discovered that 2-(6-chloro-9H-purin-9-yl)-1-(2,4-dichlorophenyl)ethan-1-one (compound **9**), named **ITH15004**, (I) inhibits P2X7 in all the experimental models employed, (II) presents high selectivity compared with other P2X subtypes, (III) is active on human, rat and mouse orthologues, (IV) reduces ATP-induced IL-1 $\beta$  release in peritoneal macrophages, (V) has good permeability through lipid membranes, and (VI) does not affect Pgp activity. All of these data suggest that **ITH15004** is able to reach the CNS and modulate neuroinflammation. We have studied the possible interactions involved in the **ITH15004** binding at the P2X7 allosteric binding pocket by molecular docking to aid further structural optimisations. Our research also revealed a potential P2X4 positive allosteric modulator (compound **36**) that may be employed as novel P2X4 selective tool.

Based on the results obtained, we state that **ITH15004** is a novel P2X7 antagonist with moderate potency and a good BBB permeability profile. It is currently employed as pharmacological tool for *in vitro* and *in vivo* studies, and as a hit compound for further medicinal chemistry programmes to develop novel therapeutic drugs for the treatment of NDDs.

## Resumen

La neuroinflamación es una condición involucrada en la patogénesis de varias enfermedades del sistema nervioso central (SNC). El receptor purinérgico P2X7 emerge como una de las posibles dianas que participan en la neuroinflamación, pues su activación por altas concentraciones de ATP, que suelen aparecer en condiciones de daño celular o tisular, desencadena una señalización inflamatoria en las células del sistema inmune, como la microglía. Por esta razón, el P2X7 se considera un sensor de señales de daño celular, de ahí que las grandes empresas farmacéuticas y diversos laboratorios académicos han desarrollado gran diversidad de potentes y eficaces antagonistas P2X7. Pero ha sido solo recientemente cuando han centrado su interés en encontrar entidades químicas capaces de inhibir este receptor en el SNC, para su uso en el tratamiento de enfermedades del cerebro.

La línea de investigación enmarcada en esta Memoria de Tesis versa sobre el descubrimiento de nuevos antagonistas P2X7 con buena permeabilidad a través de la barrera hematoencefálica (BHE) para su uso como herramientas farmacológicas y agentes terapéuticos para las enfermedades neurodegenerativas. Hemos diseñado y sintetizado 31 nuevos derivados no-nucleótidos de purina y hemos analizado su actividad farmacológica como potenciales antagonistas P2X7 en diversos modelos experimentales: (a) en células HEK293 que expresan el P2X7 humano (hP2X7), a través de estudios de acumulación de la sonda fluorescente YO-PRO-1 y del incremento de calcio citosólico medido con la sonda fluorescente Fura-2; (b) en ovocitos de *Xenopus laevis* que expresan el P2X7 humano, midiendo el bloqueo de la corriente evocada por ATP y la selectividad por P2X7 mediante la técnica de patch-clamp con fijación de voltaje a dos electrodos (TEVC); y (c) en macrófagos peritoneales de ratón para comprobar la relevancia farmacológica de nuestros compuestos, evaluando su capacidad de modular la liberación de IL-1 $\beta$ . Además, hemos sondeado su permeabilidad a través BHE con el ensayo PAMPA, y de actividad ATPasa de la glicoproteína P (gpP), un transportador protéico implicado en la resistencia a fármacos. Entre todos los compuestos, hemos descubierto que el derivado **9** (2-(6-cloro-9*H*-purin-9-il)-1-(2,4-diclorofenil)etan-1-ona), que hemos denominado **ITH15004**, (I) inhibe el P2X7 en todos los modelos experimentales empleados, (II) con alta selectividad frente a los otros subtipos P2X, (III) es activo en los ortólogos humanos, de rata y de ratón, (IV) reduce la liberación de IL-1 $\beta$  en macrófagos peritoneales, (V) tiene buena permeabilidad a través de membranas lipídicas, (VI) no aumenta significativamente la actividad de gpP. Todas estas evidencias nos sugieren que **ITH15004** puede alcanzar el SNC y modular la neuroinflamación. Por lo tanto, hemos estudiado las posibles interacciones entre el compuesto y el sitio de unión alostérico del P2X7 con metodologías computacionales de docking molecular, que

ayudarán a los estudios de optimización química posteriores. Nuestra investigación ha llevado al descubrimiento de un nuevo potencial modulador alostérico positivo del P2X4 (compuesto **36**) que se podría utilizar como herramienta farmacológica.

En base a los resultados obtenidos, consideramos que el compuesto **ITH15004** es un nuevo antagonista P2X7 de moderada potencia y buena permeabilidad de BHE. Actualmente, se está utilizando como herramienta farmacológica en estudios *in vitro* e *in vivo*, y como compuesto hit para ulteriores programas de química médica dirigidos al desarrollo de nuevos medicamentos para el tratamiento de las enfermedades neurodegenerativas.

A decorative horizontal splash of light blue and white watercolor paint, with a darker blue blotch on the right side, serving as a background for the text.

Context of the thesis



## 2. Context of the thesis

This PhD project is part of the Innovative training network (ITN) programme “PurinesDX”, a Marie Skłodowska-Curie project of the European Commission, constituted by academic and private institutions with a depth background in neuroscience and pharmacology. The purpose of the Consortium is to investigate the role of the purinergic P2X7 receptor in the pathogenesis of several neurodegenerative, neurological, and psychiatric disorders. It also aims at the training of 14 early-stage researchers during their PhD thesis, providing them with courses on transferable skills, workshops on scientific fields of interest for the network, and the participation in international congresses, all supervised by recognised experts, such as Prof. Antonio García García, Emeritus Professor of Pharmacology at University Autónoma of Madrid and President of Fundación Teófilo Hernando, who played as supervisor of this PhD work.

This PhD thesis describes the synthesis of novel P2X7 antagonists to provide novel pharmacological tools to study the role of P2X7 in neuroinflammation and to potentially develop a drug for the treatment of NDDs. The work was accomplished at the Instituto-Fundación Teófilo Hernando for drugs R&D, in the Department of Pharmacology and Therapeutics of the Faculty of Medicine of the University Autónoma of Madrid. The project was supervised by the above-mentioned Prof. Antonio García García and Dr. Cristóbal de los Ríos, “Miguel Servet II” researcher of the Health Research Institute at the University Hospital de la Princesa (Madrid). Both García’s and Ríos’ research groups have an extended experience in the study of NDDs (Calvo-Gallardo *et al.*, 2014; Fernández-Morales *et al.*, 2012; Martínez-Ramírez *et al.*, 2018; Yáñez *et al.*, 2014) and the drug R&D of new neuroprotectants (de los Ríos *et al.*, 2010; Gonzalez *et al.*, 2018; Lajarín-Cuesta *et al.*, 2018; Lorrio *et al.*, 2013; Martínez-Sanz *et al.*, 2016; Moreno-Ortega *et al.*, 2015; Romero *et al.*, 2014), focused on  $[Ca^{2+}]_c$  dynamics or the synthesis of Ser/Thr phosphatases activators, among other biological targets, to combat NDDs such as Alzheimer’s Disease.

These research groups possess all the necessary facilities and instrumentation for the synthesis of novel compounds, their purification and characterisation, as well as the computational techniques to execute the molecular design of novel compounds and their docking at the pocket of the biological target. Recently, we have introduced the methodology of microflow chemistry to optimise the chemical fabrication of potential drugs and differently substituted scaffold. Additionally, we have a platform for the screening of novel or repositioned compounds in fluorescence assays, electrophysiological tools for patch-clamp and amperometry techniques, and basic equipment for molecular biology experiments.

A horizontal watercolor splash in shades of light blue and white, with a darker blue blotch on the right side. The word "Introduction" is centered within this splash.

# Introduction

## 3. Introduction

### 3.1. The purinergic signalling

Nucleotides had always been considered energy-carrying molecules (*e.g.* ATP), intracellular messengers (*e.g.* GTP and cAMP), and the building blocks of nucleic acids. But, in 1970, Geoffrey Burnstock, taking inspiration from punctual experiments performed in the late 1920s, demonstrated that ATP was released by vagal non-adrenergic inhibitory nerves after electrical stimulation, thus attributing to ATP the function of neurotransmitters (Burnstock *et al.*, 1970). In 1976, Burnstock proposed the existence of specific receptors for nucleosides and nucleotides (Figure 1A) (Burnstock, 1976), which two years later were divided into P1 and P2 receptors, for adenosine and ATP/adenosine diphosphate (ADP), respectively. In 1985, P2 receptors were classified into two groups, the ligand-gated ion channels P2X receptors and the G protein-coupled receptors (GPCR) P2Y (Figure 1B,C) (Burnstock and Kennedy, 1985). Considering the variety of the purinergic receptors discovered and cloned at that moment (Brake *et al.*, 1994; Lustig *et al.*, 1993; Valera *et al.*, 1994; Webb *et al.*, 1993), in 1994 Abbracchio and Burnstock established the criteria for a common nomenclature (Abbracchio and Burnstock, 1994). Finally, in 2002 Janssen Pharmaceutica characterised a rat orphan GPCR that was activated by adenine and then classified as P0 receptor (Bender *et al.*, 2002). In the following subchapters, we will briefly describe the different classes of purinergic receptors.

#### 3.1.1. P0 receptors

The first discovered GPCR belonging to the P0 receptors family was the rat adenine receptor (rAdeR). Later on, other new receptors were cloned from mouse brain (mAdeR) and hamster ovary (cAdeR). They are all receptors coupled to G<sub>i</sub>α protein, whose main effect is the inhibition of 3',5'-cyclic adenosine monophosphate (Bender *et al.*, 2002; Kügelgen *et al.*, 2008). Activation of cAdeR also regulates Ca<sup>2+</sup> signalling, due to the recruitment of G<sub>q</sub>α and/or G<sub>i</sub>βγ (Thimm *et al.*, 2013). No human adenine receptor has been cloned so far, although some data suggest its existence in human astrocytoma 1321N1 cells (Gorzalka *et al.*, 2005) and human embryonic kidney (HEK293) cells (Schiedel *et al.*, 2007). P0 receptors seem to be involved in many human pathophysiological mechanisms, particularly nociception and chronic renal failure (Matthews and Dickenson, 2004; Slominska *et al.*, 2002; Wengert *et al.*, 2007). Nevertheless, many AdeR-mediated functions need to be further investigated.

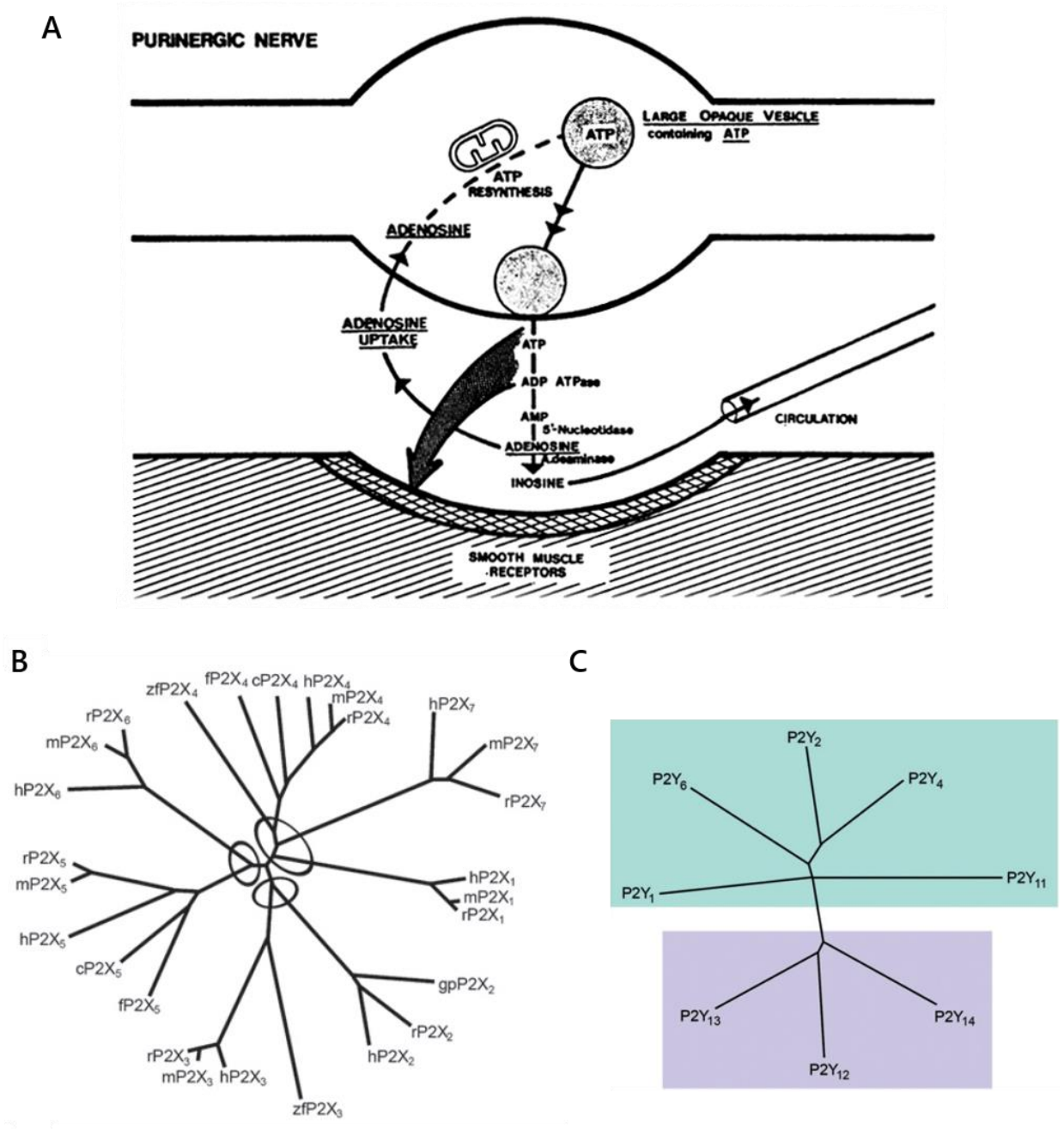


**Figure 1.** A) Original schematic representation of synthesis, storage, release and inactivation of autonomic neurotransmitters at purinergic neuromuscular junction by Geoffrey Burnstock. B-C) Phylogenetic trees (dendrograms) showing the relatedness of P2X (B) and P2Y (C) receptors. h, Human (*Homo sapiens*); r, rat (*Rattus norvegicus*); m, mouse (*Mus musculus*); gp, guinea pig (*Cavia porcellus*); c, chicken (*Gallus gallus*); zf, zebrafish (*Danio rerio*); bf, bullfrog (*Rana catesbeiana*); x, claw-toed frog (*Xenopus laevis*); f, fugu (*Takifugu rubripes*). Images adapted from Burnstock, 1972 and 2007.

### 3.1.2. P1 receptors and their potential role for the treatment of CNS diseases

The P1 receptors are GPCRs physiologically activated by adenosine (ADO). Four different subtypes have been cloned so far, A<sub>1</sub>, A<sub>2A</sub>, A<sub>2B</sub>, and A<sub>3</sub>. A<sub>1</sub> and A<sub>3</sub> receptors are coupled to G<sub>i</sub>α that decreases intracellular cAMP levels, whereas A<sub>2</sub> receptors are coupled to G<sub>s</sub>α that on the contrary increases cAMP concentration. G<sub>q</sub>α proteins are also coupled to A<sub>2B</sub> and A<sub>3</sub> receptors, regulating phospholipase (PL) C activity and inositol triphosphate (IP<sub>3</sub>) levels (Ralevic and Burnstock, 1998). Adenosine receptors have been deeply studied during the last 40 years, also thanks to the well-known methylxanthine antagonists found in nature (*e.g.* caffeine, theophylline). Being expressed on several organs, they are involved in many functions and pathologies. Lots of bioactive ligands targeting these receptors have been developed (Jacobson and Müller, 2016) and reached clinical trials, such as the A<sub>1</sub> agonist Trabodenson, which was studied in phase III for the treatment of glaucoma (Lu *et al.*, 2017), and the A<sub>3</sub> agonist IB-MECA, which was tested for rheumatoid arthritis (Figure 2) (Fishman *et al.*, 2012). Regarding the CNS, only A<sub>1</sub> and A<sub>2A</sub> subtypes have been consistently identified (Beamer *et al.*, 2016), and the A<sub>2A</sub> antagonist and xanthine derivative Istradefylline has been recently approved by the FDA as an add-on treatment to levodopa for Parkinson's Disease (PD) (Figure 2) (Chen and Cunha, 2020).

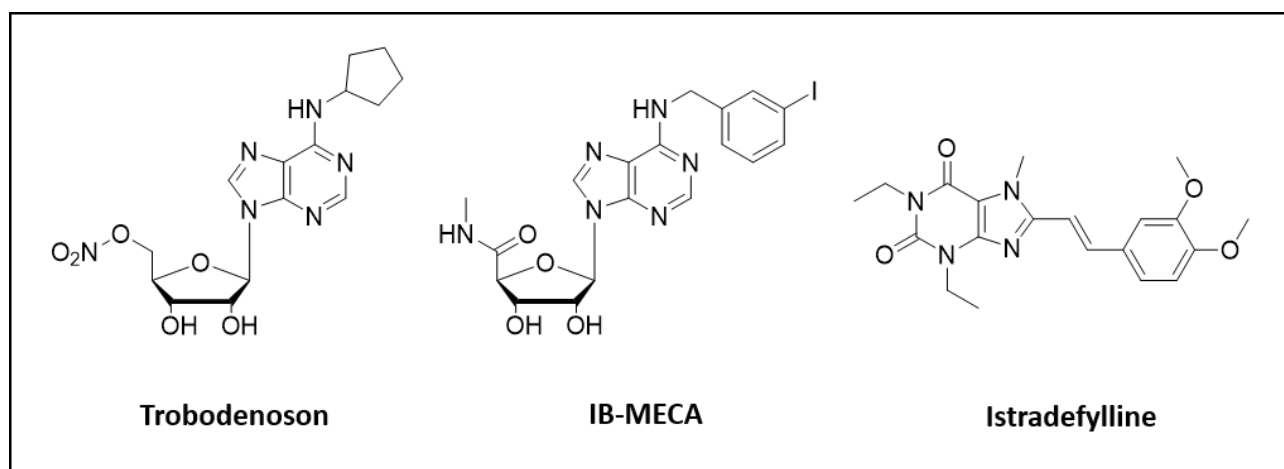


**Figure 2.** Selection of P1 receptors ligands that reached clinical trials: the A<sub>1</sub> agonist Trabodenson, the A<sub>3</sub> agonist IB-MECA, and the A<sub>2A</sub> antagonist Istradefylline, recently approved by the FDA for the treatment of PD.

### 3.1.3. P2Y receptors and their potential role for the treatment of CNS diseases

The P2Y receptors are GPCRs classified in eight subtypes: P2Y<sub>1</sub>, P2Y<sub>2</sub>, P2Y<sub>4</sub>, P2Y<sub>6</sub>, P2Y<sub>11</sub>, P2Y<sub>12</sub>, P2Y<sub>13</sub>, and P2Y<sub>14</sub>. These receptors are activated by both adenine and uridine nucleoside tri- and diphosphate (ATP, ADP, UTP and UDP), except P2Y<sub>14</sub>, whose endogenous agonists are UDP, UDP-glucose, UDP-

N-acetylglucosamine, UDP-glucuronic acid, and UDP-galactose (Abbracchio *et al.*, 2003; Carter *et al.*, 2009). On one hand, P2Y<sub>1</sub>, P2Y<sub>2</sub>, P2Y<sub>4</sub>, and P2Y<sub>6</sub> receptors are coupled to G<sub>q</sub> proteins. On the other hand, the P2Y<sub>11</sub> receptor is coupled to both G<sub>q</sub> and G<sub>s</sub>. P2Y<sub>12</sub>, P2Y<sub>13</sub>, and P2Y<sub>14</sub> receptors are coupled to G<sub>i</sub> (Figure 3) (Erb and Weisman, 2012). The most used P2Y-targeting ligands used in clinics are clopidogrel and ticagrelor, which act on the P2Y<sub>12</sub> receptor as antiaggregant drugs for acute coronary syndromes, stroke, and thrombosis (Teng, 2015). Another P2Y drug approved by the regulatory agency of Japan is Diquafosol, a P2Y<sub>2</sub>/P2Y<sub>4</sub> agonist used for dry eye disease (Jacobson and Müller, 2016).

Most of the P2Y receptors are expressed in the CNS, having functions in neuroprotection, neuroinflammation or some pathological conditions. P2Y<sub>1</sub>, P2Y<sub>2</sub>, and P2Y<sub>13</sub> receptors functions are neuroprotective (Beamer *et al.*, 2016; Fujita *et al.*, 2009; Pérez-Sen *et al.*, 2015) and can have a role in anxiety and Alzheimer's disease (AD) (Kittner *et al.*, 2003; Moore *et al.*, 2000). The P2Y<sub>4</sub>, P2Y<sub>6</sub>, and P2Y<sub>12</sub> receptors modulates microglia activation (Illes *et al.*, 2020; Rafehi *et al.*, 2017), the latest being proposed to be a marker of demyelinating lesions in amyotrophic lateral sclerosis (ALS) (Amadio *et al.*, 2014). P2Y<sub>11</sub> receptors seem to be involved in sleep disorders (Kornum *et al.*, 2011), whereas P2Y<sub>14</sub> receptors are interesting target for the treatment of chronic pain (Mufti *et al.*, 2020).

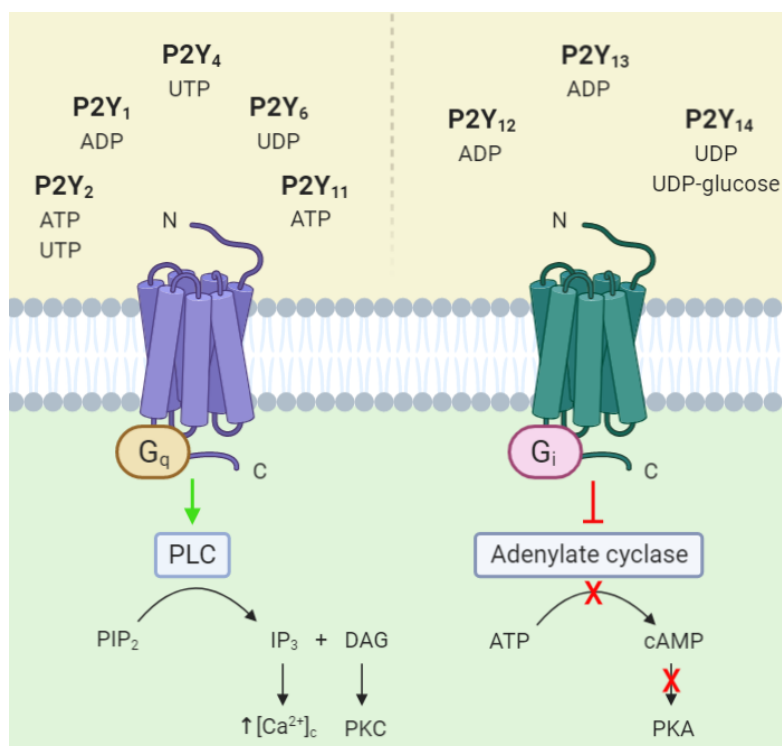


**Figure 3.** Representation of P2Y receptors, with their respective endogenous agonists, divided in two groups based on sequence homology and main signalling cascade. Image inspired by Rafehi and Müller, 2018.

### 3.1.4. P2X receptors and their potential role for the treatment of CNS diseases

The P2X receptors are ATP-gated ion channels. They are homo- or heterotrimers that can combine seven types of subunits (P2X1-7). Each subunit is composed of two  $\alpha$ -helical transmembrane domains (TM), a short intracellular *N*-terminus, a more variable in length *C*-terminus, and a large extracellular loop of 269-288 amino acids, mostly folded as  $\beta$ -sheets and loops (Kopp *et al.*, 2019). Depending on their different activation and desensitisation kinetics, P2X receptors are classified in three main groups. On the one hand, P2X1 and P2X3 are activated in the range of milliseconds and rapidly desensitise. On the other hand, the remaining subtypes are rapidly activated in about a second, but can undergo a slow or no desensitisation. In fact, P2X2, P2X4, P2X4/6, P2X2/3, and P2X2/6 slowly desensitise, while P2X5, P2X7, and P2X1/5 present a persistent current plateau during prolonged ATP stimulation (Figure 4) (Coddou *et al.*, 2011; Jacobson *et al.*, 2002).

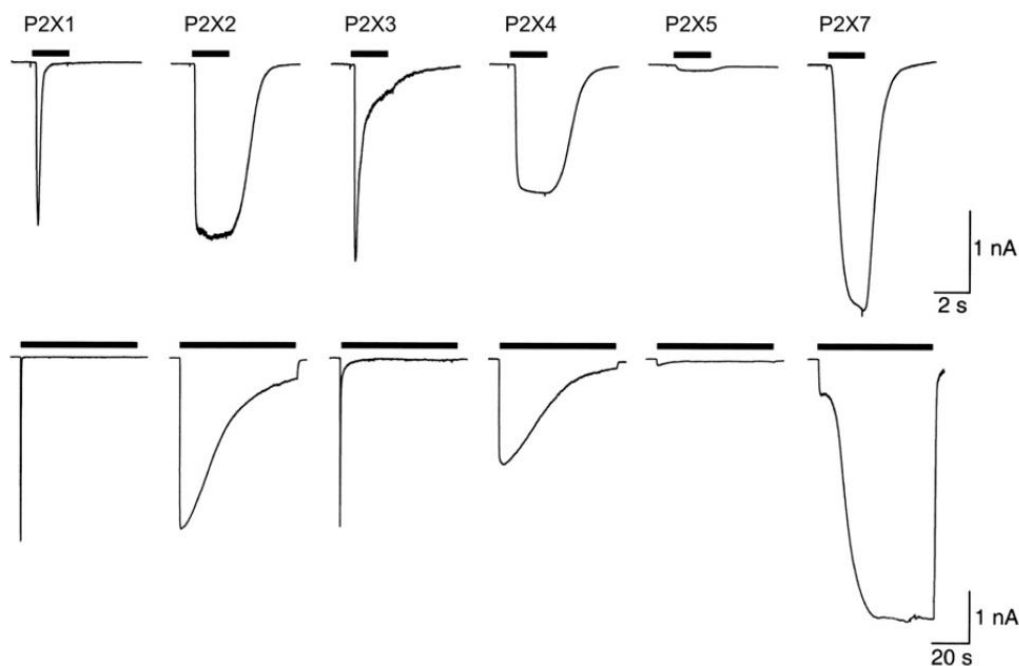


**Figure 4.** Differences on current desensitisation for each P2X subtype after 2 s (above) or 20 s (below) ATP application (30  $\mu$ M, except 1 mM for P2X7). Image taken from Khakh and North, 2012.

P2X receptors show different affinities for ATP. P2X1 is highly sensitive to ATP, with a  $pEC_{50}$  of 7.3, followed by P2X3 (6.5), P2X4 (6.3), P2X5 (6.0), P2X2 (5.9), and P2X7 (4.0). So far, no functional homomultimer receptor has been found for P2X6, and its role in pathophysiological conditions is still unknown (Jacobson, 2010), while P2X5 is usually expressed as a non-functional cytoplasmic exon-

deleted isoform (Kotnis *et al.*, 2010). With the exception of P2X5, which is permeable to Cl<sup>-</sup>, the other P2X receptors allow Na<sup>+</sup> and Ca<sup>2+</sup> influx and K<sup>+</sup> efflux, according to the electrochemical gradient of plasmalemma. Some subtypes (e.g., P2X2, P2X4, P2X7, P2X2/3, and P2X2/5) generate a pore in the membrane wide enough to let small molecules pass through (Figure 5).

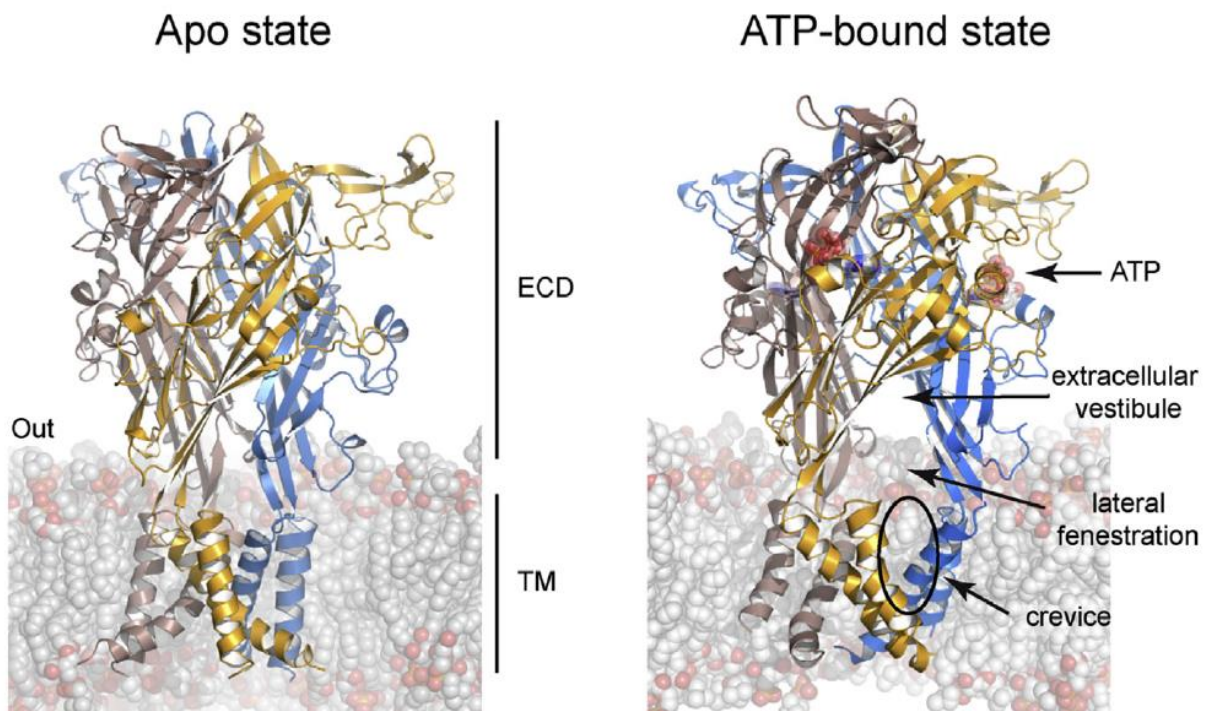


**Figure 5.** Crystal structure of zebrafish P2X4 in the close (left, PDB code 4DW0) and open (right, PDB code 4DW1) state, as example of the P2X family. The main features after receptor activation are highlighted, such as the ATP-binding pocket and the lateral fenestration that allows ion passage. ECD, extracellular domain; TM, transmembrane domain. Image taken from Habermacher *et al.*, 2016.

As far as their pharmacology, no P2X selective ligand has been commercialised yet. Few clinical trials have been performed to test P2X ligands, in particular P2X7 (see chapter 3.4) and P2X3 antagonists, such as Gefapixant (named after Geoff Burnstock), for chronic cough, asthma, pulmonary fibrosis, osteoarthritis, and bladder pain syndrome (clinicaltrials.gov). All the functional P2X receptors have been also investigated in the CNS. P2X1 showed neuroprotective properties after ischemia (Hausmann and Schmalzing, 2012), while in PD models, their activation induces the accumulation of intracellular  $\alpha$ -synuclein (Gan *et al.*, 2015). P2X2 showed antidepressant-like effects (Cao *et al.*, 2013), while P2X3 has been proposed as potential target for the treatment of epileptic seizures (Zhou *et al.*, 2016). P2X4 modulates microglia process retraction and conversion to a proinflammatory phenotype



in physiological (Illes *et al.*, 2020) and ischaemic conditions (Cheng *et al.*, 2014). P2X4 activation on microglia induces the release of brain neurotrophic factor (BDNF) and provokes systematic neuropathic pain through neuronal overexcitation (Coull *et al.*, 2005; Illes *et al.*, 2020; Tsuda *et al.*, 2003). P2X4 antagonists might also protect neurons from status epilepticus- and A $\beta_{1-42}$ -induced neuronal death (Ulmann *et al.*, 2013; Varma *et al.*, 2009). Nevertheless, P2X4 blockade favoured a microglia pro-inflammatory phenotype in the experimental autoimmune encephalomyelitis (EAE) model of multiple sclerosis (MS), while its potentiation by ivermectin ameliorated clinical manifestations of EAE, modulating myelination and macrophage phagocytosis (Zabala *et al.*, 2018). Regarding ALS, P2X4 was found on degenerating motoneurons in the spinal cord ventral horn. Finally, P2X7 is probably the most studied receptor of this family, due to its strong involvement in many neuroinflammatory disorders, and it will be extensively discussed in chapters 3.2 and 3.3.

**Table 1.** Summary of all the P1 and P2 receptors, their endogenous ligands, the main signalling pathways they activate, and the most known, used or potent ligands used for their activation/inhibition. Adapted from Calzaferrri *et al.*, 2020.

Purinergic receptors							
Family	Subtype	Receptor type	Endogenous agonist	Main signalling pathway	Most potent agonists	Most potent of common antagonists	
P1	A1	Metabotropic	Adenosine	Coupled to G <sub>i</sub> proteins	CCPA	DPCPX	Caffeine Theophylline
	A2 <sub>A</sub>			Coupled to G <sub>s</sub> proteins	CGS-21680, ATL-146e	KW-6002, SCH-58261	
	A2 <sub>B</sub>				BAY 60-6583, NECA	MRE2030F20, PBS1115	
	A3			Coupled to G <sub>i</sub> proteins	CI-IB-MECA, MRS3558	MRE3008F20, MRS-1523	
P2	P2X	Ionotropic	ATP	Permeable to Na <sup>+</sup> , Ca <sup>2+</sup> , K <sup>+</sup>	BzATP, ATP, 2-MeSATP	NF-449, IP <sub>5</sub> I	
					ATP, 2-MeSATP	RB2, iso PPADS	
					ATP, 2-MeSATP	TNP-ATP	
				ATP	5-BDBD		
				Permeable to Cl <sup>-</sup>	ATPγS, ATP	BBG	
				Permeable to Na <sup>+</sup> , Ca <sup>2+</sup> , K <sup>+</sup>	-	-	
					BzATP	JNJ- 47965567, A-804598, A-740003, KN-62	
	P2Y	Metabotropic	ADP	Coupled to G <sub>q</sub> proteins	MRS-2365	MRS-2500	
					UTP, ATP	UTP, MRS-2698	AR-C-126313
					UTP, ATP	2'-azido-dUTP	ATP, RB2, Suramin
					UDP	MRS-2696	MRS-2578
			ATP	Coupled to G <sub>q</sub> + G <sub>s</sub> proteins	ATPγS	NF-157	
					ADP	2-MeSADP	ARC-69931MX
					ADP	ADP, 2-MeSADP	ARC-69931MX
UDP					MRS-2690	-	
UDP-glucose UDP-galactose							

### 3.1.5. Targeting the enzymes of the purinergic signalling in the CNS

As all the receptors described above are activated by nucleotides or their enzymatic degradation products, the soluble and membrane proteins involved in their conversion are interesting pharmacological targets for modulating receptors activation (Figure 6).

Plasma membrane-embedded enzymes that hydrolyse extracellular nucleotides are called ectonucleotidases, and are classified in 4 different families: 1) the ecto-nucleoside triphosphate diphosphohydrolises (ENTPDases, including CD39), which are nucleotide selective and hydrolyse nucleoside tri- and di-phosphates into their respective nucleoside monophosphates; 2) the ecto-5'-nucleotidases (5'-NT, also known as CD73), which are the main producers of ADO from AMP; 3) the ecto-nucleotide pyrophosphatases/phosphodiesterases (ENPPs) that hydrolyse nucleoside tri- and diphosphates, as well as ADP-ribose and some phospholipids, but not monophosphates; and 4) the alkaline phosphatases (APs) that remove one or more phosphates from nucleosides. Other important enzymes involved in nucleotide signalling are adenosine deaminase (ADA), which converts ADO into inosine by deamination; adenylate kinase (AK), which generates ATP and AMP starting from 2 ADP; and nucleoside diphosphate kinase (NDPK), which transfers a  $\gamma$ -phosphate from a nucleoside triphosphate to a nucleoside diphosphate. This last has emerged as an interesting player in the generation of extracellular ATP by ectoNDPK-mediated inside-out nucleotide transfer (Agren *et al.*, 1974; Ronquist, 1968).

There are not many drugs capable of selectively targeting these enzymes. Pentostatin, an inhibitor of ADA, is clinically used as antimetabolite in hairy cell leukemia (Kane *et al.*, 1992). ABT-702 is a non-nucleoside blocker of AK that reached clinical trials, by decreasing chronic and acute pain, but it was discontinued later (Kowaluk *et al.*, 2000). More recently, inhibitors of ENNP1 have been disclosed as potential therapeutic agents for glioblastoma (Lee *et al.*, 2016), as well as CD39 and dual CD39/CD73 inhibitors as immunostimulators for cancer therapy, by decreasing the hydrolysis of ATP and the generation of the immunosuppressive ADO (Schäkel *et al.*, 2020). Finally, CPI-006, a monoclonal antibody targeting CD73, is currently under phase I clinical trial for immunotherapy in stably hospitalised mild or moderately symptomatic COVID-19 patients (Corvus Pharmaceuticals, Inc., 2020).

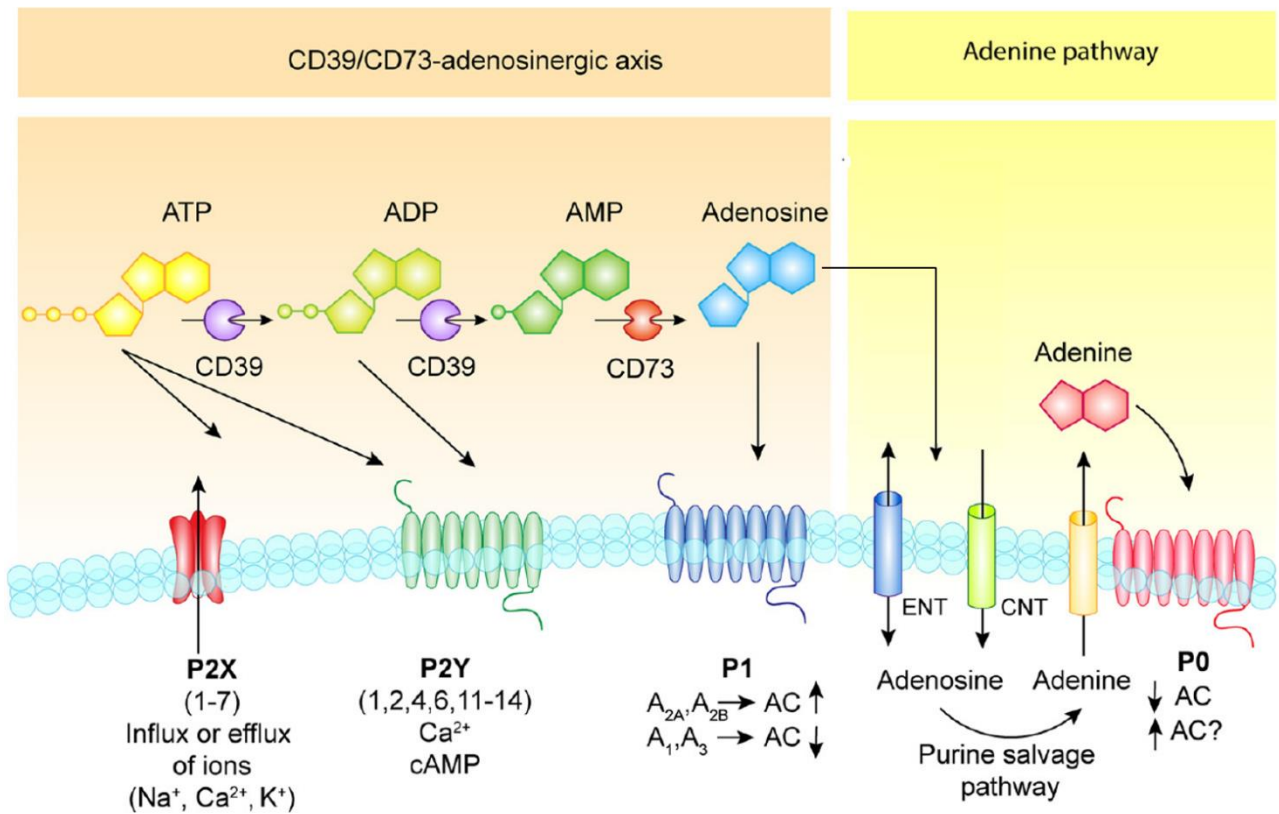


**Figure 6.** Summary of all the purinergic receptors, transporters, and metabolic enzymes involved in purinergic signalling. Image adapted from Giuliani *et al.*, 2019.

### 3.2. The P2X7 receptor

The P2X7 receptor is an ATP-gated ion channel permeable to Na<sup>+</sup>, Ca<sup>2+</sup>, and K<sup>+</sup> cations, but also to small molecules up to 900 Da weight. This receptor assembles as homotrimer, although some studies suggested that it could also form heterotrimers with P2X4 subunits (Guo *et al.*, 2007; Schneider *et al.*, 2017). P2X7 exhibits low affinity for ATP (pEC<sub>50</sub> = 4) compared with other P2X subtypes. Such characteristic seems to be due to the peculiar ATP-binding pocket of P2X7, which lacks four amino acids present in other P2X subtypes that are replaced by more bulky and hydrophobic ones (Dal Ben *et al.*, 2015; Karasawa and Kawate, 2016). This was confirmed by cryogenic electron microscopy (cryo-EM) of rat P2X7 (rP2X7) that shows some residues involved in ATP binding, different from those of the human P2X3 crystal. Nevertheless, the interactions depicted by ATP with P2X3 seem to be reasonably replaced by those found in P2X7, which does not justify a ~10-fold decrease of the ATP affinity of P2X7. The cryo-EM structure also revealed that the ATP binding pocket is less solvated than in P2X3 structure, presumably because it is a narrower pocket. Thus, any structural fluctuation would hinder ATP accessibility (McCarthy *et al.*, 2019).

P2X7 has three ATP binding sites. The pocket, also called the "binding jaws", is located at the interface of two subunits, in the so-called upper body (UB), between the head domain (Hdom) and the dorsal fin (DF). These terminology comes from the first crystal structure obtained, from the giant panda (*Ailuropoda melanoleuca*) P2X7, which has an 85% identity with the human orthologue (Karasawa and Kawate, 2016). Thanks to this crystal structure, it was confirmed that the P2X7 subunit has the same dolphin-like shape as those previously described for the human P2X3 and zebrafish P2X4 (Figure 7A) (Pasqualetto *et al.*, 2018). Each subunit comprises an UB and a lower body (LB), a Hdom, left and right flippers (LF and RF, respectively), a DF and a fluke (FL), which are the two  $\alpha$ -helix transmembrane domains, constituting the channel pore.

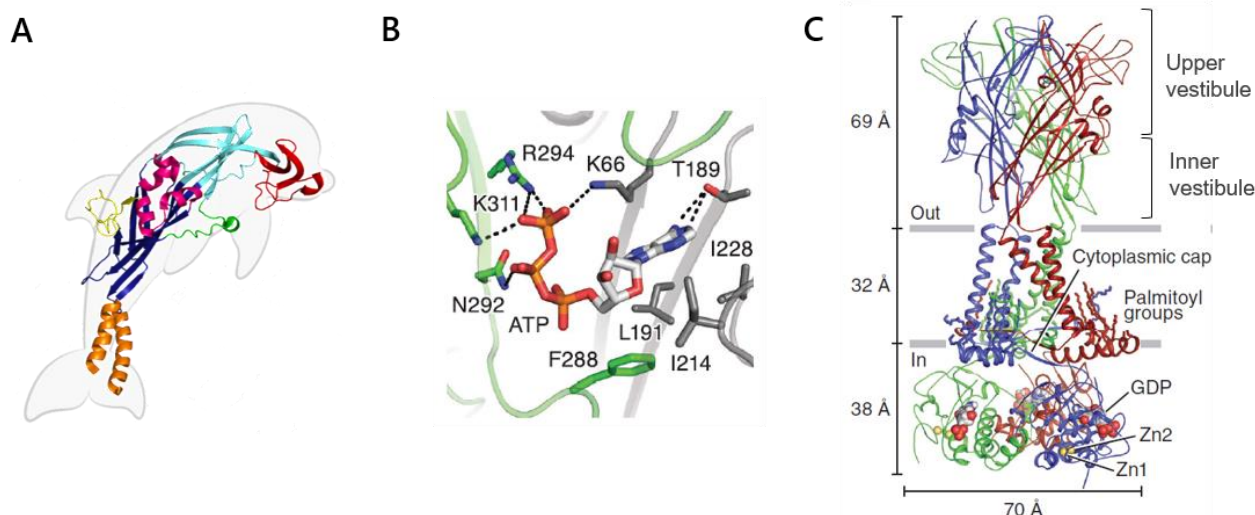


**Figure 7.** **A)** Crystal structure of the giant panda P2X7 subunit (PDB code 5U1L). The different structural parts are depicted in different colours: head domain (HDom) in red, upper body (UB) in cyan, lower body (LB) in blue, dorsal fin (DF) in yellow, left flipper (LF) in green, right flipper (RF) in magenta and the fluke (FL) in orange. **B)** Closer view of the binding pose of ATP in the rP2X7. **C)** Cryo-EM structure of rP2X7 (PDB code 6U9V). Upper and inner vestibules are highlighted, as well as the cytoplasmic cap, zinc and GDP domains, and the palmitoyl groups that anchor the C-terminus to the membrane. Images adapted from Calzaferri *et al.*, 2020 and McCarthy *et al.*, 2019.

ATP acquires a U-shaped conformation upon its binding through the interaction of phosphates to the adenine base, in a similar fashion to the ATP interaction with the class II aminoacyl transfer RNA synthetases (Figure 7B). During activation, the UB subunit shrinks toward the central axis of the receptor, leading the LB to broaden, forming fenestrations that allow the passage of ions through a lateral pathway, away from the central axis. These conformational changes result in a vertical stretch and rotation of the two TMs, thus opening the channel gate. A structural characteristic of P2X7 is that an extracellular pocket, located internally at the top of the UB, is wider than in other family subtypes. This is indeed the allosteric binding site of several antagonists, as demonstrated by the crystal of the giant panda P2X7, and in subsequent studies of mutagenesis and molecular docking (Figure 7C) (Dayel *et al.*, 2019; Karasawa and Kawate, 2016). This information helps for the design and development of new selective ligands. So far, only one additional allosteric pocket more has been proposed, located deeper in the central vestibule of the receptor, near the  $\beta$ -sheets of the lateral portals. This is the binding site mapped for P2X7 positive allosteric modulators (Figure 8) (Bidula *et al.*, 2019a).

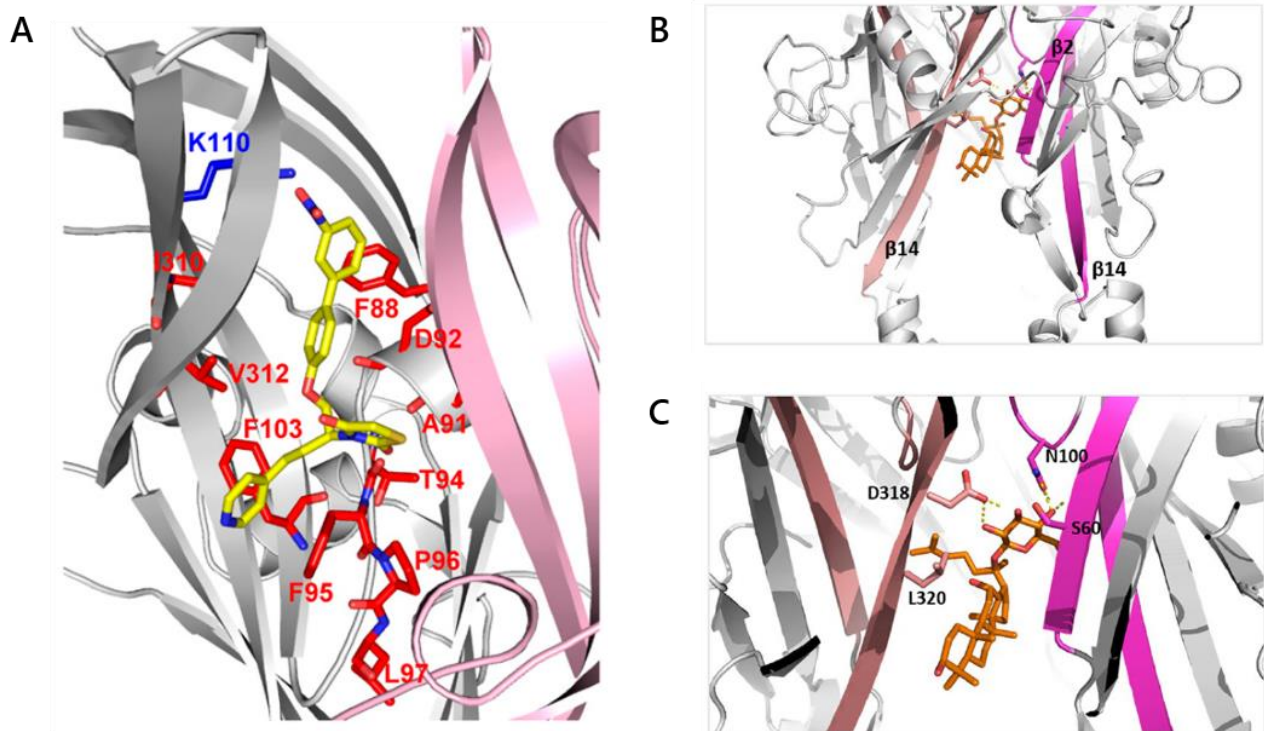


**Figure 8.** P2X7 allosteric binding pockets. **A)** Docking of the P2X7 antagonist A-11645373 at the upper vestibule of the receptor. Amino acids responsible of higher or lower P2X7 activity after mutagenesis are represented in blue and red, respectively. **B)** Docking of the positive allosteric modulator ginsenoside CK at the central vestibule of P2X7. **C)** Closer view of the binding site of ginsenoside CK. Images taken from Dayel *et al.*, 2019 and Bidula *et al.*, 2019a.

The P2X7 sensitivity to ATP is different among species (Figure 9). In detail, ATP has a higher  $pEC_{50}$  in rat P2X7 receptor than in mouse or human orthologues ( $3.40 \pm 0.10$  against  $2.70 \pm 0.07$  and  $2.80 \pm 0.06$ , respectively) (Hibell *et al.*, 2001), but it also shows lower efficacy (Donnelly-Roberts *et al.*, 2009b). These differences are also evident when the more potent 2'(3')-O-(4-benzoylbenzoyl)ATP (BzATP) is used as agonist ( $pEC_{50}$ :  $5.20 \pm 0.09$  for rat,  $< 3.5$  for mouse, and  $4.10 \pm 0.06$  for human P2X7) (Hibell *et al.*, 2001). Current kinetics was shown to be dissimilar. In fact, rP2X7 currents measured in stably transfected HEK293 cells show a higher decay time than in other orthologues under BzATP stimulation. This depends on both agonist association and dissociation rates, which are determined by protein-ligand interactions, and this implies that structural differences among species are responsible for these observations (Hibell *et al.*, 2001). Notably, Young and co-worker demonstrated that mouse P2X7 (mP2X7) sensitivity for ATP and BzATP reaches that one of rat when the amino acids present in mouse, Asp 284 and Ala127, are replaced with the corresponding amino acids present in rat, Asn and Lys (*i.e.* D284N and A127K mutations) (Young *et al.*, 2007).

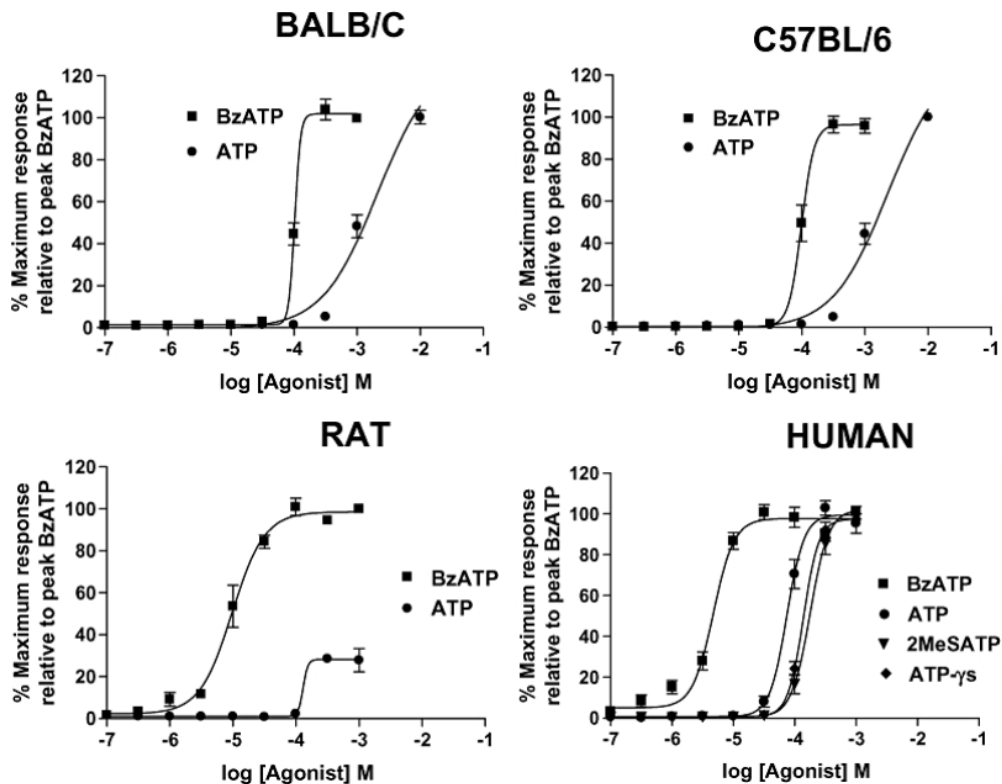


**Figure 9.** Agonist concentration-response curves to stimulate increases in P2X7-mediated  $[Ca^{2+}]_c$  (Fura-4) in P2X7-transfected human astrocytoma 1321N1 cells. Data were normalised to the peak BzATP response (%Maximum response). Data represent mean  $\pm$  SEM of 4–6 experiments. 2MeSATP, 2-methylthioadenosine 5-triphosphate; ATP $\gamma$ S, adenosine 5-[ $\gamma$ -thio]triphosphate tetralithium salt; BzATP, 2,3-O-(4-benzoylbenzoyl)-ATP. Image taken from Donnelly-Roberts *et al.*, 2009b.

Such differences in ligands potency were also observed for several allosteric modulators. For instance, AZ11645373 is a potent antagonist of human and dog P2X7 at nanomolar concentrations, but it is active only at micromolar concentrations in the mouse orthologue, and it is inactive in the rat one (Figure 10) (Michel *et al.*, 2009). These differences were attributed to the amino acid 95, which is a Phe in hP2X7 and can form a  $\pi$ - $\pi$  stacking interaction to AZ11645373, unlike the Leu 95 present in the rat orthologue (Caseley *et al.*, 2015; Michel *et al.*, 2009). A more evident example of species-dependent differences is the pharmacological activity of GW791343, a potent P2X7 antagonist in humans, but a positive allosteric modulator in rats (Michel *et al.*, 2008).



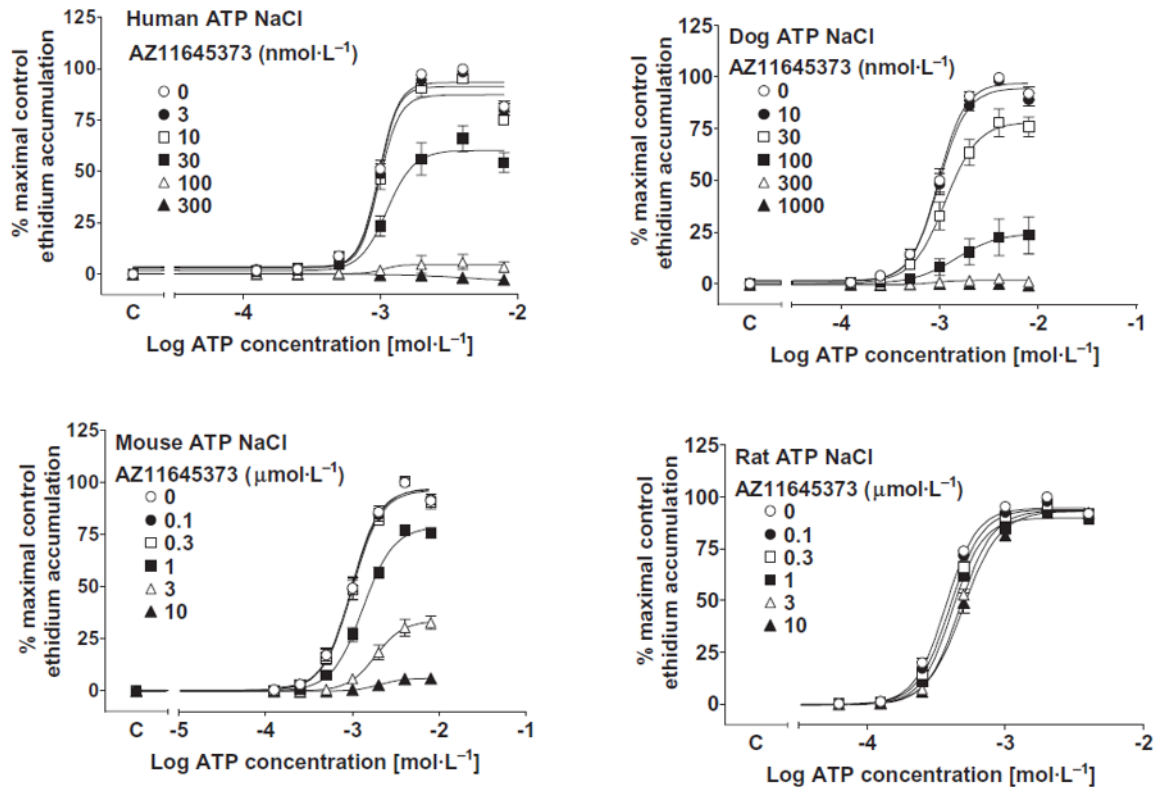


**Figure 10.** ATP concentration-response curves obtained by ethidium uptake experiments at different concentrations of the P2X7 antagonist AZ11645373 in P2X7-transfected HEK293 cell line. Basal ethidium accumulation in the absence or presence of AZ11645373 is indicated on the X-ordinate as C. The data are the mean  $\pm$  SEM of three to four separate experiments. BzATP, 2'(3')-O-(4-benzoylbenzoyl) ATP. Figure adapted from Michel *et al.*, 2009.

Another feature that distinguishes P2X7 from the other P2X subtypes is the long C-terminus (239 residues – from 356 to 595) that contains several binding domains. The first described was the *lipid interaction or putative lipopolysaccharide (LPS)-binding motif* (residues 574-589), which is homologous of the domain present in LPS-binding protein (LBP 44 % homology) and bactericidal permeability-increasing protein (BPI 31 % homology). LPS can bind to P2X7 LBP, as shown by *in vitro* experiments (Denlinger *et al.*, 2001), and it increases the potency and the effects of ATP-induced P2X7 activation, such as pyroptosis and cell death, in bone marrow-derived macrophages (Yang *et al.*, 2015). Between residues 541 and 560, an unusual  $\text{Ca}^{2+}$ -dependent calmodulin (CaM) binding motif was characterised (Roger *et al.*, 2008). It was proposed that CaM dynamically binds to this domain during repeated or prolonged stimulations, being responsible for the current facilitation detected by patch clamp techniques in rP2X7. The CaM binding also increases membrane blebbing, probably due to some interaction with proteins of the cytoskeleton (*e.g.*  $\alpha$ -actinin and F-actin among

others) (Roger *et al.*, 2008). These effects are evident when cytosolic  $\text{Ca}^{2+}$  is involved. Noteworthy, CaM cannot bind the hP2X7 C-terminus, due to the mutation of three amino acids. This correlates with the evidence that no  $\text{Ca}^{2+}$ -dependent current facilitation, but only a  $\text{Ca}^{2+}$ -independent one, has been detected in the hP2X7 orthologue (Roger *et al.*, 2010a). Other interesting motifs present in the P2X7 C-terminus have been recently disclosed with the rP2X7 cryo-EM structure (McCarthy *et al.*, 2019). Right at the juxtamembrane region of the C-terminal a C-cys anchor section was defined (residues 357-387, Figure 11). It comprises a region rich in palmitoylated cysteines anchored to the plasmatic membrane. The same happens also in the juxtamembrane region of the N-terminal (residues 1-26). The palmitoylated cysteines avoid any movement of the cytoplasmic cap, *i.e.* the region that follows the C-cys anchor in both C- and N-termini. This cap is firm and constantly assembled, impeding receptor desensitisation (McCarthy *et al.*, 2019), differently from what happens, for example, in P2X3 (Mansoor *et al.*, 2016). Curiously, the truncated variants of P2X7, *i.e.* those missing the cap or the anchor, or both, have never been reported to suffer desensitisation (Adinolfi *et al.*, 2010; Becker *et al.*, 2008; Cheewatrakoolpong *et al.*, 2005; Karasawa *et al.*, 2017). After the cytoplasmic cap, a cytoplasmic ballast has been characterised (Figure 11), which consists of the rest of the C-terminus including the domains described above. The ballast is not involved in receptor gating (McCarthy *et al.*, 2019), however two novel domains were disclosed in it by cryo-EM: two zinc-binding domains, involved in receptor trafficking and other possible intracellular signaling pathways, such as apoptosis or oxidative defense (Franklin and Costello, 2009; Furuta *et al.*, 2017), and a guanosine nucleotide binding site, which reminds to GPCRs.

P2X7 is peculiar for its pore that allows the passage of small ions, solvated organic molecules such as charged fluorescent probes, and ATP itself. There are two hypothesis that explain the existence of this pore, also defined as "macropore" (Di Virgilio *et al.*, 2018): 1) it is generated after dilation of the channel gate, or 2) it is the result of the involvement of other mechanisms (*e.g.* endocytosis) or proteins (Steinberg *et al.*, 1987). In the first case, whole-cell patch clamp experiments showed that the permeability of *N*-methyl-D-glucamine (NMDG, MW: 195 Da) through P2X7 is time-dependent (Yan *et al.*, 2008). However, this phenomenon seems to be due to unintended ionic accumulation or downstream-activated ion conductances (Li *et al.*, 2015). Single-channel experiments showed that current amplitude and permeation characteristics are stable and constant in time (Riedel *et al.*, 2007). Regarding the second hypothesis on the pore formation mechanism, the main P2X7-associated protein investigated is pannexin-1 (Qu *et al.*, 2011). However, its role in this event has not been experimentally confirmed (Alberto *et al.*, 2013). Considering all these evidences, it is now preferably stated that no pore dilation or additional proteins are involved in the generation of the P2X7

macropore, but that the pore of P2X7 is intrinsically wide, with a diameter of 8.5 Å (Riedel *et al.*, 2007). It was demonstrated that mutations or the truncation of P2X7 C-terminus avoid the permeation of small organic molecules through the pore (*e.g.* dye uptake), without changing ATP-gating properties (Adinolfi *et al.*, 2010; Cheewatrakoolpong *et al.*, 2005). It was proposed that palmitoylation of the cysteines in the C-terminus changes the composition of the lipid raft where the receptor is expressed, allowing the full pore opening (Di Virgilio *et al.*, 2018). For instance, it would move cholesterol away from the P2X7 transmembrane domains, thus inhibiting fluorescence dye uptake (Karasawa *et al.*, 2017).

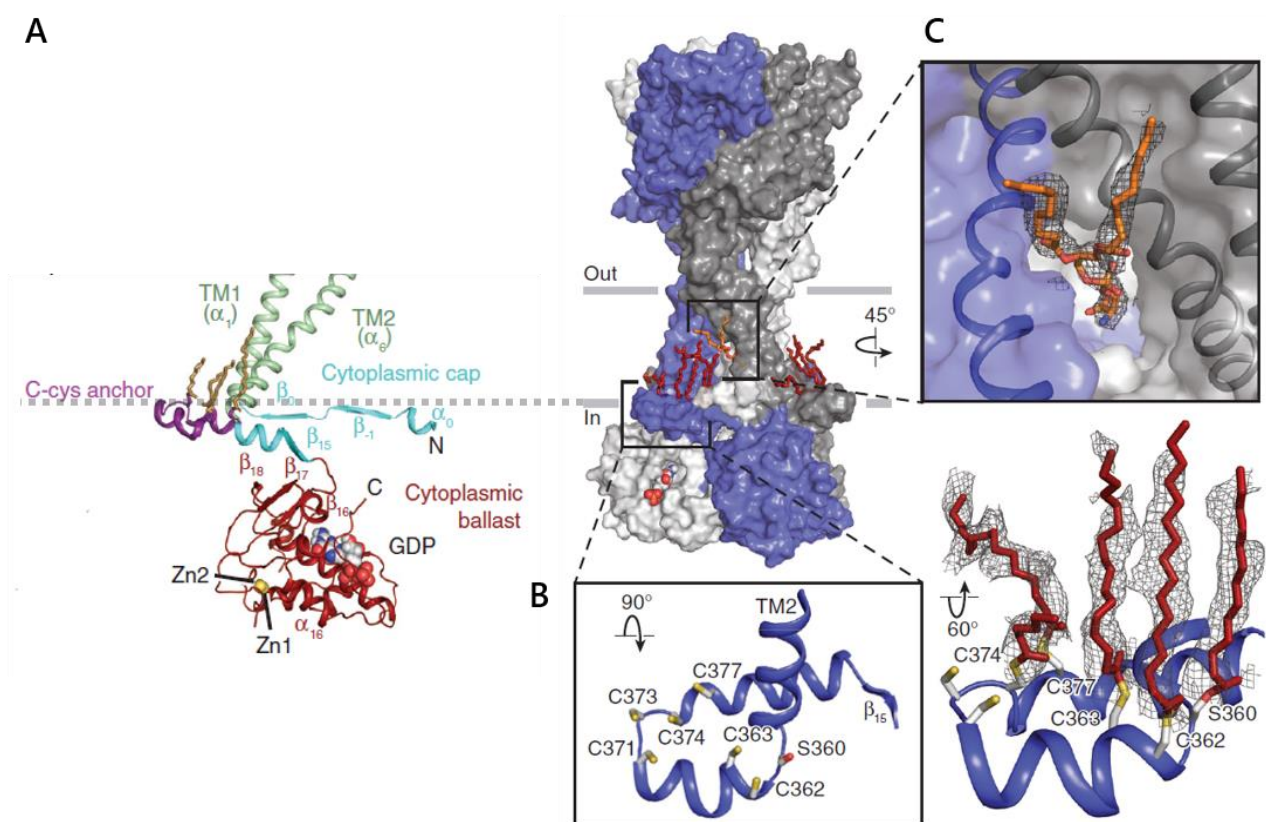


**Figure 11.** Representation of rP2X7, based on the structure disclosed by cryo-EM. **A)** P2X7 TMs and cytoplasmatic C-tail representation. The main sections and domains described in the text are highlighted. **B)** Closer view of the cysteines of the C-cys anchor. On the right, the same cysteines palmitoylated. **C)** Closer view of the phospholipid found in the middle of the channel pore. It may be involved in a flippase-like function of the receptor, but more information is needed. The images are taken from McCarthy *et al.*, 2019 and adapted to the content of this thesis.

Finally, alternative splicing and natural-occurring single-nucleotide polymorphisms (SNP) have been identified for P2X7. More than 150 SNPs in the extracellular loop and C-terminus, as well as 13 natural splice variants, have been discovered in human tissues (Jimenez-Mateos *et al.*, 2019). P2X7A is well characterised as the full-length P2X7. P2X7B isoform is particularly relevant for being the C-terminus-truncated form of the receptor. It is widely distributed in several tissues and lacks the proapoptotic actions of P2X7A (Cheewatrakoolpong *et al.*, 2005). This suggests that P2X7 responses could be finely tuned by the expression of various P2X7 isoforms. For instance, P2X7B augments NFATc1 activation and supports cell growth (Adinolfi *et al.*, 2010). P2X7K is fully functional in mice, with 8-fold higher sensitivity to agonists, slower deactivation, and augmented ability of making small organic cation to pass through its pore than the human variant (Nicke *et al.*, 2009). The influence of these and other variants on P2X7 signalling, both *in vitro* and *in vivo*, may be a confusing factor in preclinical studies in knock-out or transgenic mice. Particularly relevant could be the difference in sensitivity of these variants to the P2X7 antagonists tested, and the extrapolation of these outcomes to clinical trials in humans. Moreover, the SNPs described with altered hP2X7 functions add extra complexity to an already intricate situation (Gu *et al.*, 2001; Roger *et al.*, 2010b; Stokes *et al.*, 2010).

### 3.3. The role of P2X7 receptor in neuroinflammation and neurodegenerative diseases

Considering that P2X7 is expressed by immune and inflammatory cells, such as mast cells, NK cells, and T and B lymphocytes (Di Virgilio, 2015), and that is up-regulated in inflammatory processes, it has been considered a reliable target to treat neurodegenerative diseases (Adinolfi *et al.*, 2018). In the CNS, P2X7 is widely expressed in dendritic cells and microglia, best-known cells from the monocyte/macrophage axis.

Cell components, including ATP, are released out to the extracellular space as a result of stress or tissue damage (danger-associated molecular pattern, DAMP), causing the activation of a protective immune response. It is amply recognised that P2X7 is the main sensor for ATP during inflammation, where it is also the main trigger of the immune response, as it mediates maturation and secretion of several interleukins, mainly interleukin-1 $\beta$  (IL-1 $\beta$ ) (Ferrari *et al.*, 2006; Piccini *et al.*, 2008), but also IL-18, IL-6, and IL-1 $\alpha$  (Englezou *et al.*, 2015). IL-1 $\beta$  synthesis within immune cells requires the activation of the nuclear factor NF- $\kappa$ B, achieved by using LPS as TLR4 agonist in *in vitro* and *in vivo* models of inflammation (Di Virgilio *et al.*, 2017). IL-1 $\beta$  is firstly produced in an inactive form (pro-IL-1 $\beta$ ) that is subsequently cleaved by caspase-1, a part of the inflammasome complex. The specific inflammasome that is activated by the ATP-induced P2X7 activity is NLRP3 (Karmakar *et al.*, 2016). Decrease of intracellular K<sup>+</sup> resulted to be the main driving force for NLRP3 activation (Munoz-Planillo *et al.*, 2013). This happens through the activation of P2X7 itself, and curiously, pore function is required for NLRP3 activation, meaning that a large drop in K<sup>+</sup> is necessary (Di Virgilio *et al.*, 2017). NLRP3/P2X7 axis has also been associated to pyroptosis, a cell death mediated by inflammatory caspases (Caspase-1 and -11 in mice, Caspase-1, -4, and -5 in humans) in immune cells (de Gassart and Martinon, 2015). In particular, caspase-11 is responsible of cleaving pannexin-1, which in turn mediates ATP release and consequently extends P2X7 activation in an autocrine/paracrine fashion (Yang *et al.*, 2015). Figure 12 represents the main pathways involved in NLRP3 activation and P2X7-mediated interleukins release.

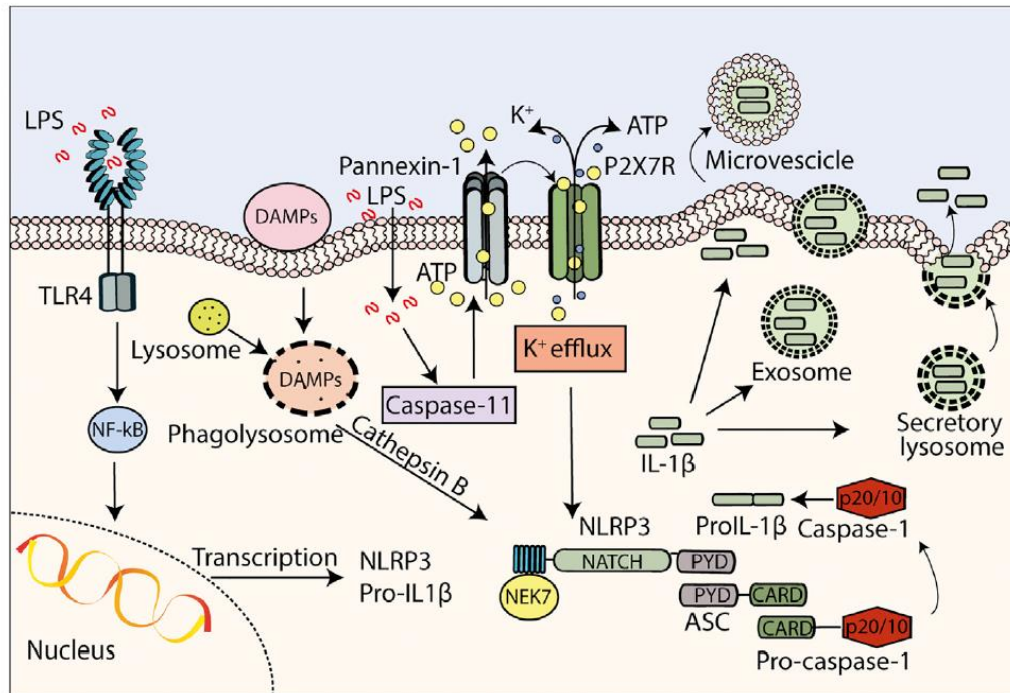


**Figure 12.** Schematic representation of IL-1 $\beta$  transcription stimulation, P2X7- or DAMPs-exerted NLRP3 activation, and IL-1 $\beta$  release, as main inflammatory signaling associated to P2X7 activation. Image taken from Di Virgilio *et al.*, 2017.

Conversely, it was demonstrated that punctual activation of P2X7 with low concentration of ATP can provoke a pseudoapoptosis state, characterised by the increase of intracellular Ca<sup>2+</sup>, uptake of mitochondrial Ca<sup>2+</sup>, and mitochondrial depolarisation, thus leading to localised Ca<sup>2+</sup> overload at the plasma membrane-mitochondria-cytoskeleton matrix, responsible for membrane blebbing (Mackenzie *et al.*, 2005). This process is reversible because the stimulus is not so intense as to activate the cytochrome *c*/caspase-3/RhoA-associated kinase (ROCK1) pathway, avoiding cell death (Figure 13). Ion fluxes and membrane blebbing are accompanied by other intracellular signals that are not necessarily related to damaging conditions, such as PLA2, PLC, and PLD activation (Kopp *et al.*, 2019). For example, PLD activity is fundamental for P2X7-dependent mitigation of intracellular pathogens (Coutinho-Silva *et al.*, 2003; Kusner and Adams, 2000). Tonic P2X7 activation, presumably under physiological conditions, also increases endoplasmic reticulum Ca<sup>2+</sup> levels with subsequent transcription factor NFATc1 activation and promotion of the cell survival and growth (Adinolfi *et al.*, 2009). Moreover, it was suggested that cells can control the pattern of expression of naturally occurring variants of the receptor to take advantage of their trophic effects when necessary (Figure 12) (Adinolfi *et al.*, 2010).

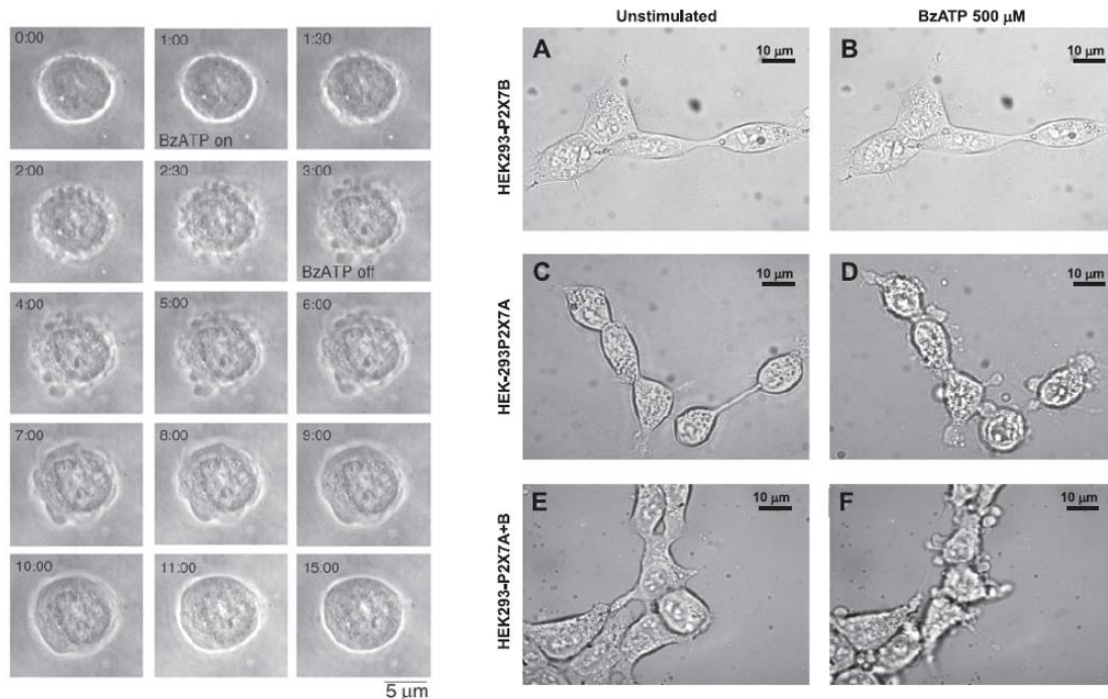


**Figure 13.** P2X7-induced membrane blebbing in P2X7-stably expressing HEK293 cells. On the left, the cell is stimulated with BzATP (100  $\mu$ M) from minute 1 to 3. Blebbing is reversible, since blebs are completely reabsorbed after 12 min washing. On the right (A-F), membrane blebbing in HEK293 cells transfected with P2X7A and/or P2X7B receptors. The naturally occurring C-terminus-truncated variant possesses trophic effects and does not trigger membrane blebbing, which is usually linked to apoptotic death. Images adapted from Mackenzie *et al.*, 2005, and Adinolfi *et al.*, 2010.

Expression of P2X7 in neurons is still controversial (Illes *et al.*, 2017; Miras-Portugal *et al.*, 2017). By contrast, macrophages are usually used as model to investigate the functional role of P2X7 in neuroinflammation. Beside their inflammatory properties, P2X7 works as a scavenger receptor in its non-activated state, thus being responsible of macrophages and microglia phagocytosis of pathogenic organisms, apoptotic cells, and debris (Figure 14) (Gu and Wiley, 2018). Additionally, P2X7 activation downregulates microglia proliferation in spinal cord, controlling phagocytosis of dead motoneurons (Rigato *et al.*, 2011), which cannot be prevented by P2X7 pharmacological antagonists (Ou *et al.*, 2018). These findings have implications on the role of the P2X7 in neurogenesis at developmental and adult stages (Leeson *et al.*, 2019), as well as in pathological conditions, such as MS. In fact, P2X7 knockout mice develop more severe clinical and pathological expression of the experimental autoimmune encephalomyelitis (EAE) model of MS than wild-type controls. This may be due to a loss of lymphocyte homeostasis, including lack of apoptosis and P2X7 scavenger functions (Chen and Brosnan, 2006).

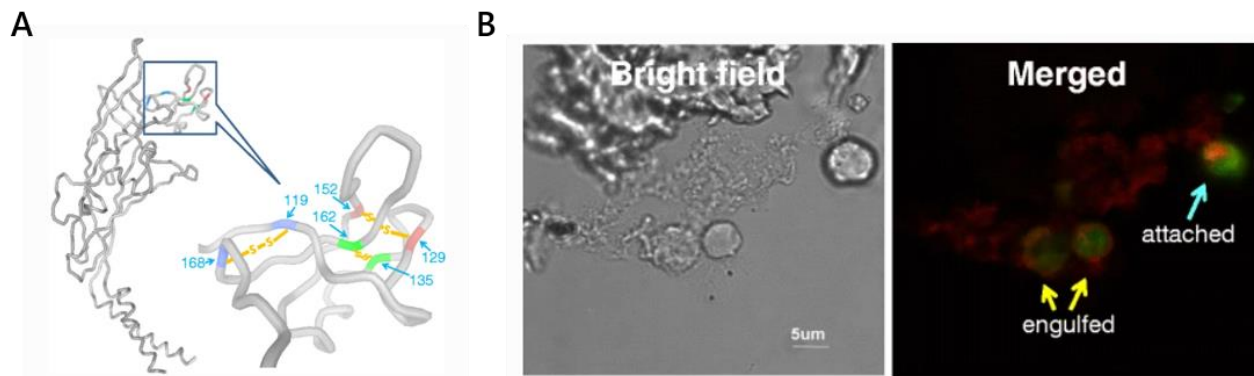


**Figure 14.** A) P2X7 model built using the crystal structure of the zebrafish P2X4. Three of the five disulfide bonds of the upper domain (the “dolphin nose”) are highlighted and were suggested to be responsible for P2X7 scavenging activity. B) Bright field and confocal image of HEK293 cells transfected with the DsRed-tagged P2X7 (red) during phagocytosis of CFSE-labelled apoptotic human tumour T-cells (HPB - green). The image shows two engulfed HPB cells and a third one that is undergoing phagocytosis. Images adapted from Wiley and Gu, 2012.

Considering the huge impact of P2X7 activity on the rise of neuroinflammation and its relationship with CNS disorders, the development of P2X7 antagonists has become a reliable pharmacological strategy in neurodegenerative diseases (Calzaferri *et al.*, 2020).

### 3.3.1. Alzheimer’s disease

AD is a neurodegenerative disorder characterised by a progressive impairment of higher cognitive function, memory loss, and altered behaviour as salient clinical symptoms (Goedert and Spillantini, 2006). Pathological hallmarks of AD are senile plaques composed of extracellular aggregates of amyloid beta peptide ( $A\beta$ ), intracellular neurofibrillary tangles formed by deposits of phosphorylated tau protein, and the shrinkage of the cerebral cortex due to extensive neuronal loss (Alzheimer, 1907; Giannakopoulos *et al.*, 2009). As for the drug treatment of AD, only some symptomatic medicines are available, namely the acetylcholinesterase inhibitors rivastigmine, donepezil, and galantamine, as well as the non-competitive antagonist of *N*-methyl-D-aspartate (NMDA) receptors for glutamate, memantine. None of these medicines delay disease progression. For about 20 years,  $A\beta$  has been the preferred drug target in the search for a medicine capable of delaying disease progression. Disappointingly, many compounds showing efficacy in murine models of AD have failed in clinical trials (Cummings *et al.*, 2019; Mehta *et al.*, 2017). Thus, doubts on the central pathogenic role of  $A\beta$  in AD may change the focus to other drug targets. In this context, the P2X7 is emerging as a potential drug target for AD (Calzaferri *et al.*, 2020).



In cellular models of AD, A $\beta$  oligomers induced P2X7 overexpression, exacerbating synaptic impairment and neuronal dyshomeostasis (Saez-Orellana *et al.*, 2018). A $\beta$  caused the release of ATP and IL-1 $\beta$  in WT microglia, and augmented plasmalemmal permeability. These effects were not observed in microglia from P2X7-deficient mice, suggesting that microglia activation requires the presence of P2X7 (Sanz *et al.*, 2009). An *in vivo* study using the AD mouse model Tg2576 reported that P2X7 is overexpressed in both astrocytes and microglia around A $\beta$  senile plaques (Parvathenani *et al.*, 2003). A second study in APP/PS1 mice found that P2X7 was mostly located in microglia that generated excessive ROS with ensuing dendrite damage. Authors correlated these findings with A $\beta$  increase and synaptotoxicity (Lee *et al.*, 2011). Additionally, A $\beta_{1-42}$  significantly elevated P2X7 expression in cultured fetal human microglia. The Ca<sup>2+</sup> signals evoked by BzATP were also increased in these cells, and were blocked by oxidised ATP (oATP). Furthermore, P2X7 co-localised with microglia in rat hippocampus injected with A $\beta_{1-42}$  (McLarnon *et al.*, 2006). Similarly, the tauopathy mouse model P3015 expressed P2X7 mainly in astrocytes (Jin *et al.*, 2018). A study in brain of AD patients showed augmented expression of P2X7 in microglia. P2X7 was predominantly expressed in association with A $\beta$  plaques and localised in immunoreactive microglia. As a proof-of-concept of P2X7 as drug target for AD, the *in vivo* inhibition of the P2X7 with Brilliant Blue G (BBG) in the J20 transgenic mice of the human mutant induced a significant decrease in hippocampal amyloid plaques, correlating with glycogen synthase kinase 3 activity decrease and  $\alpha$ -secretase activity increase (Diaz-Hernandez *et al.*, 2012). BBG also improved both cognition and increased the number of dendritic spines in hippocampal neurons of rats injected with A $\beta_{1-42}$  (Cheng *et al.*, 2014).

### 3.3.2. Parkinson's disease

PD is a neurodegenerative disease characterised by the selective loss of dopaminergic neurons in the substantia nigra pars compacta, that leads to physiopathologic alterations in the circuitry of downstream basal ganglia (Kalia and Lang, 2016). When motor symptoms first appear (*i.e.* tremor, muscle rigidity, bradykinesia), over 80 % of these neurons are lost (Reich and Savitt, 2019). The presence of Lewy bodies containing misfolded  $\alpha$ -synuclein are the hallmarks of PD (Goedert *et al.*, 2017). One pathogenic hypothesis states that dopamine acts as a natural toxin: its oxidation in the cytosol produces the neurotoxin 7-hydroxydopamine and other toxic metabolites that cause mitochondrial damage and death of dopaminergic neurons (Sulzer, 2007). PD is treated with a great variety of medicines aimed at dopamine repositioning (Reich and Savitt, 2019). Levodopa remains the central stage in the treatment of PD. To prevent its peripheral breakdown, levodopa is administered with carbidopa, a DOPA decarboxylase inhibitor. The dopamine receptor agonists pramipexole, ropinirole or rotigotine are used as add-on therapy to levodopa. Additionally, to prevent dopamine degradation, the catechol-*O*-methyl-transferase inhibitors tolcapone, entacapone,

or opicapone, as well as the mono-amine-oxidase B inhibitors selegiline, rasagiline, and safinamide are also used with levodopa to reduce wearing-off and also to delay the initiation of levodopa when used as monotherapy. Finally, the NMDA receptor antagonist amantadine and the anticholinergic trihexyphenidyl are other medications that may have levodopa sparing effects.

Nowadays, PD is considered as a multifactorial pathology involving the above-mentioned dopamine-related oxidative stress, as well as other factors such as neuroinflammation. Increasing evidence points out P2X7 as supporting player for PD progression (Calzaferri *et al.*, 2020; Savio *et al.*, 2018). For instance, *in vitro* experiments revealed that ATP and 6-hydroxydopamine (6-OHDA) induce cytotoxicity in SN4741 dopaminergic neurons via activation of P2X7 (Jun *et al.*, 2007). P2X7 was found to be upregulated in post-mortem brain of PD patients (Durrenberger *et al.*, 2012). This was explained by further observations, in which accumulation of oligomerised  $\alpha$ -synuclein mediates neurotoxicity by producing ROS and other pro-inflammatory mediators, and thus activating microglia (Stefanis, 2012). Moreover,  $\alpha$ -synuclein binds to P2X7 in microglia and stimulates P2X7 transcription (Jiang *et al.*, 2015). Microgliosis found in PD patients' brains was mimicked in rat PD models by unilateral intranigral injection of 6-OHDA. P2X7 antagonists, namely BBG and A-438079, attenuated microglia activation, mitochondrial dysfunction, and motor and memory impairment (Carmo *et al.*, 2014; Kumar *et al.*, 2017; Marcellino *et al.*, 2010). BBG was found to prevent also the loss of dopaminergic neurons (Ferrazoli *et al.*, 2017), unlike A-438079 (Marcellino *et al.*, 2010). Similarly, P2X7 deletion or pharmacological inhibition failed to afford neuroprotection in the MPTP mouse model of PD (Hracsco *et al.*, 2011).

### 3.3.3. Huntington's disease

Huntington's disease (HD) is an autosomal dominant disorder with hyperkinetic involuntary movements, progressive dementia, paranoid psychosis, and aggressiveness. When mutated, the huntingtin gene exhibits an expansion in the number of cytosine, adenine, and guanine (CAG) trinucleotide repeats in exon 1 (MacDonald, 1993). Anomalous expansion of CAG repeats produces misfolded huntingtin that forms cytoplasmic and nuclear aggregates, giving rise to neuronal loss in the cortex and in the lateral tuberal nucleus of the hypothalamus (Kremer *et al.*, 1990). These two pathogenic features have been mimicked in mouse models of HD. Drug treatment of HD patients is based on tetrabenazine, a blocker of the vesicular monoamine transporter (VMAT2) that causes dopamine depletion from presynaptic vesicles. In so doing, the drug reduces the chorea symptoms of HD patients (Savani and Login, 2007). Also, in HD mice tetrabenazine improves motor coordination deficits and protects against striatal neuron degeneration (Tang *et al.*, 2007). Recently, deuterated tetrabenazine (or deutetetrabenazine) has also been approved for the treatment of chorea in HD

patients. The substitution of hydrogen for deuterium in this drug increases its half-life, thus decreasing the administration frequency (Dean and Sung, 2018). Thus, novel drug targets to treat HD and to delay disease progression are needed. Considering the accumulation of reactive microglia (microgliosis) and the elevated values of IL-6, IL-8, and TNF- $\alpha$  observed in post-mortem brains and cerebrospinal fluid of HD patients, P2X7 has been considered as a promising target to treat HD. However, the role of P2X7 in HD has not been deeply investigated and only few facts are known about this possible relationship. Beside the P2X7 overexpression in neurons of a mouse model of HD, as well as in the striatum of post-mortem HD patients (Ollà *et al.*, 2020), an excessive P2X7-dependent Ca<sup>2+</sup> permeability has been documented (Díaz-Hernández *et al.*, 2009). In addition, neurons that express the mutant huntingtin are prone to suffer apoptosis after P2X7 stimulation. As proof-of-concept, eight-month-old mice treated with BBG recovered body weight loss and motor coordination. However, the treatment with the antagonist A-438079 did not result in any difference when compared with controls.

#### 3.3.4. Multiple sclerosis

MS is a neurodegenerative disorder in which patients show altered motor coordination, sensory disturbances, and visual deficit. This is due to immune cell infiltration, loss of oligodendrocytes and axonal damage that leads to demyelination and neuronal death (Lucchinetti *et al.*, 2011). Currently, there is no cure to this disease, however symptomatic pharmacological treatments are available, such as the administration of immunosuppressive drugs like glucocorticoids (*e.g.* methylprednisolone), interferon  $\beta$ -1, and several monoclonal antibodies (*e.g.* natalizumab) (Gholamzad *et al.*, 2019).

P2X7 involvement in MS is based on the high P2X7 expression detected in activated astrocytes and microglia in MS post-mortem patients (Narcisse *et al.*, 2005; Yiangou *et al.*, 2006). Upregulation of the P2X7 in astrocytes and oligodendrocytes was also observed in a rat model of MS (EAE) (Grygorowicz *et al.*, 2010; Matute *et al.*, 2007; Tsunoda and Fujinami, 1996). From a genetic perspective, it is noteworthy the finding that a rare variant of P2X7 receptors, *i.e.* Arg307Gln leads to loss of pore formation and function that protects against neuroinflammation in MS (Gu *et al.*, 2015). P2X7 levels remain elevated in EAE rats even after reversion of neurological symptoms, correlating with sustained astrocytosis in advanced disease stages in both EAE and MS patients (Grygorowicz *et al.*, 2011; Holley *et al.*, 2003). These data are reinforced by the recent observation of increased P2X7Rs on frontal cortex astrocytes from patients suffering from progressive MS (Amadio *et al.*, 2017). Administration of P2X7 antagonists, either BBG or oATP to EAE rats prevented ATP-induced excitotoxicity in oligodendrocytes, reduced demyelination, thus improving neurological features

(Matute *et al.*, 2007). This supports the view that P2X7R blockers could have a role in preventing or improving MS symptoms (Calzaferrri *et al.*, 2020).

### 3.3.5. Amyotrophic lateral sclerosis

ALS is a progressive neurodegenerative disorder caused by the selective loss of motor neurons in the cortex, brainstem, and spinal cord. This leads to ambulation, speech, and swallowing impairment, and compromised respiration, leading to progressive paralysis and death 3-4 years after diagnosis. Age-standardised incidence is 2.6 per 100'000 women and 3.9 per 100'000 men per year (Alonso *et al.*, 2009). Drug therapy of ALS consists in the administration of riluzole, which blocks glutamatergic transmission in the CNS by the partial inactivation of voltage-dependent sodium channels on glutamatergic nerve terminals and through the blocking of NMDA post-synaptic receptors (Doble, 1996). However, daily treatment with riluzole is able to prolong patients' life for only 2 months (Miller *et al.*, 2003). A more recently approved drug is edaravone, an antioxidant molecule that reduces oxidative stress damage in motoneurons. Treatment with edaravone provokes a delay in the development of ALS symptoms in patients in early stages of the disease and with a slow developing disease (Cruz, 2018).

Being a multifactorial pathology, ALS is a complex disorder in which several players are involved, mainly  $\text{Ca}^{2+}$  dyshomeostasis, especially in motoneurons, low capability of  $\text{Ca}^{2+}$  buffering, generation of radical oxygen species, intracellular protein accumulation (*e.g.* mutant SOD1) and neuroinflammation (Ruiz-Ruiz *et al.*, 2020a). The role of P2X7 in ALS was firstly evidenced in post-mortem spinal cord tissue of ALS patients, where P2X7 expression levels are upregulated (Yiangou *et al.*, 2006). The relationship between P2X7 activation and motoneuron death in ALS was further established in co-cultures of astrocytes and motoneurons from WT and SOD1<sup>G93A</sup> mice, a model of ALS. Repeated stimulation of P2X7 with ATP or BzATP triggered a neurotoxic phenotype in control and SOD1<sup>G93A</sup> astrocytes, inducing motoneuron death which was prevented by treatment with BBG (Gandelman *et al.*, 2010). Despite these results, which suggest a negative effect of P2X7 in ALS, genetic ablation of the receptor in SOD1<sup>G93A</sup> mice accelerated and worsened disease progression and caused earlier disease onset (Apolloni *et al.*, 2013), suggesting a dual role of the receptor in the disease and a protective activity at some disease stages. This dual role could be explained by the two different phenotypes presented by microglia upon P2X7 activation: M1 or pro-inflammatory and M2 or anti-inflammatory. M2 is believed to be predominant in the first stages of the disease, while M1 seems more prevalent at later stages, as found in aged SOD1<sup>G93A</sup> mice (Liao *et al.*, 2012; Parisi *et al.*, 2016). Moreover, P2X7 activation improves innervation and metabolism of muscles, avoiding their

atrophy, defining a different role of the receptor in peripheral tissues respect to the CNS (Fabbrizio *et al.*, 2020; Volonté *et al.*, 2020).

*In vivo* studies using different P2X7 antagonists have afforded few, sometimes controversial, results: BBG administration improved motor performance and body weight loss in some cases (Apolloni *et al.*, 2014; Bartlett *et al.*, 2017; Cervetto *et al.*, 2013); A-804598 administration did not show any significant result (Fabbrizio *et al.*, 2017); JNJ-47965567 administration from pre-onset stage of the disease to humane endpoint, resulted in delayed disease onset, improved motor performance, and body weight loss only in females (Ruiz-Ruiz *et al.*, 2020b), whereas i.p. injection from onset stage to humane endpoint did not show any improvement (Ly *et al.*, 2020). Unfortunately, no effect on survival was observed in any of these studies, which highlight the need of finding a proper administration starting point throughout the disease, as well as the perfect dosing and frequency of administration for each P2X7 antagonist, depending on their pharmacodynamics and pharmacokinetics.

### 3.4. Ligands targeting the P2X7 receptor

During the last two decades, a plethora of drugs capable of targeting P2X7 has been discovered and developed. Beside the endogenous agonist ATP (Figure 15), BzATP is a more potent full agonist of P2X7 ( $pEC_{50} = 5.3$ ) even if not selective, as also activates P2X1 ( $pEC_{50} = 8.8$ ), P2X3 ( $pEC_{50} = 7.1$ ), P2X4 ( $pEC_{50} = 6.3$ ), P2X5 ( $pEC_{50} \sim 5$ ), and P2Y11 ( $pEC_{50} = 5.1$ ) (Abdelrahman *et al.*, 2017; Bo *et al.*, 2003; Jacobson, 2010; Jacobson *et al.*, 2002). The rationale behind the increase of P2X7 agonist activity of BzATP lays on a strong  $\pi$ -cation interaction between the additional benzene rings of BzATP and Lys 127 (Young *et al.*, 2007). Several P2X7 positive allosteric modulators (PAMs) have also been described, mainly from natural sources (*e.g.* isatin, agelastine, garcilonoic acid, and ginsenosides) or drug repurposing (*e.g.* clemastine, polymixin B, tenidap, and ivermectin) (Stokes *et al.*, 2020).

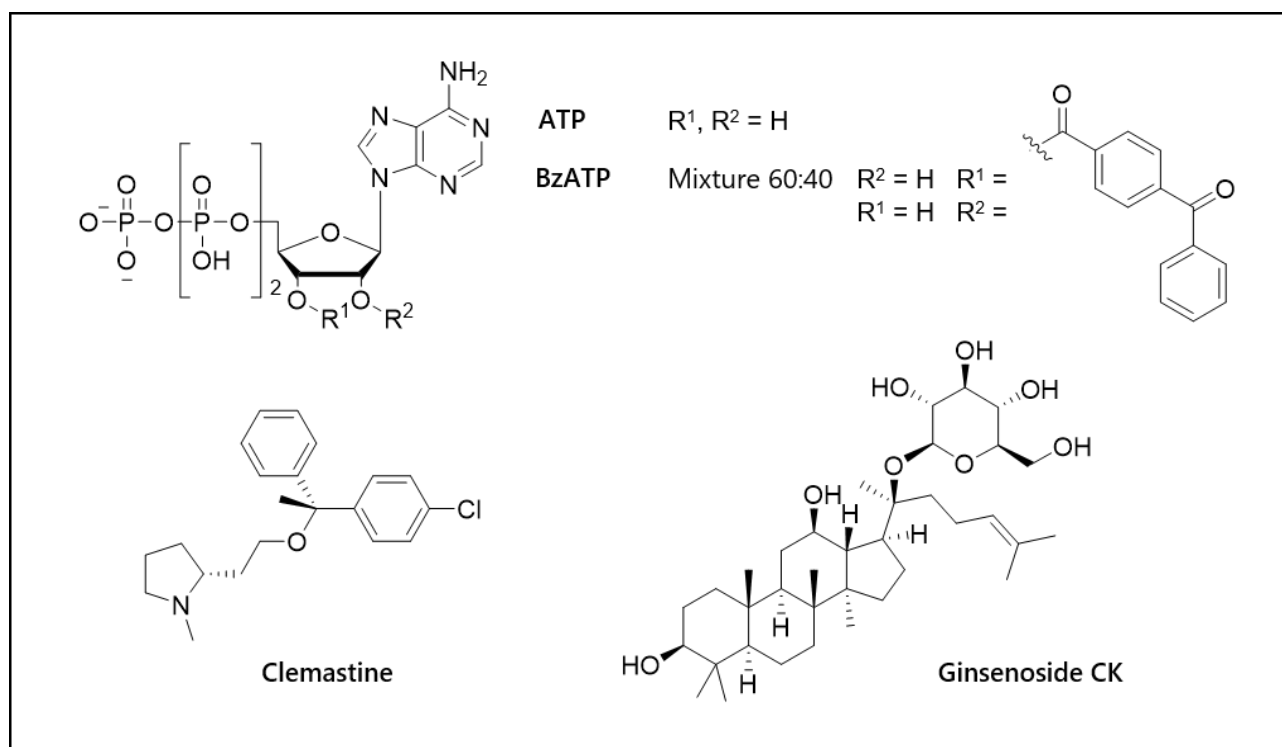


Figure 15. Agonists (above) and positive allosteric modulators (below) of the P2X7 receptor.

Most of the efforts of medicinal chemists have focused on the development of potent and selective P2X7 antagonists, supported by the potential therapeutic advantages that they could provide. One of the first P2X7 blockers discovered was the nucleotide-binding protein-reagent periodate-oxidised oATP (Figure 16) (Murgia *et al.*, 1993) that, a decade later, was found to attenuate also pro-

inflammatory signals *via* a P2 receptor-independent mechanism (Beigi *et al.*, 2003). Among the first most frequent purinergic antagonist used as pharmacological tools, the non-selective competitive P2X7 antagonist pyridoxalphosphate derivative PPADS (Huo *et al.*, 2018) stood out, as well as the non-competitive P2X7 antagonist triphenylmethane dye Brilliant Blue G (BBG) (Dayel *et al.*, 2019), the naphthylsulfonate suramin and its isoquinoline derivative KN-62 (Figure 16) (Gargett and Wiley, 1997). BBG has been largely used to study the pharmacology of P2X7, despite it also targets P2X4, P2X5, rat P2Y<sub>1</sub> and P2Y<sub>2</sub> receptors, as well as voltage-gated sodium channels (Jacobson *et al.*, 2002; Jo and Bean, 2011). BBG was initially the main compound used as proof-of-concept of the P2X7 role in neurodegenerative diseases (Apolloni *et al.*, 2014; Bartlett *et al.*, 2017; Chen *et al.*, 2014). Although its weight and neat charge compromises its permeability through the blood-brain barrier (BBB), it reaches damaged tissues of the CNS, presumably due to BBB impairment in the animal models employed (Peng *et al.*, 2009).

The search for more potent and selective P2X7 antagonists capable of reaching the CNS because of an optimised BBB permeability, mainly conducted by *Big Pharma*, has given rise to novel derivatives. The most notable medicinal chemistry projects are summarised below.

AstraZeneca was one of the first companies disclosing P2X7 antagonists (Baxter *et al.*, 2003). The first hit compound was the adamantanyl-*o*-chlorobenzamide I (Figure 17), further subjected to a hit-to-lead optimisation to improve its drug-like properties. This was achieved by replacing the benzamide with an indazolamide and the inversion of the amide moiety, resulting in compound II (Figure 17). Among the derivatives of this series, compound III stood out and would have been taken as model by other groups (Figure 17). With the attempt to improve both low solubility and metabolic stability, the incorporation of heterocycles succeeded, furnishing compounds IV, V, and VI (Figure 17) (Furber *et al.*, 2007). Replacement of these cycles with long aliphatic chains containing polar groups, gave rise to **AZD9056** (Figure 17), which entered in clinical trials for rheumatoid arthritis and Crohn's disease (Eser *et al.*, 2015; Guile *et al.*, 2009; Keystone *et al.*, 2012). Some other analogues clinical candidates were generated by linking the adamantane core to a quinoline through an amide, yielding **AZ10606120** (Figure 17). However, its high hydrophilicity was not adequate to target the CNS, so it has only been used for *in vivo* studies concerning non-CNS-related diseases. Another pharmacological tool developed by AstraZeneca is compound **AZ11645373** (Figure 17), peculiar for its thiazolidine-2,4-dione and developed through chemical optimisation after the high-throughput-screening of some cyclic imides (Alcaraz *et al.*, 2003).

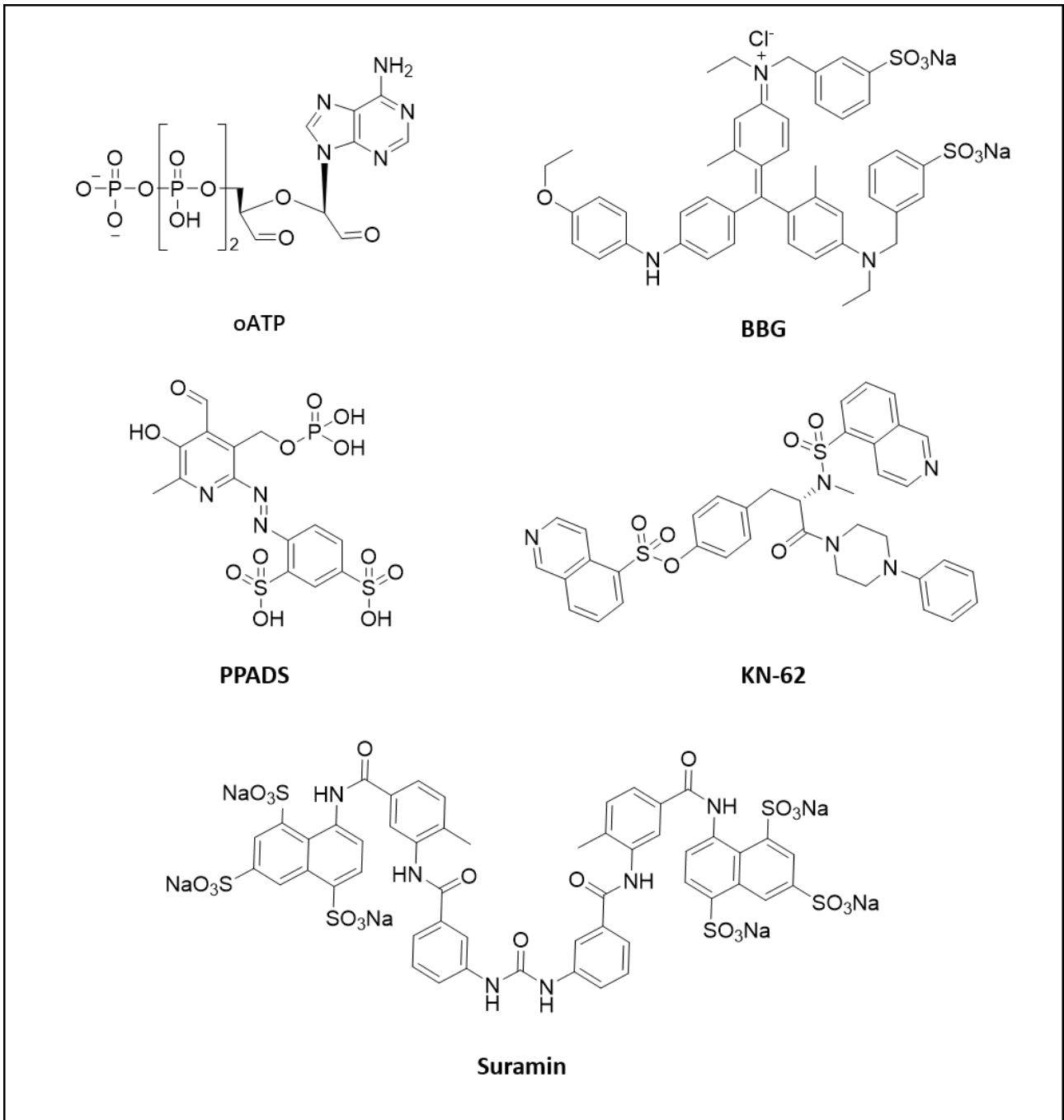
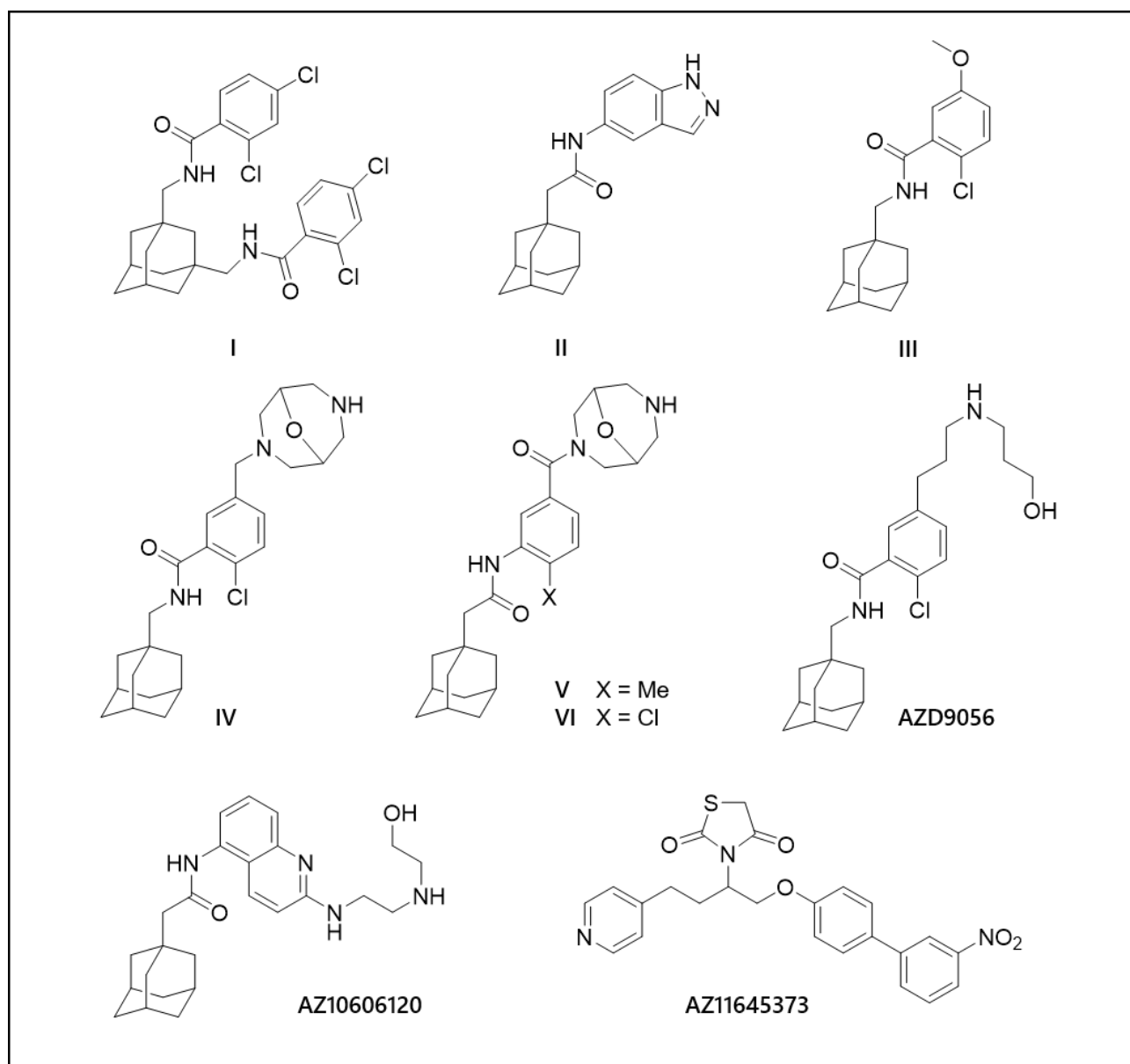


Figure 16. First generation of P2X7 antagonists.





**Figure 17.** AstraZeneca's P2X7 antagonists. AZD9056 has completed phase II clinical trial for rheumatoid arthritis and underwent a small clinical study in Crohn's disease patients.

Kim and co-workers discovered that some berberine alkaloids analogues had human P2X7 blocking activity. The chemical modifications proposed on the hit compounds, in particular the alkyls and benzyl groups, gave rise to a set of quinazolinium derivatives with  $IC_{50}$ s around 1  $\mu$ M, the most potent being the nitro-derivative **VII** ( $IC_{50}$  = 0.17 nM, 2-fold more potent than KN-62) (Figure 18) (G. E. Lee *et al.*, 2009). This compound also exhibited the highest potency to block LPS/IFN $\gamma$ -induced IL-1 $\beta$  release from THP-1 cells ( $IC_{50}$  = 175 nM). Another chemical screening identified various chiral pyrazolodiazepinones with some activity on human P2X7 receptors expressed in HEK293 cells. Such inhibition, and the related mitigation of the IL-1 $\beta$  release, improved by the incorporation of an *N*-methylindole cycle, linked by an ester to the central core (J. Y. Lee *et al.*, 2009). This led to ligands with activity similar to KN-62, such as **VIII** (Figure 18). This second family of compounds was globally less potent than the former, but presented the advantage of lacking quaternary nitrogens, thereby increasing BBB permeability. More recently, the same authors described a series of pyrimidine-2,4-dione related to KN-62, as they possess the isoquinolin-5-sulfonate and phenylpiperazine moieties in their structure (Park *et al.*, 2015). Substitution at the pending phenyl ring, as well as the presence or absence of a spacer (methyl or carbonyl) conditioned the structure-activity relationship. For instance, benzoyl analogues with different halogen substitutions afforded the best inhibitions, such as derivative **IX**, which was better than KN-62 (Figure 18). Furthermore, authors showed that piperazine substructure nicely accepted other acyl groups of hydrophobic nature (alicyclic, such as adamantyl), offering similar blockade. Compound **IX** was selected for the assessment of some of its pharmacokinetic (PK) parameters, showing high metabolic stability and low cytotoxicity and cardiac toxicity. More recently, the Kim's group have screened a library of quinoline and quinolinones looking for novel scaffolds to inhibit P2X7. They optimised their first hit compound (**X** – Figure 18), identifying the adamantly derivative **XI** (Figure 18) with efficacy in reducing sphere size of glioblastoma cells, but poor *in vitro* metabolic stability (Kwak *et al.*, 2018). The quinoline scaffold was further studied by EMD Serono (Merck KGaA), resulting in compound **XII** (Figure 18) that have very good potency on the hP2X7, and PK properties, acceptable brain penetration and efflux ratio, but only scarce rP2X7 activity, which would discourage further *in vivo* studies in rodents (Xiao *et al.*, 2019).

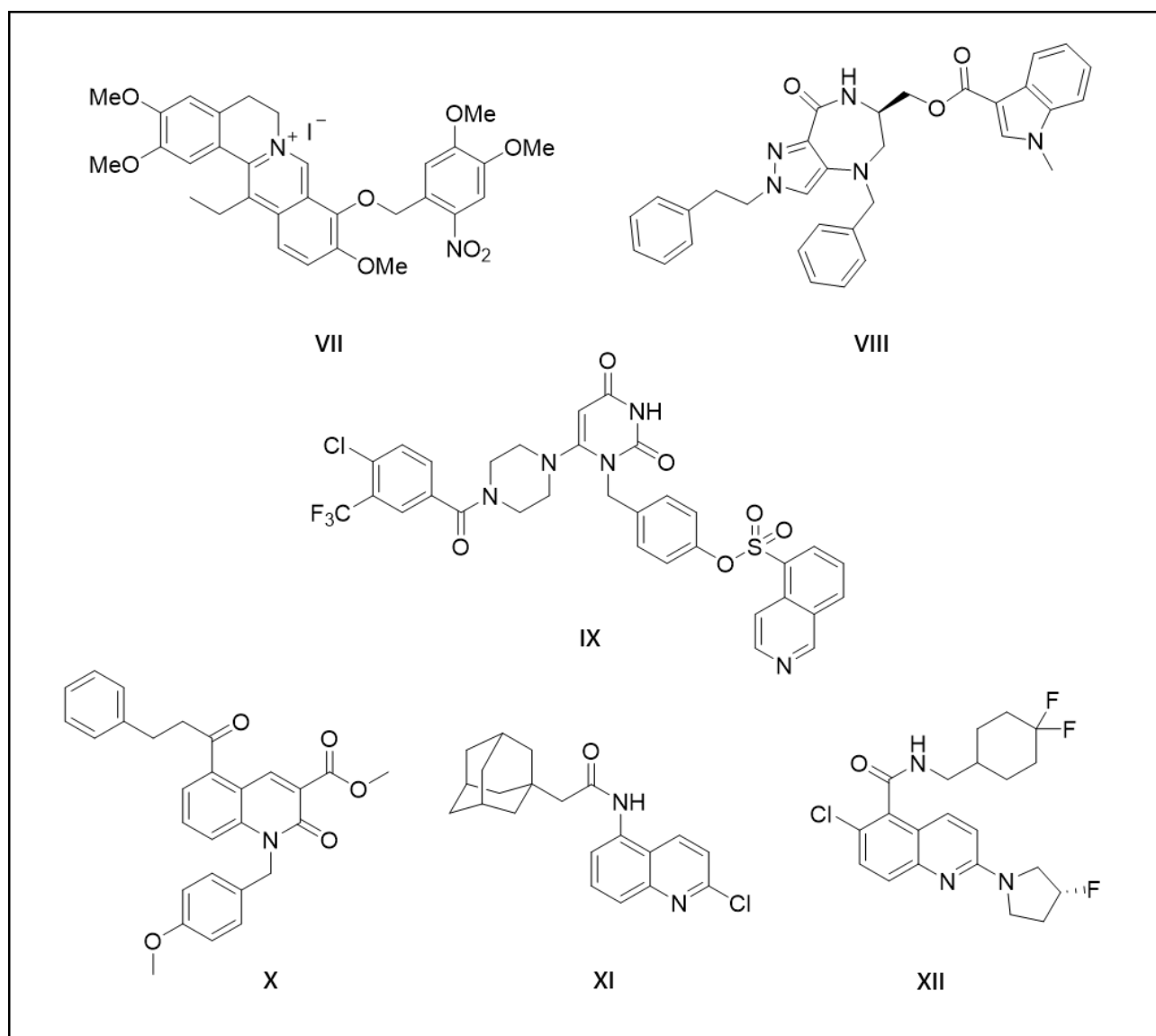


**Figure 18.** P2X7 antagonists disclosed and optimised by Kim's group. In the last row, the quinoline derivatives are shown, including compound XII, developed by the biopharmaceutical business EMD Serono.

Another approach conducted by GlaxoSmithKline was the design based on *N*-benzylacetamide. Different aryls and heterocycles were extensively probed for preparing new derivatives. The first hit, bearing an *N*-phenylpyrazole (XIII, R = Ph, X = F, Figure 19) presented poor *in vitro* stability. Attempts to improve blockade and PK profile focused mostly on replacing halogens, the amide spacer or the pyrazole ring. Indeed, the removal of the phenyl at the pyrazole (R = H, Figure 19) was essential for enhancing both properties, resulting in ligands XIV (R = H, X = F) (Chambers *et al.*, 2010) and XV (R = H, X = Cl) (Beswick *et al.*, 2010). Unfortunately, they also inhibited cytochrome P450 3A4 (CYP3A4), so the authors, guided by the information of other hit compounds, replaced the pyrazole ring, which

more metabolically-labile methyl groups, with cyclic pyroglutamic amides. Thus, CYP inhibition was avoided and P2X7 blockade improved, as in compound **XVI** (Figure 19) (Abdi *et al.*, 2010). Compound **XVI** was studied in animal models of pain but experimented a short half-life in some situations. The metabolically-labile positions present in pyroglutamic acid led to its replacement with other heterocycles, for instance the more stable imidazole, affording  $IC_{50}$ s around the nanomolar range. In addition, they presented low microsomal clearance. Among them, the unsubstituted imidazolone **XVII** stood out (Figure 19) (Abberley *et al.*, 2010).

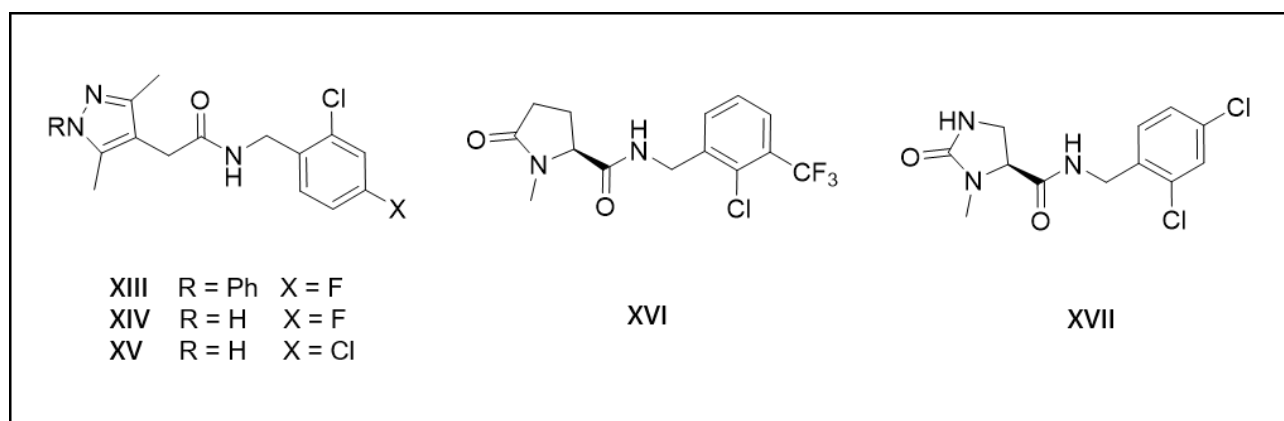


**Figure 19.** Pyroglutamic amide derivatives developed by GlaxoSmithKline as potential P2X7 antagonists.

An *o*-chlorobenzamide derivative bearing a 1,2,4-triazin-3,5-dione heterocycle showed moderate P2X7 inhibitory activity and too high *dog P* (**XVIII** – Figure 20). Theoretically, this property is compatible with high BBB permeability, but usually entails low solubility, a clear drawback for drug development. Therefore, the further chemical optimisation focused on improving the blocking activity while preparing compounds with a lower *dog P* (Duplantier *et al.*, 2011). Realizing that a huge increase of polarity at the amide compromised inhibitory activity, the long hydrophobic chain bound to the amide nitrogen was replaced by bulky alkyl, aryl or heteroaryl groups. In this work, the presence of 1-hydroxycycloheptylmethyl as substituent of the amide (**XIX** – Figure 20) lowered *dog P* to 2.9, and improved the potency to inhibit IL-1 $\beta$  release by 10-fold respect to compound **XVIII**. With this replacement in mind, *dog P* was further lowered by incorporating polar alkyl chains at the 1,2,4-triazin-3,5-dione core (**CE-224,535** – Figure 20). In addition, the potency to block IL-1 $\beta$  release was 59-fold higher than in **XIX** and, consequently, **CE-224,535** was assayed in clinical trials for

rheumatoid arthritis (Stock *et al.*, 2012). This compound was also the model followed by Kim's and coworkers for the development of their pyrimidin-2,4-diones (see above).

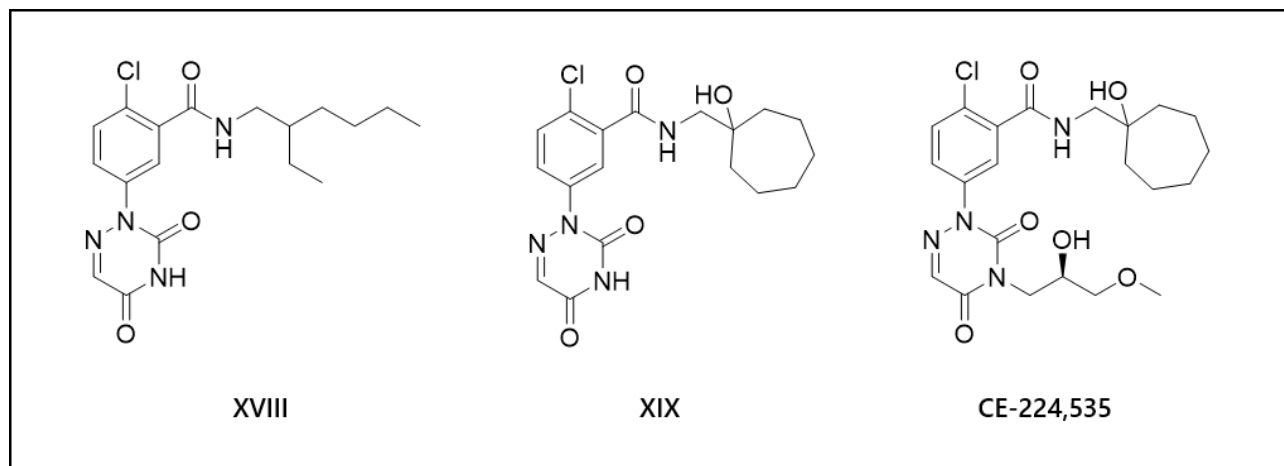


**Figure 20.** 1,2,4-triazin-3,5-dione P2X7 antagonists. CE-224,535 was tested in clinical trials for rheumatoid arthritis.

Abbott Laboratories disclosed a series of cyanoguanidines with high potency and good pharmacokinetic properties. **A-740003** (Figure 21) was the first one that stood out for its high potency to block P2X7 in the nanomolar range (Honore *et al.*, 2006). It was tested in animal models of neuropathic pain, attenuating tactile allodynia. However, further studies with its radiotracer revealed a scarce BBB permeability (Janssen *et al.*, 2014). Further modifications on this scaffold, *e.g.* retaining the isoquinoline-cyanoguanidine moiety, gave rise to cyanoguanidine-piperazine P2X7 antagonists with slight differences in activity than **A-740003** (Morytko *et al.*, 2008). Substitution of the piperazine core with a simpler (R)- $\alpha$ -methylbenzylamine resulted in **A-804598** (Figure 21), a ligand with an  $IC_{50}$  of around 10 nM in rat, mouse and human P2X7, evaluated in  $Ca^{2+}$  flux assays (Donnelly-Roberts *et al.*, 2009a). It also proved a certain stability in brain tissues at least after 1 h of oral administration (Able *et al.*, 2011). **A-740003** and **A-804598** have been both crystallised in the panda P2X7, showing that they bind in the allosteric binding pocket at the interface of two subunits' upper body (Karasawa and Kawate, 2016). Moreover, they are considered as the two P2X7 antagonists with the least differences in potency between species (Donnelly-Roberts *et al.*, 2009a).

Abbott Laboratories simultaneously developed a series of triazoles and tetrazoles bearing two differently-substituted benzenes (Carroll *et al.*, 2007; Florjancic *et al.*, 2008; Nelson *et al.*, 2006). This

wide medicinal chemistry program provided compound **A-438079** (Figure 21) as frequently used pharmacological tool. It was very appealing for its small molecular weight, good potency, and efficacy in reverting allodynia in the Chung model of neuropathic pain (Nelson *et al.*, 2006). Nevertheless, its short half-life (1 h) and low bioavailability after i.p. administration discouraged any clinical development (Guile *et al.*, 2009).

Kassiou's group has kept trusting in the adamantane cycle to get drug-like P2X7 ligands. Thus, they managed to improve the solubility of their ligands by including non-protic, highly polar moieties, such as the cyanoguanidine group, previously employed by Abbott Laboratories (O'Brien-Brown *et al.*, 2017). A large set of differentially linked adamantane-cyanoguanidine adducts was evaluated, where the 5-quinolyl derivative **XX** (Figure 21) showed the highest potency. However, its *log P* close to 5 dissuaded from further testing, and they deepened more in the more polar compound **XXI** (Figure 20), with improved PK properties, yet far from ideal. Moreover, Kassiou and co-workers took again AstraZeneca adamantanyl-*o*-chlorobenzamides (like compound **III** – Figure 17) to synthesise new derivatives defined by replacing either the *o*-chlorobenzamide group by heteroaromatic analogues, such as pyridines and diazines, or some adamantane hydrogens with fluorine atoms (Figure 21) (Wilkinson *et al.*, 2017). These chemical modifications were justified by the bioisosteric nature of fluorine respect hydrogen, which would presumably reduce lipophilicity and increase metabolic stability. However, although the experimentally obtained *log P* of the aza-analogues of **III** was slightly reduced, their blockade of hP2X7 was much worse, with compound **XXII** being the best of the series (Figure 21). With regard to the fluorinated derivatives of **III** (Figure 21), lipophilicity was substantially decreased and human P2X7 blocking activity remained in the same order of magnitude, meaning an improvement in the ligand-lipophilicity efficiency. This promising success prompted the evaluation of their PK characteristics, such as stability in liver microsomes, permeability, and CYP inhibition, as well as P-glycoprotein-addressed efflux. The trifluorinated **XXIII** (Figure 21) exhibited the highest metabolic stability, 6-fold higher than **III** and the lowest CYPs inhibition rate. In addition, **XXIII** featured the highest bioavailability together with a long brain half-life. All of these data position compound **XXIII** as a leading compound worth to be tested in further preclinical models of CNS disorders where P2X7 is implicated. More recently, Koufaki's and Nicke's groups have identified novel derivatives by replacing the adamantane and *o*-chlorobenzamide group of AstraZeneca compound **III** (Koufaki *et al.*, 2020). If the only advantageous modification on the benzamide moiety resulted to be the insertion of a nitrate ester (**XXIV** – Figure 21), the complete substitution of the adamantane

group with a nitrate ester-substituted arylcyclohexyl moiety showed good potency in the nanomolar range and may be considered as a novel scaffold for further optimisation. Curiously, the 1,4-diaryl-1,2,3-triazoles developed by the authors resemble the 1,5-diaryl-1,2,3-triazoles by Abbott Laboratories (Carroll *et al.*, 2007), without obtaining interesting potencies. This underlines that the 1,5-disubstitution is relevant for P2X7 inhibitory activity in this particular family of compounds.

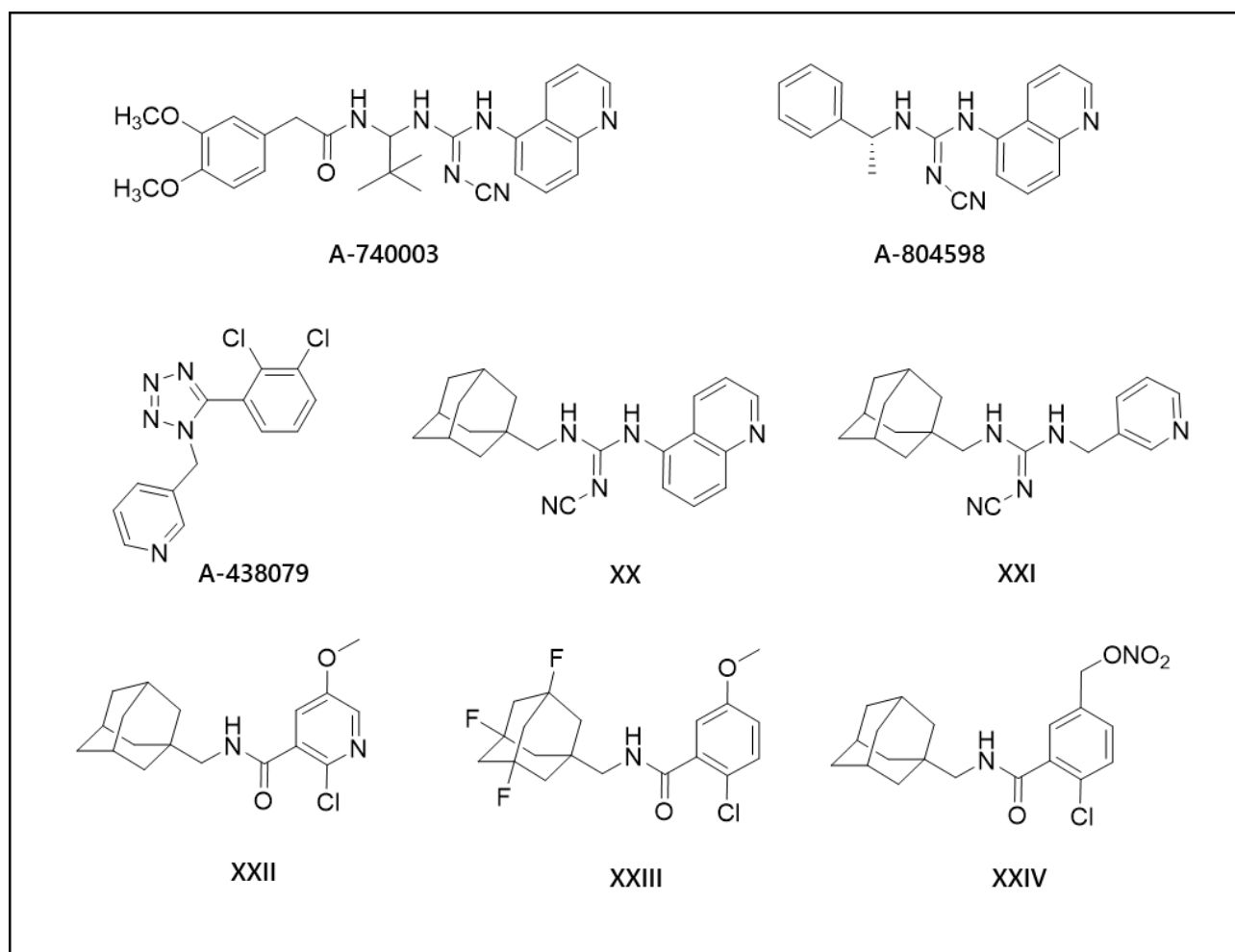


**Figure 21.** Tetrazole, cyanoguanidine, and adamantane derivatives developed by Abbott Laboratories, Kassiou's group, and Koufaki's laboratory.

A new series of heterocyclic derivatives linked to the *o*-chlorobenzamide moiety, which could be considered as a juxtaposition of **JNJ-42253432** (Letavic *et al.*, 2013) and compound **XXV** (Figure 22) (Chen *et al.*, 2010), was described by Janssen Pharmaceutica. Diverse alkylamines were probed at C2 of the quinoline core (Rech *et al.*, 2016). Their activity on the P2X7 receptor was scattered and

differences between human and mouse orthologues were found. The best compound was **XXVI**, bearing at C2 a 3-(*R*)-hydroxypyrrolidine (Figure 22), and showing good bioavailability and a significant, though time-dependent, reduction of IL-1 $\beta$  release in C57BL/6 mice. Moreover, another member of this class of ligands, **JNJ-47965567** (Figure 22), has been pharmacologically characterised and extensively used. In particular, it showed efficacy in reducing the sensitisation of amphetamine induced locomotion, although it did not exhibit robust results in models of neuropathic pain, or in the forced swim test as model of depression in rats (Bhattacharya *et al.*, 2013). **JNJ-47965567** is one of the antagonists crystallised in the giant panda P2X7 and its binding site resulted to be the same allosteric pocket as for the above mentioned ligands (Karasawa and Kawate, 2016). In parallel to the development of these last P2X7 ligands, authors have also studied the triazolopiperidine scaffold, linked to the *o*-chlorobenzamide moiety. The first trends prioritised to weigh the influence of aza-aromatic rings pending to the triazole, as exemplified by **XXVII** (X = H – Figure 22) (Savall *et al.*, 2015). Aza-aromatics helped to reduce both log P and CYP inhibition. Compound **XXVII** was selected as the lead to be optimised by fixing its pyrimidine heterocycle at N1 and replacing the 3-trifluoromethyl-2-chlorophenyl by other halogenated benzenes. However, no significant improvements were obtained in PK values, while potency diminished in some cases, and the cross activity between orthologues worsened globally. Preclinical studies showed that the incorporation of a fluorine atom (**XXVIII**, X = F – Figure 22) improved PK parameters such as bioavailability and solubility. Further studies aimed to evaluate the effect of an *R*-methylation at the piperidine C4 (Letavic *et al.*, 2017), with the idea of increasing microsomal metabolic stability and potency, in a manner similar to that one previously appreciated with the P2X7 antagonist **JNJ-54166060** (Figure 22). Actually, this compound also showed a nanomolar P2X7 blocking activity along with nice PK profile (Swanson *et al.*, 2016), but it was affected by an unaffordable CYP3A interaction. Using an *R*-methylated **XXVII** derivative at C4 as scaffold, single aza-aromatics were installed at N1 of the triazole nucleus, furnishing ligands with nanomolar-ranged potency, highlighting the 4-(*R*)-methyl derivative of **XXVIII** (**JNJ-54175446** – Figure 22); this compound lacked CYP inhibition and had elevated metabolic stability, high bioavailability, and low off-target pharmacology. Further pharmacological experiments revealed high tolerability, which led compound **JNJ-54175446** to be a candidate for clinical studies.



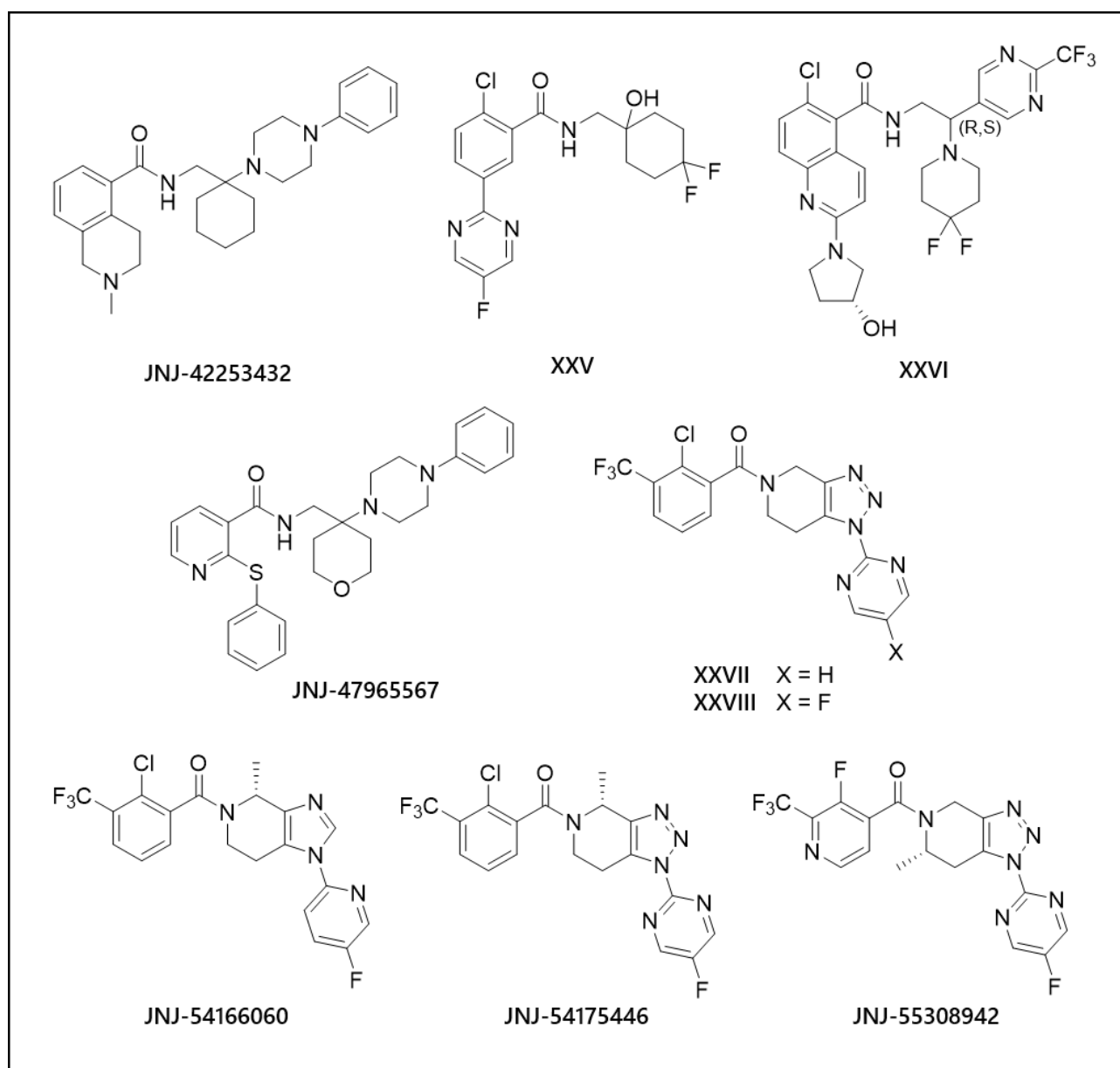


**Figure 22.** P2X7 antagonists developed by Janssen Pharmaceutica. JNJ-55308942 has completed 3 phase I clinical trials, while JNJ-54175446 has completed 7 of them, one of which in patients with major depressive disorders, and now it is in a phase II trial for the same indication.

By shuffling the methyl group from C4 to C6 with configuration inversion, a new family of triazolopiperidines was disclosed, also with different aromatic *N*-substitution at the triazole (Chrovian *et al.*, 2018). Their P2X7 activity was as good as for previous families, but featuring low solubility and poor stability. To solve these problems, benzamide was replaced by isonicotinamide, as shown in **JNJ-55308942** (Figure 22). Solubility and metabolic stability were indeed improved, but with a decrease in activity. The *para*-fluoro derivative was again the best of the family, standing out for its

increased plasma free fraction, high tolerability and cardiovascular safety. For these reasons, **JNJ-55308942** has been chosen as a second P2X7 antagonist to enter clinical trials for depression. The phase I ended in March 2018 and evaluated the safety of the compound in healthy participants. **JNJ-54175446** (Figure 22) was also tested in 2017 in healthy volunteers and patients affected by major depressive disorders (Recourt *et al.*, 2020). Currently, it has entered phase II clinical trial for the same indication, as stated in ClinicalTrials.gov database.

Currently, the efforts for the discovery and development of novel scaffold with P2X7 inhibitory activity do not give up. Martins' and Faria's groups disclosed 2-amino- or 2-hydroxyl-substituted 1,4-naphtoquinone derivatives as novel P2X7 blockers, with activity on the murine and human P2X7 orthologues and capable of reducing ATP-induced IL-1 $\beta$  release and paw edema *in vivo* (de Luna Martins *et al.*, 2020; Faria *et al.*, 2018). The most promising compounds are **XXIX**, **XXX**, and **XXXI** shown in Figure 23. The same authors discovered that aryl boronic acid derivatives (**XXXII** and **XXXIII** – Figure 23) can also inhibit P2X7, highlighting the importance of the polarity of this moiety in constituting hydrogen bonds Leu 97, Gln 98, and Ser 101 (Faria *et al.*, 2019). Moreover, they described other novel scaffolds represented by a thiodiazole core. The most promising one is compound **XXXIV** (Figure 23), although its high polarity ( $\log D = -3.7 \pm 0.2$ ) discourage its application for CNS diseases (Gonzaga *et al.*, 2019).

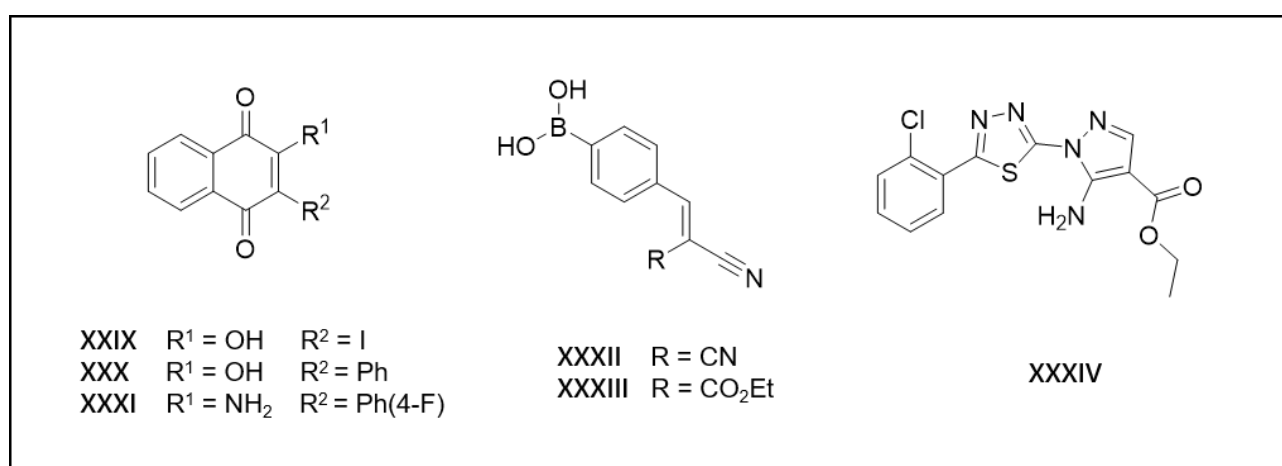


**Figure 23.** Novel scaffold recently disclosed as P2X7 antagonists: 1,4-naphtoquinones, aryl boronic acids, and thiodiazoles.

Finally, a new strategy has been recently proposed: the use of biologics, such as antibodies and nanobodies to target P2X7. Several biologics have been already developed (Table 2), but the studies on their efficacy and their therapeutic application are still very few (Koch-Nolte *et al.*, 2019).

**Table 2.** Antibodies and nanobodies that modulate the function of P2X7\*. Adapted from Koch-Nolte *et al.*, 2019.

mAb/Nb	Effect on P2X7 function	Effect on the inflammation model	References
<b>mAb L4</b>	Inhibits h- and rP2X7 gating	Inhibits ATP-induced release of IL-1 $\beta$	(Chessell <i>et al.</i> , 1998)
<b>mAb Hano43</b>	Inhibits ADP-ribosylation of mP2X7	-	(Jong <i>et al.</i> , 2016)
<b>mAb Hano44</b>	Potentiates mP2X7 gating	-	
<b>mAb 1F11</b>	Inhibits mP2X7 gating	Ameliorates exp. colitis	(Kurashima <i>et al.</i> , 2012)
<b>Nb Dano1</b>	Inhibits hP2X7 gating	Inhibits ATP-induced release of IL-1 $\beta$	(Danquah <i>et al.</i> , 2016)
<b>Nb 13A7</b>	Inhibits mP2X7 gating	Ameliorates exp. glomerulonephritis and contact dermatitis	
<b>Nb 14D5</b>	Potentiates mP2X7 gating	Aggravates exp. glomerulonephritis	
<b>Nb s+16</b>	Inhibits ADP-ribosylation of mP2X7	-	(Rissiek <i>et al.</i> , 2018)

\* *mAb*, monoclonal antibody; *Nb*, nanobody; *h*, human; *r*, rat; *m*, mouse; *exp.*, experimental.

To sum up, several P2X7 antagonists have been developed through the years, exploiting different scaffolds and molecular structures. Nevertheless, only few ligands succeeded in entering clinical trials and the majority of them in peripheral disorders (Eser *et al.*, 2015; Keystone *et al.*, 2012; Stock *et al.*, 2012). This is surely due to poor knowledge of hP2X7 structure, above all the lack of its crystal resolution, but also to the need of finding the proper drug-like properties to target the CNS, *i.e.* sufficient lipophilicity, water solubility and brain tissue half-life. That is why *BigPharma* pays more attention to assessing the receptor occupancy of the newly developed ligands, as well as their efficacy in the brain, by performing well established *ex vivo* autoradiography assays or *in vivo* microdialysis tests in animals. Table 3 summarises the pharmacodynamics, PK, and drug-likeness of a selection of P2X7 antagonists.

**Table 3.** Principal pharmacodynamic and pharmacokinetic characteristics of selected P2X7 antagonists. Adapted from Calzaferri *et al.*, 2020.

Antagonist name	Pharmacodynamic activity	Pharmacokinetic properties	Clinical trials
oATP	Irreversible	Only pharmacological tool	-
PPADS	P2X selective	Non-BBB permeable	-
BBG	P2X selective	BBB permeable	-
Suramin	No P2 selective Antitrypanosomal drug GABA <sub>A</sub> antagonist (Luo <i>et al.</i> , 2018)	Non-BBB, but circumventricular organs permeable Long half-life (around 50 days)	-
KN-62	mP2X7 selective CaM kinase II inhibitor	Only pharmacological tool	-
AZD9056	hP2X7 IC <sub>50</sub> = 12 nM	Excellent PK with daily dose (Phase 1)	Phase 2 – Rheumatoid arthritis Phase 2 – Crohn’s disease
AZ11645373	IC <sub>50</sub> = 20 nM	-	-
Pyrimidine-2,4-diones (IX)	IC <sub>50</sub> = 27 nM	High metabolic stability Low cytotoxicity and cardiac toxicity	-
Pyroglutamic derivative XVI	IC <sub>50</sub> = 3.2 nM	Metabolic stability Short half-life (1.5 h)	-
CE-224,535	IC <sub>50</sub> = 4 nM	clog P = 2.9	Phase 2 – Osteoarthritis Phase 3 – Rheumatoid arthritis
A-740003	h(r)P2X7 IC <sub>50</sub> = 40 (18) nM	Scarce BBB permeability	-
A-804598	h/r/mP2X7 IC <sub>50</sub> = 10 nM	Short brain half-life (at least 1 h)	-
A-438079	hP2X7 IC <sub>50</sub> = 100 nM	Short half-life (1 h) Low bioavailability (i.p.)	-
Trifluoroadamantane- <i>o</i> -chlorobenzamide (XXIV)	IC <sub>50</sub> = 33.9 nM	High metabolic stability High bioavailability Short brain half-life (around 1 h)	-
JNJ-47965567	hP2X7 IC <sub>50</sub> = 5.3 nM	Short brain half-life	-
JNJ-54175446	hP2X7 IC <sub>50</sub> = 3 nM	High metabolic stability High bioavailability No CYP3A4 inhibition	Phase 1 – Major depressive disorder
JNJ-55308942	hP2X7 IC <sub>50</sub> = 10 nM	High water solubility Long brain half-life (20 h in dogs)	Phase 1 – Healthy participants

Research hypothesis  
and objectives

## 4. Research hypothesis and objectives

Many potent antagonists have been developed so far, but only few participated in clinical trials, and only JNJ 54175446 has passed to phase 2 for a CNS disease, *i.e.* depression (see chapter 3.4). Hence, new tools that explore different chemical space, combining good drug-like properties and characteristics that favour permeability to the CNS, are needed. Hence, we proposed to design and synthesise new P2X7 antagonists, based on the review of scientific literature, in order to find out the molecular patterns essential for receptor inhibition, among the plethora of structures previously described. As discussed in chapter 5.1, **our hypothesis is that compounds that bear a purine core linked to an *ortho*-haloarene through a small linker should inhibit P2X7 and modulate neuroinflammation in models of CNS disorders (Figure 24). We also suggest that these compounds may have favourable physicochemical properties to be developed as potential therapeutic drugs, and to cross the BBB to act in the CNS.**

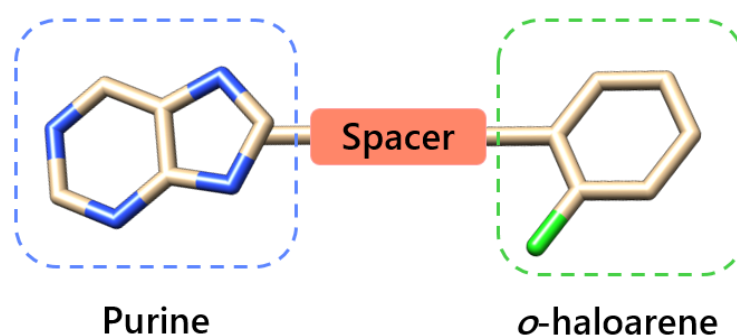


**Figure 24.** Model of our novel P2X7 antagonists, based on the review of the ligands already described in the literature (see chapter 5.1).

To verify this hypothesis, we proposed to accomplish the following objectives:

1. design, synthesis, and chemical characterisation of a series of novel non-nucleotide purine derivatives with favourable physicochemical properties to cross the BBB and reach the CNS;
2. pharmacological *in vitro* characterisation of the synthesised compounds as P2X7 antagonists;
3. early prediction of their pharmacokinetic profile to target the CNS, by the assessment of their permeability through lipid membranes and the affinity for the efflux pump P-glycoprotein;
4. docking study to predict the possible binding site of the best P2X7 antagonists of the series;
5. introduce our most promising P2X7 antagonist for its further preclinical assessment.

Results and discussion

## 5. Results and discussion

### 5.1. Design of novel non-nucleotide purine derivatives as P2X7 antagonists

An extensive review of the previously described P2X7 antagonists (see chapter 3.4) led us to the establishment of a generic structure-activity model that facilitated the design of the novel P2X7 antagonists. In fact, the majority of the ligands share a variable heterocyclic aromatic scaffold, or the corresponding aza-aliphatic cycle linked to a lipophilic group by a variable spacer (Figure 25). The most extended heterocycles have been quinolines and isoquinolines (Kwak *et al.*, 2018), like in the case of KN-62 (Figure 16), A-740003 or A-804598 (Figure 21). Many other heterocyclic scaffolds have been explored, as amply reviewed in chapter 3.4: tetrazoles, pyrazoles, tetrahydrotriazolopyridines, triazoles, triazinones, and thiadiazoles, among others.

Adamantane is a well-studied lipophilic moiety used in previous medicinal chemistry projects aiming for P2X7 antagonists (Baxter *et al.*, 2003; Furber *et al.*, 2007; O'Brien-Brown *et al.*, 2017; Wilkinson *et al.*, 2017). A plethora of attempts to replace this cycloalkane for other simpler and water-soluble moieties (Chen *et al.*, 2010; Koufaki *et al.*, 2020) or alternative polycycles (Barniol-Xicota *et al.*, 2017) have been performed because of its high lipophilicity, which would favour its distribution to the CNS, but compromises water solubility and most of the drug-likeness properties. Beside adamantane and its derivatives, other lipophilic moieties have been recruited for the design of P2X7 antagonists, such as differently-substituted benzenes (Figure 19, 22-23, chapter 3.4) (Abberley *et al.*, 2010; Carroll *et al.*, 2007; Gonzaga *et al.*, 2019; Homerin *et al.*, 2017; Morytko *et al.*, 2008).

The spacers that link the heterocyclic scaffold to the lipophilic moiety are of different nature and complexity, due to the extreme variability of the structures of so far-discovered P2X7 antagonists. We principally focused on a recurrent amide link, as firstly presented in Suramin and KN-62 (Figure 16, chapter 3.4), and later on in most of the chemical entities developed, from the AstraZeneca adamantane-*o*-chlorobenzamides (Figure 17 – chapter 3.4) (Furber *et al.*, 2007), to the subsequent quinoline derivatives (Figure 18 – chapter 3.4) (Xiao *et al.*, 2019), the pyrazole and pyroglutamic acid series (Figure 19 – chapter 3.4) (Abberley *et al.*, 2010; Abdi *et al.*, 2010; Chambers *et al.*, 2010) and the newest tetrahydrotriazolopyridine amides (Figure 22 – chapter 3.4) (Chrovian *et al.*, 2018; Letavic *et al.*, 2017; Savall *et al.*, 2015).

Considering all of these antecedents, we decided to design small molecules bearing a purine as heterocycle (Figure 25), because of its potential pharmacodynamic and pharmacokinetic properties.



The rationale behind the use of purine is acquiring affinity to P2X7, being the adenine nucleotide its endogenous ligand. Also, it has some physicochemical properties, like three hydrogen bond acceptors and good lipophilicity, that could benefit the drug-likeness of the final compounds, and their ability to act in the CNS through BBB permeation. Additionally, a purine-based compound could take advantage of the active purine and pyrimidine nucleoside transporters expressed in the BBB to get into the CNS, in particular the equilibrative nucleoside transporter 1 (ENT1) (Murakami *et al.*, 2005). This can be considered a possible strategy, such as demonstrated with Tecadenoson, an A<sub>1</sub> receptor agonist that entered clinical trials (Lepist *et al.*, 2013). Moreover, the purine scaffold has never been used for the synthesis of P2X7 antagonists, unless in nucleotide derivatives, which have been especially developed as ecto-5'-nucleotidase, P2Y or P1 ligands (Dal Ben *et al.*, 2011; Junker *et al.*, 2019; Tosh *et al.*, 2020), or as antivirals (Yates and Seley-Radtke, 2019) and anticancer drugs (Valdés *et al.*, 2018). The only well-known P2X7-inhibiting nucleotide derivative is oATP (Murgia *et al.*, 1993).

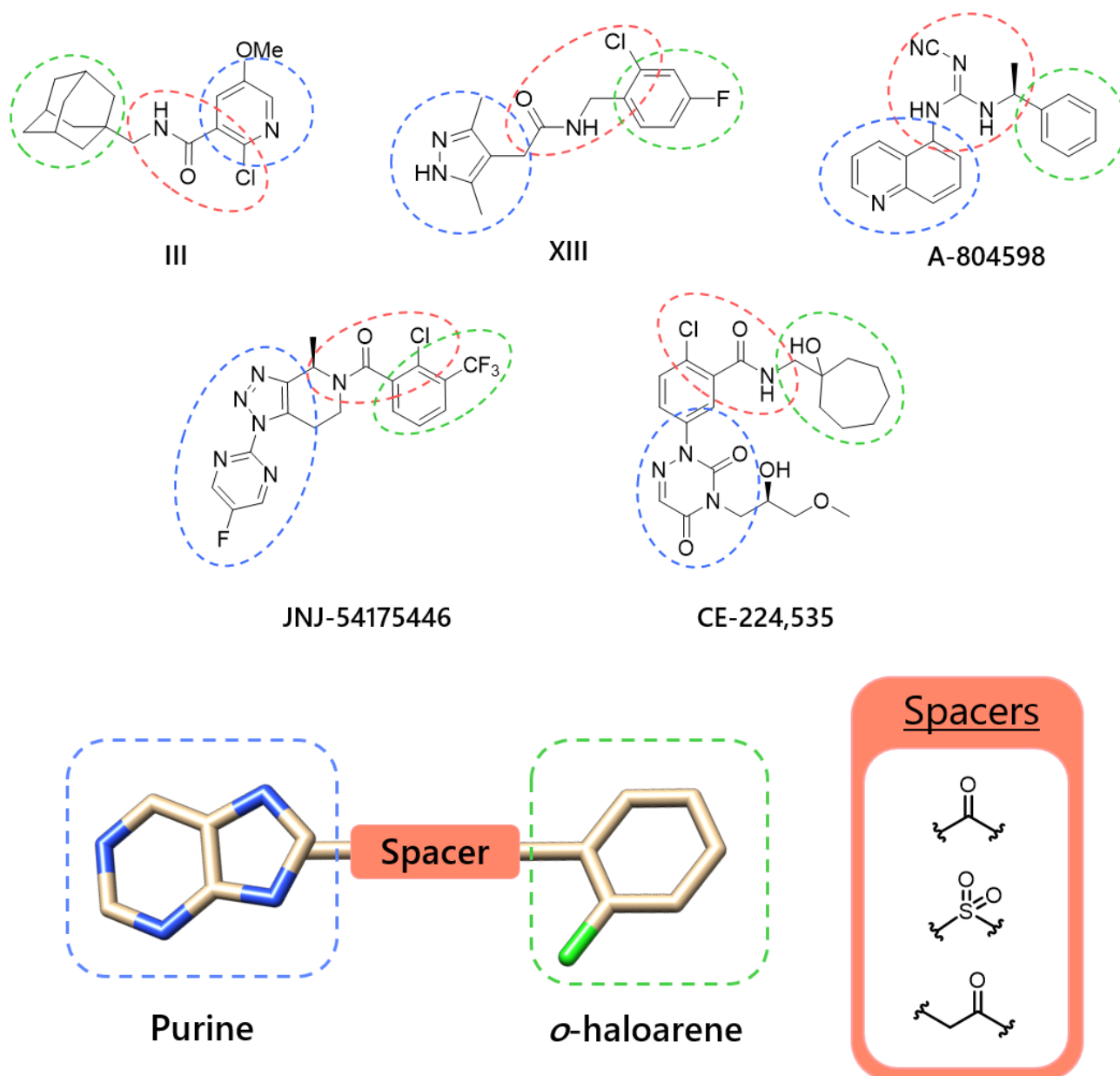
Regarding the spacer and the lipophilic scaffold, we particularly focused on the persistent *o*-substituted arylamide moiety, which has been maintained during compound optimisation of many series of molecules (Figure 25). In fact, we find an *o*-chlorobenzamide in AstraZeneca adamantane derivatives (Figure 17 – chapter 3.4) (Furber *et al.*, 2007), Pfizer triazindiones analogues (Figure 20 – chapter 3.4) (Duplantier *et al.*, 2011), Kim pyrimidinediones (Figure 18 – chapter 3.4) (Park *et al.*, 2015), and the latest tetrahydrotriazolopyrimidines by Janssen Pharmaceutica (Figure 22 – chapter 3.4) (Chrovian *et al.*, 2018; Letavic *et al.*, 2017). We accepted to include bioisosters of the *o*-substituted arylamide in our design, as we noticed that superior homologues of this moiety retained the P2X7 inhibitory activity, such as in GlaxoSmithKline's derivatives (Figure 19 – chapter 3.4), as well as the replacement with the cyanoguanidine group (Figure 21 – chapter 3.4), the carbohydrazide moiety (Barniol-Xicota *et al.*, 2017), and the tetrazole (A-438079 – Figure 21 – chapter 3.4)

The first set of compounds designed is characterised by the connection of the purine and halobenzoyl moiety with an amide group (Figure 25 and Table 4). This is the simplest and closest design according to our hypothesis. Commercially available and easily prepared scaffolds were taken into account to focus the efforts on synthesising as many diversely substituted purine analogues as possible. Additionally, we paid a careful attention to the physicochemical properties of all the potential final derivatives. Indeed, we followed the Lipinski's rules of five to obtain drug-like compounds (Bickerton *et al.*, 2012; Lipinski *et al.*, 2001), as well as the experience from our group in developing BBB-penetrant small molecules that act in the CNS (Lajarín-Cuesta *et al.*, 2018). We established then to design purine derivatives with the following characteristics:

MW [160-450]	N+O $\leq$ 5	ClogP [2-5]
PSA $\leq$ 90	NH+OH < 3	ClogD pH= 7.4 [0,4]

where MW is the molecular weight, thus the higher MW, the more difficult the passage through the BBB; N+O and NH+OH are the sum of the hydrogen bonds acceptors (HB-A) and donors (HB-D), respectively, which are essential to determine the polarity and the potential interaction with water, and therefore their solubility and their tendency to stay in extracellular or blood compartments; PSA is the polar surface area, an indicator of the electronic distribution in a molecule, and so of its polarity;  $\log P$  and  $\log D$  are the logarithms of the predicted partition and distribution coefficients, respectively. Noteworthy, the acidic constant of a molecule ( $K_a$ ) is also an important factor to evaluate whether a compound ionise in water. In fact, a charged molecule is not likely to cross the BBB. However, we designed non-ionisable compounds at physiological conditions, so we did not include  $K_a$  to the above-mentioned parameters.

The selected scaffolds and the final compounds cover the exploration of different positions on the purine ring, aiming at structure-activity relationships as soon as their pharmacological characterisation was completed. Substituents with different spatial hindrance, polarity and electronic effects on the purine were selected, particularly at position 2 and 6, including halogens (chloride, iodide and fluoride), amines, methoxides, and phenyls. Modifications at position 8 were attempted but needed further optimisation of synthetic conditions. The xanthine core was also included in our small library to explore as much chemical space as possible. Moreover, methylxanthines, like caffeine and theophylline, are known to cross the BBB through the adenine transporter although they exhibit poor lipophilic profile (Di *et al.*, 2003; McCall *et al.*, 1982). Thus, we speculated that xanthine derivatives could easily reach the CNS by using the same transporter.

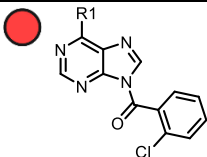
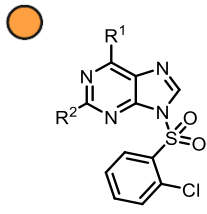
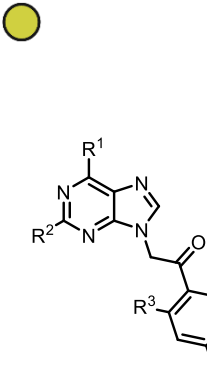
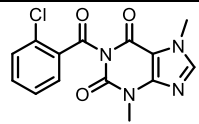
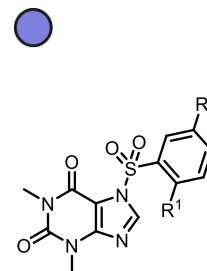


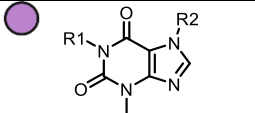
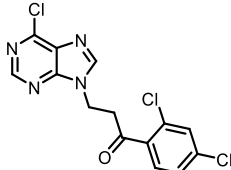
**Figure 25.** Structures of previously described P2X7 antagonists, marking the different moieties. The heterocyclic moiety (blue), the amide spacer or its isosters (red), and the lipophilic group (green) are highlighted. Below, our proposal for the design of novel P2X7 antagonists using the purine scaffold as heterocycle, three different spacers, and a o-haloarene. **III:** adamantane derivative described by AstraZeneca (Baxter *et al.*, 2003). **XIII:** pyrazole derivative described by GlaxoSmithKline (Chambers *et al.*, 2010).

First novel benzoyl-purine derivatives (Scheme 2, chapter 5.2.1) showed chemical instability in both acidic and basic conditions. Realizing that such stability is essential for drug R&D, we decided to replace the sensitive amide spacer by more stable and well-known bioisosteres (Patani and LaVoie, 1996). Hence, we designed a series of 2-chlorophenylsulfonamides using the same scaffolds chosen for the benzoyl-purine family. Simultaneously, we designed another series of superior homologues of benzoyl-purines by inserting a methylene between the free purine nitrogen at N7 or N9 position and the carbonyl group, obtaining the 2-puriny-1-arylethanone family. Further modifications were attempted to improve the pharmacological activity of the first set of compounds evaluated. Thus, halogens and other functional groups were moved, removed or inserted at either the phenyl ring or the purine core. In order to get knowledge of the P2X7 pharmacophore, we found interesting to design the superior homologue of the most potent compound of the arylethanone family (**9** – Scheme 4, chapter 5.2.3), resulting in the arylpropanone **38** (Scheme 7, chapter 5.2.3). Additionally, to explore further chemical space on the purine scaffold and evaluate whether a stable amide could maintain the activity of compound **9**, we designed an *N*1-(2-chlorobenzyl)purine derivative (**40** – Scheme 8, chapter 5.2.3) that incorporates the methylene present in arylethanones and a stable amide-like group into the purine core.

Table 4 shows the predicted physicochemical properties of the computer-aided designed purine derivatives proposed in this PhD work. Some compounds break the established limitations in one or two parameters. Nevertheless, those ligands were prepared to determine structure-activity relationships of our new compounds on P2X7. In particular, the arylsulfonyltheophylline derivatives were synthesised because 1) they offered a good option to avoid the stability issues of (2-chlorobenzoyl)purines; 2) compound **27** showed positive outcomes in the preliminary pharmacological data carried out (see chapter 5.3). Additionally, we thought that the theophylline scaffold could overcome the BBB-permeability issues, despite their low *clog P* of its derivatives, as occurs for caffeine (see chapter 5.4).

**Table 4.** Physicochemical properties for drug-likeness and BBB permeability of our novel P2X7 antagonists. Compounds are divided into the different families described next in chapter 5.2: (2-chlorobenzoyl)purines (**red**), (2-chlorosulfonyl)purines (**orange**), 1-aryl-2-purinyloethanones (**yellow**), (2-chlorobenzoyl)theobromine (**green**), arylsulfonyltheophyllines (**blue**), 1-(2,4-dichlorophenyl)-2-xanthinyl ethanones (**lilac**), other derivatives (**pink**). In red are highlighted the values that do not respect the ranges established in our hypothesis, as explained in this chapter.<sup>a</sup>

		R <sup>1</sup>	R <sup>2</sup>	R <sup>3</sup>	R <sup>4</sup>	MW	N+O	NH+OH	clogP <sup>b</sup>	PSA <sup>d</sup>
1		Cl	-	-	-	293.11	4	0	2.31	60.67
3		CH <sub>3</sub> O	-	-	-	288.69	5	0	<b>1.92</b>	60.67
4		Cl	H	-	-	329.16	5	0	2.06	77.74
5		Cl	Cl	-	-	363.60	5	0	2.97	86.12
6		CH <sub>3</sub> NH	Cl	-	-	358.20	<b>6</b>	1	2.21	<b>98.15</b>
7		CH <sub>3</sub> O	H	-	-	324.74	<b>6</b>	0	<b>1.67</b>	<b>95.35</b>
8		Cl	NH <sub>2</sub>	-	-	344.17	<b>6</b>	2	<b>1.91</b>	<b>112.14</b>
9		Cl	H	Cl	Cl	341.58	4	0	2.59	60.67
10		Cl	Cl	Cl	Cl	376.02	4	0	4.10	60.67
11		CH <sub>3</sub> NH	Cl	Cl	Cl	370.62	5	1	3.34	72.70
12		Cl	NH <sub>2</sub>	Cl	Cl	356.59	5	2	3.04	86.69
16		Ph	H	Cl	Cl	383.23	4	0	4.40	60.67
17		CH <sub>3</sub> O	H	Cl	Cl	337.16	5	0	2.80	69.90
18		Cl	H	H	Cl	307.13	4	0	2.13	60.67
19		Cl	H	H	F	290.68	4	0	2.13	60.67
21		I	H	Cl	Cl	433.03	4	0	3.33	60.67
23		I	Cl	Cl	Cl	<b>467.47</b>	4	0	4.24	60.67
25		Cl	F	Cl	Cl	359.57	4	0	3.81	60.67
26							318.72	4	0	<b>1.68</b>
27		Cl	H	H	-	354.77	5	0	<b>0.72</b>	<b>100.96</b>
28		Cl	Cl	H	-	389.21	5	0	<b>1.33</b>	<b>100.96</b>
29		Cl	F	H	-	372.76	5	0	<b>0.87</b>	<b>100.96</b>
30		Cl	CF <sub>3</sub>	H	-	422.76	5	0	<b>1.60</b>	<b>100.96</b>
31		Cl	H	Cl	-	389.21	5	0	<b>1.33</b>	<b>100.96</b>
32		F	F	H	-	356.30	5	0	<b>0.41</b>	<b>100.96</b>
33		CH <sub>3</sub>	F	H	-	352.34	5	0	<b>0.78</b>	<b>100.96</b>
34		H	H	F	-	338.31	5	0	<b>0.26</b>	<b>100.96</b>

35		CH <sub>3</sub>	R <sup>c</sup>	-	-	367.19	4	0	1.86	75.51
36		R <sup>c</sup>	CH <sub>3</sub>	-	-	367.19	4	0	1.89	75.51
38						355.60	4	0	3.43	60.67
40						309.15	3	0	2.91	50.49

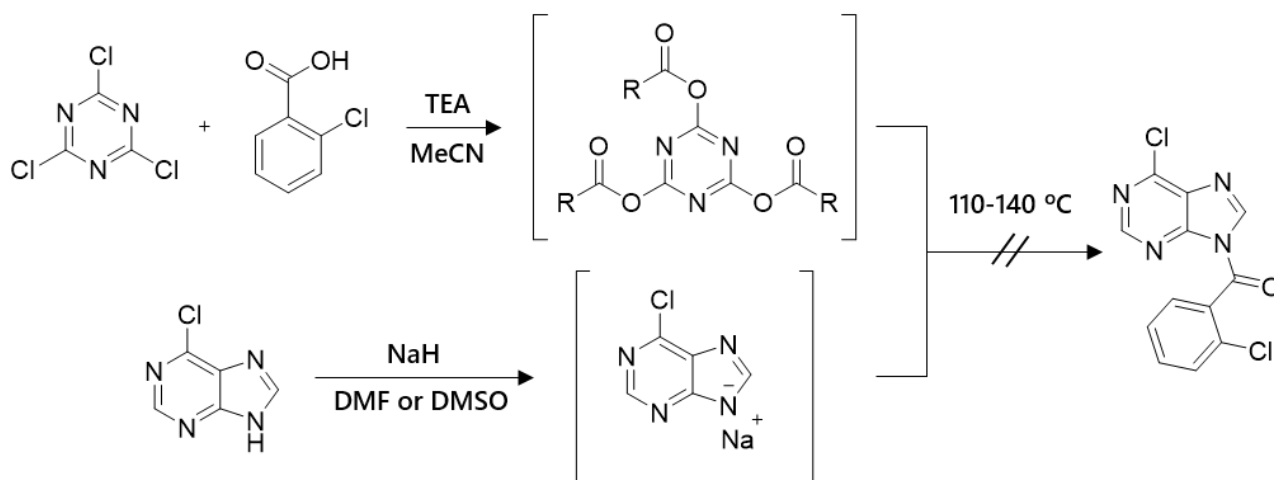
<sup>a</sup>acid constant (K<sub>a</sub>) is not included in this series of compounds, as protonation predictions suggested that they all cannot ionise at physiological conditions; <sup>b</sup>dog D [pH = 7.4] is not included because this value for these compounds is the same to dog P, as the compounds are not affected by pH at physiological conditions; <sup>c</sup>R is 2,4-dichlorobenzoylmethyl; <sup>d</sup>PSA, polar surface area.

## 5.2. Synthesis and structural characterisation of the non-nucleotide purine derivatives

### 5.2.1. 9-(2-chlorobenzoyl)purines **1** and **3**

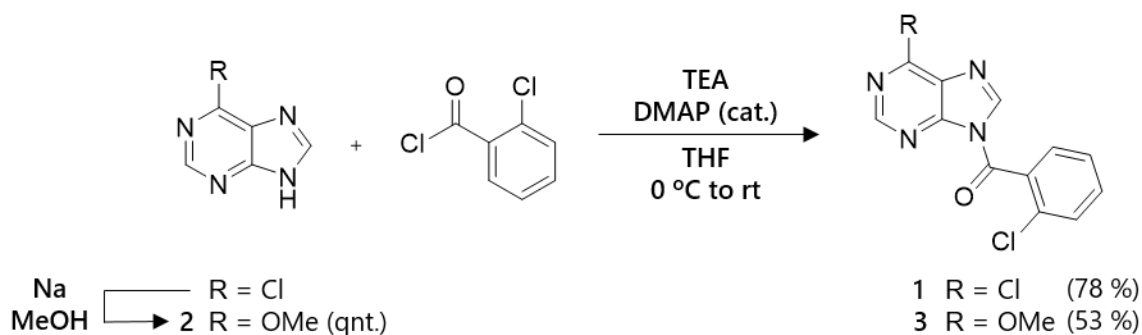
For the synthesis of the first benzoyl-purine derivatives, we resorted to the regioselective one-pot *N*-acylation of 6-chloropurine *via* 2-chlorobenzoic acid and cyanuric chloride (TCT, Scheme 1), as described by Soltani Rad and co-workers (Soltani Rad *et al.*, 2014), aware of the theoretical purine acylation at both positions N7 and N9. As shown in Scheme 1, this method provides the carboxylate-cyanuric ester intermediate that suffers the nucleophilic aromatic substitution (S<sub>N</sub>Ar) of previously NaH-deprotonated purine or pyrimidine derivatives at high temperature (110-140 °C). The use of TCT would have guaranteed the regioselective acylation at N9 (Soltani Rad *et al.*, 2014). This procedure was tested in a mixture of dimethylformamide (DMF) and acetonitrile (MeCN), as well as in dimethylsulfoxide (DMSO) and MeCN, at different temperatures (70, 110 and 125 °C) or internal pressures, without success. Analysis of the nuclear magnetic resonance (NMR) spectra of the purified reaction crude revealed that reaction did not work, only giving rise to a mixture of mono-, di- and tri-substituted adducts.

**Scheme 1.** Synthesis of *N*-(2-chlorobenzoyl)purine using cyanuric chloride as reactive. TEA, triethylamine.



We figured that 2-chlorobenzoic acid was too electron-deficient to complete the ester adduct formation. Hence, we proved the purine *N*-acylation *via* nucleophilic addition over benzoyl chloride. The election of 6-chloropurine as starting material is explained by the steric effect exerted by the chlorine that would hinder any electrophilic addition over N7, resulting in a regiochemical preference for the acylation at N9 (Ding *et al.*, 2002). We assayed this reaction at different conditions, following the protocols described by Ried and colleagues (triethylamine (TEA), DMF, rt, 18 h) (Ried *et al.*, 1989), Venkateswara Rao and co-workers (TEA, dichloromethane (DCM), 0 °C to rt, 10 h) (Venkateswara Rao *et al.*, 2013), and Changunda and colleagues (pyridine (Py), MeCN, 0 °C to rt, 5 h) (Changunda *et al.*, 2017) with no success. Nevertheless, we detected the final product in the crude, which was presumably sensitive to the weak acidic environment present in the silica gel-based column chromatographic purification. Chromatography in aluminium oxide-supported columns did not solve the problem. At last, we obtained the first final product (6-chloro-9*H*-purin-9-yl)(2-chlorophenyl)methanone (**1** – Scheme 2) using TEA and catalytic amounts of 4-dimethylaminopyridine (DMAP) as base in THF at 0 °C, following the procedure described by He (He, 2017). The crude obtained in these conditions was nicely purified by extraction in organic solvent and trituration in hexane, isolating the product **1** with a 78 % yield. Aiming at generating an analogue with a methoxy group at C6, a  $S_NAr$  reaction was promoted with Na in MeOH over the 6-chloropurine, yielding quantitatively 6-methoxypurine (**2** – Scheme 2). Following the reaction optimised for compound **1**, 6-methoxypurine gave (2-chlorophenyl)(6-methoxy-9*H*-purin-9-yl)methanone (**3** – Scheme 2) in medium yield.

Scheme 2. Synthesis of *N*-(2-chlorobenzoyl)purines *via* acylation.

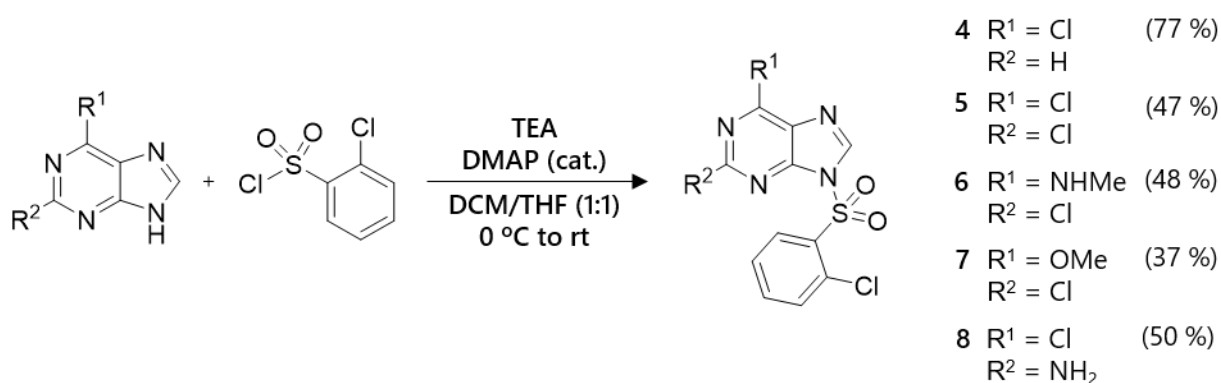


Overall, we encountered similar issues of crude purification when other starting materials were probed. Because of the high instability of this series of purine derivatives, we decided to focus our efforts on the synthesis of their more stable bioisosteres, as mentioned in chapter 5.1.

### 5.2.2. 9-(2-chlorophenyl)sulfonyl purines 4-8

To achieve the synthesis of the arylsulfonyl purine series, we initially followed the procedure described by Chen and co-workers (Chen *et al.*, 2011). The 6-chloropurine was deprotonated by NaH in dry THF, after which 2-chlorosulfonyl chloride was added dropwise at 0 °C. The 6-chloro-9-[(2-chlorophenyl)sulfonyl]-9*H*-purine (**4** – Scheme 3) was obtained after 2 h of stirring at rt with a final yield of 38 %. The same reaction using different purine derivatives still resulted in low yields. These difficulties were solved through the use of the TEA/DMAP basic catalytic system (Ananthan *et al.*, 2017). Chemical yields improved and the reaction was compatible with the presence of other nucleophile centres, as evidenced for compounds **6** and **8** (Scheme 3).

Scheme 3. Synthesis of 9-[(2-chlorophenyl)sulfonyl]-9*H*-purines *via* sulfonylation using the TEA/DMAP system.

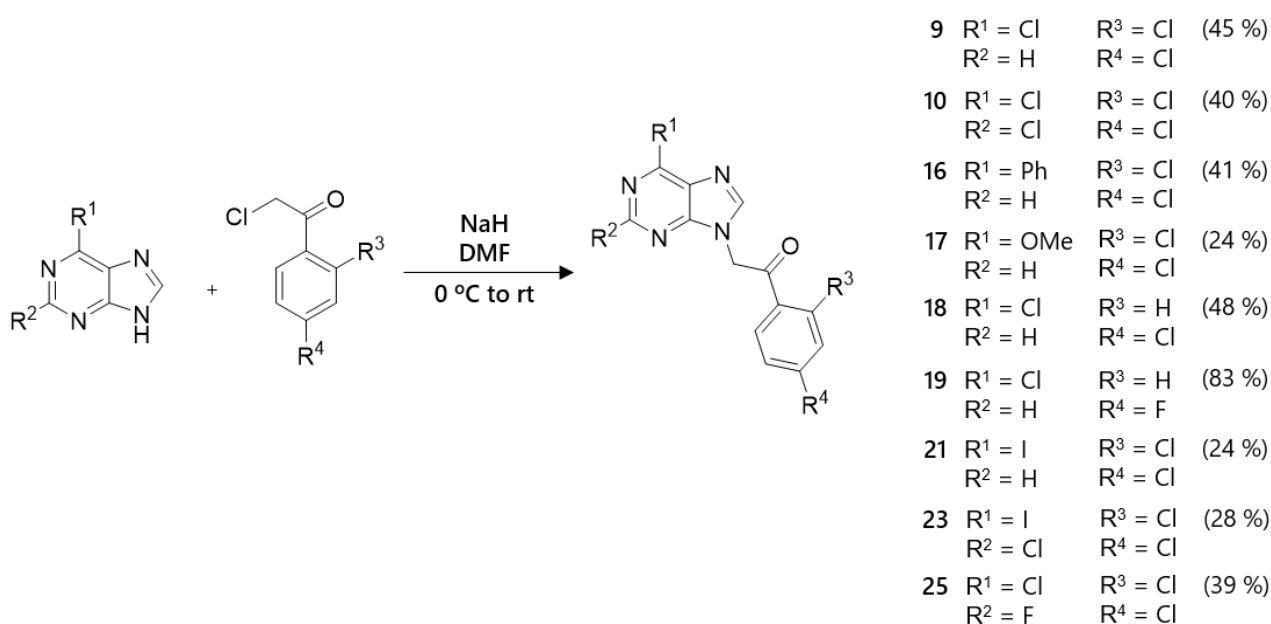




### 5.2.3. 1-Aryl-2-purinyloethanones **9-12, 16-19, 21, 23, 25, 38, 40**

For the synthesis of these derivatives, we chose to incorporate the 2,4-dichlorophenyl group as lipophilic group, being it the easiest commercially available reagent to procure (2,2',4'-trichloroacetophenone). First attempts to furnish purinyloethanone derivatives involved the nucleophilic substitution of NaH-assisted deprotonated purines over a 2-chloroacetophenone derivative in DMF and smooth conditions, according to the protocol reported by Bendels and co-workers (Bendels *et al.*, 2014), thus obtaining 2-(6-chloro-9*H*-purin-9-yl)-1-(2,4-dichlorophenyl)ethan-1-one (**9**) and 2-(2,6-dichloro-9*H*-purin-9-yl)-1-(2,4-dichlorophenyl)ethan-1-one (**10**) in low yields, presumably due to purification issues (Scheme 4).

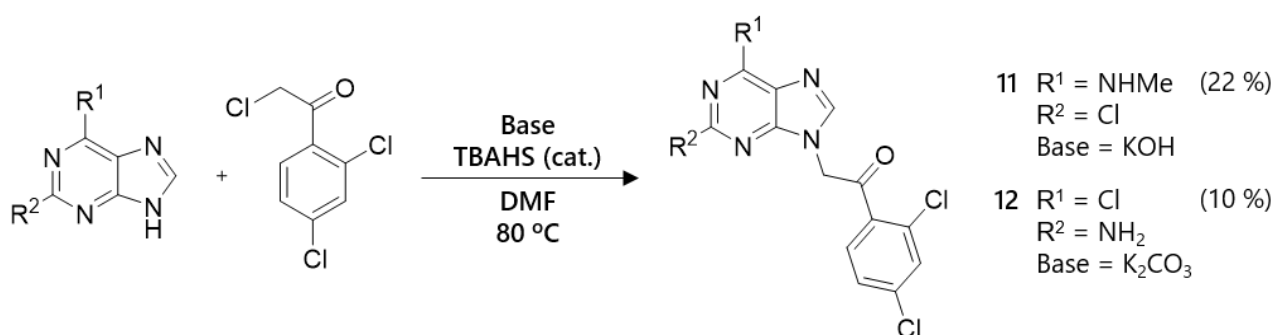
**Scheme 4.** Synthesis of 1-aryl-2-purinyloethanones *via* nucleophilic aromatic substitution by following Bendels' procedure (Bendels *et al.*, 2014).



For the synthesis of purinyloethanones bearing additional protic nucleophilic groups, such as amines, anticipating the same issues evidenced in the synthesis of **6** and **8**, alternative methodologies were performed (Scheme 5). The 2-[2-chloro-6-(methylamino)-9*H*-purin-9-yl]-1-(2,4-dichlorophenyl)ethan-1-one (**11**) was synthesised using KOH as base in DMF and tetrabutylammonium hydrogen sulfate (TBAHS) as additive (Raboisson *et al.*, 2003), while 2-(2-amino-6-chloro-9*H*-purin-9-yl)-1-(2,4-dichlorophenyl)ethan-1-one (**12** – Scheme 5) needed the use of K<sub>2</sub>CO<sub>3</sub> in DMF, as suggested by Soltani Rad and collaborators (Soltani Rad *et al.*, 2010). Both reactions underwent with low yields.

Tetrabutylammonium salts, which are usually used as transfer phase catalysts, are interestingly employed in this monophasic nucleophilic substitution reactions to increase the yield. This seems to be due to a hydrogen bond interaction of the anion with a non-ionic nucleophilic centre. However, this was well-described for tetrabutylammonium fluoride, a different onium salt than the one used in this reaction, probably explaining the reason behind the low yields (Alauddin *et al.*, 2011; Brik *et al.*, 2005).

**Scheme 5.** Synthesis of 2-aminopuriny-1-(2,4-dichlorophenyl)ethanones *via* nucleophilic aromatic substitution by following Soltani Rad's procedure (Soltani Rad *et al.*, 2010).

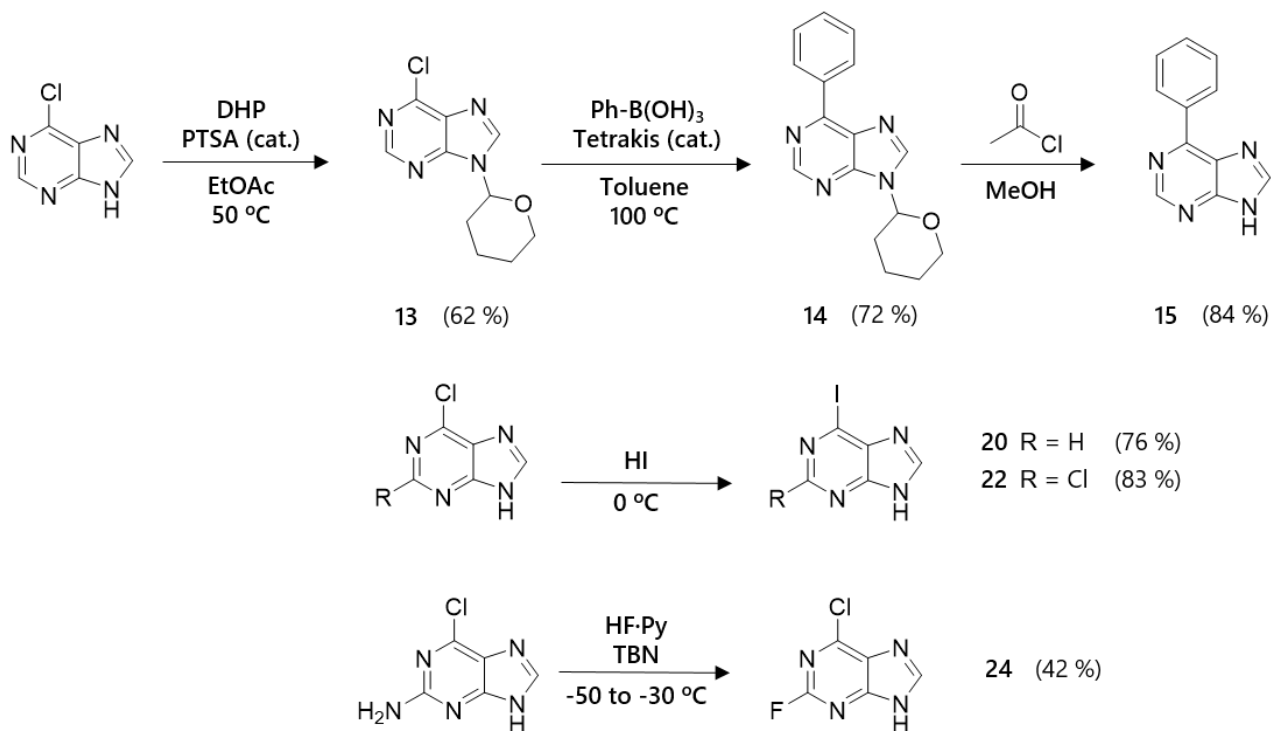


On the basis of the promising P2X7 antagonist profile of purinyethanone **9**, presented in chapter 5.3, further derivatives were prepared taking **9** as a head compound, proposing chemical modifications at both purine core and the pending phenyl ring. We kept the most optimal conditions to achieve S<sub>N</sub>2 reaction, *i.e.* NaH as base in DMF, obtaining scattered yields (**16** – **19**, **21**, **23**, **25** – Scheme 4).

For the preparation of the corresponding intermediates (Scheme 6), selected purine intermediates were accessible from commercially-available chloropurines. Protection of 6-chloropurine at position N9 with 3,4-dihydro-2*H*-pyran under mild acidic catalysis (*p*-toluensulfonic acid), which was then subjected to Suzuki-Miyaura cross-coupling reaction with phenylboronic acid, K<sub>2</sub>CO<sub>3</sub> and Pd(PPh<sub>3</sub>)<sub>4</sub> as catalyst, furnished 6-phenyl-9-(tetrahydro-2*H*-pyran-2-yl)purine (**14**) that, by selective deprotection of the THP group, gave rise to the desired intermediate **15**. Treatment of 6-chloropurine or 2,6-dichloropurine with hydroiodic acid gave 6-iodopurine **20** (76 % yield) or 2-chloro-6-iodopurine **22** (83 % yield), respectively. Incorporation of fluorine at C2 was performed by diazotisation of 2-amino-6-chloropurine with tert-butyl nitrite (TBN) in presence of hydrofluoric acid in pyridine (**24** – 42 % yield). The replacement of chlorine at C6 with fluorine was unsuccessful, despite

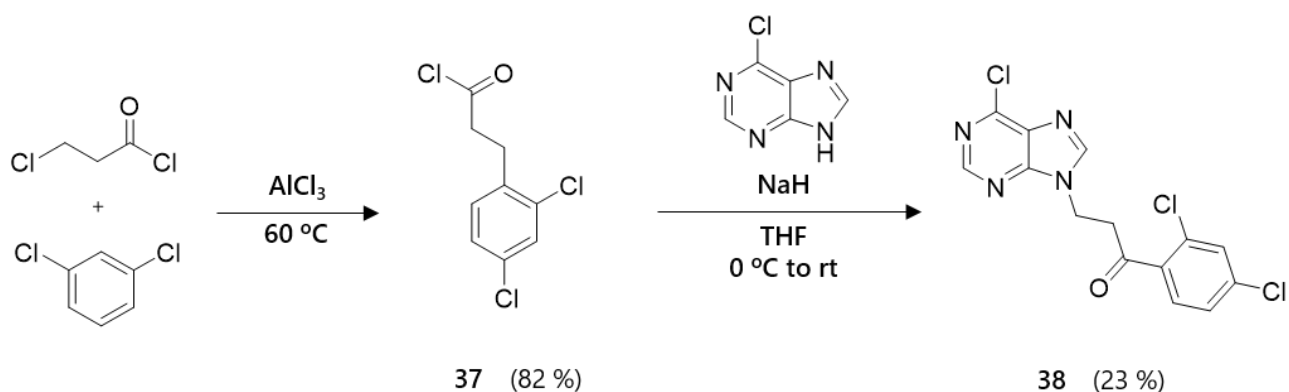
using alternative methodologies, *e.g.* via formation of a quaternary ammonium with trimethylamine substitution and subsequent fluorine nucleophilic attack using TBAF.

**Scheme 6.** Synthesis of differently substituted purine intermediates.



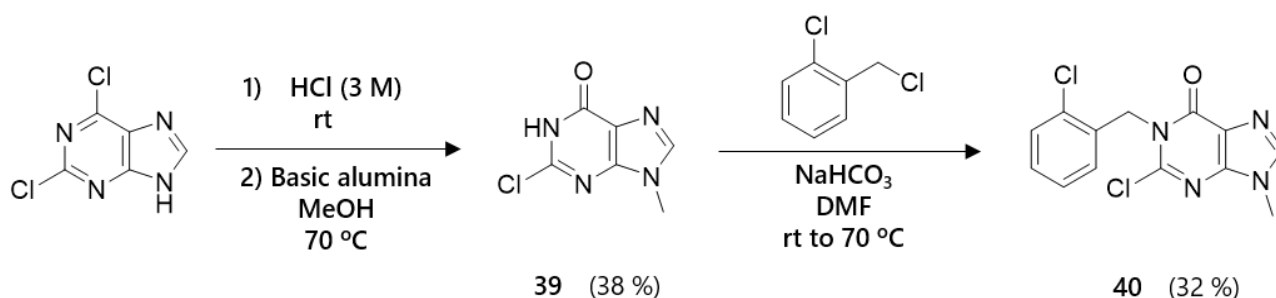
Considering the preliminary pharmacological data of compound **9**, we considered that the synthesis of its closer superior homologue, bearing a propanone as spacer instead of an ethanone, was of interest. We performed the Friedel-Crafts reaction of 1,3-dichlorobenzene with 3-chloropropanoyl chloride in presence of  $\text{AlCl}_3$ , which gave rise to 3-chloro-1-(2,4-dichlorophenyl)propan-1-one (**37**) in good yield (Scheme 7). This intermediate suffered nucleophilic substitution of 6-chloropurine under the conditions described by Bendels (Bendels *et al.*, 2014), to furnish 3-(6-chloro-9*H*-purin-9-yl)-1-(2,4-dichlorophenyl)propan-1-one (**38** – yield 23 % – Scheme 7).

**Scheme 7.** Synthesis of 3-(6-chloro-9*H*-purin-9-yl)-1-(2,4-dichlorophenyl)propan-1-one.



Our final purine derivative bears a 6-oxopurine as main scaffold, with the free N1 position as nucleophilic centre. The lipophilic moiety selected was 2-chlorobenzyl, which has a methylene that resulted to be essential for the activity of the arylpurinyl ethanone series. In detail, we chose 2,6-dichloropurine as scaffold, as it was the one used in the procedure described by Tumma and co-workers, which we took as reference (Tumma *et al.*, 2010). We first generated the 2,6-dichloropurine hydrochloride, which next underwent a reaction with MeOH and basic aluminium oxide. We successfully obtained the 2,6-dichloropurine hydrochloride and 2-chloro-9-methyl-1,9-dihydropurin-6-one (**39** – Scheme 8) in low yield. Finally, we performed the nucleophilic substitution of compound **39** over the 2-chlorobenzyl chloride with  $\text{NaHCO}_3$ , following the procedure described by Szarek and colleagues (Szarek *et al.*, 1985), which yielded 2-chloro-1-(2-chlorobenzyl)-9-methyl-1,9-dihydro-6*H*-purin-6-one (**40**) (Scheme 8).

**Scheme 8.** Synthesis of 2-chloro-1-(2-chlorobenzyl)-9-methyl-1,9-dihydro-6*H*-purin-6-one.



Regarding the regioselectivity of the alkylation reaction, we previously anticipated that we selected the 6-substituted purine scaffold expecting to direct it to N9, rather than N7 (Dalby *et al.*, 1993; Ding

*et al.*, 2002). Actually, for the synthesis of most of the compounds of this series, only one regioisomer has been successfully isolated. Nevertheless, for compound **17** we obtained both regioisomers, derived from the alkylation of either N7 or N9, identified by  $^1\text{H-NMR}$  (Figure 26). Unfortunately, we did not manage to isolate the pure N7-alkylated isomer by column chromatography. However, in its fraction, the methyl frequency signals of the two isomers are distinguishable using a 500 MHz apparatus, unlike the aromatic or the methylene peaks. Additionally, we characterised the pure N9-isomer derivative and the N7+N9 isomers mixture by  $^1\text{H-}^1\text{H}$  nuclear Overhauser's effect (NOE) spectroscopy (NOESY), to see any spatial proximity between two or more hydrogen nuclei. We supposed that the methyl group at position 6 should have been able to spatially couple to the methylene of the arylethanone when N7-isomer was analysed. In N9-alkylated purine, we could see no coupling with the methyl group. On the contrary, the methyl signal of the N7-isomer couples with the methylene and the hydrogen on the *ortho*-carbon of the aryl group (Figure 26). The N7-regioisomer was characterised also by mass spectrometry, confirming its identical molecular weight to N9-isomer. To verify additionally that the nucleophilic substitution occurred on the N9 rather than on the N7, we crystallised one of the arylpurinyloethanone derivatives and performed X-ray diffraction analysis. The compound that crystallised the easiest was **11**. The X-ray diffraction pattern confirmed that also in that case the obtained product was the N9 regioisomer (Figure 27 and Annexes, chapter 10.2). Hence, we extrapolated that all the purine scaffolds with some substituent at position 2, 6, or both gave the N9 isomer, probably due to less steric hindrance around N9, contrary to N7 (Ding *et al.*, 2002).

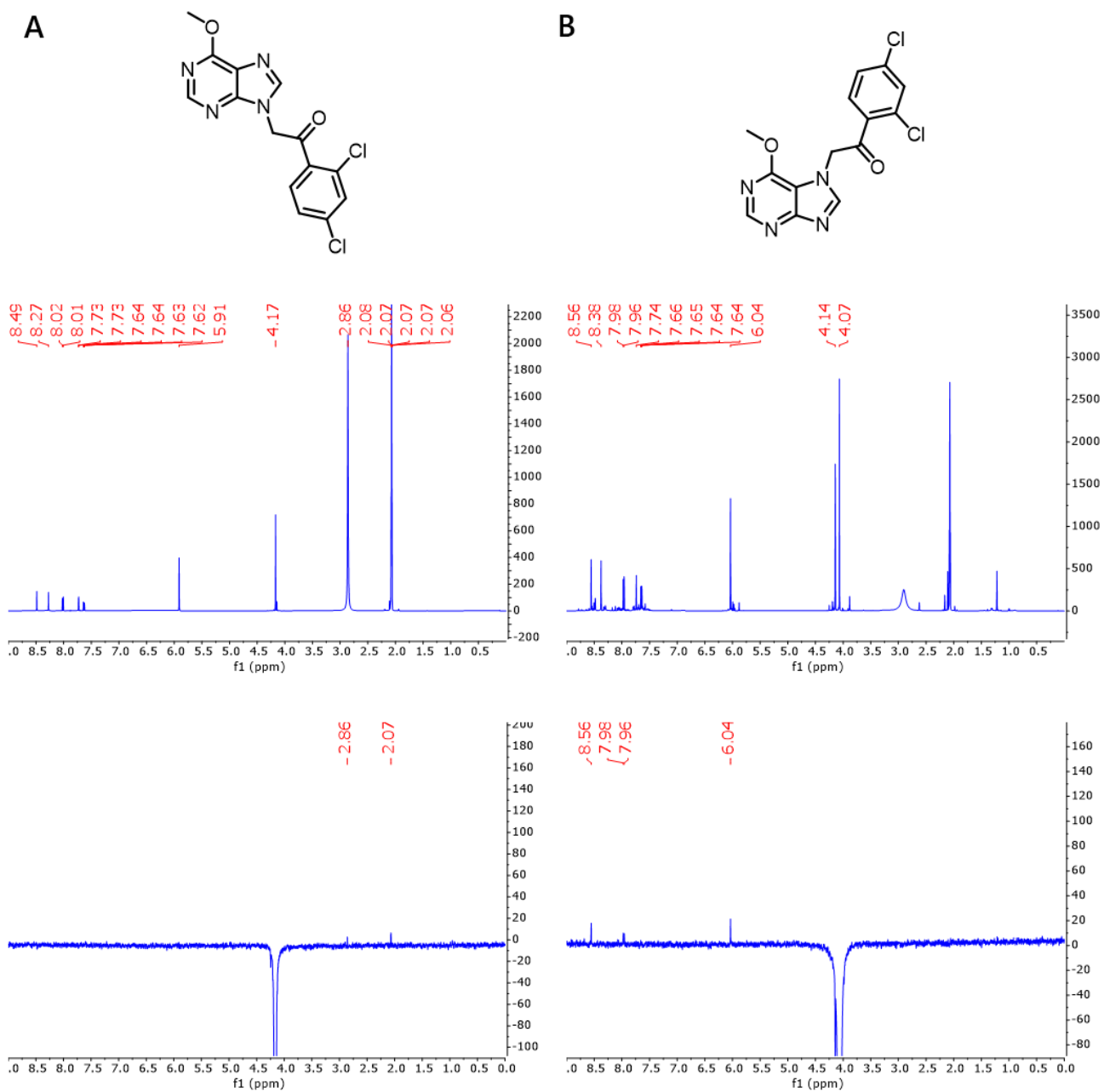
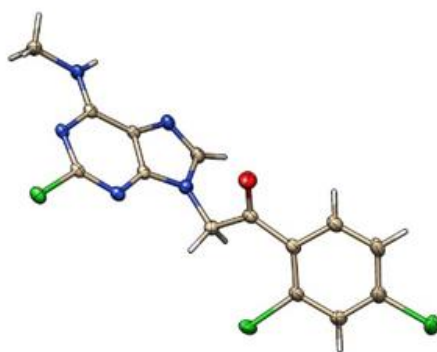


**Figure 26.** NMR spectra of the two isomers of 1-(2,4-dichlorophenyl)-2-(6-methoxypuriny)ethanone. From top to bottom, structure,  $^1\text{H}$ -NMR and  $^1\text{H}$ - $^1\text{H}$ -NOESY experiments for the N9 (A) and the mixture of N7+N9 (B) isomers.



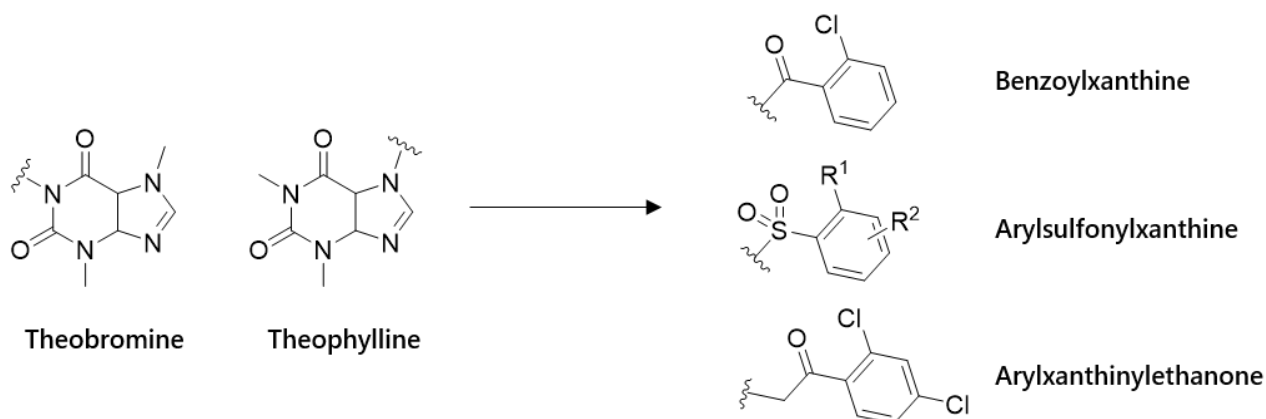
11

**Figure 27.** X-ray diffraction of 2-[2-chloro-6-(methylamino)-9*H*-purin-9-yl]-1-(2,4-dichlorophenyl)ethan-1-one 11. Atoms are distinguished by colour: carbon, grey; hydrogen, white; oxygen, red; nitrogen, blue; chlorine, green.

#### 5.2.4. Xanthine derivatives 26-36

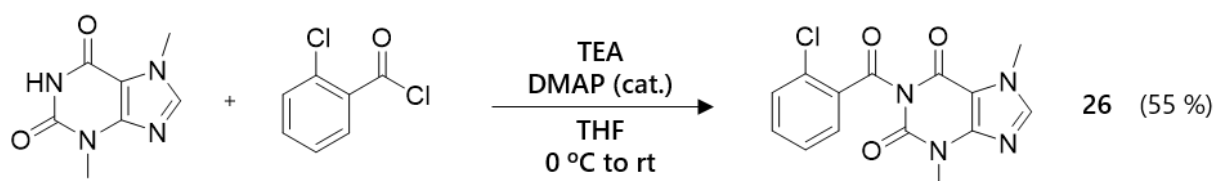
We opted to synthesise novel derivatives starting also from xanthine scaffolds, because of the considerations described in chapter 5.1 about their distribution to the CNS. We afforded novel xanthine-based compounds for each subfamily of the classification illustrated in the previous chapters (benzoyl xanthines, arylsulphonyl xanthines and arylxanthinyl ethanones – Scheme 7).

**Scheme 7.** General illustration of the three families designed using xanthine scaffolds.



The incorporation of the benzoyl residue to xanthine scaffolds, using the TEA/DMAP system protocol, suffered from the similar issues observed with the purine scaffolds, *i.e.* degradation at purification step and high rate of by-products (see chapter 5.2.1). The only successful synthesis of this series was accomplished by using theobromine as starting material. The theobromine derivative 1-(2-chlorobenzoyl)-3,7-dimethyl-3,7-dihydro-1*H*-purine-2,6-dione (**26** – Scheme 8) was accomplished by filtration of a precipitate (in EtOAc and water), extraction in EtOAc and then several washed in hexane, thus avoiding chromatography.

**Scheme 8.** Synthesis of 2-chlorobenzoyl theobromine derivative *via* acylation using the TEA/DMAP system.

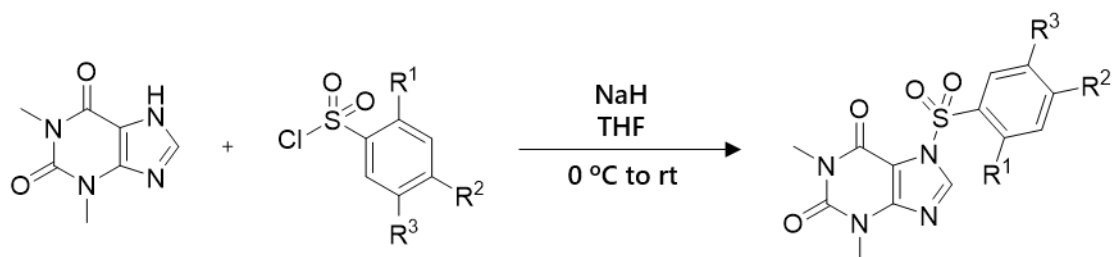


Moving to the more stable sulfone derivatives, we first used theophylline as starting material. Following the procedure used for arylsulfonyl purines, based on the use of NaH as base and 2-chlorosulfonyl chloride as electrophile in THF, we obtained 7-[(2-chlorophenyl)sulfonyl]-1,3-dimethyl-3,7-dihydro-1*H*-purine-2,6-dione (**27** – Scheme 11) in good yield. Reaction was ineffective for theobromine as starting material, presumably due to the scarce acidity and nucleophilicity of N1 (Gulevskaya and Pozharskii, 1991). Alternative bases, like diisopropylethylamine, and solvents, such as pyridine, (Jonaitis and Storer, 2004) also failed. When compound **27** was assayed together with the first batch of synthesised compounds, it showed a decent P2X7 inhibitory activity (see chapter 5.3). Hence, we synthesised further analogues under the same experimental procedure, focusing on modifying the substituents and their position on the phenyl group (Scheme 9). Yields were good in general, but the reaction to obtain the derivative possessing two chlorines at C2' and C3' did not work, presumably due to steric hindrances.

Finally, we synthesised two arylxanthinyl ethanone derivatives using theophylline and theobromine as scaffolds. We carried out the protocol described by Soltani Rad and colleagues (Soltani Rad *et al.*, 2010) previously discussed for the synthesis of the arylpurinyl ethanone **12** (Scheme 5 – chapter 5.2.3), obtaining the desired product with low yield. The incorporation of the benzoylmethyl substructure docked at the free amine in each case (Scheme 10). In particular, the regiochemistry of **35** is influenced by the steric effect of the methyl group at N3.

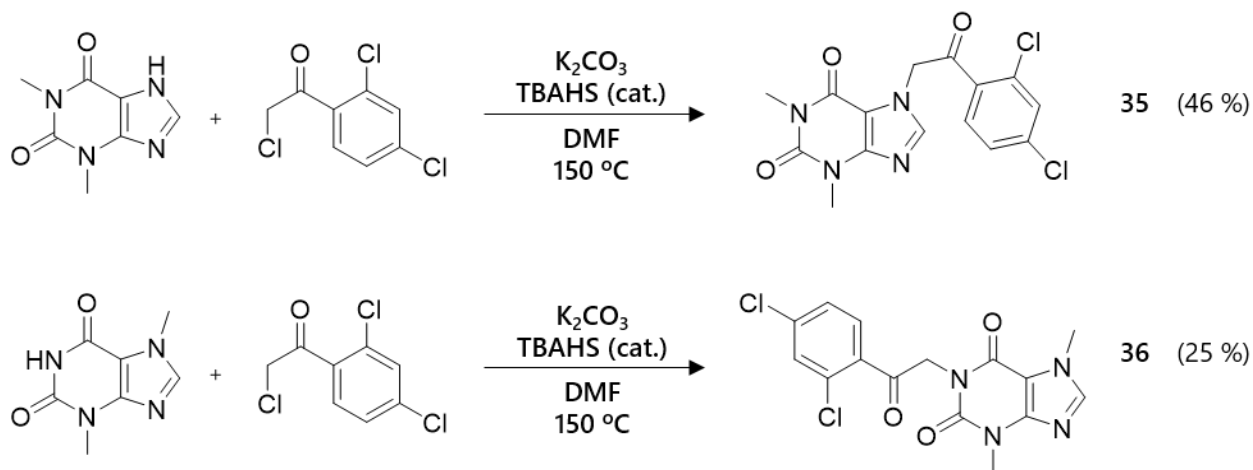


Scheme 9. Synthesis of 2-chlorosulfonyl theophylline derivatives *via* sulfonylation.

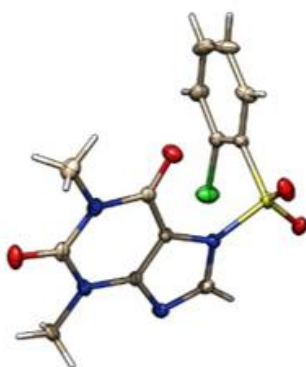


27	R <sup>1</sup> = Cl (69 %)	31	R <sup>1</sup> = Cl (73 %)
	R <sup>2</sup> = H		R <sup>2</sup> = H
	R <sup>3</sup> = H		R <sup>3</sup> = Cl
28	R <sup>1</sup> = Cl (74 %)	32	R <sup>1</sup> = F (72 %)
	R <sup>2</sup> = Cl		R <sup>2</sup> = F
	R <sup>3</sup> = H		R <sup>3</sup> = H
29	R <sup>1</sup> = Cl (54 %)	33	R <sup>1</sup> = Me (78 %)
	R <sup>2</sup> = F		R <sup>2</sup> = F
	R <sup>3</sup> = H		R <sup>3</sup> = H
30	R <sup>1</sup> = Cl (75 %)	34	R <sup>1</sup> = H (81 %)
	R <sup>2</sup> = CF <sub>3</sub>		R <sup>2</sup> = F
	R <sup>3</sup> = H		R <sup>3</sup> = H

Scheme 10. Synthesis of 1-(2,4-dichlorophenyl)-2-xanthine derivatives.



Regarding the regioselectivity of theophylline alkylation and acylation reactions, we expected them to occur at N7 position, as for the well-known alkylated xanthine derivatives, such as caffeine (Gulevskaya and Pozharskii, 1991; Zajac *et al.*, 2003). The reactions performed and their further purification gave rise to only one isomer, as occurred using the purine scaffolds. We managed to crystallise compound **27**, as reference for the whole family, and the X-ray diffraction pattern revealed that the sulfonylation is directed to N7 of the theophylline (Figure 28 and Annexes).



**27**

**Figure 28.** X-ray diffraction of 7-[(2-chlorophenyl)sulfonyl]-1,3-dimethyl-3,7-dihydro-1*H*-purine-2,6-dione **27**. Atoms are distinguished by colour: carbon, grey; hydrogen, white; oxygen, red; nitrogen, blue; sulfur, yellow; chlorine, green.

Unfortunately, we were not able to crystallise compound **35**, which comprises the theophylline scaffold and the aryloethanone, but we performed a 2D-NOESY experiment, hypothesising that if the alkylation occurred at N9, we should observe a NOE coupling between the methylene of the ethanone spacer and the methyl placed at N3. Although the lack of appreciable coupling does not completely demonstrate that the alkylation occurred at N7, this is still consistent with our hypothesis (Figure 29).

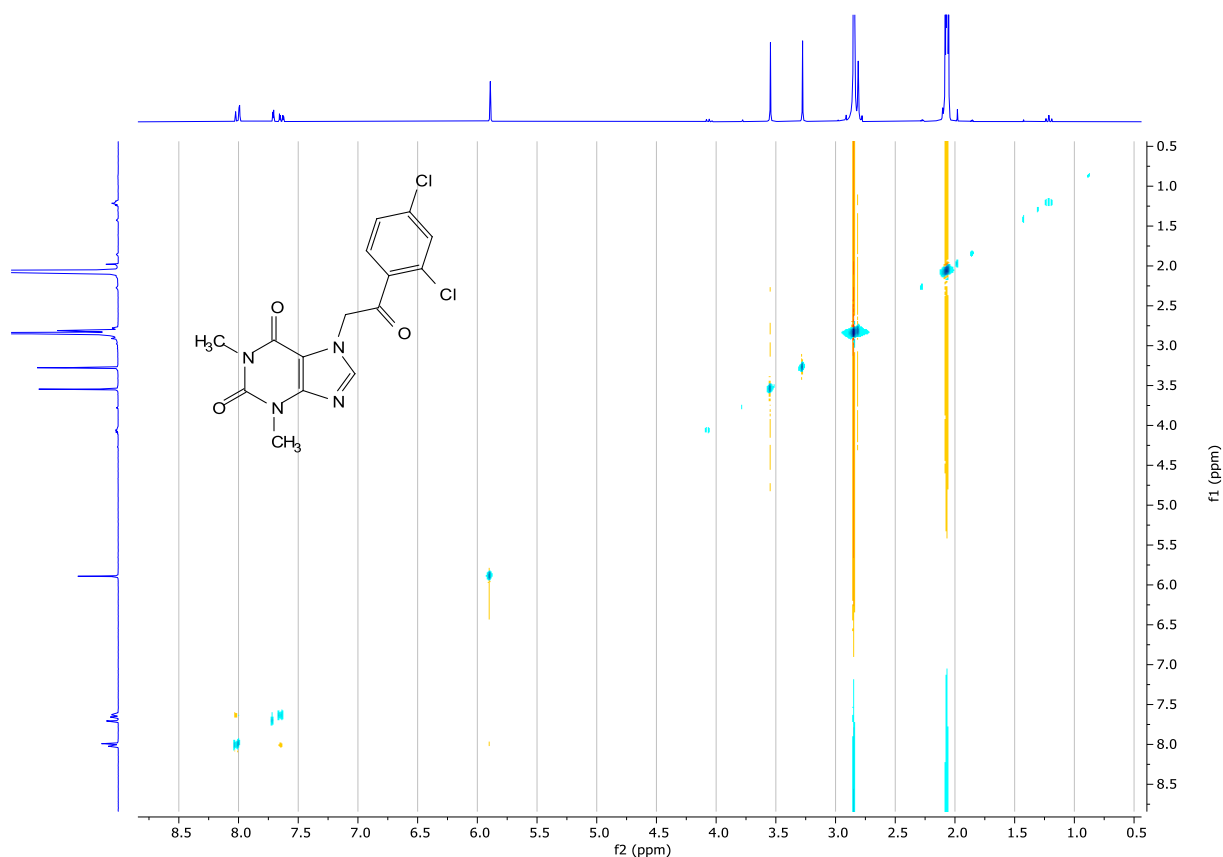


**Figure 29.** 2D-NOESY of compound 35. No spatial coupling is observable between the methylene and the N3-methyl.

### 5.2.5. Partial conclusions

From the pharmacological experiments here reported, the following partial conclusions arise:

- Novel non-nucleotide purine and xanthine derivatives were designed as potential P2X7 antagonists, taking into account our hypothesised model: the heterocycle linked to an *ortho*-substituted benzene through a carbonyl, sulfonyl, ethanoyl, propanoyl, or methylene spacer.
- Most of the compounds have favourable physicochemical properties to be administered as drugs and to reach the CNS by crossing the BBB.
- Three main series were synthesised: the unstable benzoyl purines, the arylsulfonyl purines and the 1-aryl-2-purinyletanones. We also synthesised the corresponding xanthine derivatives, using theobromine and theophylline as starting material. Final compounds were obtained with low to moderate yields, except for the arylsulfonyl xanthines, which were isolated with good yields.
- Purine acylation, sulfonylation and alkylation resulted to be regioselective at N9 position. Among all the derivatives, only the N7 isomer of compound 17 was found at low percentages.

### 5.3. Pharmacological evaluation of purine derivatives as P2X7 antagonists

#### 5.3.1. YO-PRO-1 dye uptake assay in hP2X7-overexpressing HEK293 cells

It is well known that molecules with molecular weight less than 900 Da can pass through the pore of long-activated P2X7 (Di Virgilio *et al.*, 2018; Jacobson *et al.*, 2002). This allows the measurement of their *in vitro* activity by accumulation experiments with a fluorescent dye, typically ethidium bromide, propidium iodide or 4-[(3-methyl-1,3-benzoxazol-2(3*H*)-ylidene)methyl]-1-[3-(trimethylammonio)propyl]quinolinium di-iodide (YO-PRO-1, Figure 30). This assay can be carried out in single cells using microscopy (Nicke *et al.*, 2009), or in a population of cells using a cuvette-based fluorimeter or a fluorescence plate reader, which is the best option for screening several novel compounds (Bidula *et al.*, 2019b; Gibbons *et al.*, 2001).

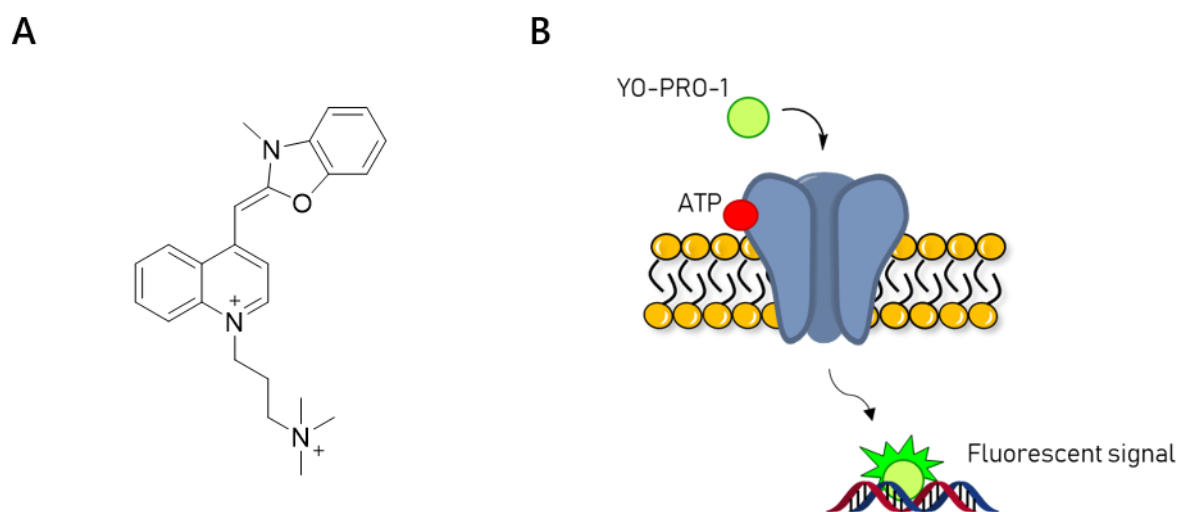
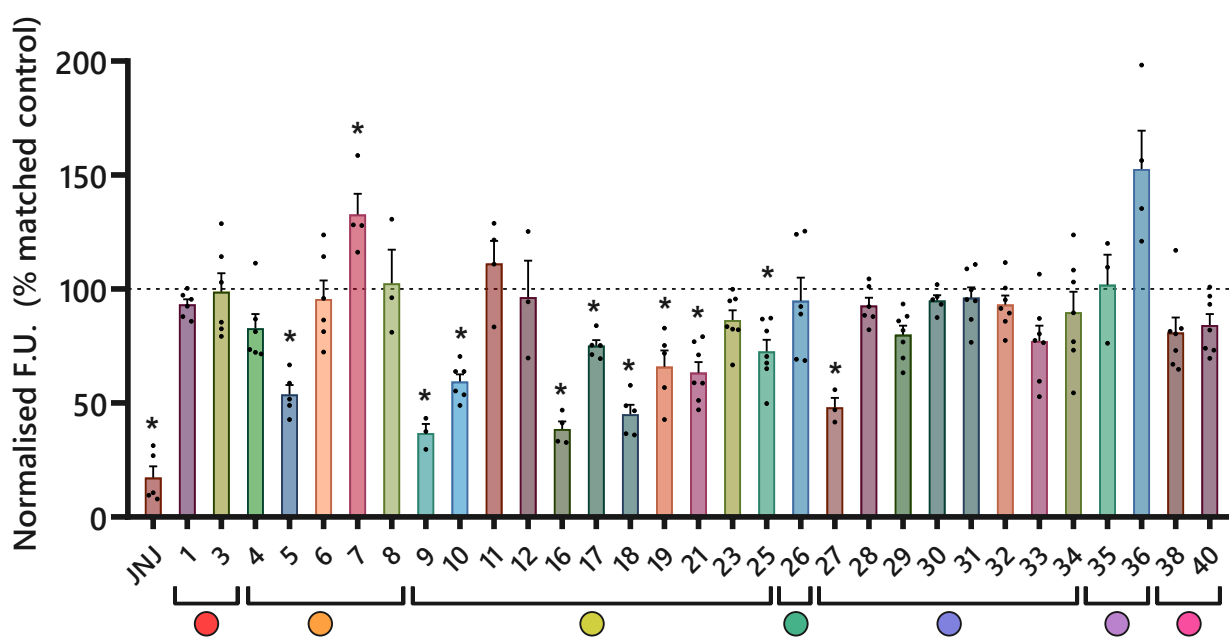


**Figure 30.** A) Chemical structure of the YO-PRO-1 dye. B) Illustration of how the YO-PRO-1 dye acts as probe for P2X7 activity. When activated by ATP or BzATP, the P2X7 pore opens and lets YO-PRO-1 permeate the cell. The dye becomes fluorescent when binds to nucleic acids. A P2X7 antagonist decreases the entrance of the dye and, subsequently, the generation of the fluorescent signal.

The YO-PRO-1 probe has excitation and emission wavelengths of 491 and 509 nm, respectively. Its fluorescence increases when it binds to nucleic acids, which are usually present inside the cells, both in the cytosol (usually RNAs) and in the nucleus. So, when the P2X7 is continuously activated by its

agonists, YO-PRO-1 can enter into the cells and fluorescence increases due to nucleic acids binding. Thus, a P2X7 antagonist would impede such fluorescence increase (Figure 30).










For this assay, we used a stably hP2X7-expressing HEK293 cell line, kindly donated by Di Virgilio's group. We screened all the final compounds at a concentration of 10  $\mu$ M, incubating them for 20 min before YO-PRO-1 (2  $\mu$ M) and BzATP application (30  $\mu$ M). YO-PRO-1 uptake responses in presence of compounds were compared with those of cells treated only with BzATP. Also, the reference compound JNJ-47965567 at a concentration of 1  $\mu$ M was used as positive control of P2X7 blockade. Several compounds exerted a significant reduction of YO-PRO-1 uptake (Figure 31). In particular, compounds **9**, **16**, and **18**, which belong to the arylpurinyl ethanone family, showed an inhibitory activity of around 50 % or more, respect to negative controls. Also, the arylsulfonyl purine **5** and the arylsulfonyl theophylline **27** showed a similar blockade. Less potent, but still significant, were the inhibitory responses of arylpurinyl ethanones **10**, **17**, **19**, **21** and **25** (Table 5).



**Figure 31.** YO-PRO-1 uptake assay of the final compounds of this work. The colour of the spots below each group of columns indicates the family of the compounds: (2-chlorobenzoyl)purines (red), (2-chlorosulfonyl)purines (orange), 1-aryl-2-purinyloethanones (yellow), (2-chlorobenzoyl)theobromine (green), arylsulfonyltheophyllines (blue), 1-(2,4-dichlorophenyl)-2-xanthinyl ethanones (lilac), other derivatives (pink). \*statistical significant (see Table 5 for further details).

This first screening showed that the arylpurinyl ethanone series resulted to be more promising than the other families, except for **5** and **27**. Regarding to SAR studies, H-bond donor groups on the purine core affected negatively the interaction to the P2X7 receptor, such as for **6**, **8**, **11** and **12** that bear an amine at position C2 or a methylamine at position C6. Some modifications at position C6 of the purine core seemed to be allowed, as well as small changes at position C2. Apparently, the xanthine core showed some antagonistic response only when bears sulfonyl as spacer (compound **27**). Neither the arylpurinyl propanone (**38**) nor the 1-benzyl-6-oxopurine derivative (**40**) provided any interesting activity. These first considerations were further confirmed in the next screening (chapter 5.3.2).

**Table 5.** Values of YO-PRO-1 uptake inhibitions for each synthesised compound (10  $\mu$ M) in hP2X7-HEK293 cells, stimulated by BzATP (30  $\mu$ M).

		Inhibition %			Inhibition %			Inhibition %
	JNJ	56 $\pm$ 5 ***		<b>12</b>	4 $\pm$ 16		<b>29</b>	20 $\pm$ 4
	<b>1</b>	7 $\pm$ 2		<b>16</b>	62 $\pm$ 3 ***		<b>30</b>	5 $\pm$ 3
	<b>3</b>	1 $\pm$ 8		<b>17</b>	25 $\pm$ 3 ***		<b>31</b>	4 $\pm$ 5
	<b>4</b>	17 $\pm$ 6		<b>18</b>	55 $\pm$ 4 ***		<b>32</b>	7 $\pm$ 4
	<b>5</b>	46 $\pm$ 4 **		<b>19</b>	34 $\pm$ 7 **	<b>33</b>	23 $\pm$ 7	
	<b>6</b>	4 $\pm$ 8		<b>21</b>	37 $\pm$ 5 ***	<b>34</b>	10 $\pm$ 1	
	<b>7</b>	nb	<b>23</b>	14 $\pm$ 4		<b>35</b>	0 $\pm$ 8	
	<b>8</b>	9 $\pm$ 9	<b>25</b>	27 $\pm$ 5 **		<b>36</b>	nb	
	<b>9</b>	63 $\pm$ 4 ***		<b>26</b>	5 $\pm$ 10		<b>38</b>	19 $\pm$ 9
	<b>10</b>	41 $\pm$ 3 ***		<b>27</b>	52 $\pm$ 4 **		<b>40</b>	16 $\pm$ 6
	<b>11</b>	2 $\pm$ 9		<b>28</b>	7 $\pm$ 3			

JNJ-47965567 (JNJ) was tested at 1  $\mu$ M. The colour of the spots indicates the family of the compounds: (2-chlorobenzoyl)purines (**red**), (2-chlorosulfonyl)purines (**orange**), 1-aryl-2-purinyloethanones (**yellow**), (2-chlorobenzoyl)theobromine (**green**), arylsulfonyltheophyllines (**blue**), 1-(2,4-dichlorophenyl)-2-xanthinyl ethanones (**lilac**), other derivatives (**pink**). Data are shown as mean  $\pm$  SEM of triplicates of at least three different cultures. \*\*p < 0.01; \*\*\*p < 0.001; nb: no blockade.

### 5.3.2. ATP currents in human P2X7 cRNA-injected *X. laevis* oocytes

To better characterise the preliminary data obtained in the YO-PRO-1 uptake assay, we decided to assess the activity of the novel compounds on ATP-elicited currents in the *Xenopus laevis* oocytes model, which allows the injection of the cRNA of the target protein (*i.e.* P2X7) directly into the cytoplasm, leading to its overexpression. This part of the project was performed during a secondment at Ludwig-Maximilians University of Munich (Germany) under the supervision of Prof. Annette Nicke, one of the principal investigators of our European Consortium "PurinesDX".

We used the two-electrode voltage-clamp (TEVC) technique to measure ATP-elicited currents, since it is considered the best choice for compounds screening. Compounds were incubated at 100  $\mu\text{M}$  for 3 min, before receptor activation occurred (ATP 300  $\mu\text{M}$ ). Compounds were tested at such a high concentration because no inhibitory action was recorded at lower concentrations. The reference compound JNJ-47965567 was used as positive control. The concentration-response curve (Figure 34C) for JNJ showed an  $\text{IC}_{50}$ , defined as drug concentration that inhibits the 50 % of the control current, about 10-fold higher than the data published from whole cell patch-clamp recordings in hP2X7-overexpressing 1321N1 cells and from radioligand binding experiments. The same could be happening with the compounds described in this work. In fact, it is known that electrophysiological experiments with oocytes can show less potent responses of pharmacological agents respect to mammalian cells due to the high amount of vitelline membrane invaginations presented in frogs' oocytes, which would hinder the access of a drug to its heterologously-expressed biological target (Goldin, 2006).

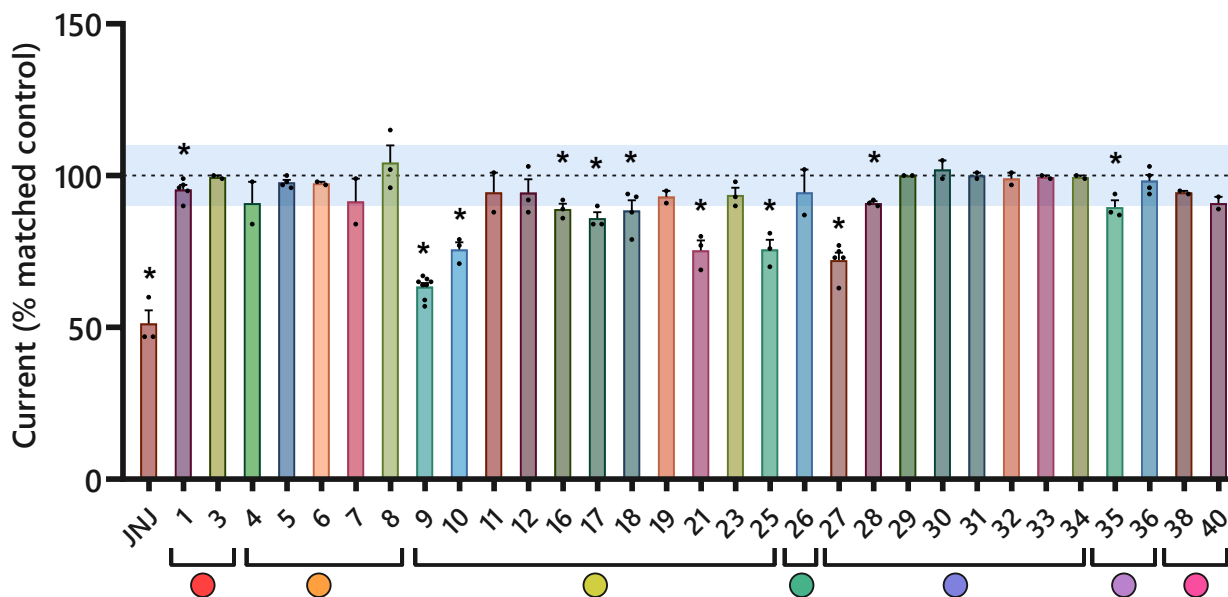











**Figure 32.** ATP (300  $\mu$ M)-induced currents measured by TEVC in *X. laevis* oocytes expressing the hP2X7. Compounds were tested at 100  $\mu$ M, except for JNJ-47965567 (JNJ), which was tested at 1  $\mu$ M. The colour of the spots below each group of columns indicates the family of the compounds: (2-chlorobenzoyl)purines (red), (2-chlorosulfonyl)purines (orange), 1-aryl-2-purinyloethanones (yellow), (2-chlorobenzoyl)theobromine (green), arylsulfonyltheophyllines (blue), 1-(2,4-dichlorophenyl)-2-xanthinyl ethanones (lilac), other derivatives (pink). The light blue area shows the variability range determined for this technique. \*statistical significant (see Table 6 for further details).

Figure 32 shows all the recorded blockade data in the hP2X7-expressing oocytes. Compounds 9, 10, 21 and 25, which belong to the arylpurinyl ethanone series, confirmed their P2X7 inhibitory activity detailed in the YO-PRO-1 experiments (Table 6). An example of such ATP current inhibition is the one elicited by compound 9, represented in Figure 32. The only arylsulfonyl xanthine capable of reducing P2X7 currents was theophylline 27, which also showed an interesting activity in the YO-PRO-1 assay.



**Table 6.** Values of ATP (300  $\mu$ M)-exerted currents for each synthesised compound (100  $\mu$ M) measured in hP2X7-expressing *X. laevis* oocytes by TEVC.

		Inhibition %				Inhibition %				Inhibition %	
		JNJ	49 $\pm$ 4 **			12	6 $\pm$ 4			29	nb
	1		5 $\pm$ 2 *		16		11 $\pm$ 2 *		30		nb
	3		0 $\pm$ 1		17		14 $\pm$ 2 *		31		nb
	4		9 $\pm$ 7		18		11 $\pm$ 3 *		32		1 $\pm$ 2
	5		2 $\pm$ 1		19		7 $\pm$ 2		33		nb
	6		2 $\pm$ 1		21		25 $\pm$ 3 *		34		nb
	7		8 $\pm$ 8		23		6 $\pm$ 2		35		10 $\pm$ 2 *
	8		nb		25		24 $\pm$ 3 *		36		2 $\pm$ 2
	9		47 $\pm$ 1 ****		26		5 $\pm$ 8		38		6 $\pm$ 1
	10		24 $\pm$ 2 **		27		28 $\pm$ 2 ***		40		9 $\pm$ 2
	11		5 $\pm$ 7		28		9 $\pm$ 1 **				

JNJ-47965567 (JNJ) was used at 1  $\mu$ M. The colour of the spots indicates the family of the compounds: (2-chlorobenzoyl)purines (**red**), (2-chlorosulfonyl)purines (**orange**), 1-aryl-2-purinyloethanones (**yellow**), (2-chlorobenzoyl)theobromine (**green**), arylsulfonyltheophyllines (**blue**), 1-(2,4-dichlorophenyl)-2-xanthinyl ethanones (**lilac**), other derivatives (**pink**). Data are shown as mean  $\pm$  SEM of at least two different oocytes coming from at least two different frogs. Statistical analysis has not been performed for  $n < 3$ . \* $p < 0.05$ ; \*\* $p < 0.01$ ; \*\*\* $p < 0.001$ ; \*\*\*\* $p < 0.0001$ ; nb: no blockade.

These five derivatives showed percentage responses comparable to the ones in the uptake assay in HEK293 cells. The other active compounds in the YO-PRO-1 screening did not show any activity in ATP currents in oocytes. This may be due to several factors. For instance, high concentrations (100  $\mu$ M) of compound could precipitate in the buffers used. This is particularly relevant when lipophilic compounds are involved, like ours, which have been designed to act in the CNS. This is the case of compound **16** (see chapter 5.3.3). Additionally, longer incubation time as in the YO-PRO-1 could have an impact on the percentage of P2X7 blockade responses. It was demonstrated that PPADS inhibits more the P2X7-dependent currents in stably transfected HEK293 cells when incubation time is increased from 0 to 10 min (Chessell *et al.*, 1998). This was confirmed in the same model in YO-PRO-1 experiments with several antagonists: maximum inhibitory response was obtained after 15 min for

PPADS and 30 min for oATP and KN62 (Michel *et al.*, 2000). The same effect was corroborated with compound **9** in hP2X7 cRNA-injected oocytes ATP currents. An incubation of 15 min instead of only 3 min augmented the percentage of inhibition from  $63 \pm 5\%$  to  $21 \pm 6\%$  (Figure 33).

Finally, all these compounds showed to be reversible, since the inhibited ATP currents were restored after 1 min of buffer perfusion. This was not the case of JNJ-47965567, which resulted to be irreversible (Figure 34D), as described by Bhattacharya and collaborators (Bhattacharya *et al.*, 2013).

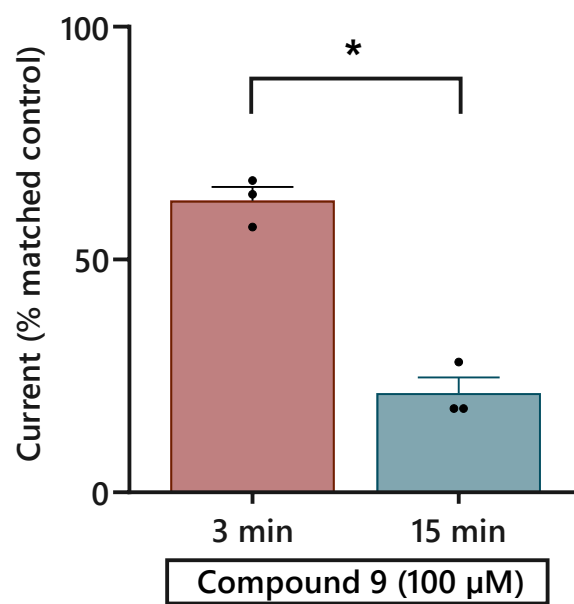


**Figure 33.** Time-dependent increase of ATP current inhibition exerted by compound **9**. Data were analysed using the t test. Three oocytes coming from at least 2 frogs were used for each group. \* $p < 0.001$ .

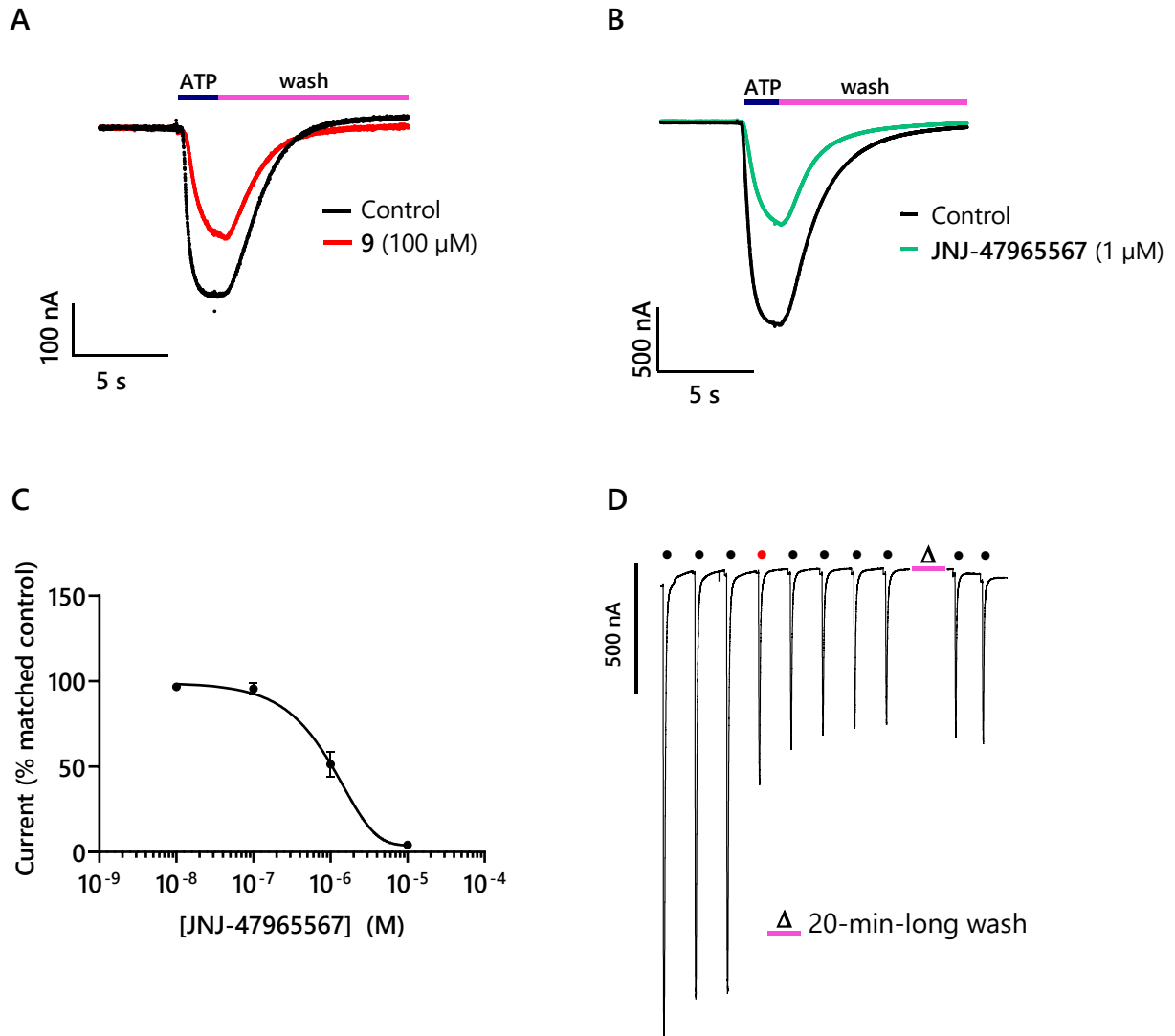


**Figure 34.** ATP current records of compound 9 (A) and positive control JNJ-47965567 (B). C) Concentration-response curve of JNJ-47965567. D) Concatenated current responses after a 2 s application of ATP (300  $\mu$ M). Black dots indicate each ATP pulse. The red dot indicates the ATP pulse after incubation (3 min) of JNJ-47965567. This P2X7 antagonist is irreversible, also after a 20-min-long wash.

### 5.3.3. Cytosolic Ca<sup>2+</sup> imaging in hP2X7-overexpressing HEK293 cell populations

Being a non-selective ion channel, P2X7 activation implies the entrance of Ca<sup>2+</sup> into the cells (Figure 35). Many fluorescent intracellular Ca<sup>2+</sup> indicators have been developed and used in the last decades (Paredes *et al.*, 2008), *e.g.* Fura-2 (Figure 35) or Fluo-4. In this study, we used the ratiometric Fura-2 dye, which emits at 510 nm when excited at 340 and 380 nm. The ratio of the emissions at the two wavelengths is directly related to the amount of Ca<sup>2+</sup> bound. The use of the ratio provides a more specific measurement, cancelling variables like cell morphology and changes in dye concentrations (Paredes *et al.*, 2008).

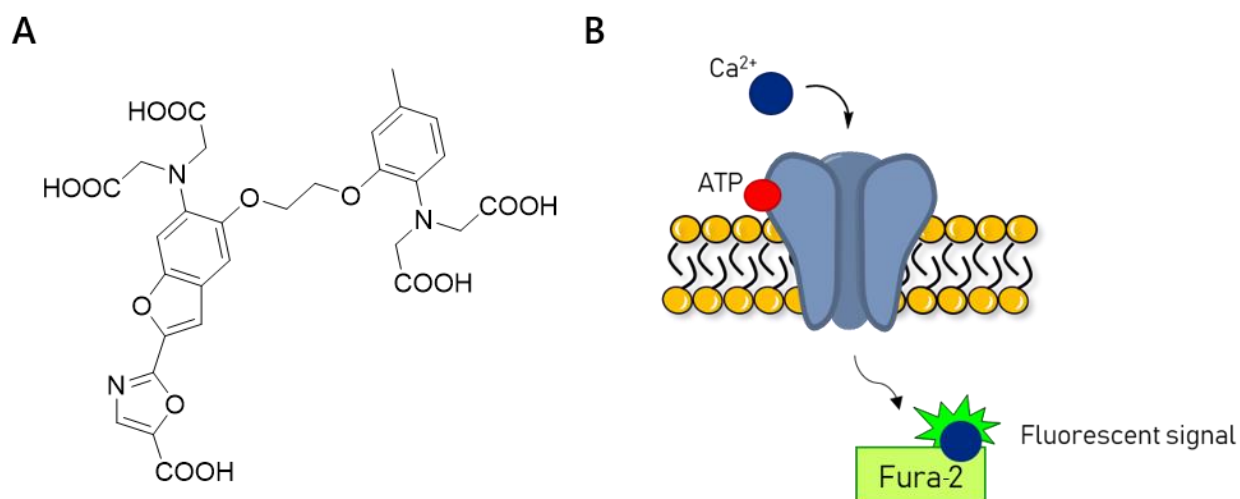


**Figure 35.** A) Structure of the FURA-2 Ca<sup>2+</sup> indicator. B) Illustration of how Ca<sup>2+</sup> influx is detected in this assay after P2X7 activation. Ca<sup>2+</sup> enters through the channel and binds to the indicator, generating a fluorescent signal.

The compounds were incubated for 15-30 min before BzATP (100  $\mu$ M) perfusion. JNJ-47965567 was used as positive control. We first tested a selected compound at a wide range of concentrations, from 0.1 to 100  $\mu$ M, to ensure the finding of any potential inhibition. Initially, we found that compound **9** could decrease the BzATP-induced Ca<sup>2+</sup> influx in a concentration-dependent way, with an IC<sub>50</sub> of 14  $\mu$ M (Figure 36). Since then, we evaluated the following compounds at 10  $\mu$ M (Figure 37).

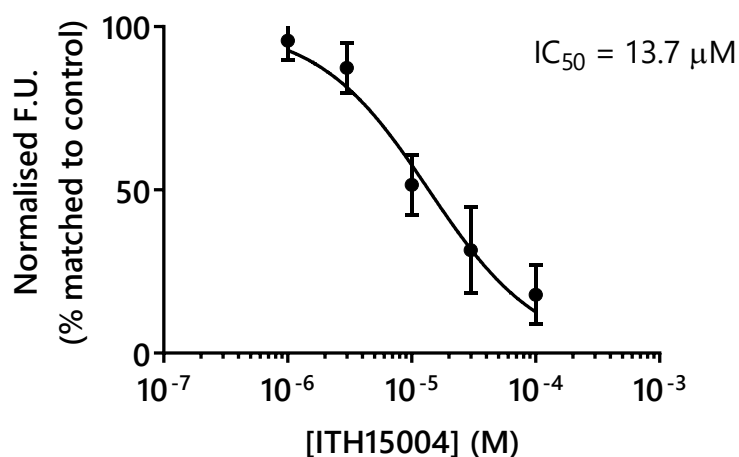


**Figure 36.** Concentration-response curve of the inhibition of compound **9** in  $[Ca^{2+}]_c$  measurements in hP2X7-HEK293 cells when stimulated by BzATP (100  $\mu$ M). Data are shown as mean  $\pm$  SEM of triplicates of three different cultures.

Compounds **16** and **21**, arylpurinyl ethanone derivatives bearing an iodine and a phenyl at position C6 of the purine core, respectively, had a significant reduction in BzATP-induced  $[Ca^{2+}]_c$  increase (Figure 37). Curiously, compound **18** showed a statistically significant decrease in  $[Ca^{2+}]_c$ , an activity that also appeared in the YO-PRO-1 assay. However, we could not observe any of that antagonistic effect on ATP currents, probably because the inhibitory activity of this derivative is less significant than others (*e.g.* those of **9**, **10** and **27**). This means that the chlorine at position C2 in the arylpurinyl ethanone series is not essential for P2X7 antagonism, but reinforces it. The 6-chloro-2-fluoropurinyl ethanone **25** showed a certain inhibitory activity in  $[Ca^{2+}]_c$  measurements, as in ATP currents recorded in the *X.laevis* oocyte model (see chapter 5.3.2) but, in this case, it was not statistically significant. Noteworthy, compound **10**, which bears two chlorines at position C2 and C6 of the purine, and the arylsulfonyl purine **27**, did not show any relevant activity in this experiment, compared to YO-PRO-1 assay and ATP currents (see chapter 5.3.1 and 5.3.2). We speculate that these compounds, among others, could permeate into the cell and have some intracellular off-target effect. In fact, intracellular  $Ca^{2+}$  is involved in the homeostasis and the promotion of intracellular functions and a cell permeable exogenous lipophilic molecule could interfere with it. Other non-specific interactions must be taken into account, such as insertion into the cellular membrane, which could lead to  $Ca^{2+}$  influx during incubation,  $[Ca^{2+}]_c$  increase, and then BzATP-elicited response decrease, among other causes.

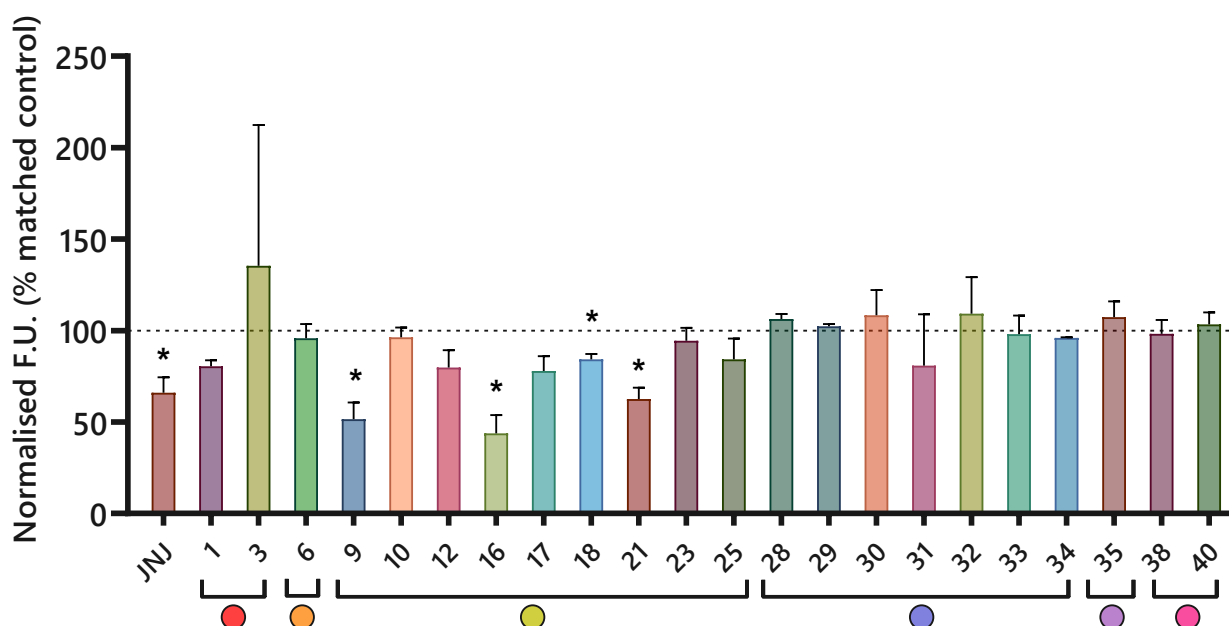


**Figure 37.** BzATP (100  $\mu\text{M}$ )-induced  $[\text{Ca}^{2+}]_c$  dynamics measured in hP2X7-HEK293 cells using Fura-2-AM as fluorescent dye. Compounds were incubated at 10  $\mu\text{M}$ , excepted for JNJ-47965567 (JNJ), which was used at 1  $\mu\text{M}$ . The colour of the spots below each group of columns indicates the family of the compounds: (2-chlorobenzoyl)purines (red), (2-chlorosulfonyl)purines (orange), 1-aryl-2-purinyloethanones (yellow), arylsulfonyltheophyllines (blue), 1-(2,4-dichlorophenyl)-2-xanthinyl ethanones (lilac), other derivatives (pink). \* statistical significant (see Table 7 for further details).

The inhibitory activity of **16** is quite interesting (Figure 37 and Table 7). It was found out in the YO-PRO-1 uptake assay, but not in ATP currents (see chapter 5.3.1 and 5.3.2). During  $[\text{Ca}^{2+}]_c$  measurements, we discovered that **16** precipitated in small crystals at 30 and 100  $\mu\text{M}$  in the test medium, which probably explains why no response was recorded in oocytes. However, the fact that the replacement of chlorine at position C6, as present in compound **9**, with a phenyl, like in **16**, is encouraging from a medicinal chemistry point of view. In fact, the phenyl group could be involved in some additional interaction at the P2X7 allosteric binding pocket (see chapter 5.5) and the insertion of further moieties could be beneficial to increase potency to the nanomolar range or to ameliorate the physicochemical properties, such as solubility. Currently, we are designing derivatives of **16** bearing hydroxyls or other halogens on this phenyl group.

**Table 7.** Values of compounds (10  $\mu$ M) inhibition on BzATP (100  $\mu$ M)-induced  $[Ca^{2+}]_c$  increase in hP2X7-HEK293 cells using Fura-2-AM as indicator.

		Inhibition %				Inhibition %			
	JNJ	66 $\pm$ 9 *		17	22 $\pm$ 8		31	2 $\pm$ 10 <sup>a</sup>	
●	1	20 $\pm$ 3 <sup>a</sup>	●	18	16 $\pm$ 3 **	●	32	nb <sup>a</sup>	
	3	nb <sup>a</sup>		21	37 $\pm$ 6 **		33	2 $\pm$ 10	
●	6	4 $\pm$ 8		23	5 $\pm$ 7		34	4 $\pm$ 0.3 <sup>a</sup>	
●	9	49 $\pm$ 9 **	●	25	16 $\pm$ 11	●	35	nb	
	10	4 $\pm$ 5		28	nb <sup>a</sup>		38	2 $\pm$ 7	
	12	20 $\pm$ 9		29	nb <sup>a</sup>		40	nb	
	16	50 $\pm$ 4 **		30	nb <sup>a</sup>				

JNJ-47965567 (JNJ) was used at 1  $\mu$ M. The colour of the spots indicates the family of the compounds: (2-chlorobenzoyl)purines (red), (2-chlorosulfonyl)purines (orange), 1-aryl-2-purinyloethanones (yellow), arylsulfonyltheophyllines (blue), 1-(2,4-dichlorophenyl)-2-xanthinyl ethanones (lilac), other derivatives (pink). Data are shown as mean  $\pm$  SEM of triplicates of three different cultures. Statistical analysis has not been performed for n < 3. <sup>a</sup> n = 2 \* p < 0.05; \*\* p < 0.01; nb: no blockade.

#### 5.3.4. P2X7-induced interleukin-1 $\beta$ release in rat peritoneal macrophages

P2X7 has an important role in inflammation, as it is also highly expressed on the membrane of immune cells. Briefly, it is well-known that P2X7 activation is one of the possible triggers of the NLRP3 inflammasome in macrophages and microglia (Burm *et al.*, 2016; Di Virgilio *et al.*, 2017). This leads to the enzymatic cut of pro-IL-1 $\beta$  into IL-1 $\beta$ , which is subsequently released from the cell (see chapter 3.3).

Thanks to a collaboration with the group of Dr. Javier Egea of the Hospital Universitario de la Princesa (Madrid) that studies the NLRP3 inflammasome, we could assess if P2X7 inhibition caused by our novel potential antagonists had a pharmacological relevance in inflammation like the blockers already described in the scientific literature, by decreasing the levels of IL-1 $\beta$  released by macrophages.

To evaluate this, we collected mouse macrophages, gathered in the peritoneum after injection of thioglycolate. They were primed with LPS, which induces the expression of pro-IL-1 $\beta$  by the activation of TLR4. Then, they were incubated with test compounds at different concentrations for 15 min, and

stimulated with ATP (5 mM) for other 30 min. The culture medium was collected and IL-1 $\beta$  levels were detected by ELISA. JNJ-47965567 was used as positive control.

Only few compounds were evaluated, in particular those synthesised in the first set. Among these, the arylpurinyl ethanone **9** and the arylsulfonyl purine **27** showed a significant inhibition of IL-1 $\beta$  release at 1  $\mu$ M (Figure 38). We studied their behaviour at different concentrations, demonstrating a concentration-response trend (Figure 39). Their blocking activity is not as potent as that of JNJ-47965567, but is apparently higher than the one obtained in the hP2X7-HEK293 cell line, since they can inhibit around the 50 % of the response at 1  $\mu$ M.

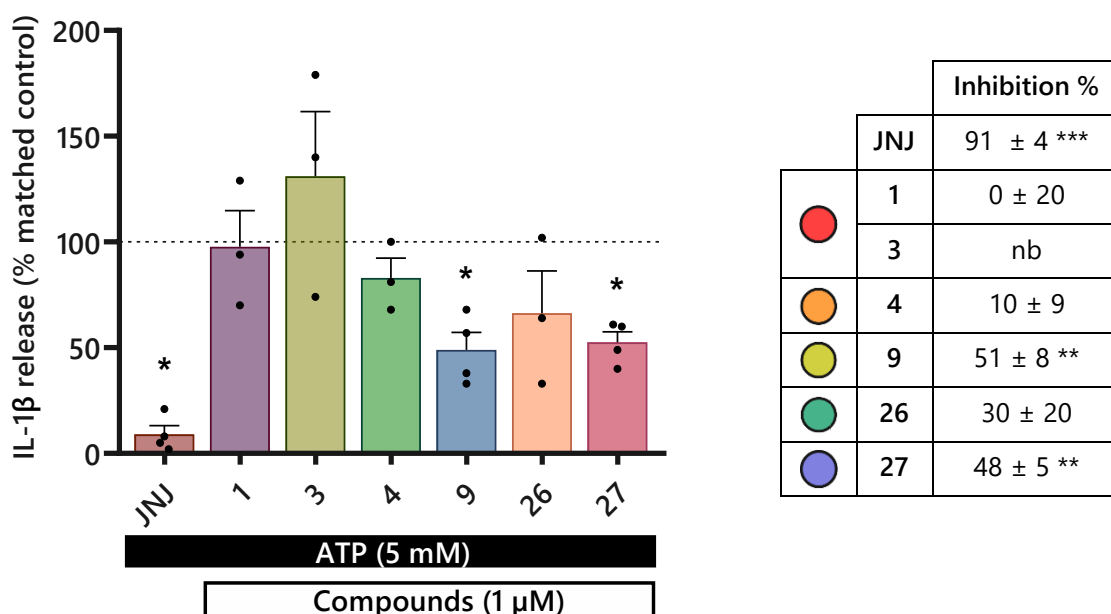


**Figure 38.** ATP-induced IL-1 $\beta$  release in mouse macrophages after 15-min-long incubation of some of our compounds. The colour of the spots indicates the family of the compounds: (2-chlorobenzoyl)purines (red), (2-chlorosulfonyl)purines (orange), 1-aryl-2-purinyloethanones (yellow), (2-chlorobenzoyl)theobromine (green), arylsulfonyltheophyllines (blue). JNJ-47965567 (JNJ) was tested at 0.1  $\mu$ M. Data are shown as mean  $\pm$  SEM of triplicates of three different mice. In the graph, \*statistical significant. In the table, \*\*p < 0.01; \*\*\*p < 0.001.



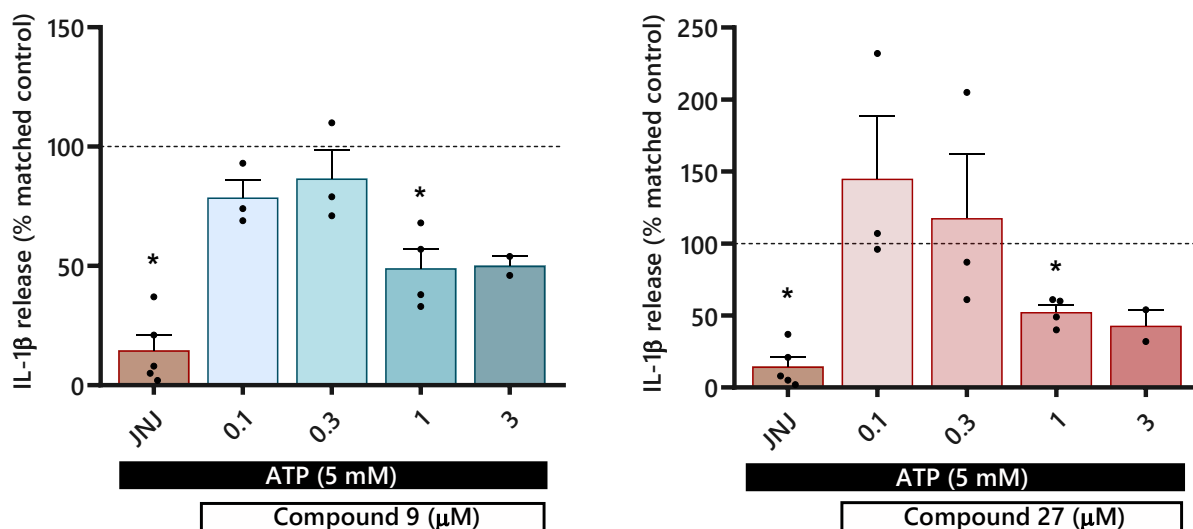


**Figure 39.** Concentration-dependent ATP-induced IL-1 $\beta$  release in mouse macrophages following incubation of compounds 9 and 27. JNJ-47965567 (JNJ) was tested at 0.1  $\mu$ M. Data are shown as mean  $\pm$  SEM of triplicates of three different mice. In the graph, \*statistically significant. See the table in Figure 38 for detailed p values.

In summary, the activity of compound 9 was confirmed, whereas the activity of 27 remains still elusive. ATP currents confirm that it has a certain inhibitory activity on P2X7, but this does not exclude that it could affect some Ca<sup>2+</sup>-mediated pathways (Swanson *et al.*, 2019; Yang *et al.*, 2019), which would explain why this arylsulfonyl purine shows a similar activity to an arylpurinyl ethanone in this model respect to the others. Other possible speculations are that this arylsulfonyl purine could directly inhibit the NLRP3 inflammasome, since other sulfonamides have been described to exhibit such an effect (Zahid *et al.*, 2019). Finally, exists the possibility that compound 27 has greater affinity for the mP2X7 than for hP2X7.

### 5.3.5. Selectivity of the non-nucleotide purine derivatives on the P2X subtypes

In order to assess the selectivity of the compounds on the P2X7 subtype, we took advantage of the *X. laevis* oocytes model described in chapter 5.3.2. In fact, it is possible to easily change the biological target expressed by these cells just by injecting the corresponding cRNA into the cytoplasm. We decided to test our compounds on several available constructs, *i.e.* rat P2X1, 2, 4 and 7 subtypes, of high physiological relevance. Additionally, the measurement of the blockade on rP2X7 allowed us to evaluate whether they showed interspecies activity, an issue that complicated drug discovery

programmes in the past. In fact, several pharmacodynamic differences have been reported for some antagonists between h/mP2X7 and rP2X7 (see chapters 3.2 and 3.4). This part of the project was also performed during the secondment at Ludwig-Maximilians University of Munich (Germany) under the supervision of Prof. Annette Nicke.

After experimental optimisation of both protein expression and effective ATP pulse (see experimental section, chapter 8.5.4), we performed an initial screening of all the compounds on the rP2X4. None of them showed P2X4 antagonistic activity but, surprisingly, some of them potentiated ATP (30  $\mu$ M)-induced currents at 100  $\mu$ M (compounds **30**, **36**, **38** and **40** – Figure 40 and Table 8), although with low reproducibility. cRNA-injected amount, oocytes destabilisation after exhaustive currents, and different basal current intensity are some of the factors that are responsible for high variability in responses. Nevertheless, we consider that the effect of compound **36** on rP2X4 is consistent and it could be also better investigated as a potential positive allosteric modulator (PAM) of this receptor, an interesting tool for the study of the myelination process of oligodendrocytes and its potential therapeutic benefit in multiple sclerosis.

Looking at the structures of those possible rP2X4 PAMs, they all share a xanthine-like core, except for **38**. Compound **30** is an arylsulfonyl theophylline, while **36** is the theobromine derivative of the arylxanthinyl ethanone series. Compound **40** shares some similarities with **36**, because of the alkylated N1 position, and the carbonyl at position C6. If the activity of **40** on rP2X4 were confirmed with further experiments, some clues on the structure-activity relationships for this family of P2X4 enhancers could be extrapolated. In fact, it seems that modifications at position C2 of the scaffold are allowed, as well as the removal of the arylethanone moiety instead of a simple benzyl, the variation of methyl position on N7 and N9 of the purine scaffold, and finally the removal of the chlorine at position 4 of the aryl group.

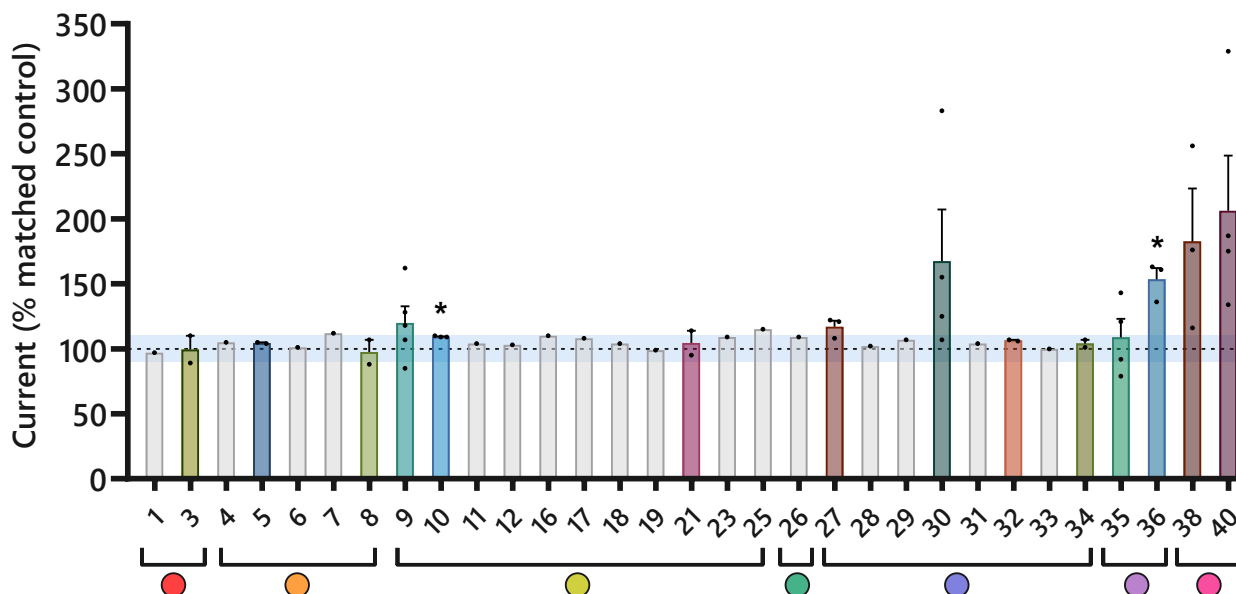


**Figure 40.** ATP (30  $\mu$ M)-induced currents measured by TEVC in rP2X4-expressing *X. laevis* oocytes. Compounds were assayed at 100  $\mu$ M. Grey bars represent compounds tested only once. The colour of the spots below each group of columns indicates the family of the compounds: (2-chlorobenzoyl)purines (red), (2-chlorosulfonyl)purines (orange), 1-aryl-2-purinyloethanones (yellow), (2-chlorobenzoyl)theobromine (green), arylsulfonyltheophyllines (blue), 1-(2,4-dichlorophenyl)-2-xanthinyl ethanones (lilac), other derivatives (pink). The light blue area shows the variability range determined for this technique. \*statistical significant (Table 8)

**Table 8.** Values of ATP (30  $\mu$ M)-induced currents for each synthesised compound (100  $\mu$ M) measured by TEVC in rP2X4-expressing *X. laevis* oocytes.

		Current %			Current %			Current %
●	3	100 $\pm$ 10 <sup>a</sup>	●	27	117 $\pm$ 5	●	35	109 $\pm$ 14
●	5	104 $\pm$ 5		30	167 $\pm$ 40		●	36
	8	97 $\pm$ 9		32	106 $\pm$ 0.5 <sup>a</sup>	●		38
●	9	120 $\pm$ 13		34	104 $\pm$ 3 <sup>a</sup>		40	206 $\pm$ 43
	10	109 $\pm$ 0.3 <sup>**</sup>						
	21	104 $\pm$ 9 <sup>a</sup>						

The colour of the spots indicates the belonging family of compounds: (2-chlorobenzoyl)purines (red), (2-chlorosulfonyl)purines (orange), 1-aryl-2-purinyloethanones (yellow), arylsulfonyltheophyllines (blue), 1-(2,4-dichlorophenyl)-2-xanthinyl ethanones (lilac), other derivatives (pink). Data are shown as mean  $\pm$  SEM of at least two different oocytes coming from at least two different frogs. Statistical analysis has not been performed for  $n < 3$ . <sup>a</sup> $n = 2$ ; <sup>\*</sup> $p < 0.05$ ; <sup>\*\*</sup> $p < 0.01$ .

Only few compounds were tested on rP2X1. Compound **9** did not show any inhibitory activity on this channel, as well as the other test compounds, *i.e.* **10**, **27**, **36** and **40**. However, these are preliminary studies that need to be refined. Only compound **5**, **9** and **21** were tested on rP2X2, having no significant inhibitory actions. The arylpurinyl derivatives **9** and **21** were finally tested on rP2X7. Compound **9** showed higher potency on rP2X7 than on the human orthologue. This was verified also by the fact that several washouts were necessary to completely restore ATP currents (Figure 41). These data not only confirm that this novel compound can inhibit P2X7, but also that it is selective for the P2X7 subtype, since it showed no effect on the other subtypes challenged (Figure 41). Analogously, its close derivative **21**, which bears an iodine instead a chlorine at C6, showed an enhanced inhibition of the rP2X7 current, compared with the inhibition found in the human orthologue. This would probably mean that the arylpurinyl ethanones that possess certain inhibitory activity on the hP2X7 would present an augmented inhibitory potency in the rat orthologue. These considerations validate our chemical design model, prompting further exploration of the chemical space under this family to discover extended antagonists, with improved pharmacokinetic properties.

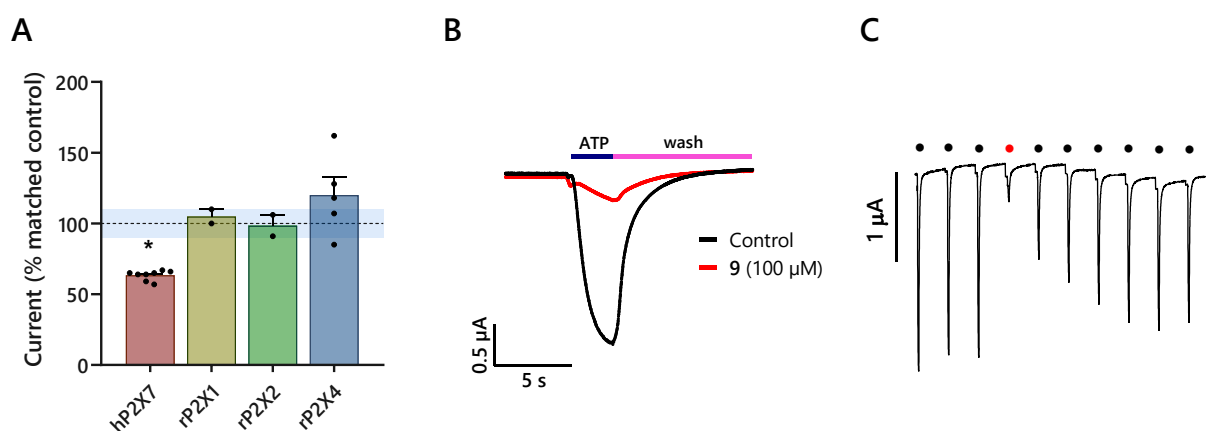


**Figure 41.** **A**) ATP-induced currents in presence of compound **9** (100 μM) on different P2X subtypes, measured by TEVC in *X. laevis* oocytes. The light blue area shows the variability range determined for this technique. **B**) Representation of an example of ATP current inhibited by compound **9** in rP2X7 receptor, expressed by *X. laevis* oocytes. **C**) Concatenated current responses after a 3 s application of ATP (30 μM). Black dots indicate each ATP pulse. The red dot indicates the ATP pulse after the incubation (3 min) of compound **9**.

### 5.3.6. Partial conclusions

From the pharmacological experiments here reported, the following partial conclusions arise:

- 1-aryl-2-purinylyl ethanones **9**, **16** and **18** (10  $\mu\text{M}$ ) inhibited the P2X7-mediated YO-PRO-1 uptake of more than 50 %, as well as did the arylsulfonyl purine **5** and theophylline **27**. Other ethanone derivatives, such as **10**, **17**, **19**, **21**, and **25** blocked less potently the receptor in this assay. The other compounds did not show any significant activity.
- ATP-induced currents in hP2X7-expressing *X. laevis* oocytes were successfully inhibited by compound **9**, **10**, **21**, and **25** (100  $\mu\text{M}$ ), which are all analogous derivatives of the ethanone series. Also, the arylsulfonyl theophylline **27** confirmed its activity as P2X7 antagonist.
- 1-aryl-2-purinylyl ethanones **9**, **16**, **18**, and **21** (10  $\mu\text{M}$ ) significantly blocked  $[\text{Ca}^{2+}]_c$  variations in hP2X7-expressing HEK293 cells, even though compound **18** showed only a small percentage of inhibition. Arylsulfonyl theophylline **27** did not inhibit BzATP-elicited  $[\text{Ca}^{2+}]_c$  influx.
- Compound **9** blocked  $[\text{Ca}^{2+}]_c$  variations in a concentration-dependent fashion, with an  $\text{IC}_{50}$  of 13.7  $\mu\text{M}$ .
- Among the small array of compounds tested in murine peritoneal macrophages, derivatives **9** and **27** (1  $\mu\text{M}$ ) stood out for their concentration-dependent blockade on the mP2X7-mediated IL-1 $\beta$  release. Thus, they are able to modulate *in vitro* neuroinflammatory cytokines release.
- Compound **9** acts selectively on the P2X7 receptor, giving no current variations when oocytes are injected with P2X1, P2X2, and P2X4 cRNAs. Compound **27** does not inhibit the P2X1 and P2X4 receptors either.
- Derivative **9** acts on human, rat and mouse P2X7 receptors, being more potent on the rat orthologue, as shown by TEVC.
- (1-aryl-2-oxoethyl)theobromine **36** potentiated consistently ATP currents in rat P2X4 receptors, working as a potential positive allosteric modulator. Arylsulfonyl theobromine **30**, 1-aryl-3-purinylyl propanone **38**, and 1-benzyl-6-oxopurine **40** also enhanced them, but further studied are necessary to confirm it.

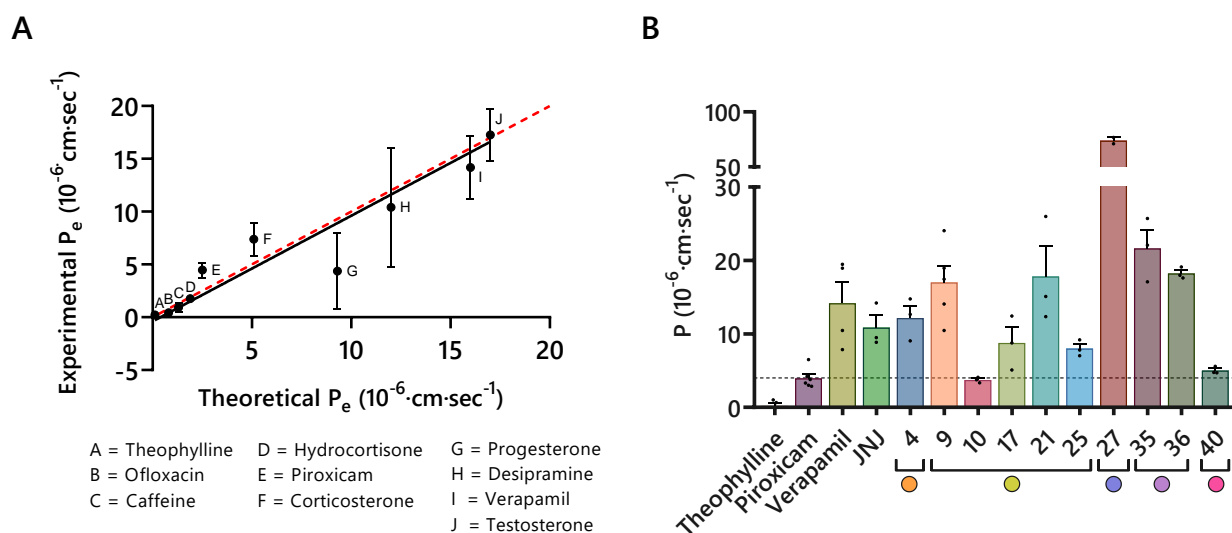
## 5.4. Evaluation of blood-brain barrier permeability

### 5.4.1. Blood-brain barrier permeability of the non-nucleotide purine derivatives

To evaluate whether the prediction of the physicochemical properties of the synthesised compounds were adequate to reach the CNS *via* the BBB, we decided to fine-tune the parallel artificial membrane permeability assay (PAMPA) in our laboratory. This *in vitro* method measures the molecular ability of compounds to cross a lipophilic membrane by passive diffusion.

First, the protocol was set up and optimised for a series of standard compounds, whose permeability values have been reported in the literature (Di *et al.*, 2003; Palomo *et al.*, 2012). These compounds cover a large range of effective permeability coefficients ( $P_e$  expressed as  $10^{-6}\cdot\text{cm}\cdot\text{s}^{-1}$ ). In detail, we used theophylline (reported  $P_e = 0.12$ ), ofloxacin ( $P_e = 0.8$ ), caffeine ( $P_e = 1.3$ ), hydrocortisone ( $P_e = 1.9$ ), piroxicam ( $P_e = 2.5$ ), corticosterone ( $P_e = 5.1$ ), progesterone ( $P_e = 9.3$ ), desipramine ( $P_e = 12$ ), verapamil ( $P_e = 16$ ) and testosterone ( $P_e = 17$ ). We reproduced these values by varying compound concentrations (100 or 150  $\mu\text{M}$ ) and time of incubation (4 or 18 h). We saw that selecting 100  $\mu\text{M}$  of compound, incubated for 4 h, allowed us to obtain  $P_e$  values consistent with the theoretical ones (Figure 42A). Progesterone is the only standard that did not give reproducible results. Compounds with high coefficients showed a high variability, which influenced the linear regression shown in Figure 42A.






Representative compounds of the different families were tested in the PAMPA assay. Most of them showed an elevated permeability that should guarantee their CNS distribution (Figure 42B and Table 9). According to Di and co-workers (Di *et al.*, 2003), the threshold value of  $P_e$  estimated for compounds that reach the CNS is  $4 \cdot 10^{-6} \text{ cm}\cdot\text{s}^{-1}$ . Among the tested compounds, **10** presents a value below 4, lower than other structural analogues, despite it bears an additional chlorine atom respect to **9**. Replacement of chlorine with fluorine (**25**) leads to a better permeability, but not as much as not functionalising the C2 position of the purine core. The *N*-sulfonylation of the purine scaffolds apparently decreased the permeability, according to PAMPA, respect to the corresponding *N*-alkylation, since compound **4** crosses lipophilic barriers in a lower rate than **9**, although they share the same purine scaffold bearing a chlorine at C6. The *N*-alkylation and the *N*-sulfonylation of theophyllines induced a huge increase of permeability, as shown by **27**, **35** and **36**, despite the xanthine core itself is not inclined to passively cross a lipophilic membrane (see caffeine as control). Finally, the xanthine-like core of compound **40** showed a decreased permeability due to the chlorine at position C2, as commented above.



**Figure 42.** A) Linear regression built with the values of ten standard compounds with known effective permeability ( $P_e$ ) for PAMPA optimisation. The red line shows the theoretical curve in case of perfect correlation between theoretical values and experimental ones at our conditions (slope = 1). The black line shows the fitting of our measurements (slope = 0.8912,  $R^2 = 0.6575$ ). B) Effective permeability ( $P_e$ ) values measured for some of the synthesised compounds. Theophylline, piroxicam and verapamil were used as controls. The colour of the spots below each group of columns indicates the belonging family of compounds: (2-chlorosulfonyl)purines (orange), 1-aryl-2-purinyloethanones (yellow), arylsulfonyltheophyllines (blue), 1-(2,4-dichlorophenyl)-2-xanthinyl ethanones (lilac), other derivatives (pink). Data are shown as mean  $\pm$  SEM of triplicates of at least three independent experiments. \*statistical significant (see Table 9 for further details).

We have previously discussed that compounds **10** and **27** could act within the cell triggering off-target effects, which could lead to ambiguous  $[\text{Ca}^{2+}]_c$  measurements or released IL-1 $\beta$  levels in macrophages. PAMPA confirmed the very high permeability of compound **27**, whereas it did not confirm that one of compound **10**. A further evaluation of whether this derivative gets stuck into the lipid membrane could explain its low permeability constant and its lack of activity on  $[\text{Ca}^{2+}]_c$  oscillations.

**Table 9.** Values of effective permeability through lipid membrane measured by PAMPA.

		$P_e$ ( $10^{-6}\cdot\text{cm}\cdot\text{s}^{-1}$ )			$P_e$ ( $10^{-6}\cdot\text{cm}\cdot\text{s}^{-1}$ )
<b>Theophylline</b>		$0.21 \pm 0.37$	<b>Verapamil</b>		$14 \pm 3$
<b>Piroxican</b>		$3.9 \pm 0.5$	<b>JNJ</b>		$11 \pm 2$
	<b>9</b>	$17 \pm 2$		<b>4</b>	$12 \pm 2$
	<b>10</b>	$3.7 \pm 0.2$		<b>27</b>	$74 \pm 3$
	<b>17</b>	$8.8 \pm 2.1$		<b>35</b>	$22 \pm 2$
	<b>21</b>	$18 \pm 4$		<b>36</b>	$18 \pm 0.4$
	<b>25</b>	$8.0 \pm 0.63$		<b>40</b>	$5.0 \pm 0.3$

The colour of the spots indicates the belonging family of compounds: (2-chlorosulfonyl)purines (**orange**), 1-aryl-2-purinyloethanones (**yellow**), arylsulfonyltheophyllines (**blue**), 1-(2,4-dichlorophenyl)-2-xanthinyl ethanones (**lilac**), other derivatives (**pink**). Data are shown as mean  $\pm$  SEM of triplicates of at least three independent experiments.

#### 5.4.2. Evaluation of compounds affinity for the P-glycoprotein efflux pump

Many xenobiotics are rejected by cells through the so-called efflux pumps. These are active transporters usually categorised into different families (Liu, 2019). One of the most studied and responsible for drug resistance is the ATP-binding cassette (ABC), which also includes the permeability glycoprotein (P-glycoprotein or Pgp). The expression of Pgp in the human brain is well known, particularly on the luminal membrane of microvessel endothelial cells (capillaries and venules in particular) (Wilhelm *et al.*, 2016). Thus, it is fundamental to evaluate if novel compounds, designed to target the CNS, are substrates of this transporter and are expelled back into the systemic circulation instead of being retained in brain tissues.

We decided to test compounds **9** and **27** with this purpose, since they showed an interesting inhibitory activity on P2X7 and high permeability through lipid membranes (PAMPA). In order to predict whether they are able to endure in the CNS, we measured their ability to stimulate the Pgp ATPase activity by an ATP luminescence assay. Together with test compounds, we also measured the effect of the well-known Pgp substrate verapamil and the P2X7 standard blocker JNJ-47965567 (JNJ), all of them tested at 10  $\mu\text{M}$  (Figure 43).



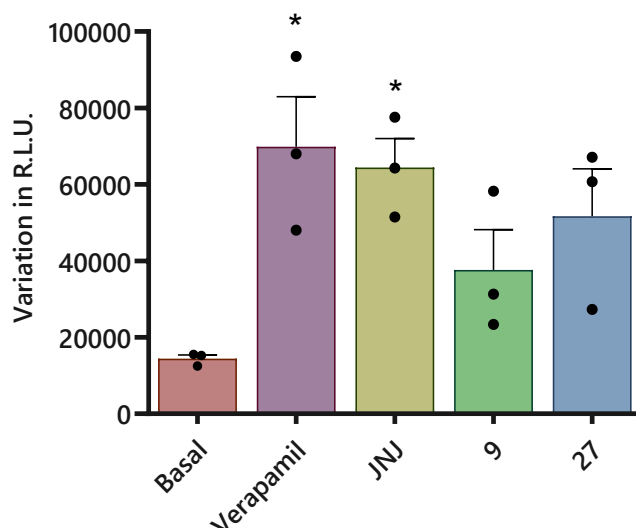


**Figure 43.** Effect of compounds **9** and **27** on Pgp ATPase activity, compared with those of the Pgp substrate verapamil and the P2X7 standard blocker JNJ-47965567 (JNJ). Data are presented as the mean  $\pm$  SEM of triplicates of three individual experiments. \* $p < 0.05$

The Pgp substrate verapamil up-regulated the ATPase activity of Pgp, measured as variation in luminescence (R.L.U. – see experimental section, chapter 8.5.7). Surprisingly, JNJ-47965567 strongly activated Pgp ATPase, too, meaning that it is likely to be an important substrate of the efflux pump. This was not reported yet in the literature, although *ex vivo* radioligand assays in rat brains demonstrated the capacity of JNJ-47965567 to endure in the CNS for at least 2 h (Bhattacharya *et al.*, 2013), with a continuously decrease in concentration during time (Letavic *et al.*, 2013). Unlike JNJ-47965567, compounds **9** and **27**, did not affect Pgp ATPase activity in a statistical significance ( $P = 0.09$  and  $0.16$ , respectively). Considering that human and rat P-glycoprotein activities are usually comparable (Jain *et al.*, 2018; O'Brien *et al.*, 2013; Suzuyama *et al.*, 2007), our data suggest that our compounds could persist in the CNS similarly or even better than JNJ-47965567, despite its enhancing activity on the Pgp.

### 5.4.3. Partial Conclusions

From the pharmacological experiments here reported, the following partial conclusions arise:

- Most of the tested compounds featured good permeability properties through lipid membranes, as assessed by PAMPA. Xanthine derivatives penetrate better than purine ones. Finally, halogens at position C2 of the purine core reduced compounds permeability.

- Compounds **9** and **27** did not act as P-glycoprotein substrates according to the Pgp ATPase assay. However, they showed a tendency to increase the enzymatic activity, though in a statistically non-significant way.
- Surprisingly, the reference compound **JNJ-47965567** increased significantly the Pgp ATPase activity.

## 5.5. Docking study of compound **9** at the allosteric pocket of the P2X7 receptor

As described in chapter 3.2, three binding pockets have been described so far for P2X7. We performed a molecular docking study to evaluate where and how the most potent compound of the series (**9**) is supposed to bind. Most of the antagonists developed so far act in the highly lipophilic allosteric binding pocket located between neighbouring subunits in the extracellular domain (Figure 44). For this reason, we ran docking experiments in this binding site using the model described by Dayel and coworkers (Table 10) (Dayel *et al.*, 2019).

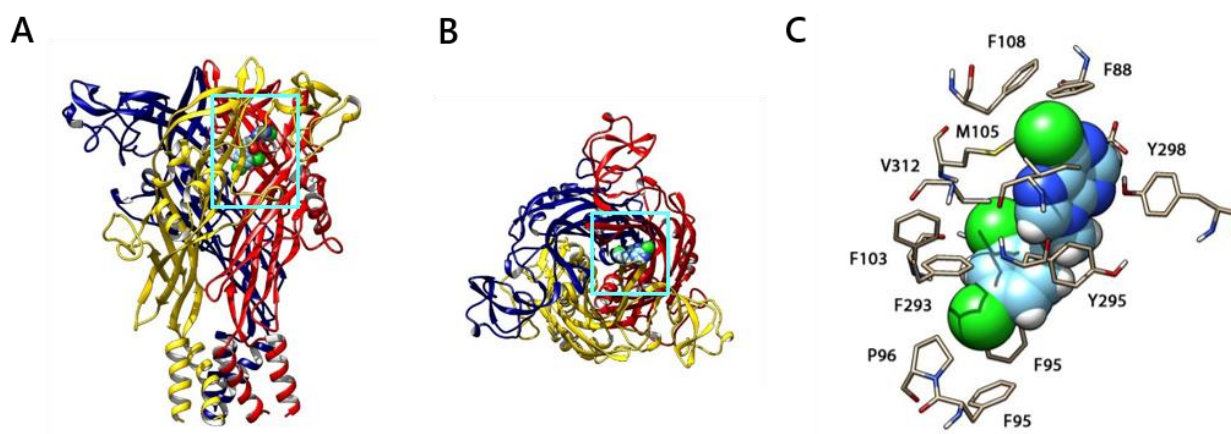


**Figure 44.** Lateral (A) and top (B) views of the ribbon-like representation of P2X7. The predicted binding site of compound **9** is indicated by the cyan frame. The residues defining the binding pocket are shown in C.

The majority of the poses obtained (between -8.8 and -8.5 kcal/mol) placed the dichloroaryl core deep into the pocket, interacting in a presumably  $\pi$ - $\pi$  stacking with Phe 95 (F95), 103 (F103), and 293

(F293), as showed by calmidazolium in the literature (Dayel *et al.*, 2019). Besides, all the antagonists crystallised with the pdP2X7 show their most lipophilic moiety in this vestibule (Karasawa and Kawate, 2016). The purine core, instead, is placed among Tyr 295 (Y295) and 298 (Y298), as well as Ile 310 (I310) and Met 105 (M105). The top area of the binding pocket is defined by the presence of Phe 88 (F88) and 108 (F108), which suggests a halogen-aromatic interaction of the chlorine at C6 with these residues (Figure 44). This would explain why polar groups at this position are not permitted to keep the biological activity of the compounds. Moreover, the replacement of the chlorine with the bulkier iodine at C6 reduces potency, considering that the distance between the halogen and F88/F108 is of about 3.5 Å (Sirimulla *et al.*, 2013). However, the presence of F88 and F108 would also justify why the replacement of the chlorine at position C6 with a phenyl group, like in compound **16**, would maintain the activity. In fact, additional  $\pi$ - $\pi$  staking interactions could be involved, in spite of its big volume. Noteworthy, many residues of this pocket have shown an essential contribution for receptor blockade in mutagenesis experiments (Dayel *et al.*, 2019; Karasawa and Kawate, 2016). Docking **9** at the orthosteric binding pocket did not achieve any result in terms of global energy. Our compound was also docked at the allosteric pocket in the central vestibule (Bidula *et al.*, 2019a), giving some possible result in term of energy (-6.3 kcal/mol the most representative), but with many uncertain binding poses. This pocket was indeed characterised for ginsenoside derivatives with positive allosteric activity (Bidula *et al.*, 2019a). Further investigations are needed to validate this *in silico* prediction and the potential involvement of these residues in ligand binding.

**Table 10.** Summary of the poses calculated by docking compound **9** and reference compound **AZ11645373** in the allosteric binding pocket of the rP2X7 receptor.

Pose	Compound 9			AZ11645373		
	Affinity (kcal/mol)	Dist. from RMSD l. b.	Best mode RMSD u.b.	Affinity (kcal/mol)	Dist. from RMSD l. b.	Best mode RMSD u.b.
1	- 8.8	0.000	0.000	- 11.2	0.000	0.000
2	- 8.8	1.321	2.041	- 11.2	3.237	5.982
3	- 8.7	2.340	3.411	- 11.1	7.153	10.479
4	- 8.7	1.857	2.261	- 11.1	7.256	10.242
5	- 8.7	2.302	3.071	- 11.1	1.192	1.804
6	- 8.6	2.857	8.352	- 11.1	7.231	10.222
7	- 8.5	2.901	7.025	- 11.0	2.393	5.765
8	- 8.5	8.760	10.224	- 11.0	3.257	10.972
9	- 8.5	4.060	9.077	- 10.9	2.277	5.366

General discussion

## 6. General discussion

Despite the efforts carried out by *Big Pharma* and *Academia* in the last decade, only two recently-discovered drugs to block P2X7 have reached clinical trials to combat neuroinflammation, JNJ-54175446 and JNJ-55308942 (Figure 22). Phases I were completed for both, including PET studies to confirm receptor occupancy in the CNS. However, only JNJ-54175446 has entered phase II for the potential treatment of a CNS disease (*i.e.* major depression) (Recourt *et al.*, 2020). Indeed, the other candidates capable of blocking P2X7 and studied in clinical trials had been proposed for the treatment of peripheral disorders (Eser *et al.*, 2015; Keystone *et al.*, 2012; Stock *et al.*, 2012). This fact evidences the critical role that PK properties play in the selection of a drug candidate for CNS disorders, besides high potency, selectivity, and interspecies blocking effect. Most of the studies reported in literature to find a proper P2X7 antagonist for CNS diseases have focused only on pharmacological potency. When a head compound has been selected, it commonly lacked an adequate PK profile to penetrate the CNS, forcing medicinal chemists to rethink all the design programmes. Such is the case of the adamantane derivatives, which showed good P2X7 antagonist effect but a mediocre PK profile ( $t_{1/2} = 0.22$  h) (O'Brien-Brown *et al.*, 2017). In this work, we have paid attention to BBB permeability, starting from the molecular design. Firstly, we selected well-known scaffolds that are present in drugs with recognised CNS activity. Then, we corroborated that the target compounds fulfilled Lipinski's rule of five. These preliminary considerations guided us to synthesise and study the pharmacological scope of novel non-nucleotide purine derivatives as potential P2X7 antagonists. The purine scaffold of these novel compounds has been linked to a lipophilic group, that is a substituted benzene, through a small spacer, namely a carbonyl, a sulfonyl, and an ethanoyl moiety. All the data obtained through the pharmacological assays revealed that these features fit the structural properties necessary to inhibit P2X7, but that more investigation is needed to fully define them.

The most potent compound of our series (**9** – 2-(6-chloro-9H-purin-9-yl)-1-(2,4-dichlorophenyl)-ethan-1-one) belongs to the family that possesses an ethanoyl group as spacer. Only compound **27**, which bears a sulfonyl spacer and a theophylline core in its structure, showed a certain blockade among the derivatives of the other families. All its derivatives lose their inhibitory potency in most of the pharmacological assays performed, leading us to consider that it might interact differently with the P2X7 receptor than purinylethanones, or even modulate secondary intercellular pathways. Hence, only deeper SAR studies by structural modification of the theophylline core of compound **27** would clarify its potential P2X7 blockade activity.

Compound **9**, which we have been named **ITH15004**, has a chlorine at C6, potentially replaceable with other halogens like iodine. However, this led to a decrease of drug potency, probably due to the larger radius that iodine presents, which do not fit the “cap” formed by F88 and F108 in the allosteric pocket of the receptor (Figure 44). Replacement of the chlorine by a phenyl, like in **16**, might be permitted by favourable  $\pi$ - $\pi$  stacking interactions, but the inclusion of some polar substituent on it would be necessary to increase compound solubility. Low solubility of **16**, in fact, led to contradictory data in this work (e.g. ATP currents in P2X7-expressing oocytes). The insertion of smaller halogens like fluorine, or non-voluminous alkyl chains at this position, has not been tested yet, as well as the effect of substituents at position C8 of the purine core. According to the SAR, small substituents at C2 are accepted with a decrease in potency, but only when chlorine is maintained at position C6, like in compounds **10** and **25**, and not **23**. However, a significant reduction in BBB-permeation is expected as happened for compound **20** in PAMPA. The removal of the chlorine at C2' at the aryl group of the ethanoyl derivatives seems detrimental to P2X7 blockade. This might be due to lipophilic interactions with V12 (Figure 44), one of the residues responsible for P2X7 inhibition with other antagonists (Dayel *et al.*, 2019; Karasawa and Kawate, 2016).

**ITH15004** elicits a concentration-dependent blockade of BzATP-evoked  $[Ca^{2+}]_c$  transients in hP2X7-HEK293 cells, with an  $IC_{50}$  of 13.7  $\mu$ M, and blocks a 63 % of the BzATP-induced YO-PRO-1 uptake at 10  $\mu$ M in the same cellular model. At 100  $\mu$ M, it decreases a 47 % of the ATP-activated currents in *X. laevis* oocytes expressing hP2X7. It also showed selectivity towards P2X7, since it did not block rat P2X1, P2X2, nor P2X4, but rP2X7. **ITH15004** also blocked mP2X7, halving the ATP-induced IL-1 $\beta$  release in LPS-primed mouse peritoneal macrophages, and exhibits a high lipophilic membrane permeability in the PAMPA, suggesting it can permeate BBB and gain access to the brain. Although its potency is in the micromolar range, its pharmacodynamic profile and BBB permeability suggest that this non-nucleotide purine derivative could serve as starting point to design and synthesise new P2X7 blockers with moderate potency. This is relevant in the context of drug side effects and safety, which can be compromised by highly potent compounds that target P2X7 in the low nanomolar range. For instance, the complete removal of P2X7 activity in a mouse model of MS caused an exacerbation of the disease, probably due to P2X7-dependent changes in lymphocytic homeostasis (Chen and Brosnan, 2006). This could be explained by the duality that characterises P2X7 receptors. Its “macropore” activation has been related to apoptosis and inflammatory signalling (Di Virgilio *et al.*, 2018), but other P2X7 functions are independent from it, such as phagocytosis and trophic events dependent on the activation of transcription factors and the increase of mitochondrial oxidative phosphorylation (Adinolfi *et al.*, 2010, 2009, 2005). Hence, it seems plausible that a proper P2X7

modulation with a mild antagonist could be more beneficial than a total blockade through a potent drug, above all in a chronic administration regimen. However, much has to be clarified to perfectly understand what the perfect pharmacological strategy could be, above all regarding CNS disorders that have usually multifactorial causes. As for ALS, enhancing the P2X7 on anti-inflammatory M2 microglia at first stages of the disease could be advantageous, while inhibiting it when microglia has already a pro-inflammatory phenotype. Additionally, P2X7 potentiation on muscles seemed to improve innervation and metabolism of myofibers (Fabbrizio *et al.*, 2020), whereas its blockade in the CNS showed to ameliorate motoneuron survival (Ruiz-Ruiz *et al.*, 2020a, 2020b; Volonté *et al.*, 2020). Likely, the design of novel active agents targeting specific domains of the P2X7 C-terminal could reveal a new way to control the positive effect of P2X7 activation, reducing those related to inflammation and cell death, being the C-terminus considered responsible of them. The modulation of the expression of trophic factors induced by an overexpression of functional C-truncated P2X7 isoforms might be considered as well.

**ITH15004** presents not only a good pharmacodynamic profile, but also an improved BBB permeability rate (Figure 42), which represents a fundamental issue that affects the development of agents targeting the CNS. This might be the case of the well-known P2X7 antagonist JNJ-47965567, which was never included in a clinical trial. Although it was demonstrated that it reaches the CNS *in vivo* (Bhattacharya *et al.*, 2013), we observed for the first time that it also increases the Pgp ATPase activity, which could jeopardise its positive effects on CNS disorders. **ITH15004** slightly increased Pgp ATPase activity (Figure 43), but not in a statistically significant fashion, respect to the basal activity of the transporter, and apparently not as much as JNJ-47965567. If further pharmacokinetic studies would confirm good absorption and metabolic stability, we may think that our novel compound could persist in the CNS more or as much as JNJ-47965567. This hypothesis is out of the scope of this work, but it underlines the necessity of a deeper focus on the pharmacokinetic parameters of potential new CNS drugs, as we have intended.

Our compound **ITH15004** is being currently used as pharmacological agent in *in vitro* and *in vivo* studies, such as in embryonal pyramidal neurons to study its effects on neurogenesis compared to other well-known P2X7 antagonists, as well as in retinal 661W and MU-PH1 cells, and the mouse Rd10, a model of retinitis pigmentosa, a degenerative disease of the eyes (Campello *et al.*, 2020). Moreover, additional effects of **ITH15004** on P2X7-dependent and -independent  $Ca^{2+}$  modulation have being studied in bovine chromaffin cells, a neuronal model that has been amply used in our research group (Carbone *et al.*, 2019; Martínez-Ramírez *et al.*, 2020). These studies confirm that our novel lead compound is a valuable pharmacological tool to investigate neuroinflammatory

implications mediated by the P2X7 receptor. Additionally, we have already designed novel derivatives to study the effects of more functionalised moiety at position C6 of the purine core, as well as position C8, which is still unexplored. Modifications on position C4' of the aryl moiety might also result in interesting novel compounds. The latest tasks of this PhD work have focused on optimising the synthesis of reactive intermediates through mild microflow conditions, aimed to be applied for the generation of several novel purine scaffolds, covering the unexplored positions mentioned above.

Our medicinal chemistry programme also disclosed some potential P2X4 positive allosteric modulators (Figure 41). Although further studies are needed for their validation, these could become new pharmacological tools for the characterisation of P2X4 in CNS disorders. In fact, P2X4 potentiation has been suggested for the treatment of alcohol abuse disorders, considering its role in modulating GABA release in neurons (Khoja *et al.*, 2018), but also of Parkinson's Disease for improving L-DOPA-induced motor behaviour (Khoja *et al.*, 2016). Additionally, P2X4 positive modulation has been proposed to increase myelination in oligodendrocytes and microglia phagocytotic activity, with benefits in the symptoms of MS mice (Domercq and Matute, 2019; Zabala *et al.*, 2018). Currently, only ivermectin, a drug already approved by the FDA for the treatment of parasites infection, and other macrocyclic lactone analogues have been studied in CNS diseases (Asatryan *et al.*, 2014; Huynh *et al.*, 2017). They showed good distribution in the CNS, but they are non-specific for the P2X4, targeting also GABA receptors, or the P2X7 (Stokes *et al.*, 2020). A deeper characterisation of 1-(1-aryl-2-oxoethyl) theobromine **36** could validate a novel pharmacological agent, as well as its chemical optimisation through modifications on both the xanthine core and the aryl moiety, as proved by the *M*1-benzyl-6-oxopurine **40**.



A decorative horizontal band with a watercolor splash effect in shades of light blue and white. The word "Conclusions" is centered within this band.

**Conclusions**

## 7. Conclusions

Based on the results of this PhD dissertation, the following **partial conclusions** can be drawn:

- The generation of novel non-nucleotide purine derivatives, comprised of a purine core linked to an *ortho*-haloarene through an ethanoyl spacer gave rise to a novel P2X7 antagonist (**ITH15004**), validating our design model.
- The total synthesis of 31 final compounds has been accomplished in low to good yields. The scarce stability of the first designed compounds (benzoylpurines) was overcome by the design of novel bioisosteres incorporating a sulfonyl or ethanoyl as spacer.
- Several 1-aryl-2-purinyl ethanones showed certain P2X7 blocking activity. **ITH15004** showed consistent blockade in all the pharmacological assays. It is also able to reduce the P2X7-mediated IL-1 $\beta$  release *ex vivo* in mouse macrophages, giving pharmacological significance to its action.
- **ITH15004** is active on mouse, rat and human receptor orthologues and it is P2X7 selective over other P2X subtypes. The screening of our compounds on different P2X subtypes disclosed a new potential P2X4 positive allosteric modulator.
- Most of our derivatives showed adequate physicochemical properties to cross the BBB and reach the CNS. They have good permeability values as assessed by PAMPA, and **ITH15004** does not significantly activate Pgp ATPase activity, suggesting that it shall not be expelled from the CNS by active transport.

Finally, the **general conclusion** is as follows:

- The overall results of this PhD dissertation allow us to conclude that the purine core can be used as main scaffold for the generation of novel non-nucleotide P2X7 antagonists, when an *ortho*-haloarene is substituted at position N9 of the purine through an ethanoyl spacer. The halogen at *ortho* position is relevant for potency, and the derivative bearing two additional chlorines at C6 and C4', namely **ITH15004**, showed the best potency and a promising brain penetration profile to act in the CNS. *Ortho*-chlorobenzene gives rise to a less potent P2X7 antagonist when it is linked to theophylline through a sulfonyl spacer at position N7. **ITH15004** represents a novel pharmacological tool for the *in vitro* and *in vivo* study of neuroinflammation where the P2X7 plays a chief role. Additionally, substitutions at C6 with a more hydrophilic aromatic ring can give rise to optimised compounds with different potency and better pharmacokinetic properties for the development of therapeutic drugs for neurodegenerative diseases.

## Conclusiones

A partir de los resultados de esta Memoria de Tesis se pueden extraer las siguientes **conclusiones parciales**:

- La síntesis de nuevos derivados no-nucleótidos de purina, que incluyen en su estructura un núcleo purínico enlazado a un *orto*-haloareno a través de una etanona como espaciador, ha dado lugar, entre todos los nuevos compuestos analizados, a un nuevo antagonista P2X7 (**ITH15004**), validando así nuestra hipótesis de trabajo.
- La síntesis de un total de 31 compuestos finales se consiguió con rendimientos de bajos a buenos. La escasa estabilidad de la primera familia de compuestos diseñados, basados en una estructura general de benzoilpurina, se superó con el diseño de nuevos bioisómeros que tienen un sulfonilo o una etanona como espaciador.
- Varias 1-*aril*-2-puriniletanonas demostraron una cierta actividad bloqueadora sobre el receptor P2X7. El compuesto **ITH15004** inhibió el receptor de manera reproducible en todos los ensayos farmacológicos empleados. **ITH15004** reduce también la liberación *ex vivo* de IL-1 $\beta$  debida a la activación del P2X7 en macrófagos de ratón, dando un significado terapéutico a su acción farmacológica.
- **ITH15004** actúa sobre el P2X7 de ratón, rata y humano, y es selectivo sobre otros subtipos P2X. El cribado de nuestros compuestos en diferentes subtipos P2X llevó al descubrimiento de un potencial modulador alostérico positivo P2X4.
- La mayoría de los nuevos derivados mostraron propiedades fisicoquímicas adecuadas para cruzar la BHE y llegar al SNC. Poseen buenos valores de permeabilidad, según lo apreciado en el ensayo PAMPA y, además, **ITH15004** no aumentó de manera estadísticamente significativa la actividad ATPasa de la gpP, sugiriendo así que no sería sustrato para este mecanismo de expulsión del SNC por transporte activo.

Para finalizar, la **conclusión general** es la siguiente:

- Los resultados globales de esta Memoria de Tesis nos permiten concluir que la purina puede ser utilizada como núcleo principal para la creación de nuevos antagonistas P2X7 no-nucleótidos, modificada químicamente por la sustitución de *orto*-haloareno en posición N9, preferentemente mediante el empleo de etanona como espaciador. El halógeno en posición *orto* parece esencial para la potencia de estos derivados, y el compuesto **ITH15004**, que lleva dos cloros adicionales

en posición C6 y C4', mostró la mejor potencia y un perfil de permeabilidad prometedor. El grupo *orto*-clorobencénico da lugar a antagonistas P2X7 menos potentes cuando enlaza una teofilina en posición N7 a través de un espaciador sulfonilo. **ITH15004** representa una herramienta farmacológica de nueva generación para el estudio *in vitro* e *in vivo* de la neuroinflamación. Además, el reemplazo del cloro en posición C6 con un anillo aromático con perfil hidrófilo puede servir como punto de partida para la optimización química de estos derivados, que presenten diferentes potencias y mejores propiedades farmacocinéticas para el desarrollo de nuevos medicamentos para el tratamiento de las enfermedades neurodegenerativas.

Experimental section

## 8. Experimental section

### 8.1. General procedures and materials

Solvents and starting materials for chemical procedures were used as supplied by Sigma-Aldrich, Merck KGaA (Madrid, Spain), unless otherwise indicated. Anhydrous and inert conditions for specific reactions were obtained by using a Schlenk line (vacuum purges and argon atmosphere). Solvents were dried and freshly distilled over its corresponding adsorbent. Reactions were controlled by thin-layer chromatography (TLC - silica gel plates from Sigma-Aldrich, Merck KGaA). Detection was made with UV light lamp at 254 nm of wavelength. Flash normal-phase column chromatography (CC) was carried out on a Isolera™ One (Biotage) automatised chromatography station, using silica gel pre-packaged cartridges, unless otherwise indicated.

### 8.2. Molecular design

The novel non-nucleotide purine derivatives were designed based on an extended review of the previous developed P2X7 antagonists. Their physicochemical properties were evaluated using computational software, such as MarvinSketch 19.18 (ChemAxon, Budapest, Hungary) and, in some cases, AutodockTools-1.5.6 (The Scripps Research Institute, La Jolla, CA, USA).

### 8.3. Chemical characterisation

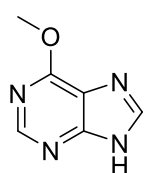
<sup>1</sup>H and <sup>13</sup>C NMR spectra were obtained in a Bruker AVANCE 300 MHz spectrometer and presented in ppm using the residual signal of proton of the corresponding deuterated solvent as internal standard. Examples of the NMR spectra acquired for each family of compounds are shown in the Annexes, chapter 10.1. MS spectra were obtained in an ABSciex QSTAR spectrometer under the high-resolution configuration with electrospray as ionization source. Melting points were obtained in a Stuart SMP-10 apparatus and are uncorrected. Purity of the tested compounds was analysed by combustion elemental analysis (Anal.) on a LECO-CHNS-932 station or by HPLC-UV with a Varian Prostar analytical liquid chromatographer. Values of C, H, and N from elemental analyses data were within 0.4 % of the calculated values for each final compound. Purity of compounds was > 95 %, except for **20** that was 93 %. X-Ray diffractions for selected compounds were acquired from a Bruker D8 Kappa series apparatus, with Mo K $\alpha$  radiation of graphite monochromator at  $\lambda = 0.71073 \text{ \AA}$ . X-Ray results are shown in Annexes. CIF files have been deposited in the Cambridge Crystallographic

Data Centre (CCDC) with the codes CCDC2023913 for compound **26**, and CCDC2023914 for compound **10**. Tested compounds do not present potential pan-assay interference compounds (PAINS) activity, according to screening in <http://zinc15.docking.org/patterns/home> (Aldrich *et al.*, 2017).

## 8.4. Synthesis

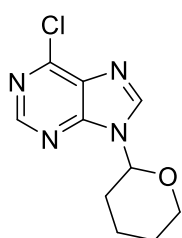
### 8.4.1. Preparation of synthetic precursors **2**, **13–15**, **20**, **22**, **24**, **37** and **39**

#### 8.4.1.1. 6-methoxypurine (**2**)



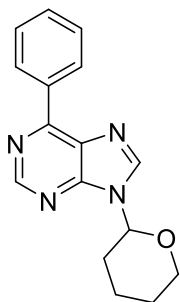
Metallic Na (200 mg, 9.1 mmol) was slowly added to MeOH (10 mL) in a flask under dry and inert conditions. After 30 min stirring at rt, 6-chloropurine (350 mg, 2.3 mmol) was added. The mixture was heated to 60 °C and stirred for 2 h. The solvent was then evaporated under reduced pressure and the crude purified by filtration through a silica plug (gradient of MeOH in DCM, 0/100 to 20/80). The filtrate was evaporated under vacuum obtaining a white powder that corresponded to **2** in quantitative yield. <sup>1</sup>H NMR (300 MHz, CD<sub>3</sub>OD) δ 8.49 (s, 1H, H2), 8.27 (s, 1H, H8), 4.18 (s, 3H, CH<sub>3</sub>).

#### 8.4.1.2. 6-chloro-9-(tetrahydro-2H-pyran-2-yl)purine (**13**)



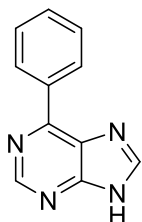
6-chloropurine (1.5 g, 9.7 mmol) and p-toluensulfonic acid (PTSA, 33 mg, 0.19 mmol) was suspended in dry EtOAc (16 mL) in dry and inert conditions. The mixture was heated up to 50 °C, and 3,4-dihydropyran (DHP, 992 μL, 11 mmol) was added dropwise over 5 min. The reaction was stirred at 50 °C for 64 h. Then, aqueous ammonia was added until pH 8. The mixture was diluted with EtOAc (10 mL) and water (10 mL). Then, the organic layer was separated, washed again with water and brine, dried over anhydrous Na<sub>2</sub>SO<sub>4</sub>, filtered, and the solvent evaporated under reduced pressure. The crude was purified by CC (gradient of EtOAc in hexane, 18/82 to 100/0), giving compound **13** as a transparent oil that solidified upon standing (1.45 g, 62 %). <sup>1</sup>H NMR (300 MHz, CDCl<sub>3</sub>) δ 8.75 (s, 1H, H2), 8.34 (s, 1H, H8), 5.80 (dd, J = 10.2 Hz, 2.6 Hz, 1H, CHO), 4.20 (dd, J = 12.8, 3.0 Hz, 1H, CH<sub>2</sub>O), 3.79 (td, J = 11.4, 3.1 Hz, 1H, CH<sub>2</sub>O), 2.28–1.96 and 1.94–1.63 (2m, 6H, (CH<sub>2</sub>)<sub>3</sub>).

#### 8.4.1.3. 6-phenyl-9-(tetrahydro-2H-pyran-2-yl)purine (14)



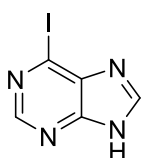
The intermediate **13** (138 mg, 0.58 mmol) was dissolved in freshly distilled toluene (6 mL) under dry and inert conditions.  $K_2CO_3$  (116 mg, 0.84 mmol) and phenylboronic acid (102 mg, 0.84 mmol) were added and the mixture was sonicated for 5 min under Ar bubbling. Tetrakis(triphenylphosphine)palladium (0) (33 mg, 29  $\mu$ mol) was added and the reaction refluxed overnight. After 15 h, the mixture was filtered and the filtrate concentrated under reduced pressure. The residue was purified by CC (gradient of EtOAc in hexane, 18/82 to 100/0), obtaining **14** as a transparent oil that solidified upon standing (117 mg, 72 %).  $^1H$  NMR (300 MHz, acetone- $d_6$ )  $\delta$  9.01–8.92 (m, 3H, H2' and H2), 8.65 (s, 1H, H8), 7.63–7.52 (m, 3H, H3', H4'), 5.90 (dd,  $J$  = 10.9, 2.4 Hz, 1H, CHO), 4.17–4.07 (m, 1H,  $CH_2O$ ), 3.82 (td,  $J$  = 11.5, 3.1 Hz, 1H,  $CH_2O$ ), 2.45–2.23, 2.20–2.08, 1.99–1.81, 1.79–1.60 (4m, 6H,  $(CH_2)_3$ ).

#### 8.4.1.4. 6-phenylpurine (15)



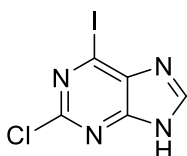
The intermediate **14** (117 mg, 0.42 mmol) was suspended in MeOH (4 mL). Acetyl chloride (8.3  $\mu$ L, 0.12 mmol) was added and the reaction was stirred at rt for 72 h. Then, the solvent was evaporated under reduced pressure, and the residue washed with water (2  $\times$  4 mL) and concentrated under vacuum, giving **15** as a white powder (69 mg, 84 %).  $^1H$  NMR (300 MHz, acetone- $d_6$ )  $\delta$  9.04–8.94 (m, 2H, H2'), 8.93 (s, 1H, H2), 8.56 (s, 1H, H8), 7.65–7.52 (m, 3H, H3', H4').

#### 8.4.1.5. 6-iodopurine (20)



Following the procedure described by Tobrman and co-workers (Tobrman and Dvořák, 2006), 6-chloropurine (100 mg, 0.65 mmol) was suspended in hydriodic acid (1 mL) at 0  $^\circ$ C and stirred for 5 h. Then, the reaction was diluted with water (2 mL) and aqueous ammonia was added until pH 9. The solvent was evaporated under reduced pressure and the residue was purified by CC (gradient of MeOH in DCM, 1/99 to 8/92). The fractions were evaporated under vacuum and the yellow powder obtained was triturated with  $Et_2O$ , obtaining **20** as a yellowish powder (121 mg, 76 %).  $^1H$  NMR (300 MHz, methanol- $d_4$ )  $\delta$  8.63 (s, 1H, H2), 8.58 (s, 1H, H8).

#### 8.4.1.6. 2-chloro-6-iodopurine (22)

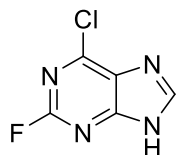


Following the procedure described by Tobrman and collaborators (Tobrman and Dvořák, 2006), 2,6-dichloropurine (100 mg, 0.53 mmol) was suspended in hydriodic acid (1 mL) at 0  $^\circ$ C. After 5 h of stirring, the reaction was diluted with water (2 mL) and aqueous ammonia was added until pH = 9. The mixture was decanted overnight, then filtered,



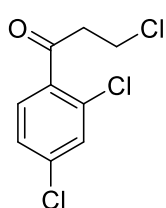
washed with water (1 mL) and dried under vacuum, obtaining **22** as a yellowish powder (123 mg, 83 %).  $^1\text{H NMR}$  (300 MHz, Acetone- $d_6$ )  $\delta$  8.60 (s, 1H, H8).

#### 8.4.1.7. 6-chloro-2-fluoropurine (**24**)



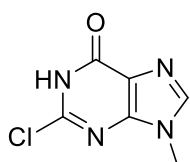
Following the procedure described by Kim and colleagues (Kim *et al.*, 2003), 2-amino-6-chloropurine (100 mg, 0.59 mmol) was added to a solution of hydrofluoric acid in pyridine (70 %, 1.5 mL) at  $-50\text{ }^\circ\text{C}$ . The reaction was allowed to warm up to  $-30\text{ }^\circ\text{C}$  and tert-butyl nitrite (105  $\mu\text{L}$ , 0.88 mmol) was added. The reaction was stirred at  $-30\text{ }^\circ\text{C}$  for 20 min, then it was quenched by adding water and ice (4 mL). The mixture was extracted with  $\text{CHCl}_3$  (5 x 3 mL) and the organic fractions washed with brine, dried over anhydrous  $\text{Na}_2\text{SO}_4$  and filtered. After solvent evaporation under vacuum, the residue was purified by CC (gradient of MeOH in DCM, 1/99 to 8/92), giving **24** as a white solid (43 mg, 42 %).  $^1\text{H NMR}$  (300 MHz, Acetone- $d_6$ )  $\delta$  8.60 (s, 1H, H8).

#### 8.4.1.8. 3-chloro-1-(2,4-dichlorophenyl)propan-1-one (**37**)



$\text{AlCl}_3$  (252 mg, 1.9 mmol) was suspended in 1,3-dichlorobenzene (920  $\mu\text{L}$ , 8 mmol) under dry and inert conditions. 3-chloropropanoyl chloride (150  $\mu\text{L}$ , 1.6 mmol) was added dropwise to the mixture, which was subsequently heated up to  $60\text{ }^\circ\text{C}$  and stirred for 4 h. The mixture was cooled down to  $0\text{ }^\circ\text{C}$  and water (2 mL) was slowly added to quench the reaction. The mixture was extracted with ethyl acetate (EtOAc; 3 x 3 mL) and the combined organic fraction was dried over anhydrous  $\text{Na}_2\text{SO}_4$ , filtered and the solvent evaporated under reduced pressure. The residue was purified by CC (gradient of EtOAc in hexane, 2/98 to 20/80). After solvent evaporation under vacuum, intermediate **37** was obtained as a clear amber oil (307 mg, 82 %).  $^1\text{H NMR}$  (300 MHz,  $\text{CDCl}_3$ )  $\delta$  7.52 (d,  $J = 8.4\text{ Hz}$ , 1H, H6'), 7.46 (d,  $J = 2.0\text{ Hz}$ , H3'), 7.34 (dd,  $J = 8.4, 2.0\text{ Hz}$ , 1H, H5'), 3.88 (t,  $J = 6.6\text{ Hz}$ , 2H,  $\text{CH}_2\text{CO}$ ), 3.76 (t,  $J = 6.6\text{ Hz}$ , 1H,  $\text{CH}_2\text{CO}$ ), 3.44 (t,  $J = 6.5\text{ Hz}$ , 1H,  $\text{CH}_2\text{Cl}$ ), 2.87 (t,  $J = 6.6\text{ Hz}$ , 1H,  $\text{CH}_2\text{Cl}$ ).

#### 8.4.1.9. 2,6-dichloropurine hydrochloride and 2-chloro-9-methyl-1,9-dihydropurin-6-one (**39**)



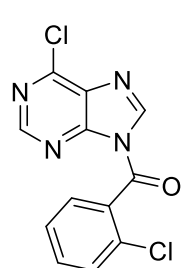
2,6-dichloropurine (100 mg, 0.53 mmol) was dissolved in a 3 M solution of HCl in cyclopentylmethylether (1 mL) under dry and inert conditions. The reaction was stirred at rt for 24 h and filtered. The resulting solid was washed with diethyl ether ( $\text{Et}_2\text{O}$ ; 2 x 1 mL) and dried under vacuum, yielding 2,6-dichloropurine hydrochloride as a yellowish powder (84 mg, 70 %).  $^1\text{H NMR}$  (300 MHz,  $\text{D}_2\text{O}$ )  $\delta$  8.64 (s, 1H, H8). Following the procedure described by Tumma and collaborators (Tumma *et al.*, 2010), 2,6-dichloropurine

hydrochloride (84 mg, 0.37 mmol) and basic alumina (38 mg) were suspended in MeOH (2 mL). The reaction was heated up to 70 °C and stirred for 24 h. Reaction was interrupted by solvent evaporation under reduced pressure and the residue purified by CC (gradient of MeOH in DCM, 2/98 to 16/84), yielding **39** as a white powder (26 mg, 38 %). <sup>1</sup>H NMR (300 MHz, acetone-d<sub>6</sub>) δ 8.32 (s, 1H, H8), 4.15 (s, 3H, CH<sub>3</sub>).

#### 8.4.2. General procedure for the synthesis of 2-chlorobenzoyl purines **1** and **3**, and 2-chlorobenzoyl theobromine **26**

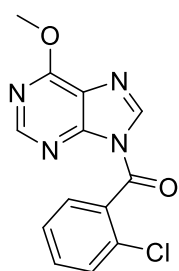
The 6-substituted purine or theobromine (1 equiv) was dissolved in freshly distilled THF (0.1 M) under dry and inert conditions. DMAP (0.05 equiv) and TEA (2 equiv) were injected and the mixture was cooled down to 0 °C. 2-chlorobenzenesulfonyl chloride (1 equiv) was added dropwise for 30 min and the mixture was allowed to reach rt while stirring. After the reaction was completed (4–6 h for purines, 24 h at rt plus 24 h at 70 °C for theobromine, TLC), the solvent was evaporated under reduced pressure, EtOAc (20 mL) and water (20 mL) were added to the crude and the two layers were separated. The aqueous layer was extracted again with EtOAc (10 mL) and the combined organic fraction was washed with brine, dried over anhydrous Na<sub>2</sub>SO<sub>4</sub>, and filtered. The solvent was concentrated under reduced pressure and the residue purified by trituration in hexane several times to yield pure product.

##### 8.4.2.1. (6-chloro-9*H*-purin-9-yl)(2-chlorophenyl)methanone (**1**)



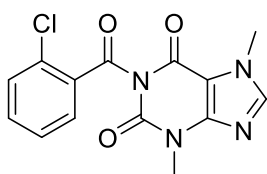
6-chloropurine (227 mg, 1.5 mmol), 2-chlorobenzenesulfonyl chloride (186 μL, 1.5 mmol), DMAP (9 mg, 73.7 μmol) and TEA (410 μL, 3 mmol) in THF (15 mL) yielded **1** as a white powder (337 mg, 78 %). <sup>1</sup>H NMR (300 MHz, acetone-d<sub>6</sub>) δ 9.02 (s, 1H, H2), 8.61 (s, 1H, H8), 7.88–7.52 (m, 4H, Ar). <sup>13</sup>C NMR (75.4 MHz, acetone-d<sub>6</sub>) δ 164.0, 154.1, 152.1, 151.9, 145.5, 134.4, 133.7, 133.6, 132.3, 131.3, 131.0, 128.4. HRMS (ESI+) mass calcd for C<sub>12</sub>H<sub>6</sub>Cl<sub>2</sub>N<sub>4</sub>O (m/z) 292.9991 [M + H]<sup>+</sup>; found, 292.9994. Mp 133–135 °C. Anal. calcd for C<sub>12</sub>H<sub>6</sub>Cl<sub>2</sub>N<sub>4</sub>O: C, 49.17; H, 2.06; N, 19.12. Found: C, 48.78; H, 2.40; N, 19.50.

#### 8.4.2.2. (2-chlorophenyl)(6-methoxy-9H-purin-9-yl)methanone (3)



6-Methoxypurine (3, 100 mg, 0.67 mmol), 2-chlorobenzenesulfonyl chloride (84.5  $\mu\text{L}$ , 0.67 mmol), DMAP (4 mg, 33.3  $\mu\text{mol}$ ) and TEA (177  $\mu\text{L}$ , 1.3 mmol) in THF (6.5 mL) yielded **3** as a white powder (102 mg, 53 %).  $^1\text{H}$  NMR (300 MHz, acetone- $d_6$ )  $\delta$  8.74 (s, 1H, H2), 8.34 (s, 1H, H8), 7.80–7.52 (m, 4H, Ar), 4.15 (s, 3H,  $\text{CH}_3$ ).  $^{13}\text{C}$  NMR (75.4 MHz, acetone- $d_6$ )  $\delta$  164.6, 162.3, 154.3, 152.3, 145.5, 142.1, 134.4, 134.1, 132.2, 131.1, 130.9, 128.4, 123.4, 54.8. HRMS (ESI+) mass calcd for  $\text{C}_{13}\text{H}_9\text{ClN}_4\text{O}_2$  ( $m/z$ ) 311.0306 [ $\text{M} + \text{Na}$ ] $^+$ ; found, 311.0302. Mp 169–171  $^\circ\text{C}$ . Anal. calcd for  $\text{C}_{13}\text{H}_9\text{ClN}_4\text{O}_2$ : C, 54.09; H, 3.14; N, 19.41. Found: C, 54.00; H, 3.06; N, 18.95.

#### 8.4.2.3. 1-(2-chlorobenzoyl)-3,7-dimethyl-3,7-dihydro-1H-purine-2,6-dione (26)



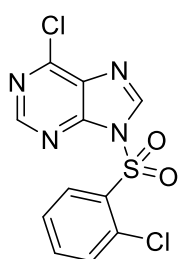
Theobromine (3,7-dimethyl-3,7-dihydro-1H-purine-2,6-dione, 200 mg, 1.1 mmol), 2-chlorobenzoyl chloride (141  $\mu\text{L}$ , 1.1 mmol), DMAP (7 mg, 57.3  $\mu\text{mol}$ ) and TEA (309  $\mu\text{L}$ , 2.2 mmol) in THF (11 mL) yielded **26** as a white powder (196 mg, 55 %).  $^1\text{H}$  NMR (300 MHz, acetone- $d_6$ )  $\delta$  8.01 (d,  $J = 7.9$  Hz, 1H, H6'), 7.95 (s, 1H, H8), 7.70–7.60 (m, 2H, Ar), 7.48 (t,  $J = 7.4$  Hz, 1H, Ar), 3.97 (s, 1H, N7- $\text{CH}_3$ ), 3.47 (s, 1H, N3- $\text{CH}_3$ ).  $^{13}\text{C}$  NMR (75.4 MHz, acetone- $d_6$ )  $\delta$  167.8, 154.6, 151.2, 150.8, 144.5, 135.5, 134.9, 133.6, 132.6, 128.4, 108.1, 33.8. HRMS (ESI+) mass calcd for  $\text{C}_{14}\text{H}_{11}\text{ClN}_4\text{O}_3$  ( $m/z$ ) 341.0411 [ $\text{M} + \text{Na}$ ] $^+$ ; found, 341.0398. Mp 182–183  $^\circ\text{C}$ . Anal. calcd for  $\text{C}_{14}\text{H}_{11}\text{ClN}_4\text{O}_3$ : C, 52.76; H, 3.48; N, 17.58. Found: C, 52.66; H, 3.38; N, 17.56.

#### 8.4.3. General procedure for the synthesis of sulfonamides **4–8** and **27–34**

**Method A.** The purine derivative (1 equiv) was dissolved in freshly distilled DCM and THF (1:1, 0.1 M) under dry and inert conditions. DMAP (0.2 equiv) and TEA (2 equiv) were added and the mixture was cooled down to 0  $^\circ\text{C}$ . 2-chlorobenzenesulfonyl chloride (2 equiv) was added dropwise for 30 min. The mixture was stirred at rt and, after completion (2–4 h, TLC), the solvent was removed under reduced pressure. The crude was dissolved in EtOAc (30 mL) and water (20 mL) and the two layers were separated. The aqueous layer was extracted again with EtOAc (10 mL) and the combined organic fraction was washed with brine, dried over anhydrous  $\text{Na}_2\text{SO}_4$ , and filtered. The solvent was evaporated under reduced pressure and the residue purified by CC or trituration to yield the pure product.

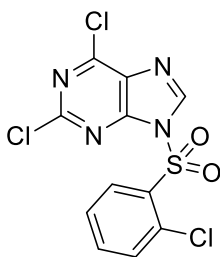
**Method B.** Theophylline (1,3-dimethyl-3,9-dihydro-1*H*-purine-2,6-dione, 1 equiv) was suspended in freshly distilled THF (0.05 M) in dry and inert conditions. The mixture was cooled down to 0 °C, NaH (60 % dispersion in mineral oil, 1.2 equiv) was added, and the reaction was stirred at rt for 30 min. The corresponding arylsulfonyl chloride derivative (1.2 equiv) was dissolved in dry THF (1 mL) and added to the reaction dropwise at 0 °C for 15 min. The reaction was stirred at rt and, after completion (4–48 h, TLC), the solvent was evaporated under reduced pressure. The residue was dissolved in EtOAc (30 mL) and water (30 mL). The layers were separated and the aqueous one was extracted again with EtOAc (20 mL). The combined organic fraction was washed with brine, dried over anhydrous Na<sub>2</sub>SO<sub>4</sub> and filtered. The solvent was evaporated under reduced pressure and the residue purified by CC to yield the pure product.

#### 8.4.3.1. 6-chloro-9-[(2-chlorophenyl)sulfonyl]-9*H*-purine (4)



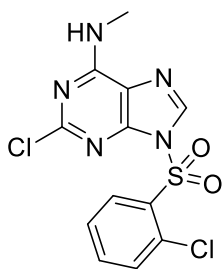
Following method A, 6-chloropurine (100 mg, 0.65 mmol), 2-chlorobenzenesulfonyl chloride (176  $\mu$ L, 1.3 mmol), DMAP (16 mg, 129  $\mu$ mol) and TEA (180  $\mu$ L, 1.3 mmol) in DCM/THF (6.5 mL) yielded **4** as a white powder (165 mg, 77 %) after trituration with cold MeOH. <sup>1</sup>H NMR (300 MHz, acetone-d<sub>6</sub>)  $\delta$  9.05 (s, 1H, H2), 8.70 (s, 1H, H8), 8.60 (dd, *J* = 7.9, 1.9 Hz, 1H, H6'), 7.93–7.74 (m, 2H, H4', H5'), 7.67 (dd, *J* = 7.9, 1.5 Hz, 1H, H3'). <sup>13</sup>C NMR (75.4 MHz, acetone-d<sub>6</sub>)  $\delta$  154.2, 152.1, 151.4, 145.5, 138.3, 134.6, 134.5, 133.4, 133.1, 129.1. HRMS (ESI+) mass calcd for C<sub>11</sub>H<sub>6</sub>Cl<sub>2</sub>N<sub>4</sub>O<sub>2</sub>S (m/z) 328.9661 [M + H]<sup>+</sup>; found, 328.9663. Mp 172 °C (dec). Anal. calcd for C<sub>11</sub>H<sub>6</sub>Cl<sub>2</sub>N<sub>4</sub>O<sub>2</sub>S: C, 40.14; H, 1.84; N, 17.02; S, 9.74. Found: C, 40.12; H, 2.06; N, 16.66; S, 9.75.

#### 8.4.3.2. 2,6-dichloro-9-[(2-chlorophenyl)sulfonyl]-9*H*-purine (5)



Following method A, 2,6-dichloropurine (100 mg, 0.53 mmol), 2-chlorobenzenesulfonyl chloride (144  $\mu$ L, 1.1 mmol), DMAP (13 mg, 106  $\mu$ mol) and TEA (147  $\mu$ L, 1.1 mmol) in DCM/THF (5.3 mL) yielded **5** as a white powder (90 mg, 47 %) after purification by CC (gradient of EtOAc in hexane, 0/100 to 50/50). <sup>1</sup>H NMR (300 MHz, acetone-d<sub>6</sub>)  $\delta$  9.07 (s, 1H, H8), 8.58 (dd, *J* = 8.0, 1.9 Hz, 1H, H6'), 7.95–7.75 (m, 2H, H4', H5'), 7.70 (dd, *J* = 7.9, 1.2 Hz, 1H, H3'). <sup>13</sup>C NMR (75.4 MHz, acetone-d<sub>6</sub>)  $\delta$  154.7, 153.0, 152.8, 146.2, 138.6, 134.8, 134.4, 133.7, 133.6, 132.9, 129.3. HRMS (ESI+) mass calcd for C<sub>11</sub>H<sub>5</sub>Cl<sub>3</sub>N<sub>4</sub>O<sub>2</sub>S (m/z) 362.9271 [M + H]<sup>+</sup>; found, 362.9285. Mp 156 °C (dec). Anal. calcd for C<sub>11</sub>H<sub>5</sub>Cl<sub>3</sub>N<sub>4</sub>O<sub>2</sub>S: C, 36.34; H, 1.39; N, 15.41; S, 8.82. Found: C, 36.06; H, 1.58; N, 15.20; S, 9.14.

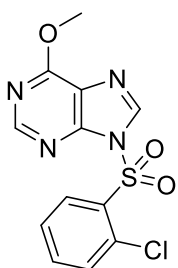
8.4.3.3. 2-chloro-9-[(2-chlorophenyl)sulfonyl]-*N*-methyl-9*H*-purin-6-amine (6)



Following method A, 2-chloro-*N*-methylpurin-6-amine (100 mg, 0.54 mmol), 2-chlorobenzenesulfonyl chloride (148  $\mu$ L, 1.1 mmol), DMAP (13 mg, 118  $\mu$ mol) and TEA (152  $\mu$ L, 1.1 mmol) in DCM/THF (6 mL) yielded **6** as a white powder (94 mg, 48 %) after purification by CC (gradient of EtOAc in hexane, 12/88 to 100/0).  $^1\text{H}$  NMR (300 MHz, acetone- $d_6$ )  $\delta$  8.55–8.46 (m, 2H, H8, H6'), 7.91–7.71 (m, 2H, H5', H4'), 7.67 (dd,  $J$  = 7.9, 1.4 Hz, 1H, H3'), 7.55 (bs, 1H, NH), 3.07 (d,  $J$  = 4.4 Hz, 3H, CH<sub>3</sub>).

$^{13}\text{C}$  NMR (75.4 MHz, DMSO- $d_6$ )  $\delta$  155.4, 154.9, 147.9, 139.6, 137.4, 133.2, 133.1, 132.4, 131.3, 126.2, 118.4, 27.2. HRMS (ESI+) mass calcd for C<sub>12</sub>H<sub>9</sub>Cl<sub>2</sub>N<sub>5</sub>O<sub>2</sub>S (m/z) 357.9926 [M + H]<sup>+</sup>; found, 357.9932. Mp 235 °C (dec). HPLC-UV ( $\lambda$  = 260 nm), purity > 95 %.

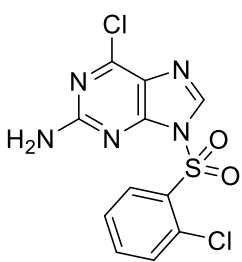
8.4.3.4. 9-[(2-chlorophenyl)sulfonyl]-6-methoxy-9*H*-purine (7)



Following method A, 6-methoxypurine (2 – 90 mg, 0.60 mmol), 2-chlorobenzenesulfonyl chloride (163  $\mu$ L, 1.2 mmol), DMAP (15 mg, 120  $\mu$ mol) and TEA (167  $\mu$ L, 1.2 mmol) in DCM/THF (6 mL) yielded **7** as a white powder (72 mg, 37 %) after purification by trituration with cold MeOH.  $^1\text{H}$  NMR (300 MHz, acetone- $d_6$ )  $\delta$  8.76 (s, 1H, H2), 8.57 (dd,  $J$  = 7.9, 1.9 Hz, 1H, H6'), 8.43 (s, 1H, H8), 7.85–7.77 (m, 2H, H4', H5'), 7.66 (dd,  $J$  = 7.8, 1.5 Hz, 1H, H3'), 4.13 (s, 3H, CH<sub>3</sub>).

$^{13}\text{C}$  NMR (75.4 MHz, acetone- $d_6$ )  $\delta$  162.2, 154.5, 151.5, 142.3, 138.0, 134.9, 134.6, 133.2, 133.1, 129.0, 122.6, 54.9. HRMS (ESI+) mass calcd for C<sub>12</sub>H<sub>9</sub>ClN<sub>4</sub>O<sub>3</sub>S (m/z) 346.9976 [M + Na]<sup>+</sup>; found, 346.9980. Mp 158 °C (dec). Anal. calcd for C<sub>12</sub>H<sub>9</sub>ClN<sub>4</sub>O<sub>3</sub>S: C, 44.38; H, 2.79; N, 17.25; S, 9.87. Found: C, 44.48; H, 2.99; N, 16.94; S, 9.93.

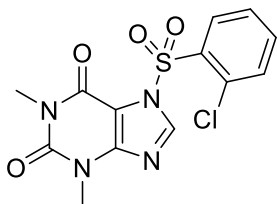
8.4.3.5. 6-chloro-9-[(2-chlorophenyl)sulfonyl]-9*H*-purin-2-amine (8)



Following method A, 6-chloropurin-2-amine (100 mg, 0.59 mmol), 2-chlorobenzenesulfonyl chloride (161  $\mu$ L, 1.2 mmol), DMAP (14 mg, 118  $\mu$ mol) and TEA (164  $\mu$ L, 1.2 mmol) in DCM/THF (6 mL) yielded **8** as a white powder (102 mg, 50 %) after purification by CC (gradient of EtOAc in hexane, 12/88 to 85/15).  $^1\text{H}$  NMR (300 MHz, acetone- $d_6$ )  $\delta$  8.51–8.42 (m, 2H, H8, H6'), 7.84 (td,  $J$

= 7.7, 1.7 Hz, 1H, H5'), 7.77–7.62 (m, 2H, H3', H4'), 6.52 (bs, 2H, NH<sub>2</sub>).  $^{13}\text{C}$  NMR (75.4 MHz, CDCl<sub>3</sub>)  $\delta$  161.8, 153.5, 152.5, 140.8, 137.9, 135.0, 134.7, 133.3, 133.2, 128.9, 125.1. HRMS (ESI+) mass calcd for C<sub>11</sub>H<sub>7</sub>Cl<sub>2</sub>N<sub>5</sub>O<sub>2</sub>S (m/z) 343.9770 [M + H]<sup>+</sup> and 365.9589 [M + Na]<sup>+</sup>; found, 343.9765 and 365.9573. Mp 200 °C (dec). Anal. calcd for C<sub>11</sub>H<sub>7</sub>Cl<sub>2</sub>N<sub>5</sub>O<sub>2</sub>S: C, 38.39; H, 2.05; N, 20.35; S, 9.32. Found: C, 38.66; H, 2.37; N, 19.91; S, 9.23.

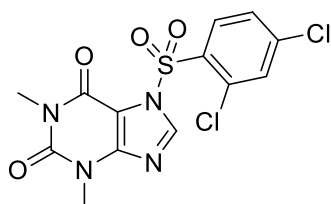
8.4.3.6. 7-[(2-chlorophenyl)sulfonyl]-1,3-dimethyl-3,7-dihydro-1*H*-purine-2,6-dione (27)



Following method B, theophylline (60 mg, 0.33 mmol), 2-chlorobenzenesulfonyl chloride (55  $\mu$ L, 0.40 mmol), NaH (60 % dispersion in mineral oil, 16 mg, 0.4 mmol) in THF (5.5 mL) yielded **27** as a white powder (82 mg, 69 %) after purification by CC (gradient of EtOAc in hexane, 12/88 to

100/0). The compound was recrystallised in DCM and acetone by slow evaporation to obtain crystals for X-Ray diffraction (supporting info).  $^1\text{H}$  NMR (300 MHz, acetone- $d_6$ )  $\delta$  8.70 (s, 1H, H8), 8.60 (dd,  $J$  = 8.1, 1.7 Hz, 1H, H6'), 7.88–7.84, 7.76–7.66 (2m, 3H, Ar), 3.52 (s, 3H, N3- $\text{CH}_3$ ), 3.16 (s, 3H, N1- $\text{CH}_3$ ).  $^{13}\text{C}$  NMR (75.4 MHz,  $\text{CDCl}_3$ )  $\delta$  153.6, 152.0, 151.8, 151.3, 145.4, 138.0, 136.1, 134.6, 133.3, 132.8, 128.6, 28.5. HRMS (ESI+) mass calcd for  $\text{C}_{13}\text{H}_{11}\text{ClN}_4\text{O}_4\text{S}$  ( $m/z$ ) 377.0081 [ $\text{M} + \text{Na}$ ] $^+$ ; found, 377.0070. Mp 212  $^\circ\text{C}$  (dec). HPLC-UV ( $\lambda$  = 287 nm), purity > 99 %.

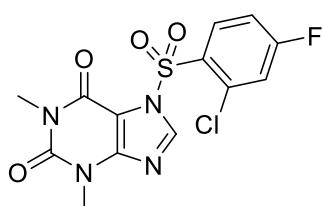
8.4.3.7. 7-[(2,4-dichlorophenyl)sulfonyl]-1,3-dimethyl-3,7-dihydro-1*H*-purine-2,6-dione (28)



Following method B, theophylline (100 mg, 0.55 mmol), 2,4-dichlorobenzenesulfonyl chloride (163 mg, 0.67 mmol), NaH (60 % dispersion in mineral oil, 27 mg, 0.67 mmol) in THF (11 mL) yielded **28** as a white powder (160 mg, 74 %) after purification by CC (gradient of

EtOAc in hexane, 12/88 to 95/5).  $^1\text{H}$  NMR (300 MHz,  $\text{CDCl}_3$ )  $\delta$  8.59 (d,  $J$  = 9.2 Hz, 1H, H6'), 8.43 (s, 1H, H8), 7.61–7.47 (m, 2H, H3', H5'), 3.60 (s, 3H, N3- $\text{CH}_3$ ), 3.30 (s, 3H, N1- $\text{CH}_3$ ).  $^{13}\text{C}$  NMR (75.4 MHz,  $\text{CDCl}_3$ )  $\delta$  152.9, 151.2, 150.6, 144.0, 142.9, 136.2, 133.9, 132.0, 131.7, 127.9, 105.7, 30.3, 28.6. HRMS (ESI+) mass calcd for  $\text{C}_{13}\text{H}_{10}\text{Cl}_2\text{N}_4\text{O}_4\text{S}$  ( $m/z$ ) 410.9692 [ $\text{M} + \text{Na}$ ] $^+$ ; found, 410.9687. Mp 206–208  $^\circ\text{C}$ . Anal. Calcd for  $\text{C}_{13}\text{H}_{10}\text{Cl}_2\text{N}_4\text{O}_4\text{S}$ : C, 40.12; H, 2.59; N, 14.40; S, 8.24. Found: C, 40.19; H, 2.71; N, 14.22; S, 8.25.

8.4.3.8. 7-[(2-chloro-4-fluorophenyl)sulfonyl]-1,3-dimethyl-3,7-dihydro-1*H*-purine-2,6-dione (29)

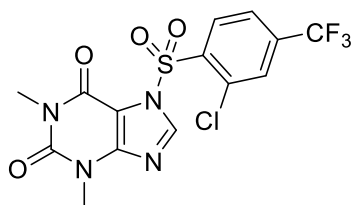


Following method B, theophylline (100 mg, 0.55 mmol), 2-chloro-4-fluorobenzenesulfonyl chloride (97  $\mu$ L, 0.67 mmol), NaH (60 % dispersion in mineral oil, 27 mg, 0.67 mmol) in THF (11 mL) yielded **29** as a white powder (112 mg, 54 %) after purification by CC (gradient of EtOAc in

hexane, 12/88 to 100/0).  $^1\text{H}$  NMR (300 MHz,  $\text{CDCl}_3$ )  $\delta$  8.69 (dd,  $J$  = 9.0, 5.7 Hz, 1H, H6'), 8.43 (s, 1H, H8), 7.34–7.20 (m, 2H, H3', H5'), 3.60 (s, 3H, N3- $\text{CH}_3$ ), 3.29 (s, 3H, N1- $\text{CH}_3$ ).  $^{13}\text{C}$  NMR (75.4 MHz,  $\text{CDCl}_3$ )

$\delta$  166.4 (d,  $J = 263.9$  Hz), 153.0, 151.3, 150.6, 144.0, 138.0 (d,  $J = 10.6$  Hz), 135.2 (d,  $J = 11.3$  Hz), 134.3, 129.8, 119.6 (d,  $J = 25.6$  Hz), 115.1 (d,  $J = 21.9$  Hz), 105.8, 30.3, 28.6. HRMS (ESI+) mass calcd for  $C_{13}H_{10}ClFN_4O_4S$  ( $m/z$ ) 394.9987 [ $M + Na$ ] $^+$ ; found, 394.9980. Mp 220–222 °C. Anal. calcd for  $C_{13}H_{10}ClFN_4O_4S$ : C, 41.89; H, 2.70; N, 15.03; S, 8.60. Found: C, 41.85; H, 2.82; N, 14.85; S, 8.72.

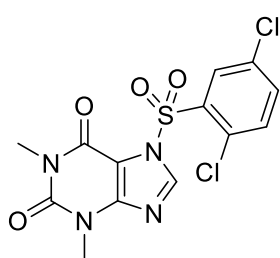
8.4.3.9. 7-([2-chloro-4-(trifluoromethyl)phenyl]sulfonyl)-1,3-dimethyl-3,7-dihydro-1*H*-purine-2,6-dione (30)



Following method B, theophylline (100 mg, 0.55 mmol), 2-chloro-4-(trifluoromethyl)benzenesulfonyl chloride (186 mg, 0.67 mmol), NaH (60 % dispersion in mineral oil, 27 mg, 0.67 mmol) in THF (11 mL) yielded **30** as a white powder (177 mg, 75 %) after purification by CC

(gradient of EtOAc in hexane, 15/85 to 100/0).  $^1H$  NMR (300 MHz,  $CDCl_3$ )  $\delta$  8.80 (d,  $J = 8.4$  Hz, 1H, H6'), 8.46 (s, 1H, H8), 7.84 (dd,  $J = 8.4, 1.7$  Hz, 1H, H5'), 7.75 (d,  $J = 1.7$  Hz, 1H, H3'), 3.60 (s, 3H, N3- $CH_3$ ), 3.28 (s, 3H, N1- $CH_3$ ).  $^{13}C$  NMR (75.4 MHz,  $CDCl_3$ )  $\delta$  153.0, 151.2, 150.6, 144.0, 138.0 (q,  $J = 31.7$  Hz), 136.92, 136.1, 133.9, 129.0 (q,  $J = 3.8$  Hz), 124.4 (q,  $J = 3.8$  Hz), 122.2 (d,  $J = 273.7$  Hz), 105.8, 30.4, 28.6. HRMS (ESI+) mass calcd for  $C_{14}H_{10}ClF_3N_4O_4S$  ( $m/z$ ) 444.9955 [ $M + Na$ ] $^+$ ; found, 444.9954. Mp 210 °C (dec). Anal. calcd for  $C_{14}H_{10}ClF_3N_4O_4S$ : C, 39.77; H, 2.38; N, 13.25; S, 7.58. Found: C, 39.93; H, 2.55; N, 12.99; S, 7.76.

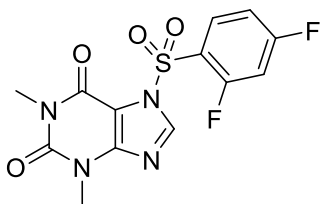
8.4.3.10. 7-[(2,5-dichlorophenyl)sulfonyl]-1,3-dimethyl-3,7-dihydro-1*H*-purine-2,6-dione (31)



Following method B, theophylline (100 mg, 0.55 mmol), 2,5-dichlorobenzenesulfonyl chloride (163 mg, 0.67 mmol), NaH (60 % dispersion in mineral oil, 27 mg, 0.67 mmol) in THF (11 mL) yielded **31** as a white powder (157 mg, 73 %) after purification by CC (gradient of EtOAc in hexane, 15/85 to 100/0).  $^1H$  NMR (300 MHz,  $CDCl_3$ )  $\delta$  8.62 (d,  $J = 2.5$  Hz, 1H, H6'), 8.43 (s, 1H, H8), 7.60 (dd,  $J = 8.6, 2.5$  Hz, 1H, H4'), 7.42 (d,  $J = 8.6$  Hz, 1H, H3'), 3.59 (s, 3H, N3- $CH_3$ ), 3.30 (s, 3H, N1- $CH_3$ ).

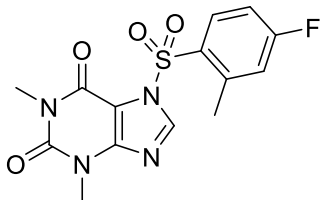
$^{13}C$  NMR (75.4 MHz,  $CDCl_3$ )  $\delta$  152.8, 151.3, 150.5, 144.0, 136.4, 134.9, 134.8, 133.8, 132.8, 131.1, 105.8, 30.3, 28.6. HRMS (ESI+) mass calcd for  $C_{13}H_{10}Cl_2N_4O_4S$  ( $m/z$ ) 410.9692 [ $M + Na$ ] $^+$ ; found, 410.9686. Mp 222 °C (dec). Anal. calcd for  $C_{13}H_{10}Cl_2N_4O_4S$ : C, 40.12; H, 2.59; N, 14.40; S, 8.24. Found: C, 40.34; H, 2.78; N, 14.23; S, 8.52.

8.4.3.11. 7-[(2,4-difluorophenyl)sulfonyl]-1,3-dimethyl-3,7-dihydro-1*H*-purine-2,6-dione (32)



Following method B, theophylline (100 mg, 0.55 mmol), 2,4-difluorobenzenesulfonyl chloride (141 mg, 0.67 mmol), NaH (60 % dispersion in mineral oil, 27 mg, 0.67 mmol) in THF (11 mL) yielded 32 as a white powder (142 mg, 72 %) after purification by CC (gradient of EtOAc in hexane, 10/90 to 80/20). <sup>1</sup>H NMR (300 MHz, CDCl<sub>3</sub>) δ 8.48 (ddd, J = 9.0, 8.1, 5.9 Hz, 1H, H6'), 8.37 (d, J = 1.2 Hz, 1H, H8), 7.16 (dddd, J = 8.9, 7.6, 2.4, 1.1 Hz, 1H, H5'), 6.93 (ddd, J = 10.4, 8.2, 2.4 Hz, 1H, H3'), 3.60 (s, 3H, N3CH<sub>3</sub>), 3.31 (s, 3H, N1CH<sub>3</sub>). <sup>13</sup>C NMR (75.4 MHz, CDCl<sub>3</sub>) δ 167.8 (dd, J = 12.1, 262.4 Hz), 160.5 (dd, J = 12.8, 261.6 Hz), 153.0, 151.3, 150.6, 143.0, 135.8 (d, J = 11.31 Hz), 120.8 (dd, J = 3.8, 12.1 Hz), 112.7 (dd, J = 3.8, 22.6 Hz), 105.9 (dd, J = 24.9, 26.4 Hz), 105.8, 30.3, 28.6. HRMS (ESI+) mass calcd for C<sub>13</sub>H<sub>10</sub>F<sub>2</sub>N<sub>4</sub>O<sub>4</sub>S (m/z) 379.0283 [M + Na]<sup>+</sup>; found, 379.0269. Mp 194 °C (dec). Anal. calcd for C<sub>13</sub>H<sub>10</sub>F<sub>2</sub>N<sub>4</sub>O<sub>4</sub>S: C, 43.82; H, 2.83; N, 15.72; S, 9.00. Found: C, 43.83; H, 2.96; N, 15.63; S, 9.12.

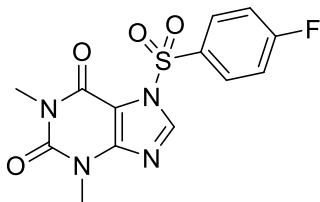
8.4.3.12. 7-[(4-fluoro-2-methylphenyl)sulfonyl]-1,3-dimethyl-3,7-dihydro-1*H*-purine-2,6-dione (33)



Following method B, theophylline (100 mg, 0.55 mmol), 4-fluoro-2-methylbenzenesulfonyl chloride (97 μL, 0.67 mmol), NaH (60 % dispersion in mineral oil, 27 mg, 0.67 mmol) in THF (11 mL) yielded 33 as a white powder (152 mg, 78 %) after purification by CC (gradient of EtOAc in hexane, 10/90 to 80/20). <sup>1</sup>H NMR (300 MHz, CDCl<sub>3</sub>) δ 8.57 (dd, J = 9.0, 5.5 Hz, 1H, H6'), 8.38 (s, 1H, H8), 7.17 (ddd, J = 9.5, 7.6, 2.6 Hz, 1H, H5'), 6.99 (dd, J = 9.0, 2.6, 1H, H3'), 3.59 (s, 3H, N3-CH<sub>3</sub>), 3.30 (s, 3H, N1-CH<sub>3</sub>), 2.51 (s, 3H, C2'-CH<sub>3</sub>). <sup>13</sup>C NMR (75.4 MHz, CDCl<sub>3</sub>) δ 166.6 (d, J = 263.1 Hz), 153.0, 151.3, 150.6, 142.7, 142.2 (d, J = 9.8 Hz), 137.1 (d, J = 10.6 Hz), 130.3 (d, J = 3.0 Hz), 119.7 (d, J = 22.6 Hz), 114.1 (d, J = 21.9 Hz), 106.1, 30.3, 28.6, 20.4 (d, J = 1.1 Hz). HRMS (ESI+) mass calcd for C<sub>14</sub>H<sub>13</sub>FN<sub>4</sub>O<sub>4</sub>S (m/z) 375.0533 [M + Na]<sup>+</sup>; found, 375.0535. Mp 216–218 °C (dec). Anal. calcd for C<sub>14</sub>H<sub>13</sub>FN<sub>4</sub>O<sub>4</sub>S: C, 47.72; H, 3.72; N, 15.90; S, 9.10. Found: C, 47.63; H, 3.83; N, 15.64; S, 9.18.



8.4.3.13. 7-[(4-fluorophenyl)sulfonyl]-1,3-dimethyl-3,7-dihydro-1*H*-purine-2,6-dione (**34**)



Following method B, theophylline (100 mg, 0.55 mmol), 4-fluorobenzenesulfonyl chloride (130 mg, 0.67 mmol), NaH (60 % dispersion in mineral oil, 27 mg, 0.67 mmol) in THF (11 mL) yielded **34** as a white powder (152 mg, 81 %) after purification by CC (gradient of EtOAc in hexane, 10/90 to 100/0). <sup>1</sup>H NMR (300 MHz, CDCl<sub>3</sub>) δ 8.42–8.21 (m, 3H, H2', H8), 7.36–7.20 (m, 2H, H3'), 3.57 (s, 3H, N3-CH<sub>3</sub>), 3.36 (s, 3H, N1-CH<sub>3</sub>). <sup>13</sup>C NMR (75.4 MHz, CDCl<sub>3</sub>) δ 166.9 (d, J = 260.13), 153.1, 151.3, 150.8, 142.2, 133.0 (d, J = 10.6 Hz), 132.4 (d, J = 3.1 Hz), 117.1 (d, J = 22.6 Hz), 106.1, 30.3, 28.7. HRMS (ESI+) mass calcd for C<sub>13</sub>H<sub>11</sub>FN<sub>4</sub>O<sub>4</sub>S (m/z) 361.0377 [M + Na]<sup>+</sup> and 699.0862 [2M + Na]<sup>+</sup>; found, 361.0366 and 699.0841. Mp 223 °C (dec). Anal. calcd for C<sub>13</sub>H<sub>11</sub>FN<sub>4</sub>O<sub>4</sub>S: C, 46.15; H, 3.28; N, 16.56; S, 9.48. Found: C, 46.05; H, 3.41; N, 16.45; S, 9.21.

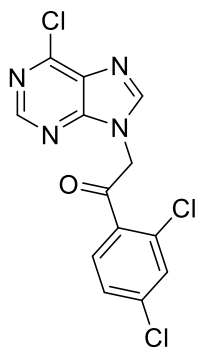
8.4.4. General procedure for the preparation of purinyl/xanthinyl-2,4-dichlorophenylethanones/propanones **9-10, 12, 16-19, 21, 23, 25, 35-36, 38**

**Method A.** The purine derivative used as starting material (1 equiv) was dissolved in dry DMF (0.05 M) under dry and inert conditions and cooled down to 0 °C. NaH (60 % dispersion in mineral oil, 1.2 equiv) was added and the resulting mixture stirred at rt for 30 min (Bendels *et al.*, 2014). The corresponding 2-chloro-1-arylethan-1-one (1.5 equiv), dissolved in dry DMF (1 mL), was added dropwise at 0 °C over 45 min. The reaction was allowed to reach rt. After completion (15–40 h, TLC), the solvent was evaporated under vacuum and the residue dissolved in EtOAc (30 mL) and water (20 mL). The layers were decanted and the aqueous phase was extracted with EtOAc (2 × 10 mL). The combined organic fraction was washed with brine, dried over anhydrous Na<sub>2</sub>SO<sub>4</sub>, filtered, and the solvent evaporated under reduced pressure. The crude was purified by CC or trituration.

**Method B.** The purine or xanthine derivative used as starting material (1 equiv), 2-chloro-1-(2,4-dichlorophenyl)ethan-1-one (1.2 equiv), TBAHS (0.05 equiv), and K<sub>2</sub>CO<sub>3</sub> (1 equiv) were dissolved in dry DMF (0.2 M) under dry and inert conditions. The mixture was then heated up to 150 °C in a sealed tube. After completion (1–6 h, TLC), the solvent was evaporated under vacuum, the residue retrieved with CH<sub>2</sub>Cl<sub>2</sub> (10 mL), and washed with water (2 × 4 mL). The organic fraction was dried over anhydrous

Na<sub>2</sub>SO<sub>4</sub>, filtered, and the solvent evaporated under reduced pressure. The crude was eventually purified by CC.

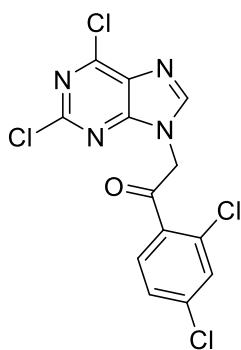
8.4.4.1. 2-(6-chloro-9*H*-purin-9-yl)-1-(2,4-dichlorophenyl)ethan-1-one (**9**)



Following method A, 6-chloropurine (100 mg, 0.65 mmol), 2-chloro-1-(2,4-dichlorophenyl)ethan-1-one (224 mg, 0.97 mmol), NaH (60 % dispersion in mineral oil, 31 mg, 776 μmol) in dry DMF (11 mL) yielded **9** as a white powder (50 mg, 45 %) after purification by CC (gradient of EtOAc in hexane, 16/84 to 100/0). <sup>1</sup>H NMR (300 MHz, acetone-d<sub>6</sub>) δ 8.71 (s, 1H, H<sub>2</sub>), 8.55 (s, 1H, H<sub>8</sub>), 8.03 (d, J = 8.4 Hz, 1H, H<sub>6'</sub>), 7.73 (d, J = 2.0 Hz, 1H, H<sub>3'</sub>), 7.63 (dd, J = 8.4, 2.0 Hz, 1H, H<sub>5'</sub>), 6.01 (s, 2H, CH<sub>2</sub>). <sup>13</sup>C NMR (75.4 MHz, acetone-d<sub>6</sub>) δ 193.4, 153.6, 152.8, 151.0, 148.3, 139.4, 134.9, 133.9,

132.7, 132.2, 131.8, 128.8, 53.2. HRMS (ESI+) mass calcd for C<sub>13</sub>H<sub>7</sub>Cl<sub>3</sub>N<sub>4</sub>O (m/z) 340.9758 [M + H]<sup>+</sup>; found, 340.9759. Mp 166–168 °C. Anal. calcd for C<sub>13</sub>H<sub>7</sub>Cl<sub>3</sub>N<sub>4</sub>O: C, 45.71; H, 2.07; N, 16.40. Found: C, 45.69; H, 1.89; N, 16.50.

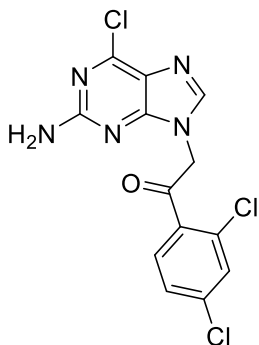
8.4.4.2. 2-(2,6-dichloro-9*H*-purin-9-yl)-1-(2,4-dichlorophenyl)ethan-1-one (**10**)



Following method A, 2,6-dichloropurine (100 mg, 0.53 mmol), 2-chloro-1-(2,4-dichlorophenyl)ethan-1-one (183 mg, 0.79 mmol), NaH (60 % dispersion in mineral oil, 25 mg, 635 μmol) in dry DMF (18 mL) yielded **10** as a yellowish powder (65 mg, 40 %) after purification by CC (gradient of EtOAc in hexane, 12/88 to 100/0) and trituration in Et<sub>2</sub>O. <sup>1</sup>H NMR (300 MHz, acetone-d<sub>6</sub>) δ 8.57 (s, 1H, H<sub>8</sub>), 8.05 (d, J = 8.4 Hz, 1H, H<sub>6'</sub>), 7.73 (d, J = 2.0 Hz, 1H, H<sub>3'</sub>), 7.63 (dd, J = 8.4, 2.0 Hz, 1H, H<sub>5'</sub>), 6.01 (s, 2H, CH<sub>2</sub>). <sup>13</sup>C NMR (75.4 MHz, acetone-d<sub>6</sub>) δ 192.9,

155.2, 153.1, 151.7, 149.3, 139.6, 134.6, 134.1, 132.9, 131.9, 131.6, 128.9, 53.4. HRMS (ESI+) mass calcd for C<sub>13</sub>H<sub>6</sub>Cl<sub>4</sub>N<sub>4</sub>O (m/z) 374.9368 [M + H]<sup>+</sup>; found, 374.9374. Mp 136–138 °C. Anal. calcd for C<sub>13</sub>H<sub>6</sub>Cl<sub>4</sub>N<sub>4</sub>O: C, 41.53; H, 1.61; N, 14.90. Found: C, 41.78; H, 1.93; N, 14.81.

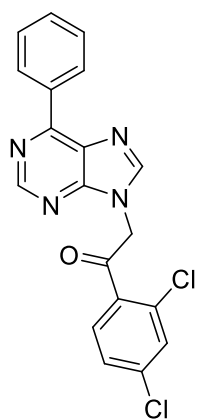
8.4.4.3. 2-(2-amino-6-chloro-9*H*-purin-9-yl)-1-(2,4-dichlorophenyl)ethan-1-one (12)



Following method B, 6-chloropurin-2-amine (100 mg, 0.53 mmol), 2-chloro-1-(2,4-dichlorophenyl)ethan-1-one (145 mg, 0.65 mmol), TBAHS (10 mg, 29  $\mu$ mol), and  $K_2CO_3$  (81 mg, 0.59 mmol) in dry DMF (3 mL), yielded **12** as a brown powder (15 mg, 10 %) after 30 h of reaction time at 80  $^{\circ}C$ , and purification by CC (gradient of MeOH in DCM, 1/99 to 8/92) and trituration in cold EtOAc.  $^1H$  NMR (300 MHz, acetone- $d_6$ )  $\delta$  8.03 (s, 1H, H8), 7.96 (d,  $J$  = 8.4 Hz, 1H, H6'), 7.70 (d,  $J$  = 2.0 Hz, 1H, H3'), 7.60 (dd,  $J$  = 8.4, 2.0 Hz, 1H, H5'), 6.17 (br, 2H,  $NH_2$ ),

5.69 (s, 2H,  $CH_2$ ).  $^{13}C$  NMR (75.4 MHz, acetone- $d_6$ )  $\delta$  194.1, 161.1, 155.6, 151.3, 144.3, 139.2, 135.3, 133.7, 132.6, 131.6, 128.8, 125.1, 52.6. HRMS (ESI+) mass calcd for  $C_{13}H_8Cl_3N_5O$  ( $m/z$ ) 355.9867 [ $M + H$ ] $^+$ ; found, 355.9873. Mp 208–209  $^{\circ}C$  (dec). HPLC-UV ( $\lambda$  = 306 nm), purity > 99 %.

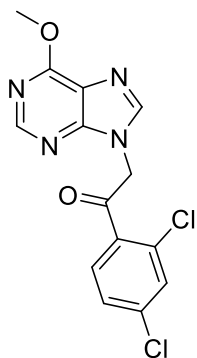
8.4.4.4. 1-(2,4-dichlorophenyl)-2-(6-phenyl-9*H*-purin-9-yl)ethan-1-one (16)



Following method A, 6-phenylpurine (**15** – 55 mg, 0.28 mmol), 2-chloro-1-(2,4-dichlorophenyl)ethan-1-one (97 mg, 0.42 mmol), NaH (60 % dispersion in mineral oil, 13 mg, 336  $\mu$ mol) in dry DMF (7 mL) yielded **16** as a yellowish powder (55 mg, 41 %) after purification by CC (gradient of EtOAc in hexane, 15/85 to 100/0).  $^1H$  NMR (300 MHz, acetone- $d_6$ )  $\delta$  9.04–8.98 (m, 2H, C6-Ar), 8.94 (s, 1H, H2), 8.56 (s, 1H, H8), 8.04 (d,  $J$  = 8.4 Hz, 1H, H6'), 7.73 (d,  $J$  = 2.0 Hz, 1H, H3'), 7.68–7.51 (m, 4H, C6-Ar, H5'), 5.99 (s, 2H,  $CH_2$ ).  $^{13}C$  NMR (75.4 MHz, acetone- $d_6$ )  $\delta$  194.0, 154.4, 154.1, 153.1, 147.3, 139.3, 137.0, 135.2, 133.8, 132.6, 131.9, 131.7, 131.5, 130.8, 129.4, 128.8,

52.7. HRMS (ESI+) mass calcd for  $C_{19}H_{12}Cl_2N_4O$  ( $m/z$ ) 383.0460 [ $M + H$ ] $^+$ ; found, 383.0465. Mp 160–162  $^{\circ}C$ . Anal. calcd for  $C_{19}H_{12}Cl_2N_4O$ : C, 59.55; H, 3.16; N, 14.62. Found: C, 59.58; H, 3.43; N, 14.48.

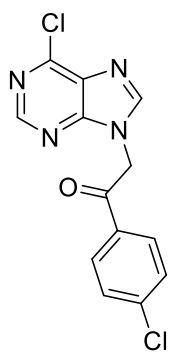
8.4.4.5. 1-(2,4-dichlorophenyl)-2-(6-methoxy-9*H*-purin-9-yl)ethan-1-one (17)



Following method A, 6-methoxypurine (**2** – 100 mg, 0.67 mmol), 2-chloro-1-(2,4-dichlorophenyl)ethan-1-one (223 mg, 1.0 mmol), NaH (60 % dispersion in mineral oil, 32 mg, 799  $\mu$ mol) in dry DMF (11 mL) yielded **17** as a yellowish powder (53 mg, 24 %) after purification by CC (gradient of acetone in hexane, 12/88 to 80/20).  $^1H$  NMR (300 MHz, acetone- $d_6$ )  $\delta$  8.47 (s, 1H, H2), 8.25 (s, 1H, H8), 7.99 (d,  $J$  = 8.4 Hz, 1H, H6'), 7.71 (d,  $J$  = 2.1 Hz, 1H, H3'), 7.61 (dd,  $J$  = 8.3, 2.2 Hz, 1H, H5'), 5.89 (s, 2H,  $CH_2$ ), 4.15 (s, 3H,  $CH_3$ ).  $^{13}C$  NMR (75.4 MHz, acetone- $d_6$ )  $\delta$  194.0, 161.9, 153.7, 152.7,

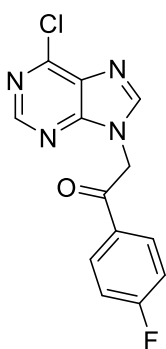
144.7, 139.1, 135.2, 133.6, 132.5, 131.6, 128.7, 121.8, 54.4, 52.8. HRMS (ESI+) mass calcd for  $C_{14}H_{10}Cl_2N_4O_2$  (m/z) 337.0253 [M + H]<sup>+</sup>; found, 337.0256. Mp 158 °C (dec). Anal. calcd for  $C_{14}H_{10}Cl_2N_4O_2$ : C, 49.87; H, 2.99; N, 16.62. Found: C, 50.01; H, 3.11; N, 16.38.

8.4.4.6. 2-(6-chloro-9*H*-purin-9-yl)-1-(4-chlorophenyl)ethan-1-one (**18**)



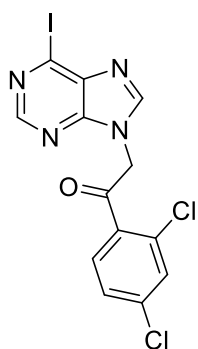
Following method A, 6-chloropurine (100 mg, 0.65 mmol), 2-chloro-1-(2,4-dichlorophenyl)ethan-1-one (183 mg, 0.97 mmol), NaH (60 % dispersion in mineral oil, 31 mg, 796  $\mu$ mol) in dry DMF (10 mL) yielded **18** as a white powder (95 mg, 48 %) after purification by CC (gradient of acetone in hexane, 10/90 to 80/20). <sup>1</sup>H NMR (300 MHz, acetone-d<sub>6</sub>)  $\delta$  8.69 (s, 1H, H2), 8.53 (s, 1H, H8), 8.20 (d, J = 8.6 Hz, 2H, H2'), 7.68 (d, J = 8.6 Hz, 2H, H3'), 6.12 (s, 2H, CH<sub>2</sub>). <sup>13</sup>C NMR (75.4 MHz, acetone-d<sub>6</sub>)  $\delta$  191.6, 153.8, 152.7, 150.9, 148.5, 141.0, 134.0, 132.2, 131.0, 130.3, 50.8. HRMS (ESI+) mass calcd for  $C_{13}H_8Cl_2N_4O$  (m/z) 307.0147 [M + H]<sup>+</sup>; found, 307.0161. Mp 217 °C (dec.). Anal. calcd for  $C_{13}H_8Cl_2N_4O$ : C, 50.84; H, 2.63; N, 18.24. Found: C, 50.77; H, 2.78; N, 18.26.

8.4.4.7. 2-(6-chloro-9*H*-purin-9-yl)-1-(4-fluorophenyl)ethan-1-one (**19**)



Following method A, 6-chloropurine (100 mg, 0.65 mmol), 2-chloro-1-(4-fluorophenyl)ethan-1-one (167 mg, 0.97 mmol), NaH (60 % dispersion in mineral oil, 31 mg, 796  $\mu$ mol) in dry DMF (10 mL) yielded **19** as a white powder (156 mg, 83 %) after purification by CC (gradient of EtOAc in hexane, 12/88 to 100/0). <sup>1</sup>H NMR (300 MHz, acetone-d<sub>6</sub>)  $\delta$  8.69 (s, 1H, H2), 8.54 (s, 1H, H8), 8.27 (ddd, J = 8.9, 4.6, 1.7 Hz, 2H, H2'), 7.46–7.34 (m, 2H, H3'), 6.12 (s, 2H, CH<sub>2</sub>). <sup>13</sup>C NMR (75.4 MHz, acetone-d<sub>6</sub>)  $\delta$  191.0, 167.1 (d, J = 253.3 Hz), 153.6, 152.5, 150.8, 148.4, 132.1 (d, J = 9.8 Hz), 131.9, 131.9, 116.9 (d, J = 21.9 Hz), 50.6. HRMS (ESI+) mass calcd for  $C_{13}H_8ClFN_4O$  (m/z) 291.0443 [M + H]<sup>+</sup>; found, 291.0454. Mp 162–165 °C. Anal. calcd for  $C_{13}H_8ClFN_4O$ : C, 53.72; H, 2.77; N, 19.27. Found: C, 53.86; H, 2.93; N, 19.37.

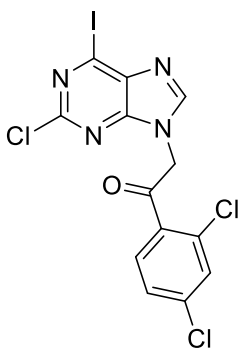
8.4.4.8. 1-(2,4-dichlorophenyl)-2-(6-iodo-9*H*-purin-9-yl)ethan-1-one (**21**)



Following method A, 6-iodopurine (**20** – 50 mg, 0.20 mmol), 2-chloro-1-(2,4-dichlorophenyl)ethan-1-one (70 mg, 0.34 mmol), NaH (60 % dispersion in mineral oil, 12 mg, 304  $\mu\text{mol}$ ) in dry DMF (3.5 mL) yielded **21** as a white powder (21 mg, 24 %) after purification by CC (gradient of EtOAc in hexane, 15/85 to 100/0).  $^1\text{H}$  NMR (300 MHz, acetone- $d_6$ )  $\delta$  8.58 (s, 1H, H2), 8.53 (s, 1H, H8), 8.02 (d,  $J = 8.4$  Hz, 1H, H6'), 7.72 (s, 1H, H3'), 7.63 (d,  $J = 8.6$  Hz, 1H, H5'), 5.97 (s, 2H,  $\text{CH}_2$ ).  $^{13}\text{C}$  NMR (75.4 MHz, acetone- $d_6$ )  $\delta$  193.5, 152.8, 147.5, 139.4, 139.3, 134.9, 133.9, 132.7, 131.8, 128.9,

122.3, 53.2. HRMS (ESI+) mass calcd for  $\text{C}_{13}\text{H}_7\text{Cl}_2\text{IN}_4\text{O}$  ( $m/z$ ), 432.9114 [ $\text{M} + \text{H}$ ] $^+$ ; found, 432.9102. Mp 172  $^\circ\text{C}$  (dec). HPLC-UV ( $\lambda = 260$  nm): purity 93 %.

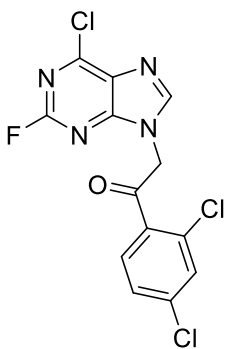
8.4.4.9. 2-(2-chloro-6-iodo-9*H*-purin-9-yl)-1-(2,4-dichlorophenyl)ethan-1-one (**23**)



Following method A, 2-chloro-6-iodopurine (**22** – 69 mg, 0.25 mmol), 2-chloro-1-(2,4-dichlorophenyl)ethan-1-one (85 mg, 0.37 mmol), NaH (60 % dispersion in mineral oil, 15 mg, 369  $\mu\text{mol}$ ) in dry DMF (4 mL) yielded **23** as a yellowish powder (30 mg, 28 %) after purification by trituration in  $\text{Et}_2\text{O}$ .  $^1\text{H}$  NMR (300 MHz, acetone- $d_6$ )  $\delta$  8.55 (s, 1H, H8), 8.04 (d,  $J = 8.4$  Hz, 1H, H6'), 7.73 (d,  $J = 2.1$  Hz, 1H, H3'), 7.63 (dd,  $J = 8.4, 2.1$  Hz, 1H, H5'), 5.97 (s, 2H,  $\text{CH}_2$ ).  $^{13}\text{C}$  NMR (75.4 MHz, acetone- $d_6$ )  $\delta$  191.9, 151.7, 150.1, 147.5, 138.5, 138.0, 133.5, 133.0, 131.8, 130.8,

127.8, 121.7, 52.2. HRMS (ESI+) mass calcd for  $\text{C}_{13}\text{H}_6\text{Cl}_3\text{IN}_4\text{O}$  ( $m/z$ ) 466.8724 [ $\text{M} + \text{H}$ ] $^+$ ; found, 466.8721. Mp 214–215  $^\circ\text{C}$  (dec). HPLC-UV ( $\lambda = 284$  nm): purity > 99 %.

8.4.4.10. 2-(6-chloro-2-fluoro-9*H*-purin-9-yl)-1-(2,4-dichlorophenyl)ethan-1-one (**25**)

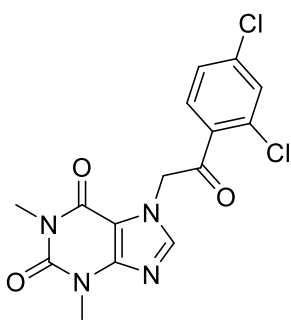


Following method A, 6-chloro-2-fluoropurine (**24** – 42 mg, 0.24 mmol), 2-chloro-1-(2,4-dichlorophenyl)ethan-1-one (82 mg, 0.36 mmol), NaH (60 % dispersion in mineral oil, 15 mg, 365  $\mu\text{mol}$ ) in dry DMF (4 mL) yielded **25** as a yellow oil (34 mg, 39 %) after purification by CC (gradient of acetone in hexane, 6/94 to 50/50).  $^1\text{H}$  NMR (300 MHz, acetone- $d_6$ )  $\delta$  8.55 (s, 1H, H8), 8.04 (d,  $J = 8.4$  Hz, 1H, H6'), 7.73 (d,  $J = 2.0$  Hz, 1H, H3'), 7.63 (dd,  $J = 8.4, 2.0$  Hz, 1H, H5'), 5.98 (s, 2H,  $\text{CH}_2$ ).  $^{13}\text{C}$  NMR (75.4 MHz, acetone- $d_6$ )  $\delta$  191.9, 157.9 (d,  $J = 214.9$  Hz), 154.7 (d,  $J =$

17.3 Hz), 151.4 (d,  $J = 18.1$  Hz), 148.2 (d,  $J = 3.0$  Hz), 138.5, 133.6, 133.0, 131.8, 130.8, 130.1 (d,  $J = 6.8$

Hz), 127.8, 52.3. HRMS (ESI+) mass calcd for  $C_{13}H_6Cl_3FN_4O$  ( $m/z$ ) 358.9663 [ $M + H$ ]<sup>+</sup>; found, 358.9657. Mp 134 °C. HPLC-UV ( $\lambda = 260$  nm): purity > 98 %.

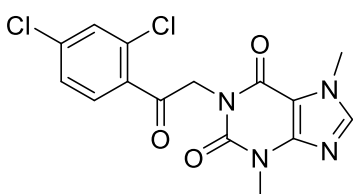
8.4.4.11. 9-[2-(2,4-dichlorophenyl)-2-oxoethyl]-1,3-dimethyl-3,9-dihydro-1*H*-purine-2,6-dione (35)



Following method B, theophylline (1,3-dimethyl-3,9-dihydro-1*H*-purine-2,6-dione, 70 mg, 0.39 mmol), 2-chloro-1-(2,4-dichlorophenyl)ethan-1-one (104 mg, 0.47 mmol), TBAHS (7 mg, 19  $\mu$ mol), and  $K_2CO_3$  (54 mg, 0.39 mmol) in dry DMF (2 mL), yielded **35** as a white powder (65 mg, 46 %) after purification by CC (gradient of MeOH in EtOAc, 1/99 to 10/90) and trituration in  $Et_2O$ . <sup>1</sup>H NMR (300 MHz, acetone- $d_6$ )  $\delta$  8.04–7.94 (m, 2H, H8, H6'), 7.69 (d,  $J = 2.1$  Hz, 1H, H3'), 7.62 (dd,  $J = 8.4, 2.1$  Hz, 1H, H5'), 5.87 (s, 2H,  $CH_2$ ), 3.53 (s, 3H, N3- $CH_3$ ), 3.26 (s, 3H, N1- $CH_3$ ).

<sup>13</sup>C NMR (75.4 MHz, acetone- $d_6$ )  $\delta$  194.1, 156.2, 152.4, 149.7, 144.0, 139.1, 135.6, 133.5, 132.7, 131.5, 128.8, 107.7, 55.8, 28.0. HRMS (ESI+) mass calcd for  $C_{15}H_{12}Cl_2N_4O_3$  ( $m/z$ ) 367.0359 [ $M + H$ ]<sup>+</sup>; found, 367.0368. Mp 198–199 °C. HPLC-UV ( $\lambda = 260$  nm), purity > 96 %.

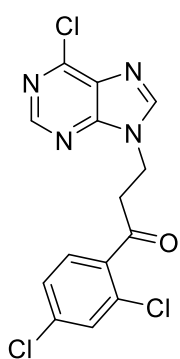
8.4.4.12. 1-[2-(2,4-dichlorophenyl)-2-oxoethyl]-3,7-dimethyl-3,7-dihydro-1*H*-purine-2,6-dione (36)



Following method B, theobromine (3,7-dimethyl-3,7-dihydro-1*H*-purine-2,6-dione, 70 mg, 0.39 mmol), 2-chloro-1-(2,4-dichlorophenyl)ethan-1-one (104 mg, 0.47 mmol), TBAHS (7 mg, 19  $\mu$ mol), and  $K_2CO_3$  (54 mg, 0.39 mmol) in dry DMF (2 mL) yielded **36** as a brown powder (36 mg, 25 %) after purification by CC (gradient of MeOH in EtOAc, 0/100 to 4/96) and trituration in  $Et_2O$ .

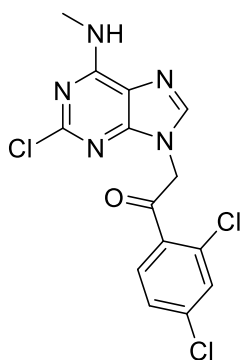
<sup>1</sup>H NMR (300 MHz, acetone- $d_6$ )  $\delta$  7.89 (s, 1H, H8), 7.86 (d,  $J = 8.3$  Hz, 2H, H6'), 7.67 (d,  $J = 2.0$  Hz, 1H, H3'), 7.58 (dd,  $J = 8.4, 2.0$  Hz, 1H, H5'), 5.28 (s, 2H,  $CH_2$ ), 3.99 (s, 3H, N7- $CH_3$ ), 3.51 (s, 3H, N3- $CH_3$ ). <sup>13</sup>C NMR (75.4 MHz, acetone- $d_6$ )  $\delta$  195.4, 155.3, 152.0, 150.2, 143.9, 138.4, 136.6, 133.1, 132.1, 131.3, 128.6, 50.2, 33.8. HRMS (ESI+) mass calcd for  $C_{15}H_{12}Cl_2N_4O_3$  ( $m/z$ ) 367.0359 [ $M + H$ ]<sup>+</sup>; found, 367.0367. Mp 196 °C (dec.). Anal. calcd for  $C_{15}H_{12}Cl_2N_4O_3$ : C, 49.07; H, 3.29; N, 15.26. Found: C, 49.05; H, 3.39; N, 15.19.

#### 8.4.4.13. 3-(6-chloro-9*H*-purin-9-yl)-1-(2,4-dichlorophenyl)propan-1-one (38)



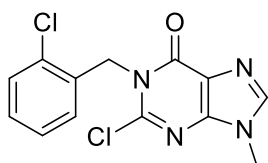
Following method A, 6-chloropurine (75 mg, 0.49 mmol), intermediate **37** (174 mg, 0.73 mmol), NaH (60 % dispersion in mineral oil, 23 mg, 586  $\mu$ mol) in dry DMF (10 mL) yielded **38** as a white powder (40 mg, 23 %) after purification by CC (gradient of EtOAc in hexane, 20/80 to 100/0).  $^1\text{H}$  NMR (300 MHz, acetone- $d_6$ )  $\delta$  8.70 (s, 1H, H2), 8.55 (s, 1H, H8), 7.72 (d,  $J = 8.4$  Hz, 1H, H6'), 7.58 (d,  $J = 2.1$  Hz, 1H, H3'), 7.48 (dd,  $J = 8.4, 2.0$  Hz, 1H, H5'), 4.80 (t,  $J = 6.3$  Hz, 2H, NCH<sub>2</sub>), 3.81 (t,  $J = 6.3$  Hz, 2H, CH<sub>2</sub>CO).  $^{13}\text{C}$  NMR (75.4 MHz, acetone- $d_6$ )  $\delta$  198.3, 152.3, 151.4, 149.7, 147.2, 137.2, 136.6, 131.9, 131.5, 130.9, 130.3, 127.5, 41.3, 39.1. HRMS (ESI+) mass calcd for C<sub>14</sub>H<sub>9</sub>Cl<sub>3</sub>N<sub>4</sub>O (m/z) 354.9914 [M + H]<sup>+</sup>; found, 354.9919. Mp 140 °C (dec). HPLC-UV ( $\lambda = 256$  nm), purity > 98 %.

#### 8.4.5. Synthesis of 2-[2-chloro-6-(methylamino)-9*H*-purin-9-yl]-1-(2,4-dichlorophenyl)ethan-1-one (**11**)



2-chloro-*N*-methylpurin-6-amine (60 mg, 0.33 mmol), TBAHS (5.5 mg, 16  $\mu$ mol) and KOH (18 mg, 0.33 mmol) were suspended in dry DMF (2 mL) under dry and inert conditions. 2-chloro-1-(2,4-dichlorophenyl)ethan-1-one (80 mg, 0.36 mmol) was dissolved in dry DMF (0.5 mL) and added dropwise to the reaction at 0 °C over 45 min. The reaction was stirred at rt for 26 h and then it was diluted with cold water (6 mL) and EtOAc (7 mL). The mixture was stirred for 30 min after which the two layers were separated. The aqueous fraction was extracted with EtOAc (3 x 3 mL) and the combined organic layer was washed with brine, dried over anhydrous Na<sub>2</sub>SO<sub>4</sub>, filtered, and evaporated under reduced pressure. The crude was purified by CC (gradient of EtOAc in hexane, 18/82 to 100/0). After solvent evaporation, the solid was triturated with Et<sub>2</sub>O, furnishing **11** as a white solid (27 mg, 22 %). The compound was recrystallised in EtOAc by slow evaporation to obtain crystals for X-Ray diffraction.  $^1\text{H}$  NMR (300 MHz, acetone- $d_6$ )  $\delta$  8.02 (s, 1H, H8), 7.98 (d,  $J = 8.4$  Hz, 1H, H6'), 7.70 (d,  $J = 2.1$  Hz, 1H, H3'), 7.61 (dd,  $J = 8.4, 2.1$  Hz, 1H, H5'), 7.24 (bs, 1H, NH), 5.75 (s, 2H, CH<sub>2</sub>), 3.12 (s, 3H, CH<sub>3</sub>).  $^{13}\text{C}$  NMR (75.4 MHz, acetone- $d_6$ )  $\delta$  193.9, 157.1, 154.3, 142.4, 139.1, 135.1, 133.6, 132.5, 131.5, 128.6, 119.2, 52.5, 27.7. HRMS (ESI+) mass calcd for C<sub>14</sub>H<sub>10</sub>Cl<sub>3</sub>N<sub>5</sub>O (m/z) 370.0023 [M + H]<sup>+</sup>; found, 370.0041. Mp 213 °C (dec). Anal. calcd for C<sub>14</sub>H<sub>10</sub>Cl<sub>3</sub>N<sub>5</sub>O·H<sub>2</sub>O: C, 43.27; H, 3.11; N, 18.02. Found: C, 43.33; H, 2.80; N, 17.99.

#### 8.4.6. Synthesis of 2-chloro-1-(2-chlorobenzyl)-9-methyl-1,9-dihydro-6H-purin-6-one (**40**)



Following the procedure described by Szarek and collaborators (Szarek *et al.*, 1985), NaHCO<sub>3</sub> (35 mg, 0.42 mmol) was added to a solution of intermediate **39** (24 mg, 0.13 mmol) in DMF (1 mL). The reaction was stirred at rt for 30 min. 1-chloro-2-(chloromethyl)benzene (40  $\mu$ L, 0.31 mmol) was added dropwise and the mixture heated up to 75 °C and stirred overnight. The solvent was evaporated under reduced pressure and the residue retrieved with water (3 mL) and extracted with EtOAc (3  $\times$  2 mL). The combined organic layer was washed with brine, dried over anhydrous Na<sub>2</sub>SO<sub>4</sub>, filtered, and the solvent evaporated under reduced pressure. Purification was performed by CC (gradient of EtOAc in hexane, 15/85 to 80/20), giving **40** as a brownish powder (10 mg, 32 %). <sup>1</sup>H NMR (300 MHz, acetone-d<sub>6</sub>)  $\delta$  8.44 (s, 1H, H<sub>8</sub>), 7.51 (dd, J = 7.8, 1.5 Hz, 1H, H<sub>3'</sub>), 7.35 (m, 2H, H<sub>4'</sub>, H<sub>5'</sub>), 7.08 (dd, J = 7.6, 1.9 Hz, 1H, H<sub>6'</sub>), 5.77 (s, 2H, CH<sub>2</sub>), 4.07 (s, 3H, CH<sub>3</sub>). <sup>13</sup>C NMR (75.4 MHz, acetone-d<sub>6</sub>)  $\delta$  161.4, 153.8, 152.3, 143.8, 133.5, 132.8, 129.9, 129.8, 129.7, 127.6, 120.3, 54.4, 45.0. HRMS (ESI+) mass calcd for C<sub>13</sub>H<sub>10</sub>Cl<sub>2</sub>N<sub>4</sub>O (m/z) 309.0304 [M + H]<sup>+</sup>; found, 309.0308. Mp 146–149 °C. HPLC-UV ( $\lambda$  = 250 nm): purity > 95 %.

## 8.5. Pharmacological methods

### 8.5.1. HEK293-hP2X7 cell culture

The human embryonic kidney cell line that stably expresses the human P2X7 isoform A (hP2X7-HEK293), was generously donated by Francesco di Virgilio's group (University of Ferrara, Italy). HEK293-hP2X7 cells were kept in 75 cm<sup>2</sup> flasks under DMEM-F12 culture medium enriched with 50 units/mL penicillin and 50  $\mu$ g/mL streptomycin, 10% FBS bovine serum and 0.2 mg/mL of geneticin (G-418 sulfate, Roche Diagnostics GmbH, Mannheim, Germany), which was used as a selection reagent. Cells grew up to 95 % confluence in an incubator with a constant atmosphere of 5 % CO<sub>2</sub>, saturated humidity and temperature of 37 °C. For culture plating, cells were detached using Trypsin-EDTA 0.05 %, counted and seeded in 96-well black, clear-bottomed plates (Corning Inc. Kennebunk ME, USA) at a different density depending on the experiment. Experiments were performed 24–48 h after plating.



### 8.5.2. YO-PRO-1 iodide uptake

hP2X7-HEK293 cells were seeded at a density of 400,000 cells/well. After 48 h, culture medium was removed and the cells were incubated with Mg<sup>2+</sup>-free Krebs-HEPES buffer containing (in mM): 144 NaCl, 5.9 KCl, 11 glucose, 10 HEPES, and 0.2 CaCl<sub>2</sub> at pH 7.4. Test compounds were incubated for 20 min, YO-PRO-1 probe (2 μM) was applied, and subsequently cells were stimulated with BzATP (30 μM). Changes in the fluorescence (excitation at 485 nm and emission at 520 nm) were measured for 25 min using a fluorescence multi-well plate reader (Fluostar, BMG Labtech, Offenburg, Germany). Responses are normalised respect to the maximum (F<sub>max</sub>) and the minimum (F<sub>min</sub>) of the fluorescence values per well. F<sub>max</sub> was obtained by adding 0.5 % Triton X-100 at the end of the experiment, while F<sub>min</sub> was measured by subsequently adding 2 M MnCl<sub>2</sub>. Data were calculated following the formula  $F = (F_x - F_0)/(F_{max} - F_{min})$ , where F<sub>x</sub> is the maximum fluorescence obtained for the test compounds and F<sub>0</sub> is the averaged basal fluorescence before YO-PRO-1 injection.

### 8.5.3. Fura-2 Ca<sup>2+</sup> measurements

hP2X7-HEK293 cells were seeded at a density of 50,000 cells/well and, after 24–48 h, were loaded with 8 μM Fura-2-AM (Invitrogen or Biotium, USA) for 1 h at 37 °C. Fura-2-AM is the acetoxymethyl ester of Fura-2. The esterification conveys cell permeability to this probe, which is readily hydrolysed by endogenous esterases to give the actual Ca<sup>2+</sup> detector. After incubation, loading medium was washed with Tyrode solution without Mg<sup>2+</sup> (in mM): 137 NaCl, 10 HEPES, 2 CaCl<sub>2</sub>, 4 KCl, and 10 glucose at pH 7.4. Test compounds were incubated for 15–30 min. Fura-2 Ca<sup>2+</sup> measurements were carried out with a fluorescence multi-well plate reader (Fluostar Optima, BMG, Germany). Cells were alternatively excited by 340 and 380 nm wavelength lights and fluorescence emitted recovered with a 520/10 nm filter for both excitation wavelengths. After a few cycles of basal fluorescence recording, the P2X7 agonist BzATP was injected to get a final concentration of 100 μM. Fluorescence was transformed to [Ca<sup>2+</sup>]<sub>c</sub> with the Grynkiewicz's equation (Grynkiewicz *et al.*, 1985). Each experimental condition was performed in triplicates and averaged. Blockade is expressed as percentage of the maximum [Ca<sup>2+</sup>]<sub>c</sub> increase elicited by BzATP in control Tyrode-only wells.

### 8.5.4. Electrophysiological measurements

cDNA of human His-P2X7 was synthesised (GeneArt String DNA fragment, Life Technologies/Thermo Fisher Scientific Inc.) and cloned together with the poly-A tail from the pNKS2 vector (Gloor *et al.*,

1995) into a modified pUC19 vector. Rat P2X7 cDNA was present in pSGem (Nicke *et al.*, 2009) and rat P2X1 and P2X2 subunits were present in pNKS2 (Gloor *et al.*, 1995). Capped cRNAs were formed from linearised templates using the mMESSAGE mMACHINE® Kit (Ambion™, Austin, Texas, USA). Oocytes were kindly donated by Prof. Luis Pardo (MPI for Experimental Medicine, Göttingen) or from EcoCyte Bioscience (Dortmund, Germany), injected with 50 nL of cRNA (0.5 mg/mL for rP2X1, rP2X4 and hP2X7; 0.1 mg/mL for rP2X2; 25 µg/mL for rP2X7), and incubated for 1–2 days at 16–18 °C before recordings were performed in a low divalent-cation solution (90 mM NaCl, 1 mM KCl, 0.5 mM CaCl<sub>2</sub>, 5 mM HEPES) as previously described (Beissner *et al.*, 2012). Current responses to ATP (300 µM for hP2X7, 30 µM for rP2X4 and rP2X7, and 10 µM for rP2X2 and rP2X1) were measured by two-electrode voltage clamp (TEVC) technique at –70 mV, using a Turbo Tec 05X Amplifier (NPI Electronic, Tamm, Germany) and Cell Works software. One electrode records the membrane potential and the other injects the current, without the need of creating a patch in the membrane. This technique is very sensitive, due to the high expression of the receptor of interest that allows the detection of currents from 30 nA to 100 µA intensity. The resistance of the electrodes on the membrane was lower than 1.2 MΩ, while the current leak was greater than –0.12 µA. A rapid exchange of solution, about 300 ms, was reached with a 50 µL oocyte chamber with a funnel shape, combined with a fast flow (150 µL/s), fed through a manifold built immediately above the oocyte (Figure 45).

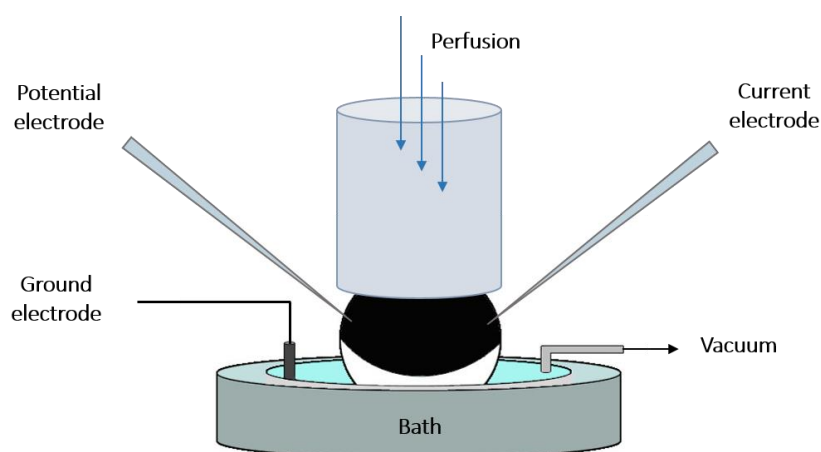


**Figure 45.** Schematic illustration of the set-up used for two-electrode voltage clamp (TEVC) in *Xenopus laevis* oocytes.

Compounds were directly diluted in the recording chamber and incubated for 3 min without perfusion. ATP pulses were applied for 2 s (3 s for rP2X7 subtype) at 4-min intervals, followed by 58 s of perfusion. Current responses of test compounds were recorded only after three stable currents

of ATP, as negative control. A variation within  $\pm 10\%$  respect to the previous current was accepted as indeterminate error.

#### 8.5.5. Isolation of murine peritoneal macrophages and IL-1 $\beta$ detection

Murine peritoneal macrophages (MPMs) were obtained from 6–8 weeks old C57BL/6 mice. Twenty-four hours before macrophages extraction, mice were intraperitoneally injected with 1 mL of 3.8 % Brewer's thioglycolate medium in order to attract circulating macrophages to the peritoneal cavity. The day after, mice were euthanised by cervical dislocation and the abdominal skin was retracted to expose the peritoneal wall. Great attention was paid to mitigate animal suffering, according to the EU Council Directive guidelines. Procedures were approved by the Universidad Autónoma de Madrid (UAM) Ethics Committee. Ten millilitres of cold sterile PBS were injected in the peritoneal cavity with a 20-G needle, and the peritoneal content was obtained by aspirating the fluid with the same syringe and needle. The peritoneal exudate cells were centrifuged at 4 °C for 10 min at 1000 rpm, and cell pellet was re-suspended in 1 mL of cold DMEM high glucose (Gibco) supplemented with 10 % FBS (Gibco) and 100 U/mL penicillin/streptomycin (Lonza). Cells were counted with a Neubauer chamber and cell concentration was adjusted to  $1\text{--}3 \times 10^6$  cells/mL. Macrophages were seeded in 24-well plates at a density of  $3 \times 10^5$  cells/well and primed with 1  $\mu\text{g/mL}$  of LPS (*E. coli* 026:B6 serotype; Sigma-Aldrich) in DMEM high glucose + 10 % FBS for 4 h. After this time, LPS-containing medium was removed and fresh DMEM with no FBS, but the testing compounds, was added for 15 min. ATP (Sigma-Aldrich) at 5 mM of concentration was then added for 30 min and cell supernatants were collected and frozen at  $-20\text{ }^\circ\text{C}$  for IL-1 $\beta$  detection. IL-1 $\beta$  (pg/mL) in the collected cell supernatants was quantified using a specific ELISA kit. Supernatant samples were obtained from the treated MPMs and subjected to the ELISA analysis according to the supplier recommendations (R&D systems).

#### 8.5.6. Parallel artificial membrane permeability assay (PAMPA)

A lipophilic membrane was prepared by dissolving porcine brain polar lipid extract (Avanti, Merck) in dodecane (Sigma-Aldrich) at a concentration of 20 mg/mL and injecting 4  $\mu\text{L}$  of it on the membrane of each well of a 96-well Multiscreen® Filter Plate (Reference: MAIPNTR10, Millipore, Merck). Compound solutions were prepared at 100  $\mu\text{M}$  in PBS at pH 7.4 (Sigma-Aldrich, Merck). Blank solution contained 1 % of DMSO. Each well was then filled with 180  $\mu\text{L}$  of compounds or blank

solution, whereas the corresponding wells of the acceptor Multiscreen® 96-well tray (MAMCS9610, Millipore, Merck) were filled with an equal amount of PBS at pH 7.4. The filter plate was inserted in the acceptor tray and incubated at rt for 4 h. A volume of 150 µL of the content of the acceptor plate was transferred to a UV-transparent 96-well plate (MSCPNUV40, Millipore, Merck) for absorbance measurements. The absorbance of the compounds at initial and equilibrium concentrations (100 µM and 50 µM, respectively) was also measured. Compounds absorption spectra were recorded by a SPECTROstar Nano Microplate Reader (BMG Labtech, Orterberg, Germany) and corrected by blank absorption spectra. Concentrations and permeability values were calculated with the following equations:

$$P(10^{-6} \cdot \text{cm} \cdot \text{s}^{-1}) = K \cdot -\ln(1 - C_{ac}/C_{eq})$$

$$K = V/2 \cdot a \cdot t$$

$$C_{ac} = A_{ac} \cdot C_0/A_0$$

$$C_{eq} = A_{eq} \cdot C_0/A_0$$

where V is the volume of solutions during the experiment (180 µL); a is the membrane area in cm<sup>2</sup>; t is the time of incubation in seconds; C<sub>0</sub> is the starting concentration of compound solutions; A<sub>0</sub> is the compounds absorbance measured at starting concentration; A<sub>eq</sub> is the compounds absorbance measured at equilibrium concentration, as if it was completely membrane permeable; A<sub>ac</sub> is the absorbance of the solutions in the acceptor plate. The wavelength at maximum absorbance was considered for calculations for each compound (240 nm for JNJ-47965567; 264 nm for **4**, **9**, **10**, **21**, **35**, **36** and **40**; 274 nm for theophylline, **5** and **25**; 284 nm for verapamil and **27**; 365 nm for piroxicam). All data are presented as mean ± SEM of triplicates of three individual experiments performed in three different days.

#### 8.5.7. P-glycoprotein ATPase activity assay

Human P-glycoprotein ATPase activity was measured using the luminescence-based Pgp-glo™ Assay System (Promega, Madison, WI, USA). The assay was performed according to manufacturer's protocol (freely available at Promega webpage). Briefly, DMSO-dissolved reference or test compounds were diluted in Pgp-assay buffer at a concentration of 10 µM, and plated in a white opaque 96-well plate. Pgp membranes (1.25 mg/mL) were added into each well. After the addition

of MgATP (final concentration 5 mM), the plate was incubated for 1.5 h. ATP detection reagent was added and the plate was incubated again at rt for 20 min. The ATP detection reagent contains the firefly luciferase enzyme and its substrate, luciferin. In the presence of ATP, luciferin is oxidised into oxyluciferin, releasing light, which is detected by a microplate luminometer (Orion II, Berthold Technologies GmbH & Co. KG, Germany) (Figure 46). Data were processed according to manufacturer's protocol. Basal relative luminescence unit (R.L.U) variation was calculated as the R.L.U. difference of  $\text{Na}_3\text{VO}_4$ -treated wells and non-treated wells R.L.U.  $\text{Na}_3\text{VO}_4$  is an inhibitor of Pgp, and the result of this calculation represents the Pgp basal consumption of ATP. Compounds R.L.U. variation was calculated as the R.L.U. difference of  $\text{Na}_3\text{VO}_4$ -treated wells and compound-treated wells.

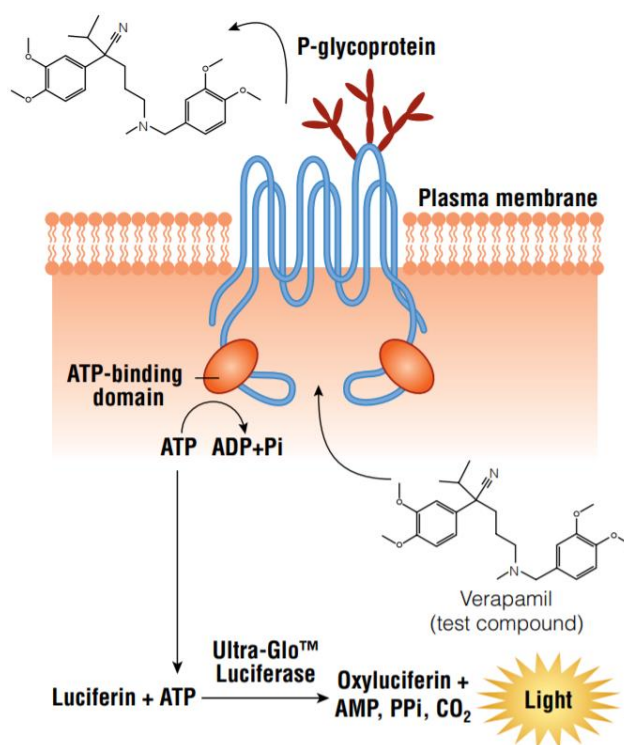


**Figure 46.** Representation of the efflux transport of Verapamil through the Pgp pump. The Pgp ATPase assay uses the firefly luciferase enzyme to measure residual ATP after Pgp activity. Image taken from Pgp-Glo™ protocol (available online for free).


### 8.5.8. Molecular docking

The ligand was docked with the permission of Dr. Ralf Schmid in the homology model of the hP2X7 published by Dayel and collaborators (Dayel *et al.*, 2019). Molecules 3D conformations were

generated using Open Babel (O'Boyle *et al.*, 2011). The ligand was docked in two previously described allosteric binding pockets of the hP2X7 (Bidula *et al.*, 2019a; Dayel *et al.*, 2019; Karasawa and Kawate, 2016) and in the orthosteric binding pocket, using a squared grid with side of 22–26 Å. Docking was performed using AutodockTools and Autodock Vina (Trott and Olson, 2010) and represented using UCSF Chimera (Pettersen *et al.*, 2004).

#### 8.5.9. Data analysis

The statistically significant differences were analysed by the one sample t test or the one-way analysis of variance (ANOVA) using Prism 8.0.1 (GraphPad). Groups of data were considered statistically different when  $p < 0.05$ .

A horizontal watercolor splash in shades of light blue and white, with a darker blue blotch on the right side. The word "References" is centered within this splash.

## References

## 9. References

- Abberley, L., Bebius, A., Beswick, P.J., Billinton, A., Collis, K.L., Dean, D.K., Fonfria, E., Gleave, R.J., Medhurst, S.J., Michel, A.D., Moses, A.P., Patel, S., Roman, S.A., Scoccitti, T., Smith, B., Steadman, J.G.A., Walter, D.S., 2010. Identification of 2-oxo-N-(phenylmethyl)-4-imidazolidinecarboxamide antagonists of the P2X7 receptor. *Bioorg. Med. Chem. Lett.* 20, 6370–6374. <https://doi.org/10.1016/j.bmcl.2010.09.101>
- Abbracchio, M.P., Boeynaems, J.M., Barnard, E.A., Boyer, J.L., Kennedy, C., Miras-Portugal, M.T., King, B.F., Gachet, C., Jacobson, K.A., Weisman, G.A., Burnstock, G., 2003. Characterization of the UDP-glucose receptor (re-named here the P2Y14 receptor) adds diversity to the P2Y receptor family. *Trends Pharmacol Sci* 24, 52–5. [https://doi.org/10.1016/S0165-6147\(02\)00038-X](https://doi.org/10.1016/S0165-6147(02)00038-X)
- Abbracchio, M.P., Burnstock, G., 1994. Purinoceptors: Are there families of P2X and P2Y purinoceptors? *Pharmacol. Ther.* 64, 445–475. [https://doi.org/10.1016/0163-7258\(94\)00048-4](https://doi.org/10.1016/0163-7258(94)00048-4)
- Abdelrahman, A., Namasivayam, V., Hinz, S., Schiedel, A.C., Köse, M., Burton, M., El-Tayeb, A., Gillard, M., Bajorath, J., de Ryck, M., Müller, C.E., 2017. Characterization of P2X4 receptor agonists and antagonists by calcium influx and radioligand binding studies. *Biochem. Pharmacol.* 125, 41–54. <https://doi.org/10.1016/j.bcp.2016.11.016>
- Abdi, M.H., Beswick, P.J., Billinton, A., Chambers, L.J., Charlton, A., Collins, S.D., Collis, K.L., Dean, D.K., Fonfria, E., Gleave, R.J., Lejeune, C.L., Livermore, D.G., Medhurst, S.J., Michel, A.D., Moses, A.P., Page, L., Patel, S., Roman, S.A., Senger, S., Slingsby, B., Steadman, J.G.A., Stevens, A.J., Walter, D.S., 2010. Discovery and structure–activity relationships of a series of pyroglutamic acid amide antagonists of the P2X7 receptor. *Bioorg. Med. Chem. Lett.* 20, 5080–5084. <https://doi.org/10.1016/j.bmcl.2010.07.033>
- Able, S.L., Fish, R.L., Bye, H., Booth, L., Logan, Y.R., Nathaniel, C., Hayter, P., Katugampola, S.D., 2011. Receptor localization, native tissue binding and ex vivo occupancy for centrally penetrant P2X7 antagonists in the rat. *Br. J. Pharmacol.* 162, 405–414. <https://doi.org/10.1111/j.1476-5381.2010.01025.x>
- Adinolfi, E., Callegari, M.G., Cirillo, M., Pinton, P., Giorgi, C., Cavagna, D., Rizzuto, R., Virgilio, F.D., 2009. Expression of the P2X7 Receptor Increases the Ca<sup>2+</sup> Content of the Endoplasmic Reticulum, Activates NFATc1, and Protects from Apoptosis. *J. Biol. Chem.* 284, 10120–10128. <https://doi.org/10.1074/jbc.M805805200>
- Adinolfi, E., Callegari, M.G., Ferrari, D., Bolognesi, C., Minelli, M., Wieckowski, M.R., Pinton, P., Rizzuto, R., Di Virgilio, F., 2005. Basal Activation of the P2X7 ATP Receptor Elevates Mitochondrial Calcium and Potential, Increases Cellular ATP Levels, and Promotes Serum-independent Growth. *Mol. Biol. Cell* 16, 3260–3272. <https://doi.org/10.1091/mbc.e04-11-1025>
- Adinolfi, E., Cirillo, M., Woltersdorf, R., Falzoni, S., Chiozzi, P., Pellegatti, P., Callegari, M.G., Sandonà, D., Markwardt, F., Schmalzing, G., Virgilio, F.D., 2010. Trophic activity of a naturally occurring truncated isoform of the P2X7 receptor. *FASEB J.* 24, 3393–3404. <https://doi.org/10.1096/fj.09-153601>
- Adinolfi, E., Giuliani, A.L., De Marchi, E., Pegoraro, A., Orioli, E., Di Virgilio, F., 2018. The P2X7 receptor: A main player in inflammation. *Biochem. Pharmacol.* 151, 234–244. <https://doi.org/10.1016/j.bcp.2017.12.021>



- Agren, G., Pontén, J., Ronquist, G., Westermarck, B., 1974. Nucleoside diphosphate kinase at the cell surface of neoplastic human cells in culture. *J. Cell. Physiol.* 83, 91–101. <https://doi.org/10.1002/jcp.1040830113>
- Alauddin, M.M., Miller, J.M., Clark, J.H., 2011. An investigation of the effects of the medium and the type of fluoride on the hydrogen bond assisted alkylation of phenols. *Can. J. Chem.* <https://doi.org/10.1139/v84-043>
- Alberto, A.V.P., Faria, R.X., Couto, C.G.C., Ferreira, L.G.B., Souza, C.A.M., Teixeira, P.C.N., Fróes, M.M., Alves, L.A., 2013. Is pannexin the pore associated with the P2X7 receptor? *Naunyn. Schmiedebergs Arch. Pharmacol.* 386, 775–787. <https://doi.org/10.1007/s00210-013-0868-x>
- Alcaraz, L., Baxter, A., Bent, J., Bowers, K., Braddock, M., Cladingboel, D., Donald, D., Fagura, M., Furber, M., Laurent, C., Lawson, M., Mortimore, M., McCormick, M., Roberts, N., Robertson, M., 2003. Novel P2X7 receptor antagonists. *Bioorg. Med. Chem. Lett.* 13, 4043–4046. <https://doi.org/10.1016/j.bmcl.2003.08.033>
- Aldrich, C., Bertozzi, C., Georg, G.I., Kiessling, L., Lindsley, C., Liotta, D., Merz, K.M., Schepartz, A., Wang, S., 2017. The Ecstasy and Agony of Assay Interference Compounds. *ACS Chem. Neurosci.* 8, 420–423. <https://doi.org/10.1021/acschemneuro.7b00064>
- Alonso, A., Logroscino, G., Jick, S.S., Hernan, M.A., 2009. Incidence and lifetime risk of motor neuron disease in the United Kingdom: a population-based study. *Eur J Neurol* 16, 745–51.
- Alzheimer, A., 1907. Über eine eigenartige Erkrankung der Hirnrinde. *Allgemeine Z. Für Psychiatr. Psychisch-Gerichtl. Med.* 64, 146–148.
- Amadio, S., Parisi, C., Montilli, C., Carrubba, A.S., Apolloni, S., Volonté, C., 2014. P2Y12 Receptor on the Verge of a Neuroinflammatory Breakdown [WWW Document]. *Mediators Inflamm.* <https://doi.org/10.1155/2014/975849>
- Amadio, S., Parisi, C., Piras, E., Fabbriozzi, P., Apolloni, S., Montilli, C., Luchetti, S., Ruggieri, S., Gasperini, C., Laghi-Pasini, F., Battistini, L., Volonte, C., 2017. Modulation of P2X7 Receptor during Inflammation in Multiple Sclerosis. *Front Immunol* 8, 1529. <https://doi.org/10.3389/fimmu.2017.01529>
- Ananthan, S., Augelli-Szafran, C.E., Galemno, R., Gupta, V., Moukha-Chafiq, O., Suto, M., 2017. Pyrrolopyrimidine Compounds, Use as Inhibitors of the Kinase Lrrk2, and Methods for Preparation Thereof. WO2017106771A1.
- Apolloni, S., Amadio, S., Parisi, C., Matteucci, A., Potenza, R.L., Armida, M., Popoli, P., D'Ambrosi, N., Volonte, C., 2014. Spinal cord pathology is ameliorated by P2X7 antagonism in a SOD1-mutant mouse model of amyotrophic lateral sclerosis. *Model Mech* 7, 1101–9. <https://doi.org/10.1242/dmm.017038>
- Apolloni, S., Parisi, C., Pesaresi, M.G., Rossi, S., Carri, M.T., Cozzolino, M., Volonte, C., D'Ambrosi, N., 2013. The NADPH oxidase pathway is dysregulated by the P2X7 receptor in the SOD1-G93A microglia model of amyotrophic lateral sclerosis. *J Immunol* 190, 5187–95. <https://doi.org/10.4049/jimmunol.1203262>
- Asatryan, L., Yardley, M.M., Khoja, S., Trudell, J.R., Hyunh, N., Louie, S.G., Petasis, N.A., Alkana, R.L., Davies, D.L., 2014. Avermectins differentially affect ethanol intake and receptor function: implications for

- developing new therapeutics for alcohol use disorders. *Int. J. Neuropsychopharmacol.* 17, 907–916. <https://doi.org/10.1017/S1461145713001703>
- Barniol-Xicota, M., Kwak, S.-H., Lee, S.-D., Caseley, E., Valverde, E., Jiang, L.-H., Kim, Y.-C., Vázquez, S., 2017. Escape from adamantane: Scaffold optimization of novel P2X7 antagonists featuring complex polycycles. *Bioorg. Med. Chem. Lett.* 27, 759–763. <https://doi.org/10.1016/j.bmcl.2017.01.039>
- Bartlett, R., Sluyter, V., Watson, D., Sluyter, R., Yerbury, J.J., 2017. P2X7 antagonism using Brilliant Blue G reduces body weight loss and prolongs survival in female SOD1(G93A) amyotrophic lateral sclerosis mice. *PeerJ* 5, e3064. <https://doi.org/10.7717/peerj.3064>
- Baxter, A., Bent, J., Bowers, K., Braddock, M., Brough, S., Fagura, M., Lawson, M., McInally, T., Mortimore, M., Robertson, M., Weaver, R., Webborn, P., 2003. Hit-to-Lead studies: The discovery of potent adamantane amide P2X7 receptor antagonists. *Bioorg. Med. Chem. Lett.* 13, 4047–4050. <https://doi.org/10.1016/j.bmcl.2003.08.034>
- Beamer, E., Göloncsér, F., Horváth, G., Bekő, K., Otrókosi, L., Koványi, B., Sperlágh, B., 2016. Purinergic mechanisms in neuroinflammation: An update from molecules to behavior. *Neuropharmacology, Special Issue: Purines in Neurodegeneration and Neuroregeneration* 104, 94–104. <https://doi.org/10.1016/j.neuropharm.2015.09.019>
- Becker, D., Woltersdorf, R., Boldt, W., Schmitz, S., Braam, U., Schmalzing, G., Markwardt, F., 2008. The P2X7 Carboxyl Tail Is a Regulatory Module of P2X7 Receptor Channel Activity. *J. Biol. Chem.* 283, 25725–25734. <https://doi.org/10.1074/jbc.M803855200>
- Beigi, R.D., Kertesy, S.B., Aquilina, G., Dubyak, G.R., 2003. Oxidized ATP (oATP) attenuates proinflammatory signaling via P2 receptor-independent mechanisms. *Br J Pharmacol* 140, 507–19. <https://doi.org/10.1038/sj.bjp.0705470>
- Beissner, M., Dutertre, S., Schemm, R., Danker, T., Sporning, A., Grubmüller, H., Nicke, A., 2012. Efficient Binding of 4/7  $\alpha$ -Conotoxins to Nicotinic  $\alpha 4\beta 2$  Receptors Is Prevented by Arg185 and Pro195 in the  $\alpha 4$  Subunit. *Mol. Pharmacol.* 82, 711–718. <https://doi.org/10.1124/mol.112.078683>
- Bendels, S., Grether, U., Kimbara, A., Nettekoven, M., Roever, S., Rogers-Evans, M., Schulz-Gasch, T., 2014. Purine Derivatives as Cb2 Receptor Agonists. WO2014177490A1.
- Bender, E., Buist, A., Jurzak, M., Langlois, X., Baggerman, G., Verhasselt, P., Ercken, M., Guo, H.-Q., Wintolders, C., Wyngaert, I.V. den, Oers, I.V., Schoofs, L., Luyten, W., 2002. Characterization of an orphan G protein-coupled receptor localized in the dorsal root ganglia reveals adenine as a signaling molecule. *Proc. Natl. Acad. Sci.* 99, 8573–8578. <https://doi.org/10.1073/pnas.122016499>
- Beswick, P.J., Billinton, A., Chambers, L.J., Dean, D.K., Fonfria, E., Gleave, R.J., Medhurst, S.J., Michel, A.D., Moses, A.P., Patel, S., Roman, S.A., Roomans, S., Senger, S., Stevens, A.J., Walter, D.S., 2010. Structure-activity relationships and in vivo activity of (1H-pyrazol-4-yl)acetamide antagonists of the P2X(7) receptor. *Bioorg Med Chem Lett* 20, 4653–6. <https://doi.org/10.1016/j.bmcl.2010.05.107>

- Bhattacharya, A., Wang, Q., Ao, H., Shoblock, J.R., Lord, B., Aluisio, L., Fraser, I., Nepomuceno, D., Neff, R.A., Welty, N., Lovenberg, T.W., Bonaventure, P., Wickenden, A.D., Letavic, M.A., 2013. Pharmacological characterization of a novel centrally permeable P2X7 receptor antagonist: JNJ-47965567. *Br J Pharmacol* 170, 624–40. <https://doi.org/10.1111/bph.12314>
- Bickerton, G.R., Paolini, G.V., Besnard, J., Muresan, S., Hopkins, A.L., 2012. Quantifying the chemical beauty of drugs. *Nat. Chem.* 4, 90–98. <https://doi.org/10.1038/nchem.1243>
- Bidula, S.M., Cromer, B.A., Walpole, S., Angulo, J., Stokes, L., 2019a. Mapping a novel positive allosteric modulator binding site in the central vestibule region of human P2X7. *Sci. Rep.* 9, 3231. <https://doi.org/10.1038/s41598-019-39771-5>
- Bidula, S.M., Dhuna, K., Helliwell, R., Stokes, L., 2019b. Positive allosteric modulation of P2X7 promotes apoptotic cell death over lytic cell death responses in macrophages. *Cell Death Dis.* 10, 1–16. <https://doi.org/10.1038/s41419-019-2110-3>
- Bo, X., Jiang, L.-H., Wilson, H.L., Kim, M., Burnstock, G., Surprenant, A., North, R.A., 2003. Pharmacological and Biophysical Properties of the Human P2X5 Receptor. *Mol. Pharmacol.* 63, 1407–1416. <https://doi.org/10.1124/mol.63.6.1407>
- Brake, A.J., Wagenbach, M.J., Julius, D., 1994. New structural motif for ligand-gated ion channels defined by an ionotropic ATP receptor. *Nature* 371, 519–523. <https://doi.org/10.1038/371519a0>
- Brik, A., Wu, C.-Y., Best, M.D., Wong, C.-H., 2005. Tetrabutylammonium fluoride-assisted rapid N9-alkylation on purine ring: Application to combinatorial reactions in microtiter plates for the discovery of potent sulfotransferase inhibitors in situ. *Bioorg. Med. Chem.* 13, 4622–4626. <https://doi.org/10.1016/j.bmc.2005.02.066>
- Burm, S.M., Zuiderwijk-Sick, E.A., Weert, P.M., Bajramovic, J.J., 2016. ATP-induced IL-1 $\beta$  secretion is selectively impaired in microglia as compared to hematopoietic macrophages. *Glia* 64, 2231–2246. <https://doi.org/10.1002/glia.23059>
- Burnstock, G., 2007. Purine and pyrimidine receptors. *Cell. Mol. Life Sci.* 64, 1471. <https://doi.org/10.1007/s00018-007-6497-0>
- Burnstock, G., 1976. Do some nerve cells release more than one transmitter? *Neuroscience* 1, 239–248. [https://doi.org/10.1016/0306-4522\(76\)90054-3](https://doi.org/10.1016/0306-4522(76)90054-3)
- Burnstock, G., 1972. Purinergic nerves. *Pharmacol. Rev.* 24, 509–581.
- Burnstock, G., Campbell, G., Satchell, D., Smythe, A., 1970. Evidence that adenosine triphosphate or a related nucleotide is the transmitter substance released by non-adrenergic inhibitory nerves in the gut. *Br. J. Pharmacol.* 40, 668–688.
- Burnstock, G., Kennedy, C., 1985. Is there a basis for distinguishing two types of P2-purinoceptor? *Gen. Pharmacol. Vasc. Syst.* 16, 433–440. [https://doi.org/10.1016/0306-3623\(85\)90001-1](https://doi.org/10.1016/0306-3623(85)90001-1)

- Calvo-Gallardo, E., Pascual, R. de, Fernández-Morales, J.-C., Arranz-Tagarro, J.-A., Maroto, M., Nanclares, C., Gandía, L., de Diego, A.M.G., Padín, J.-F., García, A.G., 2014. Depressed excitability and ion currents linked to slow exocytotic fusion pore in chromaffin cells of the SOD1G93A mouse model of amyotrophic lateral sclerosis. *Am. J. Physiol.-Cell Physiol.* 308, C1–C19. <https://doi.org/10.1152/ajpcell.00272.2014>
- Calzaferri, F., Ruiz - Ruiz, C., Diego, A.M.G., Pascual, R., Méndez - López, I., Cano - Abad, M.F., Maneu, V., Ríos, C., Gandía, L., García, A.G., 2020. The purinergic P2X7 receptor as a potential drug target to combat neuroinflammation in neurodegenerative diseases. *Med. Res. Rev. med.* 21710. <https://doi.org/10.1002/med.21710>
- Campello, L., Kutsyr, O., Noailles, A., Michalska, P., Fernández-Sánchez, L., Martínez-Gil, N., Ortuño-Lizarán, I., Sánchez-Sáez, X., Juan, E. de, Lax, P., León, R., García, A.G., Cuenca, N., Maneu, V., 2020. New Nrf2-Inducer Compound ITH12674 Slows the Progression of Retinitis Pigmentosa in the Mouse Model rd10 | *Cell Physiol Biochem. Cell. Physiol. Biochem.* 54, 142–159.
- Cao, X., Li, L.-P., Wang, Q., Wu, Q., Hu, H.-H., Zhang, M., Fang, Y.-Y., Zhang, J., Li, S.-J., Xiong, W.-C., Yan, H.-C., Gao, Y.-B., Liu, J.-H., Li, X.-W., Sun, L.-R., Zeng, Y.-N., Zhu, X.-H., Gao, T.-M., 2013. Astrocyte-derived ATP modulates depressive-like behaviors. *Nat. Med.* 19, 773–777. <https://doi.org/10.1038/nm.3162>
- Carbone, E., Borges, R., Eiden, L.E., García, A.G., Hernández-Cruz, A., 2019. Chromaffin Cells of the Adrenal Medulla: Physiology, Pharmacology, and Disease. *Compr. Physiol.* 9, 1443–1502. <https://doi.org/10.1002/cphy.c190003>
- Carmo, M.R., Menezes, A.P., Nunes, A.C., Pliassova, A., Rolo, A.P., Palmeira, C.M., Cunha, R.A., Canas, P.M., Andrade, G.M., 2014. The P2X7 receptor antagonist Brilliant Blue G attenuates contralateral rotations in a rat model of Parkinsonism through a combined control of synaptotoxicity, neurotoxicity and gliosis. *Neuropharmacology* 81, 142–52. <https://doi.org/10.1016/j.neuropharm.2014.01.045>
- Carroll, W.A., Kalvin, D.M., Perez Medrano, A., Florjancic, A.S., Wang, Y., Donnelly-Roberts, D.L., Namovic, M.T., Grayson, G., Honoré, P., Jarvis, M.F., 2007. Novel and potent 3-(2,3-dichlorophenyl)-4-(benzyl)-4H-1,2,4-triazole P2X7 antagonists. *Bioorg. Med. Chem. Lett.* 17, 4044–4048. <https://doi.org/10.1016/j.bmcl.2007.04.075>
- Carter, R.L., Fricks, I.P., Barrett, M.O., Burianek, L.E., Zhou, Y., Ko, H., Das, A., Jacobson, K.A., Lazarowski, E.R., Harden, T.K., 2009. Quantification of Gi-mediated inhibition of adenylyl cyclase activity reveals that UDP is a potent agonist of the human P2Y14 receptor. *Mol. Pharmacol.* 76, 1341–1348. <https://doi.org/10.1124/mol.109.058578>
- Caseley, E.A., Muench, S.P., Baldwin, S.A., Simmons, K., Fishwick, C.W., Jiang, L.-H., 2015. Docking of competitive inhibitors to the P2X7 receptor family reveals key differences responsible for changes in response between rat and human. *Bioorg. Med. Chem. Lett.* 25, 3164–3167. <https://doi.org/10.1016/j.bmcl.2015.06.001>

- Cervetto, C., Frattaroli, D., Maura, G., Marcoli, M., 2013. Motor neuron dysfunction in a mouse model of ALS: gender-dependent effect of P2X7 antagonism. *Toxicology* 311, 69–77. <https://doi.org/10.1016/j.tox.2013.04.004>
- Chambers, L.J., Stevens, A.J., Moses, A.P., Michel, A.D., Walter, D.S., Davies, D.J., Livermore, D.G., Fonfria, E., Demont, E.H., Vimal, M., Theobald, P.J., Beswick, P.J., Gleave, R.J., Roman, S.A., Senger, S., 2010. Synthesis and structure–activity relationships of a series of (1H-pyrazol-4-yl)acetamide antagonists of the P2X7 receptor. *Bioorg. Med. Chem. Lett.* 20, 3161–3164. <https://doi.org/10.1016/j.bmcl.2010.03.096>
- Changunda, C.R.K., Basson, A.E., van Vuuren, S.F., Rousseau, A.L., Bode, M.L., 2017. Palladium-catalysed cross-coupling as a key step in the synthesis of pyridyl-benzamides, -benzylamines and -sulfonamides. *Tetrahedron* 73, 137–147. <https://doi.org/10.1016/j.tet.2016.11.071>
- Cheewatrakoolpong, B., Gilcrest, H., Anthes, J.C., Greenfeder, S., 2005. Identification and characterization of splice variants of the human P2X7 ATP channel. *Biochem. Biophys. Res. Commun.* 332, 17–27. <https://doi.org/10.1016/j.bbrc.2005.04.087>
- Chen, J., Li, C.-M., Wang, J., Ahn, S., Wang, Z., Lu, Y., Dalton, J.T., Miller, D.D., Li, W., 2011. Synthesis and antiproliferative activity of novel 2-aryl-4-benzoyl-imidazole derivatives targeting tubulin polymerization. *Bioorg. Med. Chem.* 19, 4782–4795. <https://doi.org/10.1016/j.bmc.2011.06.084>
- Chen, J.-F., Cunha, R.A., 2020. The belated US FDA approval of the adenosine A2A receptor antagonist istradefylline for treatment of Parkinson's disease. *Purinergic Signal.* 16, 167–174. <https://doi.org/10.1007/s11302-020-09694-2>
- Chen, L., Brosnan, C.F., 2006. Exacerbation of Experimental Autoimmune Encephalomyelitis in P2X7R – / – Mice: Evidence for Loss of Apoptotic Activity in Lymphocytes. *J. Immunol.* 176, 3115–3126. <https://doi.org/10.4049/jimmunol.176.5.3115>
- Chen, X., Hu, J., Jiang, L., Xu, S., Zheng, B., Wang, C., Zhang, J., Wei, X., Chang, L., Wang, Q., 2014. Brilliant Blue G improves cognition in an animal model of Alzheimer's disease and inhibits amyloid-beta-induced loss of filopodia and dendrite spines in hippocampal neurons. *Neuroscience* 279, 94–101. <https://doi.org/10.1016/j.neuroscience.2014.08.036>
- Chen, X., Pierce, B., Naing, W., Grapperhaus, M.L., Phillion, D.P., 2010. Discovery of 2-chloro-N-((4,4-difluoro-1-hydroxycyclohexyl)methyl)-5-(5-fluoropyrimidin-2-yl)benzamide as a potent and CNS penetrable P2X7 receptor antagonist. *Bioorg. Med. Chem. Lett.* 20, 3107–3111. <https://doi.org/10.1016/j.bmcl.2010.03.094>
- Cheng, R.-D., Ren, J.-J., Zhang, Y.-Y., Ye, X.-M., 2014. P2X4 receptors expressed on microglial cells in post-ischemic inflammation of brain ischemic injury. *Neurochem. Int.* 67, 9–13. <https://doi.org/10.1016/j.neuint.2014.01.011>
- Chessell, I.P., Michel, A.D., Humphrey, P.P.A., 1998. Effects of antagonists at the human recombinant P2X7 receptor. *Br. J. Pharmacol.* 124, 1314–1320. <https://doi.org/10.1038/sj.bjp.0701958>

- Chrovian, C.C., Soyode-Johnson, A., Peterson, A.A., Gelin, C.F., Deng, X., Dvorak, C.A., Carruthers, N.I., Lord, B., Fraser, I., Aluisio, L., Coe, K.J., Scott, B., Koudriakova, T., Schoetens, F., Sepassi, K., Gallacher, D.J., Bhattacharya, A., Letavic, M.A., 2018. A Dipolar Cycloaddition Reaction To Access 6-Methyl-4,5,6,7-tetrahydro-1H-[1,2,3]triazolo[4,5-c]pyridines Enables the Discovery Synthesis and Preclinical Profiling of a P2X7 Antagonist Clinical Candidate. *J. Med. Chem.* 61, 207–223. <https://doi.org/10.1021/acs.jmedchem.7b01279>
- Coddou, C., Yan, Z., Obsil, T., Huidobro-Toro, J.P., Stojilkovic, S.S., 2011. Activation and Regulation of Purinergic P2X Receptor Channels. *Pharmacol. Rev.* <https://doi.org/10.1124/pr.110.003129>
- Corvus Pharmaceuticals, Inc., 2020. Study of CPI-006 as Immunotherapy for Hospitalized COVID-19 Patients [WWW Document]. URL <https://www.clinicaltrials.gov/ct2/show/NCT04464395?term=ecto-nucleotidase&draw=2&rank=1> (accessed 12.17.20).
- Coull, J.A.M., Beggs, S., Boudreau, D., Boivin, D., Tsuda, M., Inoue, K., Gravel, C., Salter, M.W., De Koninck, Y., 2005. BDNF from microglia causes the shift in neuronal anion gradient underlying neuropathic pain. *Nature* 438, 1017–1021. <https://doi.org/10.1038/nature04223>
- Coutinho-Silva, R., Stahl, L., Raymond, M.-N., Jungas, T., Verbeke, P., Burnstock, G., Darville, T., Ojcius, D.M., 2003. Inhibition of Chlamydial Infectious Activity due to P2X7R-Dependent Phospholipase D Activation. *Immunity* 19, 403–412. [https://doi.org/10.1016/S1074-7613\(03\)00235-8](https://doi.org/10.1016/S1074-7613(03)00235-8)
- Cruz, M.P., 2018. Edaravone (Radicava): A Novel Neuroprotective Agent for the Treatment of Amyotrophic Lateral Sclerosis. *P T* 43, 25–28.
- Cummings, J.L., Tong, G., Ballard, C., 2019. Treatment Combinations for Alzheimer’s Disease: Current and Future Pharmacotherapy Options. *J Alzheimers Dis* 67, 779–794. <https://doi.org/10.3233/JAD-180766>
- Dal Ben, D., Buccioni, M., Lambertucci, C., Marucci, G., Thomas, A., Volpini, R., 2015. Purinergic P2X receptors: Structural models and analysis of ligand-target interaction. *Eur. J. Med. Chem.* 89, 561–580. <https://doi.org/10.1016/j.ejmech.2014.10.071>
- Dal Ben, D., Buccioni, M., Lambertucci, C., Marucci, G., Volpini, R., Cristalli, G., 2011. The importance of alkynyl chain presence for the activity of adenine nucleosides/nucleotides on purinergic receptors. *Curr. Med. Chem.* 18, 1444–1463. <https://doi.org/10.2174/092986711795328391>
- Dalby, C., Bleasdale, C., Clegg, W., Elsegood, M.R.J., Golding, B.T., Griffin, R.J., 1993. Regiospecific Alkylation of 6-Chloropurine and 2,6-Dichloropurine at N7 by Transient Protection of N3/N9 by Methylcobaloxime. *Angew. Chem. Int. Ed. Engl.* 32, 1696–1697. <https://doi.org/10.1002/anie.199316961>
- Danquah, W., Meyer-Schwesinger, C., Rissiek, B., Pinto, C., Serracant-Prat, A., Amadi, M., Iacenda, D., Knop, J.-H., Hammel, A., Bergmann, P., Schwarz, N., Assunção, J., Rotthier, W., Haag, F., Tolosa, E., Bannas, P., Boué-Grabot, E., Magnus, T., Laeremans, T., Stortelers, C., Koch-Nolte, F., 2016. Nanobodies that block gating of the P2X7 ion channel ameliorate inflammation. *Sci. Transl. Med.* 8, 366ra162–366ra162. <https://doi.org/10.1126/scitranslmed.aaf8463>

- Dayel, A.B., Evans, R.J., Schmid, R., 2019. Mapping the Site of Action of Human P2X7 Receptor Antagonists AZ11645373, Brilliant Blue G, KN-62, Calmidazolium, and ZINC58368839 to the Intersubunit Allosteric Pocket. *Mol. Pharmacol.* 96, 355–363. <https://doi.org/10.1124/mol.119.116715>
- de los Ríos, C., Egea, J., Marco-Contelles, J., León, R., Samadi, A., Iriepa, I., Moraleda, I., Gálvez, E., García, A.G., López, M.G., Villarroya, M., Romero, A., 2010. Synthesis, Inhibitory Activity of Cholinesterases, and Neuroprotective Profile of Novel 1,8-Naphthyridine Derivatives. *J. Med. Chem.* 53, 5129–5143. <https://doi.org/10.1021/jm901902w>
- de Luna Martins, D., Borges, A.A., e Silva, N.A. do A., Faria, J.V., Hoelz, L.V.B., de Souza, H.V.C.M., Bello, M.L., Boechat, N., Ferreira, V.F., Faria, R.X., 2020. P2X7 receptor inhibition by 2-amino-3-aryl-1,4-naphthoquinones. *Bioorganic Chem.* 104, 104278. <https://doi.org/10.1016/j.bioorg.2020.104278>
- Dean, M., Sung, V.W., 2018. Review of deutetrabenazine: a novel treatment for chorea associated with Huntington's disease. *Drug Devel Ther* 12, 313–319. <https://doi.org/10.2147/DDDT.S138828>
- de Gassart, A., Martinon, F., 2015. Pyroptosis: Caspase-11 Unlocks the Gates of Death. *Immunity* 43, 835–837. <https://doi.org/10.1016/j.immuni.2015.10.024>
- Denlinger, L.C., Fiset, P.L., Sommer, J.A., Watters, J.J., Prabhu, U., Dubyak, G.R., Proctor, R.A., Bertics, P.J., 2001. Cutting edge: the nucleotide receptor P2X7 contains multiple protein- and lipid-interaction motifs including a potential binding site for bacterial lipopolysaccharide. *J Immunol* 167, 1871–6.
- Di, L., Kerns, E.H., Fan, K., McConnell, O.J., Carter, G.T., 2003. High throughput artificial membrane permeability assay for blood–brain barrier. *Eur. J. Med. Chem.* 38, 223–232. [https://doi.org/10.1016/S0223-5234\(03\)00012-6](https://doi.org/10.1016/S0223-5234(03)00012-6)
- Di Virgilio, F., 2015. P2X receptors and inflammation. *Curr Med Chem* 22, 866–77.
- Di Virgilio, F., Dal Ben, D., Sarti, A.C., Giuliani, A.L., Falzoni, S., 2017. The P2X7 Receptor in Infection and Inflammation. *Immunity* 47, 15–31. <https://doi.org/10.1016/j.immuni.2017.06.020>
- Di Virgilio, F., Schmalzing, G., Markwardt, F., 2018. The Elusive P2X7 Macropore. *Trends Cell Biol* 28, 392–404. <https://doi.org/10.1016/j.tcb.2018.01.005>
- Díaz-Hernández, J.I., Gómez-Villafuertes, R., León-Otegui, M., Hontecillas-Prieto, L., Del Puerto, A., Trejo, J.L., Lucas, J.J., Garrido, J.J., Gualix, J., Miras-Portugal, M.T., Díaz-Hernández, M., 2012. In vivo P2X7 inhibition reduces amyloid plaques in Alzheimer's disease through GSK3beta and secretases. *Neurobiol Aging* 33, 1816–28. <https://doi.org/10.1016/j.neurobiolaging.2011.09.040>
- Díaz-Hernández, M., Díez-Zaera, M., Sánchez-Nogueiro, J., Gómez-Villafuertes, R., Canals, J.M., Alberch, J., Miras-Portugal, M.T., Lucas, J.J., 2009. Altered P2X7-receptor level and function in mouse models of Huntington's disease and therapeutic efficacy of antagonist administration. *FASEB J* 23, 1893–906. <https://doi.org/10.1096/fj.08-122275>
- Ding, S., Gray, N.S., Wu, X., Ding, Q., Schultz, P.G., 2002. A Combinatorial Scaffold Approach toward Kinase-Directed Heterocycle Libraries. *J. Am. Chem. Soc.* 124, 1594–1596. <https://doi.org/10.1021/ja0170302>

- Doble, A., 1996. The pharmacology and mechanism of action of riluzole. *Neurology* 47, S233-41.
- Domercq, M., Matute, C., 2019. Targeting P2X4 and P2X7 receptors in multiple sclerosis. *Curr. Opin. Pharmacol., Cancer Immunomodulation* 47, 119–125. <https://doi.org/10.1016/j.coph.2019.03.010>
- Donnelly-Roberts, D.L., Namovic, M.T., Han, P., Jarvis, M.F., 2009a. Mammalian P2X7 receptor pharmacology: comparison of recombinant mouse, rat and human P2X7 receptors. *Br J Pharmacol* 157, 1203–14. <https://doi.org/10.1111/j.1476-5381.2009.00233.x>
- Donnelly-Roberts, D.L., Namovic, M.T., Surber, B., Vaidyanathan, S.X., Perez-Medrano, A., Wang, Y., Carroll, W.A., Jarvis, M.F., 2009b. [3H]A-804598 ([3H]2-cyano-1-[(1S)-1-phenylethyl]-3-quinolin-5-ylguanidine) is a novel, potent, and selective antagonist radioligand for P2X7 receptors. *Neuropharmacology, Ligand-Gated Ion Channels* 56, 223–229. <https://doi.org/10.1016/j.neuropharm.2008.06.012>
- Duplantier, A.J., Dombroski, M.A., Subramanyam, C., Beaulieu, A.M., Chang, S.P., Gabel, C.A., Jordan, C., Kalgutkar, A.S., Kraus, K.G., Labasi, J.M., Mussari, C., Perregaux, D.G., Shepard, R., Taylor, T.J., Trevena, K.A., Whitney-Pickett, C., Yoon, K., 2011. Optimization of the physicochemical and pharmacokinetic attributes in a 6-azauracil series of P2X7 receptor antagonists leading to the discovery of the clinical candidate CE-224,535. *Bioorg Med Chem Lett* 21, 3708–11. <https://doi.org/10.1016/j.bmcl.2011.04.077>
- Durrenberger, P.F., Grunblatt, E., Fernando, F.S., Monoranu, C.M., Evans, J., Riederer, P., Reynolds, R., Dexter, D.T., 2012. Inflammatory Pathways in Parkinson's Disease; A BNE Microarray Study. *Park. Dis* 2012, 214714. <https://doi.org/10.1155/2012/214714>
- Englezou, P.C., Rothwell, S.W., Ainscough, J.S., Brough, D., Landsiedel, R., Verkhatsky, A., Kimber, I., Dearman, R.J., 2015. P2X7R activation drives distinct IL-1 responses in dendritic cells compared to macrophages. *Cytokine, ICIS Awardee Reviews* 74, 293–304. <https://doi.org/10.1016/j.cyto.2015.05.013>
- Erb, L., Weisman, G.A., 2012. Coupling of P2Y receptors to G proteins and other signaling pathways. *Wiley Interdiscip Rev Membr Transp Signal* 1, 789–803. <https://doi.org/10.1002/wmts.62>
- Eser, A., Colombel, J.F., Rutgeerts, P., Vermeire, S., Vogelsang, H., Braddock, M., Persson, T., Reinisch, W., 2015. Safety and Efficacy of an Oral Inhibitor of the Purinergic Receptor P2X7 in Adult Patients with Moderately to Severely Active Crohn's Disease: A Randomized Placebo-controlled, Double-blind, Phase IIa Study. *Inflamm Bowel Dis* 21, 2247–53. <https://doi.org/10.1097/MIB.0000000000000514>
- Fabrizio, P., Amadio, S., Apolloni, S., Volonte, C., 2017. P2X7 Receptor Activation Modulates Autophagy in SOD1-G93A Mouse Microglia. *Front Cell Neurosci* 11, 249. <https://doi.org/10.3389/fncel.2017.00249>
- Fabrizio, P., Apolloni, S., Bianchi, A., Salvatori, I., Valle, C., Lanzuolo, C., Bendotti, C., Nardo, G., Volonté, C., 2020. P2X7 activation enhances skeletal muscle metabolism and regeneration in SOD1G93A mouse model of amyotrophic lateral sclerosis. *Brain Pathol. Zurich Switz.* 30, 272–282. <https://doi.org/10.1111/bpa.12774>
- Faria, R.X., de Jesus Hiller, N., Salles, J.P., Resende, J.A.L.C., Diogo, R.T., von Ranke, N.L., Bello, M.L., Rodrigues, C.R., Castro, H.C., de Luna Martins, D., 2019. Arylboronic acids inhibit P2X7 receptor function and the



acute inflammatory response. *J. Bioenerg. Biomembr.* 51, 277–290. <https://doi.org/10.1007/s10863-019-09802-x>

- Faria, R.X., Oliveira, F.H., Salles, J.P., Oliveira, A.S., von Ranke, N.L., Bello, M.L., Rodrigues, C.R., Castro, H.C., Louvis, A.R., Martins, D.L., Ferreira, V.F., 2018. 1,4-Naphthoquinones potently inhibiting P2X7 receptor activity. *Eur. J. Med. Chem.* 143, 1361–1372. <https://doi.org/10.1016/j.ejmech.2017.10.033>
- Fernández-Morales, J.-C., Arranz-Tagarro, J.-A., Calvo-Gallardo, E., Maroto, M., Padín, J.-F., García, A.G., 2012. Stabilizers of Neuronal and Mitochondrial Calcium Cycling as a Strategy for Developing a Medicine for Alzheimer's Disease. *ACS Chem. Neurosci.* 3, 873–883. <https://doi.org/10.1021/cn3001069>
- Ferrari, D., Pizzirani, C., Adinolfi, E., Lemoli, R.M., Curti, A., Idzko, M., Panther, E., Di Virgilio, F., 2006. The P2X7 receptor: a key player in IL-1 processing and release. *J Immunol* 176, 3877–83.
- Ferrazoli, E.G., de Souza, H.D., Nascimento, I.C., Oliveira-Giacomelli, A., Schwindt, T.T., Britto, L.R., Ulrich, H., 2017. Brilliant Blue G, But Not Fenofibrate, Treatment Reverts Hemiparkinsonian Behavior and Restores Dopamine Levels in an Animal Model of Parkinson's Disease. *Cell Transpl.* 26, 669–677. <https://doi.org/10.3727/096368917X695227>
- Fishman, P., Bar-Yehuda, S., Liang, B.T., Jacobson, K.A., 2012. Pharmacological and therapeutic effects of A3 adenosine receptor agonists. *Drug Discov. Today* 17, 359–366. <https://doi.org/10.1016/j.drudis.2011.10.007>
- Florjancic, A.S., Peddi, S., Perez-Medrano, A., Li, B., Namovic, M.T., Grayson, G., Donnelly-Roberts, D.L., Jarvis, M.F., Carroll, W.A., 2008. Synthesis and in vitro activity of 1-(2,3-dichlorophenyl)-N-(pyridin-3-ylmethyl)-1H-1,2,4-triazol-5-amine and 4-(2,3-dichlorophenyl)-N-(pyridin-3-ylmethyl)-4H-1,2,4-triazol-3-amine P2X7 antagonists. *Bioorg. Med. Chem. Lett.* 18, 2089–2092. <https://doi.org/10.1016/j.bmcl.2008.01.095>
- Franklin, R.B., Costello, L.C., 2009. The important role of the apoptotic effects of zinc in the development of cancers. *J. Cell. Biochem.* 106, 750–757. <https://doi.org/10.1002/jcb.22049>
- Fujita, T., Tozaki - Saitoh, H., Inoue, K., 2009. P2Y1 receptor signaling enhances neuroprotection by astrocytes against oxidative stress via IL-6 release in hippocampal cultures. *Glia* 57, 244–257. <https://doi.org/10.1002/glia.20749>
- Furber, M., Alcaraz, L., Bent, J.E., Beyerbach, A., Bowers, K., Braddock, M., Caffrey, M.V., Cladingboel, D., Collington, J., Donald, D.K., Fagura, M., Ince, F., Kinchin, E.C., Laurent, C., Lawson, M., Luker, T.J., Mortimore, M.M.P., Pimm, A.D., Riley, R.J., Roberts, N., Robertson, M., Theaker, J., Thorne, P.V., Weaver, R., Webborn, P., Willis, P., 2007. Discovery of Potent and Selective Adamantane-Based Small-Molecule P2X7 Receptor Antagonists/Interleukin-1 $\beta$  Inhibitors. *J. Med. Chem.* 50, 5882–5885. <https://doi.org/10.1021/jm700949w>
- Furuta, T., Mukai, A., Ohishi, A., Nishida, K., Nagasawa, K., 2017. Oxidative stress-induced increase of intracellular zinc in astrocytes decreases their functional expression of P2X7 receptors and engulfing activity. *Metallomics* 9, 1839–1851. <https://doi.org/10.1039/C7MT00257B>

- Gan, M., Moussaud, S., Jiang, P., McLean, P.J., 2015. Extracellular ATP induces intracellular alpha-synuclein accumulation via P2X1 receptor-mediated lysosomal dysfunction. *Neurobiol. Aging* 36, 1209–1220. <https://doi.org/10.1016/j.neurobiolaging.2014.10.037>
- Gandelman, M., Peluffo, H., Beckman, J.S., Cassina, P., Barbeito, L., 2010. Extracellular ATP and the P2X7 receptor in astrocyte-mediated motor neuron death: implications for amyotrophic lateral sclerosis. *J Neuroinflammation* 7, 33. <https://doi.org/10.1186/1742-2094-7-33>
- Gargett, C.E., Wiley, J.S., 1997. The isoquinoline derivative KN-62 a potent antagonist of the P2Z-receptor of human lymphocytes. *Br J Pharmacol* 120, 1483–90. <https://doi.org/10.1038/sj.bjpp.0701081>
- Gholamzad, M., Ebtekar, M., Ardestani, M.S., Azimi, M., Mahmodi, Z., Mousavi, M.J., Aslani, S., 2019. A comprehensive review on the treatment approaches of multiple sclerosis: currently and in the future. *Inflamm. Res.* 68, 25–38. <https://doi.org/10.1007/s00011-018-1185-0>
- Giannakopoulos, P., Kovari, E., Gold, G., von Gunten, A., Hof, P.R., Bouras, C., 2009. Pathological substrates of cognitive decline in Alzheimer's disease. *Front Neurol Neurosci* 24, 20–9. <https://doi.org/10.1159/000197881>
- Gibbons, S.J., Washburn, K.B., Talamo, B.R., 2001. P2X(7) receptors in rat parotid acinar cells: formation of large pores. *J. Auton. Pharmacol.* 21, 181–190. <https://doi.org/10.1046/j.1365-2680.2001.00224.x>
- Giuliani, A.L., Sarti, A.C., Di Virgilio, F., 2019. Extracellular nucleotides and nucleosides as signalling molecules. *Immunol. Lett.*, Special issue: The immune side of ectoenzymes 205, 16–24. <https://doi.org/10.1016/j.imlet.2018.11.006>
- Gloor, S., Pongs, O., Schmalzing, G., 1995. A vector for the synthesis of cRNAs encoding Myc epitope-tagged proteins in xenopus laevis oocytes. *Gene* 160, 213–217. [https://doi.org/10.1016/0378-1119\(95\)00226-V](https://doi.org/10.1016/0378-1119(95)00226-V)
- Goedert, M., Jakes, R., Spillantini, M.G., 2017. The Synucleinopathies: Twenty Years On. *J Park. Dis* 7, S51–S69. <https://doi.org/10.3233/JPD-179005>
- Goedert, M., Spillantini, M.G., 2006. A century of Alzheimer's disease. *Science* 314, 777–81. <https://doi.org/10.1126/science.1132814>
- Goldin, A.L., 2006. Expression of Ion Channels in Xenopus Oocytes, in: *Expression and Analysis of Recombinant Ion Channels*. John Wiley & Sons, Ltd, pp. 1–25. <https://doi.org/10.1002/3527608095.ch1>
- Gonzaga, D.T.G., Oliveira, F.H., Ranke, N.L. von, Pinho, G.Q., Salles, J.P., Bello, M.L., Rodrigues, C.R., Castro, H.C., Souza, H.V.C.M. de, Reis, C.R.C., Leme, R.P.P., Mafra, J.C.M., Pinheiro, L.C.S., Hoelz, L.V.B., Boechat, N., Faria, R.X., 2019. Synthesis, Biological Evaluation, and Molecular Modeling Studies of New Thiadiazole Derivatives as Potent P2X7 Receptor Inhibitors. *Front. Chem.* 7. <https://doi.org/10.3389/fchem.2019.00261>
- Gonzalez, D., Arribas, R.L., Viejo, L., Lajarin-Cuesta, R., de Los Rios, C., 2018. Substituent effect of N-benzylated gramine derivatives that prevent the PP2A inhibition and dissipate the neuronal Ca<sup>2+</sup> overload, as a

- multitarget strategy for the treatment of Alzheimer's disease. *Bioorg. Med. Chem.* 26, 2551–2560. <https://doi.org/10.1016/j.bmc.2018.04.019>
- Gorzalka, S., Vittori, S., Volpini, R., Cristalli, G., von Kügelgen, I., Müller, C.E., 2005. Evidence for the functional expression and pharmacological characterization of adenine receptors in native cells and tissues. *Mol. Pharmacol.* 67, 955–964. <https://doi.org/10.1124/mol.104.006601>
- Grygorowicz, T., Struzynska, L., Sulkowski, G., Chalimoniuk, M., Sulejczak, D., 2010. Temporal expression of P2X7 purinergic receptor during the course of experimental autoimmune encephalomyelitis. *Neurochem Int* 57, 823–9. <https://doi.org/10.1016/j.neuint.2010.08.021>
- Grygorowicz, T., Sulejczak, D., Struzynska, L., 2011. Expression of purinergic P2X7 receptor in rat brain during the symptomatic phase of experimental autoimmune encephalomyelitis and after recovery of neurological deficits. *Acta Neurobiol Exp Wars* 71, 65–73.
- Grynkiewicz, G., Poenie, M., Tsien, R.Y., 1985. A new generation of Ca<sup>2+</sup> indicators with greatly improved fluorescence properties. *J. Biol. Chem.* 260, 3440–3450.
- Gu, B.J., Field, J., Dutertre, S., Ou, A., Kilpatrick, T.J., Lechner-Scott, J., Scott, R., Lea, R., Taylor, B.V., Stankovich, J., Butzkueven, H., Gresle, M., Laws, S.M., Petrou, S., Hoffjan, S., Akkad, D.A., Graham, C.A., Hawkins, S., Glaser, A., Bedri, S.K., Hillert, J., Matute, C., Antiguada, A., Consortium, A.Nz., Wiley, J.S., 2015. A rare P2X7 variant Arg307Gln with absent pore formation function protects against neuroinflammation in multiple sclerosis. *Hum Mol Genet* 24, 5644–54. <https://doi.org/10.1093/hmg/ddv278>
- Gu, B.J., Wiley, J.S., 2018. P2X7 as a scavenger receptor for innate phagocytosis in the brain. *Br. J. Pharmacol.* 175, 4195–4208. <https://doi.org/10.1111/bph.14470>
- Gu, B.J., Zhang, W., Worthington, R.A., Sluyter, R., Dao-Ung, P., Petrou, S., Barden, J.A., Wiley, J.S., 2001. A Glu-496 to Ala Polymorphism Leads to Loss of Function of the Human P2X7 Receptor. *J. Biol. Chem.* 276, 11135–11142. <https://doi.org/10.1074/jbc.M010353200>
- Guile, S.D., Alcaraz, L., Birkinshaw, T.N., Bowers, K.C., Ebdon, M.R., Furber, M., Stocks, M.J., 2009. Antagonists of the P2X7 Receptor. From Lead Identification to Drug Development. *J. Med. Chem.* 52, 3123–3141. <https://doi.org/10.1021/jm801528x>
- Gulevskaya, A.V., Pozharskii, A.F., 1991. Synthesis of N-substituted xanthines (review). *Chem. Heterocycl. Compd.* 27, 1–23. <https://doi.org/10.1007/BF00633208>
- Guo, C., Masin, M., Qureshi, O.S., Murrell-Lagnado, R.D., 2007. Evidence for functional P2X4/P2X7 heteromeric receptors. *Mol Pharmacol* 72, 1447–56. <https://doi.org/10.1124/mol.107.035980>
- Habermacher, C., Dunning, K., Chataigneau, T., Grutter, T., 2016. Molecular structure and function of P2X receptors. *Neuropharmacology, Special Issue: Purines in Neurodegeneration and Neuroregeneration* 104, 18–30. <https://doi.org/10.1016/j.neuropharm.2015.07.032>
- Hausmann, R., Schmalzing, G., 2012. P2X1 and P2X2 Receptors in the Central Nervous System as Possible Drug Targets [WWW Document]. *CNS Neurol. Disord. - Drug Targets*. URL <https://www.eurekaselect.com/104069/article> (accessed 12.20.20).

- He, K., 2017. Novel Inhibitors of Protein Kinases. WO2017066193A1.
- Hibell, A., Thompson, K., Simon, J., Xing, M., Humphrey, P., Michel, A., 2001. Species- and agonist-dependent differences in the deactivation-kinetics of P2X7 receptors. *Naunyn. Schmiedebergs Arch. Pharmacol.* 363, 639–648. <https://doi.org/10.1007/s002100100412>
- Holley, J.E., Gveric, D., Newcombe, J., Cuzner, M.L., Gutowski, N.J., 2003. Astrocyte characterization in the multiple sclerosis glial scar. *Neuropathol Appl Neurobiol* 29, 434–44.
- Homerin, G., Lipka, E., Rigo, B., Millet, R., Dezitter, X., Furman, C., Ghinet, A., 2017. Discovery of highly functionalized scaffolds: Pyrroloimidazolediones as P2X7 receptor antagonists. *Tetrahedron* 73, 5327–5336.
- Honore, P., Donnelly-Roberts, D., Namovic, M.T., Hsieh, G., Zhu, C.Z., Mikusa, J.P., Hernandez, G., Zhong, C., Gauvin, D.M., Chandran, P., Harris, R., Medrano, A.P., Carroll, W., Marsh, K., Sullivan, J.P., Faltynek, C.R., Jarvis, M.F., 2006. A-740003 [N-(1-[(Cyanoimino)(5-quinolinylamino) methyl]amino)-2,2-dimethylpropyl)-2-(3,4-dimethoxyphenyl)acetamide], a Novel and Selective P2X7 Receptor Antagonist, Dose-Dependently Reduces Neuropathic Pain in the Rat. *J. Pharmacol. Exp. Ther.* 319, 1376–1385. <https://doi.org/10.1124/jpet.106.111559>
- Hracsko, Z., Baranyi, M., Csolle, C., Goloncser, F., Madarasz, E., Kittel, A., Sperlagh, B., 2011. Lack of neuroprotection in the absence of P2X7 receptors in toxin-induced animal models of Parkinson's disease. *Mol Neurodegener* 6, 28. <https://doi.org/10.1186/1750-1326-6-28>
- Huo, H., Fryatt, A.G., Farmer, L.K., Schmid, R., Evans, R.J., 2018. Mapping the binding site of the P2X receptor antagonist PPADS reveals the importance of orthosteric site charge and the cysteine-rich head region. *J. Biol. Chem.* 293, 12820–12831. <https://doi.org/10.1074/jbc.RA118.003737>
- Huynh, N., Arabian, N., Naito, A., Louie, S., Jakowec, M.W., Asatryan, L., Davies, D.L., 2017. Preclinical development of moxidectin as a novel therapeutic for alcohol use disorder. *Neuropharmacology* 113, 60–70. <https://doi.org/10.1016/j.neuropharm.2016.09.016>
- Illes, P., Khan, T.M., Rubini, P., 2017. Neuronal P2X7 Receptors Revisited: Do They Really Exist? *J Neurosci* 37, 7049–7062. <https://doi.org/10.1523/JNEUROSCI.3103-16.2017>
- Illes, P., Rubini, P., Ulrich, H., Zhao, Y., Tang, Y., 2020. Regulation of Microglial Functions by Purinergic Mechanisms in the Healthy and Diseased CNS. *Cells* 9. <https://doi.org/10.3390/cells9051108>
- Jacobson, K.A., 2010. P2X and P2Y Receptors Scientific Review [WWW Document]. Tocris Biosci. URL <https://www.tocris.com/literature/scientific-reviews/p2x-and-p2y-receptors> (accessed 12.20.20).
- Jacobson, K.A., Jarvis, M.F., Williams, M., 2002. Purine and pyrimidine (P2) receptors as drug targets. *J Med Chem* 45, 4057–93.
- Jacobson, K.A., Müller, C.E., 2016. Medicinal chemistry of adenosine, P2Y and P2X receptors. *Neuropharmacology, Special Issue: Purines in Neurodegeneration and Neuroregeneration* 104, 31–49. <https://doi.org/10.1016/j.neuropharm.2015.12.001>

- Jain, S., Grandits, M., Ecker, G.F., 2018. Interspecies comparison of putative ligand binding sites of human, rat and mouse P-glycoprotein. *Eur. J. Pharm. Sci.* 122, 134–143. <https://doi.org/10.1016/j.ejps.2018.06.022>
- Janssen, B., Vugts, D.J., Funke, U., Spaans, A., Schuit, R.C., Kooijman, E., Rongen, M., Perk, L.R., Lammertsma, A.A., Windhorst, A.D., 2014. Synthesis and initial preclinical evaluation of the P2X7 receptor antagonist [(1)(1)C]A-740003 as a novel tracer of neuroinflammation. *J Label. Comp Radiopharm* 57, 509–16. <https://doi.org/10.1002/jlcr.3206>
- Jiang, T., Hoekstra, J., Heng, X., Kang, W., Ding, J., Liu, J., Chen, S., Zhang, J., 2015. P2X7 receptor is critical in alpha-synuclein--mediated microglial NADPH oxidase activation. *Neurobiol Aging* 36, 2304–2318. <https://doi.org/10.1016/j.neurobiolaging.2015.03.015>
- Jimenez-Mateos, E.M., Smith, J., Nicke, A., Engel, T., 2019. Regulation of P2X7 receptor expression and function in the brain. *Brain Res. Bull., Purinergic Signaling as a target for emerging neurotherapeutics* 151, 153–163. <https://doi.org/10.1016/j.brainresbull.2018.12.008>
- Jin, H., Han, J., Resing, D., Liu, H., Yue, X., Miller, R.L., Schoch, K.M., Miller, T.M., Perlmutter, J.S., Egan, T.M., Tu, Z., 2018. Synthesis and in vitro characterization of a P2X7 radioligand [(123)I]TZ6019 and its response to neuroinflammation in a mouse model of Alzheimer disease. *Eur J Pharmacol* 820, 8–17. <https://doi.org/10.1016/j.ejphar.2017.12.006>
- Jo, S., Bean, B.P., 2011. Inhibition of neuronal voltage-gated sodium channels by brilliant blue G. *Mol Pharmacol* 80, 247–57. <https://doi.org/10.1124/mol.110.070276>
- Jonaitis, D., Storer, R., 2004. Crystalline and Amorphous Forms of Beta-L-2'-Deoxythymidine. WO2004012687A2.
- Jong, R.N. de, Beurskens, F.J., Verploegen, S., Strumane, K., Kampen, M.D. van, Voorhorst, M., Horstman, W., Engelberts, P.J., Oostindie, S.C., Wang, G., Heck, A.J.R., Schuurman, J., Parren, P.W.H.I., 2016. A Novel Platform for the Potentiation of Therapeutic Antibodies Based on Antigen-Dependent Formation of IgG Hexamers at the Cell Surface. *PLOS Biol.* 14, e1002344. <https://doi.org/10.1371/journal.pbio.1002344>
- Jun, D.J., Kim, J., Jung, S.Y., Song, R., Noh, J.H., Park, Y.S., Ryu, S.H., Kim, J.H., Kong, Y.Y., Chung, J.M., Kim, K.T., 2007. Extracellular ATP mediates necrotic cell swelling in SN4741 dopaminergic neurons through P2X7 receptors. *J Biol Chem* 282, 37350–8. <https://doi.org/10.1074/jbc.M707915200>
- Junker, A., Renn, C., Dobelmann, C., Namasivayam, V., Jain, S., Losenkova, K., Irjala, H., Duca, S., Balasubramanian, R., Chakraborty, S., Börgel, F., Zimmermann, H., Yegutkin, G.G., Müller, C.E., Jacobson, K.A., 2019. Structure–Activity Relationship of Purine and Pyrimidine Nucleotides as Ecto-5' -Nucleotidase (CD73) Inhibitors. *J. Med. Chem.* 62, 3677–3695. <https://doi.org/10.1021/acs.jmedchem.9b00164>
- Kalia, L.V., Lang, A.E., 2016. Parkinson disease in 2015: Evolving basic, pathological and clinical concepts in PD. *Nat Rev Neurol* 12, 65–6. <https://doi.org/10.1038/nrneurol.2015.249>
- Kane, B.J., Kuhn, J.G., Roush, M.K., 1992. Pentostatin: an adenosine deaminase inhibitor for the treatment of hairy cell leukemia. *Ann. Pharmacother.* 26, 939–947. <https://doi.org/10.1177/106002809202600718>

- Karasawa, A., Kawate, T., 2016. Structural basis for subtype-specific inhibition of the P2X7 receptor. *Elife* 5. <https://doi.org/10.7554/eLife.22153>
- Karasawa, A., Michalski, K., Mikhelzon, P., Kawate, T., 2017. The P2X7 receptor forms a dye-permeable pore independent of its intracellular domain but dependent on membrane lipid composition. *eLife* 6, e31186. <https://doi.org/10.7554/eLife.31186>
- Karmakar, M., Katsnelson, M.A., Dubyak, G.R., Pearlman, E., 2016. Neutrophil P2X7 receptors mediate NLRP3 inflammasome-dependent IL-1beta secretion in response to ATP. *Nat Commun* 7, 10555. <https://doi.org/10.1038/ncomms10555>
- Keystone, E.C., Wang, M.M., Layton, M., Hollis, S., McInnes, I.B., Team, D.C.S., 2012. Clinical evaluation of the efficacy of the P2X7 purinergic receptor antagonist AZD9056 on the signs and symptoms of rheumatoid arthritis in patients with active disease despite treatment with methotrexate or sulphasalazine. *Ann Rheum Dis* 71, 1630–5. <https://doi.org/10.1136/annrheumdis-2011-143578>
- Khakh, B.S., North, R.A., 2012. Neuromodulation by Extracellular ATP and P2X Receptors in the CNS. *Neuron* 76, 51–69. <https://doi.org/10.1016/j.neuron.2012.09.024>
- Khoja, S., Huynh, N., Asatryan, L., Jakowec, M.W., Davies, D.L., 2018. Reduced expression of purinergic P2X4 receptors increases voluntary ethanol intake in C57BL/6J mice. *Alcohol* 68, 63–70. <https://doi.org/10.1016/j.alcohol.2017.09.004>
- Khoja, S., Shah, V., Garcia, D., Asatryan, L., Jakowec, M.W., Davies, D.L., 2016. Role of purinergic P2X4 receptors in regulating striatal dopamine homeostasis and dependent behaviors. *J. Neurochem.* 139, 134–148. <https://doi.org/10.1111/jnc.13734>
- Kim, H.S., Ohno, M., Xu, B., Kim, H.O., Choi, Y., Ji, X.D., Maddileti, S., Marquez, V.E., Harden, T.K., Jacobson, K.A., 2003. 2-Substitution of Adenine Nucleotide Analogues Containing a Bicyclo[3.1.0]hexane Ring System Locked in a Northern Conformation: Enhanced Potency as P2Y1 Receptor Antagonists. *J. Med. Chem.* 46, 4974–4987. <https://doi.org/10.1021/jm030127+>
- Kittner, H., Franke, H., Fischer, W., Schultheis, N., Krügel, U., Illes, P., 2003. Stimulation of P2Y1 receptors causes anxiolytic-like effects in the rat elevated plus-maze: implications for the involvement of P2Y1 receptor-mediated nitric oxide production. *Neuropsychopharmacol. Off. Publ. Am. Coll. Neuropsychopharmacol.* 28, 435–444. <https://doi.org/10.1038/sj.npp.1300043>
- Koch-Nolte, F., Eichhoff, A., Pinto-Espinoza, C., Schwarz, N., Schäfer, T., Menzel, S., Haag, F., Demeules, M., Gondé, H., Adriouch, S., 2019. Novel biologics targeting the P2X7 ion channel. *Curr. Opin. Pharmacol., Cancer Immunomodulation* 47, 110–118. <https://doi.org/10.1016/j.coph.2019.03.001>
- Kopp, R., Krautloher, A., Ramírez-Fernández, A., Nicke, A., 2019. P2X7 Interactions and Signaling – Making Head or Tail of It. *Front. Mol. Neurosci.* 12. <https://doi.org/10.3389/fnmol.2019.00183>
- Kornum, B.R., Kawashima, M., Faraco, J., Lin, L., Rico, T.J., Hesselson, S., Axtell, R.C., Kuipers, H., Weiner, K., Hamacher, A., Kassack, M.U., Han, F., Knudsen, S., Li, J., Dong, X., Winkelmann, J., Plazzi, G., Nevsimalova, S., Hong, S.-C., Honda, Y., Honda, M., Högl, B., Ton, T.G.N., Montplaisir, J., Bourgin, P., Kemlink, D.,

- Huang, Y.-S., Warby, S., Einen, M., Eshragh, J.L., Miyagawa, T., Desautels, A., Ruppert, E., Hesla, P.E., Poli, F., Pizza, F., Frauscher, B., Jeong, J.-H., Lee, S.-P., Strohl, K.P., Longstreth, W.T., Kvale, M., Dobrovolna, M., Ohayon, M.M., Nepom, G.T., Wichmann, H.-E., Rouleau, G.A., Gieger, C., Levinson, D.F., Gejman, P.V., Meitinger, T., Peppard, P., Young, T., Jennum, P., Steinman, L., Tokunaga, K., Kwok, P.-Y., Risch, N., Hallmayer, J., Mignot, E., 2011. Common variants in P2RY11 are associated with narcolepsy. *Nat. Genet.* 43, 66–71. <https://doi.org/10.1038/ng.734>
- Kotnis, S., Bingham, B., Vasilyev, D.V., Miller, S.W., Bai, Y., Yeola, S., Chanda, P.K., Bowlby, M.R., Kaftan, E.J., Samad, T.A., Whiteside, G.T., 2010. Genetic and Functional Analysis of Human P2X5 Reveals a Distinct Pattern of Exon 10 Polymorphism with Predominant Expression of the Nonfunctional Receptor Isoform. *Mol. Pharmacol.* 77, 953–960. <https://doi.org/10.1124/mol.110.063636>
- Koufaki, M., Pournara, D., Durner, A., Kritsi, E., Papakostas, A., Zoumpoulakis, P., Nicke, A., 2020. Design, synthesis, and in vitro evaluation of novel P2X7 antagonists. *ChemMedChem* n/a. <https://doi.org/10.1002/cmdc.202000303>
- Kowaluk, E.A., Mikusa, J., Wismer, C.T., Zhu, C.Z., Schweitzer, E., Lynch, J.J., Lee, C.H., Jiang, M., Bhagwat, S.S., Gomtsyan, A., McKie, J., Cox, B.F., Polakowski, J., Reinhart, G., Williams, M., Jarvis, M.F., 2000. ABT-702 (4-amino-5-(3-bromophenyl)-7-(6-morpholino-pyridin-3-yl)pyrido[2,3-d]pyrimidine), a novel orally effective adenosine kinase inhibitor with analgesic and anti-inflammatory properties. II. In vivo characterization in the rat. *J. Pharmacol. Exp. Ther.* 295, 1165–1174.
- Kremer, H.P., Roos, R.A., Dingjan, G., Marani, E., Bots, G.T., 1990. Atrophy of the hypothalamic lateral tuberal nucleus in Huntington's disease. *J. Neuropathol Exp Neurol* 49, 371–82.
- Kügelgen, I. von, Schiedel, A.C., Hoffmann, K., Alsdorf, B.B.A., Abdelrahman, A., Müller, C.E., 2008. Cloning and Functional Expression of a Novel Gi Protein-Coupled Receptor for Adenine from Mouse Brain. *Mol. Pharmacol.* 73, 469–477. <https://doi.org/10.1124/mol.107.037069>
- Kumar, S., Mishra, A., Krishnamurthy, S., 2017. Purinergic Antagonism Prevents Mitochondrial Dysfunction and Behavioral Deficits Associated with Dopaminergic Toxicity Induced by 6-OHDA in Rats. *Neurochem Res* 42, 3414–3430. <https://doi.org/10.1007/s11064-017-2383-9>
- Kurashima, Y., Amiya, T., Nochi, T., Fujisawa, K., Haraguchi, T., Iba, H., Tsutsui, H., Sato, S., Nakajima, S., Iijima, H., Kubo, M., Kunisawa, J., Kiyono, H., 2012. Extracellular ATP mediates mast cell-dependent intestinal inflammation through P2X7 purinoceptors. *Nat. Commun.* 3, 1034. <https://doi.org/10.1038/ncomms2023>
- Kusner, D.J., Adams, J., 2000. ATP-Induced Killing of Virulent Mycobacterium tuberculosis Within Human Macrophages Requires Phospholipase D. *J. Immunol.* 164, 379–388. <https://doi.org/10.4049/jimmunol.164.1.379>
- Kwak, S.-H., Shin, S., Lee, J.-H., Shim, J.-K., Kim, M., Lee, S.-D., Lee, A., Bae, J., Park, J.-H., Abdelrahman, A., Müller, C.E., Cho, S.K., Kang, S.-G., Bae, M.A., Yang, J.Y., Ko, H., Goddard, W.A., Kim, Y.-C., 2018. Synthesis and structure-activity relationships of quinolinone and quinoline-based P2X7 receptor antagonists and

- their anti-sphere formation activities in glioblastoma cells. *Eur. J. Med. Chem.* 151, 462–481. <https://doi.org/10.1016/j.ejmech.2018.03.023>
- Lajarín-Cuesta, R., Arribas, R.L., Nanclares, C., García-Frutos, E.M., Gandía, L., de los Ríos, C., 2018. Design and synthesis of multipotent 3-aminomethylindoles and 7-azaindoles with enhanced protein phosphatase 2A-activating profile and neuroprotection. *Eur. J. Med. Chem.* 157, 294–309. <https://doi.org/10.1016/j.ejmech.2018.07.030>
- Lee, G.E., Lee, H.S., Lee, S.D., Kim, J.H., Kim, W.K., Kim, Y.C., 2009. Synthesis and structure-activity relationships of novel, substituted 5,6-dihydrodibenzo[a,g]quinolizinium P2X7 antagonists. *Bioorg Med Chem Lett* 19, 954–8. <https://doi.org/10.1016/j.bmcl.2008.11.088>
- Lee, H.G., Won, S.M., Gwag, B.J., Lee, Y.B., 2011. Microglial P2X(7) receptor expression is accompanied by neuronal damage in the cerebral cortex of the APPswe/PS1dE9 mouse model of Alzheimer's disease. *Exp Mol Med* 43, 7–14. <https://doi.org/10.3858/emm.2011.43.1.001>
- Lee, J.Y., Yu, J., Cho, W.J., Ko, H., Kim, Y.C., 2009. Synthesis and structure-activity relationships of pyrazolodiazepine derivatives as human P2X7 receptor antagonists. *Bioorg Med Chem Lett* 19, 6053–8. <https://doi.org/10.1016/j.bmcl.2009.09.053>
- Lee, S.Y., Perotti, A., De Jonghe, S., Herdewijn, P., Hanck, T., Müller, C.E., 2016. Thiazolo[3,2-a]benzimidazol-3(2H)-one derivatives: Structure-activity relationships of selective nucleotide pyrophosphatase/phosphodiesterase1 (NPP1) inhibitors. *Bioorg. Med. Chem.* 24, 3157–3165. <https://doi.org/10.1016/j.bmc.2016.05.046>
- Leeson, H.C., Chan-Ling, T., Lovelace, M.D., Brownlie, J.C., Gu, B.J., Weible, M.W., 2019. P2X7 receptor signaling during adult hippocampal neurogenesis. *Neural Regen. Res.* 14, 1684–1694. <https://doi.org/10.4103/1673-5374.257510>
- Lepist, E.-I., Damaraju, V.L., Zhang, J., Gati, W.P., Yao, S.Y.M., Smith, K.M., Karpinski, E., Young, J.D., Leung, K.H., Cass, C.E., 2013. Transport of A1 Adenosine Receptor Agonist Tecadenoson by Human and Mouse Nucleoside Transporters: Evidence for Blood-Brain Barrier Transport by Murine Equilibrative Nucleoside Transporter 1 mENT1. *Drug Metab. Dispos.* 41, 916–922. <https://doi.org/10.1124/dmd.112.049858>
- Letavic, M.A., Lord, B., Bischoff, F., Hawryluk, N.A., Pieters, S., Rech, J.C., Sales, Z., Velter, A.I., Ao, H., Bonaventure, P., Contreras, V., Jiang, X., Morton, K.L., Scott, B., Wang, Q., Wickenden, A.D., Carruthers, N.I., Bhattacharya, A., 2013. Synthesis and Pharmacological Characterization of Two Novel, Brain Penetrating P2X7 Antagonists. *ACS Med Chem Lett* 4, 419–22. <https://doi.org/10.1021/ml400040v>
- Letavic, M.A., Savall, B.M., Allison, B.D., Aluisio, L., Andres, J.I., De Angelis, M., Ao, H., Beauchamp, D.A., Bonaventure, P., Bryant, S., Carruthers, N.I., Ceusters, M., Coe, K.J., Dvorak, C.A., Fraser, I.C., Gelin, C.F., Koudriakova, T., Liang, J., Lord, B., Lovenberg, T.W., Otieno, M.A., Schoetens, F., Swanson, D.M., Wang, Q., Wickenden, A.D., Bhattacharya, A., 2017. 4-Methyl-6,7-dihydro-4H-triazolo[4,5-c]pyridine-Based P2X7 Receptor Antagonists: Optimization of Pharmacokinetic Properties Leading to the Identification of a Clinical Candidate. *J Med Chem* 60, 4559–4572. <https://doi.org/10.1021/acs.jmedchem.7b00408>



- Li, M., Toombes, G.E.S., Silberberg, S.D., Swartz, K.J., 2015. Physical basis of apparent pore dilation of ATP-activated P2X receptor channels. *Nat. Neurosci.* 18, 1577–1583. <https://doi.org/10.1038/nn.4120>
- Liao, B., Zhao, W., Beers, D.R., Henkel, J.S., Appel, S.H., 2012. Transformation from a neuroprotective to a neurotoxic microglial phenotype in a mouse model of ALS. *Exp Neurol* 237, 147–52. <https://doi.org/10.1016/j.expneurol.2012.06.011>
- Lipinski, C.A., Lombardo, F., Dominy, B.W., Feeney, P.J., 2001. Experimental and computational approaches to estimate solubility and permeability in drug discovery and development settings. *PLoS One* 6, e15862. The article was originally published in *Advanced Drug Delivery Reviews* 23 (1997) 3–25.1. *Adv. Drug Deliv. Rev.*, Special issue dedicated to Dr. Eric Tomlinson, *Advanced Drug Delivery Reviews, A Selection of the Most Highly Cited Articles, 1991-1998* 46, 3–26. [https://doi.org/10.1016/S0169-409X\(00\)00129-0](https://doi.org/10.1016/S0169-409X(00)00129-0)
- Liu, X., 2019. Transporter-Mediated Drug-Drug Interactions and Their Significance. *Adv. Exp. Med. Biol.* 1141, 241–291. [https://doi.org/10.1007/978-981-13-7647-4\\_5](https://doi.org/10.1007/978-981-13-7647-4_5)
- Lorrio, S., Romero, A., González-Lafuente, L., Lajarín-Cuesta, R., Martínez-Sanz, F.J., Estrada, M., Samadi, A., Marco-Contelles, J., Rodríguez-Franco, M.I., Villarroja, M., López, M.G., de los Ríos, C., 2013. PP2A ligand ITH12246 protects against memory impairment and focal cerebral ischemia in mice. *ACS Chem. Neurosci.* 4, 1267–1277. <https://doi.org/10.1021/cn400050p>
- Lu, L.J., Tsai, J.C., Liu, J., 2017. Novel Pharmacologic Candidates for Treatment of Primary Open-Angle Glaucoma. *Yale J. Biol. Med.* 90, 111–118.
- Lucchinetti, C.F., Popescu, B.F., Bunyan, R.F., Moll, N.M., Roemer, S.F., Lassmann, H., Bruck, W., Parisi, J.E., Scheithauer, B.W., Giannini, C., Weigand, S.D., Mandrekar, J., Ransohoff, R.M., 2011. Inflammatory cortical demyelination in early multiple sclerosis. *N Engl J Med* 365, 2188–97. <https://doi.org/10.1056/NEJMoa1100648>
- Luo, H., Wood, K., Shi, F.D., Gao, F., Chang, Y., 2018. Suramin is a novel competitive antagonist selective to alpha1beta2gamma2 GABAA over rho1 GABAC receptors. *Neuropharmacology* 141, 148–157. <https://doi.org/10.1016/j.neuropharm.2018.08.036>
- Lustig, K.D., Shiau, A.K., Brake, A.J., Julius, D., 1993. Expression cloning of an ATP receptor from mouse neuroblastoma cells. *Proc. Natl. Acad. Sci.* 90, 5113–5117. <https://doi.org/10.1073/pnas.90.11.5113>
- Ly, D., Dongol, A., Cuthbertson, P., Guy, T.V., Geraghty, N.J., Sophocleous, R.A., Sin, L., Turner, B.J., Watson, D., Yerbury, J.J., Sluyter, R., 2020. The P2X7 receptor antagonist JNJ-47965567 administered thrice weekly from disease onset does not alter progression of amyotrophic lateral sclerosis in SOD1G93A mice. *Purinergic Signal.* 16, 109–122. <https://doi.org/10.1007/s11302-020-09692-4>
- MacDonald, M.E., 1993. on behalf of the Huntington's Disease Collaborative Research Group. A novel gene containing a trinucleotide repeat that is expanded and unstable on Huntington's disease chromosomes. The Huntington's Disease Collaborative Research Group. *Cell* 72, 971–83.

- Mackenzie, A.B., Young, M.T., Adinolfi, E., Surprenant, A., 2005. Pseudoapoptosis Induced by Brief Activation of ATP-gated P2X7 Receptors. *J. Biol. Chem.* 280, 33968–33976. <https://doi.org/10.1074/jbc.M502705200>
- Mansoor, S.E., Lü, W., Oosterheert, W., Shekhar, M., Tajkhorshid, E., Gouaux, E., 2016. X-ray structures define human P2X<sub>3</sub> receptor gating cycle and antagonist action. *Nature* 538, 66–71. <https://doi.org/10.1038/nature19367>
- Marcellino, D., Suarez-Boomgaard, D., Sanchez-Reina, M.D., Aguirre, J.A., Yoshitake, T., Yoshitake, S., Hagman, B., Kehr, J., Agnati, L.F., Fuxe, K., Rivera, A., 2010. On the role of P2X(7) receptors in dopamine nerve cell degeneration in a rat model of Parkinson's disease: studies with the P2X(7) receptor antagonist A-438079. *J Neural Transm Vienna* 117, 681–7. <https://doi.org/10.1007/s00702-010-0400-0>
- Martinez-Ramirez, C., Baraibar, A.M., Nanclares, C., Mendez-Lopez, I., Gomez, A., Munoz, M.P., de Diego, A.M.G., Gandia, L., Casarejos, M.J., Garcia, A.G., 2018. Altered excitability and exocytosis in chromaffin cells from the R6/1 mouse model of Huntington's disease is linked to over-expression of mutated huntingtin. *J Neurochem* 147, 454–476. <https://doi.org/10.1111/jnc.14585>
- Martínez-Ramírez, C., Gil-Gómez, I., G de Diego, A.M., García, A.G., 2020. Acute reversible SERCA blockade facilitates or blocks exocytosis, respectively in mouse or bovine chromaffin cells. *Pflugers Arch.* <https://doi.org/10.1007/s00424-020-02483-1>
- Martínez-Sanz, F.J., Lajarín-Cuesta, R., González-Lafuente, L., Moreno-Ortega, A.J., Punzón, E., Cano-Abad, M.F., de los Ríos, C., 2016. Neuroprotective profile of pyridothiazepines with blocking activity of the mitochondrial Na<sup>+</sup>/Ca<sup>2+</sup> exchanger. *Eur. J. Med. Chem.* 109, 114–123. <https://doi.org/10.1016/j.ejmech.2015.12.043>
- Matthews, E.A., Dickenson, A.H., 2004. Effects of spinally administered adenine on dorsal horn neuronal responses in a rat model of inflammation. *Neurosci. Lett.* 356, 211–214. <https://doi.org/10.1016/j.neulet.2003.11.057>
- Matute, C., Torre, I., Perez-Cerda, F., Perez-Samartin, A., Alberdi, E., Etxebarria, E., Arranz, A.M., Ravid, R., Rodriguez-Antiguedad, A., Sanchez-Gomez, M., Domercq, M., 2007. P2X(7) receptor blockade prevents ATP excitotoxicity in oligodendrocytes and ameliorates experimental autoimmune encephalomyelitis. *J Neurosci* 27, 9525–33. <https://doi.org/10.1523/JNEUROSCI.0579-07.2007>
- McCall, A.L., Millington, W.R., Wurtman, R.J., 1982. Blood-brain barrier transport of caffeine: Dose-related restriction of adenine transport. *Life Sci.* 31, 2709–2715. [https://doi.org/10.1016/0024-3205\(82\)90715-9](https://doi.org/10.1016/0024-3205(82)90715-9)
- McCarthy, A.E., Yoshioka, C., Mansoor, S.E., 2019. Full-Length P2X7 Structures Reveal How Palmitoylation Prevents Channel Desensitization. *Cell* 179, 659-670.e13. <https://doi.org/10.1016/j.cell.2019.09.017>
- McLarnon, J.G., Ryu, J.K., Walker, D.G., Choi, H.B., 2006. Upregulated expression of purinergic P2X(7) receptor in Alzheimer disease and amyloid-beta peptide-treated microglia and in peptide-injected rat hippocampus. *J Neuropathol Exp Neurol* 65, 1090–7. <https://doi.org/10.1097/01.jnen.0000240470.97295.d3>

- Mehta, D., Jackson, R., Paul, G., Shi, J., Sabbagh, M., 2017. Why do trials for Alzheimer's disease drugs keep failing? A discontinued drug perspective for 2010–2015. *Expert Opin Investig Drugs* 26, 735–739. <https://doi.org/10.1080/13543784.2017.1323868>
- Michel, A.D., Clay, W.C., Ng, S.W., Roman, S., Thompson, K., Condreay, J.P., Hall, M., Holbrook, J., Livermore, D., Senger, S., 2008. Identification of regions of the P2X7 receptor that contribute to human and rat species differences in antagonist effects. *Br. J. Pharmacol.* 155, 738–751. <https://doi.org/10.1038/bjp.2008.306>
- Michel, A.D., Kaur, R., Chessell, I.P., Humphrey, P.P.A., 2000. Antagonist effects on human P2X7 receptor-mediated cellular accumulation of YO-PRO-1. *Br. J. Pharmacol.* 130, 513–520. <https://doi.org/10.1038/sj.bjp.0703368>
- Michel, A.D., Ng, S.-W., Roman, S., Clay, W.C., Dean, D.K., Walter, D.S., 2009. Mechanism of action of species-selective P2X7 receptor antagonists. *Br. J. Pharmacol.* 156, 1312–1325. <https://doi.org/10.1111/j.1476-5381.2009.00135.x>
- Miller, R.G., Mitchell, J.D., Lyon, M., Moore, D.H., 2003. Riluzole for amyotrophic lateral sclerosis (ALS)/motor neuron disease (MND). *Amyotroph Lateral Scler Mot. Neuron Disord* 4, 191–206.
- Miras-Portugal, M.T., Sebastian-Serrano, A., de Diego Garcia, L., Diaz-Hernandez, M., 2017. Neuronal P2X7 Receptor: Involvement in Neuronal Physiology and Pathology. *J Neurosci* 37, 7063–7072. <https://doi.org/10.1523/JNEUROSCI.3104-16.2017>
- Moore, D., Chambers, J., Waldvogel, H., Faull, R., Emson, P., 2000. Regional and cellular distribution of the P2Y(1) purinergic receptor in the human brain: striking neuronal localisation. *J. Comp. Neurol.* 421, 374–384. [https://doi.org/10.1002/\(sici\)1096-9861\(20000605\)421:3<374::aid-cne6>3.0.co;2-z](https://doi.org/10.1002/(sici)1096-9861(20000605)421:3<374::aid-cne6>3.0.co;2-z)
- Moreno-Ortega, A.J., Martínez-Sanz, F.J., Lajarín-Cuesta, R., de Los Rios, C., Cano-Abad, M.F., 2015. Benzothiazepine CGP37157 and its 2'-isopropyl analogue modulate Ca<sup>2+</sup> entry through CALHM1. *Neuropharmacology* 95, 503–510. <https://doi.org/10.1016/j.neuropharm.2015.02.016>
- Morytko, M.J., Betschmann, P., Woller, K., Ericsson, A., Chen, H., Donnelly-Roberts, D.L., Namovic, M.T., Jarvis, M.F., Carroll, W.A., Rafferty, P., 2008. Synthesis and in vitro activity of N'-cyano-4-(2-phenylacetyl)-N-o-tolylpiperazine-1-carboximidamide P2X7 antagonists. *Bioorg. Med. Chem. Lett.* 18, 2093–2096. <https://doi.org/10.1016/j.bmcl.2008.01.094>
- Mufti, F., Jung, Y.-H., Giancotti, L.A., Yu, J., Chen, Z., Phung, N.B., Jacobson, K.A., Salvemini, D., 2020. P2Y14 Receptor Antagonists Reverse Chronic Neuropathic Pain in a Mouse Model. *ACS Med. Chem. Lett.* 11, 1281–1286. <https://doi.org/10.1021/acsmchemlett.0c00115>
- Munoz-Planillo, R., Kuffa, P., Martinez-Colon, G., Smith, B.L., Rajendiran, T.M., Nunez, G., 2013. K(+) efflux is the common trigger of NLRP3 inflammasome activation by bacterial toxins and particulate matter. *Immunity* 38, 1142–53. <https://doi.org/10.1016/j.immuni.2013.05.016>
- Murakami, H., Ohkura, A., Takanaga, H., Matsuo, H., Koyabu, N., Naito, M., Tsuruo, T., Ohtani, H., Sawada, Y., 2005. Functional characterization of adenosine transport across the BBB in mice. *Int. J. Pharm.* 290, 37–44. <https://doi.org/10.1016/j.ijpharm.2004.11.005>

- Murgia, M., Hanau, S., Pizzo, P., Rippa, M., Di Virgilio, F., 1993. Oxidized ATP. An irreversible inhibitor of the macrophage purinergic P2Z receptor. *J Biol Chem* 268, 8199–203.
- Narcisse, L., Scemes, E., Zhao, Y., Lee, S.C., Brosnan, C.F., 2005. The cytokine IL-1beta transiently enhances P2X7 receptor expression and function in human astrocytes. *Glia* 49, 245–58. <https://doi.org/10.1002/glia.20110>
- Nelson, D.W., Gregg, R.J., Kort, M.E., Perez-Medrano, A., Voight, E.A., Wang, Y., Grayson, G., Namovic, M.T., Donnelly-Roberts, D.L., Niforatos, W., Honore, P., Jarvis, M.F., Faltynek, C.R., Carroll, W.A., 2006. Structure – Activity Relationship Studies on a Series of Novel, Substituted 1-Benzyl-5-phenyltetrazole P2X7 Antagonists. *J. Med. Chem.* 49, 3659–3666. <https://doi.org/10.1021/jm051202e>
- Nicke, A., Kuan, Y.-H., Masin, M., Rettinger, J., Marquez-Klaka, B., Bender, O., Górecki, D.C., Murrell-Lagnado, R.D., Soto, F., 2009. A Functional P2X7 Splice Variant with an Alternative Transmembrane Domain 1 Escapes Gene Inactivation in P2X7 Knock-out Mice. *J. Biol. Chem.* 284, 25813–25822. <https://doi.org/10.1074/jbc.M109.033134>
- O’Boyle, N.M., Banck, M., James, C.A., Morley, C., Vandermeersch, T., Hutchison, G.R., 2011. Open Babel: An open chemical toolbox. *J. Cheminformatics* 3, 33. <https://doi.org/10.1186/1758-2946-3-33>
- O’Brien, F.E., Clarke, G., Dinan, T.G., Cryan, J.F., Griffin, B.T., 2013. Human P-glycoprotein differentially affects antidepressant drug transport: relevance to blood–brain barrier permeability. *Int. J. Neuropsychopharmacol.* 16, 2259–2272. <https://doi.org/10.1017/S1461145713000692>
- O’Brien-Brown, J., Jackson, A., Reekie, T.A., Barron, M.L., Werry, E.L., Schiavini, P., McDonnell, M., Munoz, L., Wilkinson, S., Noll, B., Wang, S., Kassiou, M., 2017. Discovery and pharmacological evaluation of a novel series of adamantyl cyanoguanidines as P2X7 receptor antagonists. *Eur J Med Chem* 130, 433–439. <https://doi.org/10.1016/j.ejmech.2017.02.060>
- Ollà, I., Santos-Galindo, M., Elorza, A., Lucas, J.J., 2020. P2X7 Receptor Upregulation in Huntington’s Disease Brains. *Front. Mol. Neurosci.* 13. <https://doi.org/10.3389/fnmol.2020.567430>
- Ou, A., Gu, B.J., Wiley, J.S., 2018. The scavenger activity of the human P2X7 receptor differs from P2X7 pore function by insensitivity to antagonists, genetic variation and sodium concentration: Relevance to inflammatory brain diseases. *Biochim. Biophys. Acta BBA - Mol. Basis Dis.* 1864, 1051–1059. <https://doi.org/10.1016/j.bbadis.2018.01.012>
- Palomo, V., Perez, D.I., Perez, C., Morales-Garcia, J.A., Soteras, I., Alonso-Gil, S., Encinas, A., Castro, A., Campillo, N.E., Perez-Castillo, A., Gil, C., Martinez, A., 2012. 5-Imino-1,2,4-Thiadiazoles: First Small Molecules As Substrate Competitive Inhibitors of Glycogen Synthase Kinase 3. *J. Med. Chem.* 55, 1645–1661. <https://doi.org/10.1021/jm201463v>
- Paredes, R.M., Etzler, J.C., Watts, L.T., Zheng, W., Lechleiter, J.D., 2008. Chemical calcium indicators. *Methods, Optical Methods in Calcium Signaling* 46, 143–151. <https://doi.org/10.1016/j.ymeth.2008.09.025>

- Parisi, C., Napoli, G., Amadio, S., Spalloni, A., Apolloni, S., Longone, P., Volonte, C., 2016. MicroRNA-125b regulates microglia activation and motor neuron death in ALS. *Cell Death Differ* 23, 531–41. <https://doi.org/10.1038/cdd.2015.153>
- Park, J.H., Lee, G.E., Lee, S.D., Ko, H., Kim, Y.C., 2015. Structure-activity relationship studies of pyrimidine-2,4-dione derivatives as potent P2X7 receptor antagonists. *Eur J Med Chem* 106, 180–93. <https://doi.org/10.1016/j.ejmech.2015.10.036>
- Parvathenani, L.K., Tertyshnikova, S., Greco, C.R., Roberts, S.B., Robertson, B., Posmantur, R., 2003. P2X7 mediates superoxide production in primary microglia and is up-regulated in a transgenic mouse model of Alzheimer's disease. *J Biol Chem* 278, 13309–17. <https://doi.org/10.1074/jbc.M209478200>
- Pasqualetto, G., Brancale, A., Young, M.T., 2018. The Molecular Determinants of Small-Molecule Ligand Binding at P2X Receptors. *Front Pharmacol* 9, 58. <https://doi.org/10.3389/fphar.2018.00058>
- Patani, G.A., LaVoie, E.J., 1996. Bioisosterism: A Rational Approach in Drug Design. *Chem. Rev.* 96, 3147–3176. <https://doi.org/10.1021/cr950066q>
- Peng, W., Cotrina, M.L., Han, X., Yu, H., Bekar, L., Blum, L., Takano, T., Tian, G.F., Goldman, S.A., Nedergaard, M., 2009. Systemic administration of an antagonist of the ATP-sensitive receptor P2X7 improves recovery after spinal cord injury. *Proc Natl Acad Sci U A* 106, 12489–93. <https://doi.org/10.1073/pnas.0902531106>
- Pérez-Sen, R., Queipo, M.J., Morente, V., Ortega, F., Delicado, E., Miras-Portugal, M.T., 2015. Neuroprotection Mediated by P2Y13 Nucleotide Receptors in Neurons. *Comput. Struct. Biotechnol. J.* 13, 160–168. <https://doi.org/10.1016/j.csbj.2015.02.002>
- Pettersen, E.F., Goddard, T.D., Huang, C.C., Couch, G.S., Greenblatt, D.M., Meng, E.C., Ferrin, T.E., 2004. UCSF Chimera—A visualization system for exploratory research and analysis. *J. Comput. Chem.* 25, 1605–1612. <https://doi.org/10.1002/jcc.20084>
- Piccini, A., Carta, S., Tassi, S., Lasiglie, D., Fossati, G., Rubartelli, A., 2008. ATP is released by monocytes stimulated with pathogen-sensing receptor ligands and induces IL-1beta and IL-18 secretion in an autocrine way. *Proc Natl Acad Sci U A* 105, 8067–72. <https://doi.org/10.1073/pnas.0709684105>
- Qu, Y., Misaghi, S., Newton, K., Gilmour, L.L., Louie, S., Cupp, J.E., Dubyak, G.R., Hackos, D., Dixit, V.M., 2011. Pannexin-1 Is Required for ATP Release during Apoptosis but Not for Inflammasome Activation. *J. Immunol.* 186, 6553–6561. <https://doi.org/10.4049/jimmunol.1100478>
- Raboisson, P., Lugnier, C., Muller, C., Reimund, J.-M., Schultz, D., Pinna, G., Le Bec, A., Basaran, H., Desaubry, L., Gaudiot, F., Seloum, M., Bourguignon, J.-J., 2003. Design, synthesis and structure-activity relationships of a series of 9-substituted adenine derivatives as selective phosphodiesterase type-4 inhibitors. *Eur. J. Med. Chem.* 38, 199–214. [https://doi.org/10.1016/S0223-5234\(02\)01446-0](https://doi.org/10.1016/S0223-5234(02)01446-0)
- Rafehi, M., Malik, E.M., Neumann, A., Abdelrahman, A., Hanck, T., Namasivayam, V., Müller, C.E., Baqi, Y., 2017. Development of Potent and Selective Antagonists for the UTP-Activated P2Y4 Receptor. *J. Med. Chem.* 60, 3020–3038. <https://doi.org/10.1021/acs.jmedchem.7b00030>

- Ralevic, V., Burnstock, G., 1998. Receptors for purines and pyrimidines. *Pharmacol. Rev.* 50, 413–492.
- Rech, J.C., Bhattacharya, A., Branstetter, B.J., Love, C.J., Leenaerts, J.E., Coymans, L.P., Eckert, W.A., 3rd, Ao, H., Wang, Q., Chaplan, S.R., Wickenden, A.D., Lebsack, A.D., Breitenbucher, J.G., 2016. The discovery and preclinical characterization of 6-chloro-N-(2-(4,4-difluoropiperidin-1-yl)-2-(2-(trifluoromethyl)pyrimidin-5-yl)ethyl)quinoline-5-carboxamide based P2X7 antagonists. *Bioorg Med Chem Lett* 26, 4781–4784. <https://doi.org/10.1016/j.bmcl.2016.08.029>
- Recourt, K., van der Aart, J., Jacobs, G., de Kam, M., Drevets, W., van Nueten, L., Kanhai, K., Siebenga, P., Zuiker, R., Ravenstijn, P., Timmers, M., van Gerven, J., de Boer, P., 2020. Characterisation of the pharmacodynamic effects of the P2X7 receptor antagonist JNJ-54175446 using an oral dexamphetamine challenge model in healthy males in a randomised, double-blind, placebo-controlled, multiple ascending dose trial. *J. Psychopharmacol. (Oxf.)* 34, 1030–1042. <https://doi.org/10.1177/0269881120914206>
- Reich, S.G., Savitt, J.M., 2019. Parkinson's Disease. *Med Clin North Am* 103, 337–350. <https://doi.org/10.1016/j.mcna.2018.10.014>
- Ried, W., Woithe, H., Müller, A., 1989. Strukturaufklärung von N6-, 9- und 7-Acyladeninen durch 1H- und 13C-NMR-Spektroskopie von Festkörpern und in Lösung. *Helv. Chim. Acta* 72, 1597–1607. <https://doi.org/10.1002/hlca.19890720720>
- Riedel, T., Schmalzing, G., Markwardt, F., 2007. Influence of Extracellular Monovalent Cations on Pore and Gating Properties of P2X7 Receptor-Operated Single-Channel Currents. *Biophys. J.* 93, 846–858. <https://doi.org/10.1529/biophysj.106.103614>
- Rigato, C., Buckinx, R., Le - Corronc, H., Rigo, J.M., Legendre, P., 2011. Pattern of invasion of the embryonic mouse spinal cord by microglial cells at the time of the onset of functional neuronal networks. *Glia* 59, 675–695. <https://doi.org/10.1002/glia.21140>
- Rissiek, B., Lukowiak, M., Raczkowski, F., Magnus, T., Mittrücker, H.-W., Koch-Nolte, F., 2018. In Vivo Blockade of Murine ARTC2.2 During Cell Preparation Preserves the Vitality and Function of Liver Tissue-Resident Memory T Cells. *Front. Immunol.* 9. <https://doi.org/10.3389/fimmu.2018.01580>
- Roger, S., Gillet, L., Baroja-Mazo, A., Surprenant, A., Pelegrin, P., 2010a. C-terminal Calmodulin-binding Motif Differentially Controls Human and Rat P2X7 Receptor Current Facilitation. *J. Biol. Chem.* 285, 17514–17524. <https://doi.org/10.1074/jbc.M109.053082>
- Roger, S., Mei, Z.-Z., Baldwin, J.M., Dong, L., Bradley, H., Baldwin, S.A., Surprenant, A., Jiang, L.-H., 2010b. Single nucleotide polymorphisms that were identified in affective mood disorders affect ATP-activated P2X7 receptor functions. *J. Psychiatr. Res.* 44, 347–355. <https://doi.org/10.1016/j.jpsychires.2009.10.005>
- Roger, S., Pelegrin, P., Surprenant, A., 2008. Facilitation of P2X7 Receptor Currents and Membrane Blebbing via Constitutive and Dynamic Calmodulin Binding. *J. Neurosci.* 28, 6393–6401. <https://doi.org/10.1523/JNEUROSCI.0696-08.2008>

- Romero, A., Egea, J., González-Muñoz, G.C., Martí n de Saavedra, M.D., del Barrio, L., Rodríguez-Franco, M.I., Conde, S., López, M.G., Villarroya, M., de los Ríos, C., 2014. ITH12410/SC058: A New Neuroprotective Compound with Potential in the Treatment of Alzheimer's Disease. *ACS Chem. Neurosci.* 5, 770–775. <https://doi.org/10.1021/cn500131t>
- Ronquist, G., 1968. Formation of extracellular adenosine triphosphate by human erythrocytes. *Acta Physiol. Scand.* 74, 594–605. <https://doi.org/10.1111/j.1748-1716.1968.tb04270.x>
- Ruiz-Ruiz, C., Calzaferri, F., García, A.G., 2020a. P2X7 receptor antagonism as a potential therapy in amyotrophic lateral sclerosis. *Front. Mol. Neurosci.* 13, 93. <https://doi.org/10.3389/fnmol.2020.00093>
- Ruiz-Ruiz, C., García-Magro, N., Negredo, P., Avendaño, C., Bhattacharya, A., Ceusters, M., García, A.G., 2020b. Chronic administration of P2X7 receptor antagonist JNJ-47965567 delays disease onset and progression, and improves motor performance in ALS SOD1G93A female mice. *Dis. Model. Mech.* 13. <https://doi.org/10.1242/dmm.045732>
- Saez-Orellana, F., Fuentes-Fuentes, M.C., Godoy, P.A., Silva-Grecchi, T., Panes, J.D., Guzman, L., Yevenes, G.E., Gavilan, J., Egan, T.M., Aguayo, L.G., Fuentealba, J., 2018. P2X receptor overexpression induced by soluble oligomers of amyloid beta peptide potentiates synaptic failure and neuronal dyshomeostasis in cellular models of Alzheimer's disease. *Neuropharmacology* 128, 366–378. <https://doi.org/10.1016/j.neuropharm.2017.10.027>
- Sanz, J.M., Chiozzi, P., Ferrari, D., Colaianna, M., Idzko, M., Falzoni, S., Fellin, R., Trabace, L., Di Virgilio, F., 2009. Activation of microglia by amyloid- $\beta$  requires P2X7 receptor expression. *J Immunol* 182, 4378–85. <https://doi.org/10.4049/jimmunol.0803612>
- Savall, B.M., Wu, D., De Angelis, M., Carruthers, N.I., Ao, H., Wang, Q., Lord, B., Bhattacharya, A., Letavic, M.A., 2015. Synthesis, SAR, and Pharmacological Characterization of Brain Penetrant P2X7 Receptor Antagonists. *ACS Med Chem Lett* 6, 671–6. <https://doi.org/10.1021/acsmedchemlett.5b00089>
- Savani, A.A., Login, I.S., 2007. Tetrabenazine as antichorea therapy in Huntington disease: a randomized controlled trial. *Neurology* 68, 797; author reply 797. <https://doi.org/10.1212/01.wnl.0000259143.52138.5c>
- Savio, L.E.B., de Andrade Mello, P., da Silva, C.G., Coutinho-Silva, R., 2018. The P2X7 Receptor in Inflammatory Diseases: Angel or Demon? *Front Pharmacol* 9, 52. <https://doi.org/10.3389/fphar.2018.00052>
- Schäkel, L., Schmies, C.C., Idris, R.M., Luo, X., Lee, S.-Y., Lopez, V., Mirza, S., Vu, T.H., Pelletier, J., Sévigny, J., Namasivayam, V., Müller, C.E., 2020. Nucleotide Analog ARL67156 as a Lead Structure for the Development of CD39 and Dual CD39/CD73 Ectonucleotidase Inhibitors. *Front. Pharmacol.* 11, 1294. <https://doi.org/10.3389/fphar.2020.01294>
- Schiedel, A.C., Meyer, H., Alsdorf, B.B.A., Gorzalka, S., Brüssel, H., Müller, C.E., 2007. [3H]Adenine is a suitable radioligand for the labeling of G protein-coupled adenine receptors but shows high affinity to bacterial contaminations in buffer solutions. *Purinergic Signal.* 3, 347–358. <https://doi.org/10.1007/s11302-007-9060-4>

- Schneider, M., Prudic, K., Pippel, A., Klapperstück, M., Braam, U., Müller, C.E., Schmalzing, G., Markwardt, F., 2017. Interaction of Purinergic P2X4 and P2X7 Receptor Subunits. *Front. Pharmacol.* 8. <https://doi.org/10.3389/fphar.2017.00860>
- Sirimulla, S., Bailey, J.B., Vegesna, R., Narayan, M., 2013. Halogen Interactions in Protein–Ligand Complexes: Implications of Halogen Bonding for Rational Drug Design. *J. Chem. Inf. Model.* 53, 2781–2791. <https://doi.org/10.1021/ci400257k>
- Slominska, E.M., Szolkiewicz, M., Smolenski, R.T., Rutkowski, B., Swierczynski, J., 2002. High plasma adenine concentration in chronic renal failure and its relation to erythrocyte ATP. *Nephron* 91, 286–291. <https://doi.org/10.1159/000058406>
- Soltani Rad, M.N., Behrouz, S., Asrari, Z., Khalafi-Nezhad, A., 2014. A simple and regioselective one-pot procedure for the direct N-acylation of some purine and pyrimidine nucleobases via carboxylic acids using cyanuric chloride. *Monatshefte Für Chem. - Chem. Mon.* 145, 1933–1940. <https://doi.org/10.1007/s00706-014-1270-1>
- Soltani Rad, M.N., Khalafi-Nezhad, A., Behrouz, S., 2010. Synthesis of some novel hydrazono acyclic nucleoside analogues. *Beilstein J. Org. Chem.* 6, 49. <https://doi.org/10.3762/bjoc.6.49>
- Stefanis, L., 2012. alpha-Synuclein in Parkinson's disease. *Cold Spring Harb Perspect Med* 2, a009399. <https://doi.org/10.1101/cshperspect.a009399>
- Steinberg, T.H., Newman, A.S., Swanson, J.A., Silverstein, S.C., 1987. ATP4- permeabilizes the plasma membrane of mouse macrophages to fluorescent dyes. *J. Biol. Chem.* 262, 8884–8888.
- Stock, T.C., Bloom, B.J., Wei, N., Ishaq, S., Park, W., Wang, X., Gupta, P., Mebus, C.A., 2012. Efficacy and safety of CE-224,535, an antagonist of P2X7 receptor, in treatment of patients with rheumatoid arthritis inadequately controlled by methotrexate. *J Rheumatol* 39, 720–7. <https://doi.org/10.3899/jrheum.110874>
- Stokes, L., Bidula, S.M., Bibič, L., Allum, E., 2020. To Inhibit or Enhance? Is There a Benefit to Positive Allosteric Modulation of P2X Receptors? *Front. Pharmacol.* 11. <https://doi.org/10.3389/fphar.2020.00627>
- Stokes, L., Fuller, S.J., Sluyter, R., Skarratt, K.K., Gu, B.J., Wiley, J.S., 2010. Two haplotypes of the P2X7 receptor containing the Ala-348 to Thr polymorphism exhibit a gain-of-function effect and enhanced interleukin-1 $\beta$  secretion. *FASEB J.* 24, 2916–2927. <https://doi.org/10.1096/fj.09-150862>
- Sulzer, D., 2007. Multiple hit hypotheses for dopamine neuron loss in Parkinson's disease. *Trends Neurosci* 30, 244–50. <https://doi.org/10.1016/j.tins.2007.03.009>
- Suzuyama, N., Katoh, M., Takeuchi, T., Yoshitomi, S., Higuchi, T., Asashi, S., Yokoi, T., 2007. Species Differences of Inhibitory Effects on P - glycoprotein - mediated Drug Transport. *J. Pharm. Sci.* 96, 1609–1618. <https://doi.org/10.1002/jps.20787>
- Swanson, D.M., Savall, B.M., Coe, K.J., Schoetens, F., Koudriakova, T., Skaptason, J., Wall, J., Rech, J., Deng, X., De Angelis, M., Everson, A., Lord, B., Wang, Q., Ao, H., Scott, B., Sepassi, K., Lovenberg, T.W., Carruthers, N.I., Bhattacharya, A., Letavic, M.A., 2016. Identification of (R)-(2-Chloro-3-(trifluoromethyl)phenyl)(1-



- (5-fluoropyridin-2-yl)-4-methyl-6,7-dihydro-1H-imidazo[4,5-c]pyridin-5(4H)-yl)methanone (JNJ 54166060), a Small Molecule Antagonist of the P2X7 receptor. *J Med Chem* 59, 8535–48. <https://doi.org/10.1021/acs.jmedchem.6b00989>
- Swanson, K.V., Deng, M., Ting, J.P.-Y., 2019. The NLRP3 inflammasome: molecular activation and regulation to therapeutics. *Nat. Rev. Immunol.* 19, 477–489. <https://doi.org/10.1038/s41577-019-0165-0>
- Szarek, W.A., Pinto, B.M., Iwakawa, M., 1985. Synthesis and biological activity of nucleoside analogs involving modifications in the carbohydrate ring. *Can. J. Chem.* <https://doi.org/10.1139/v85-354>
- Tang, T.S., Chen, X., Liu, J., Bezprozvanny, I., 2007. Dopaminergic signaling and striatal neurodegeneration in Huntington's disease. *J Neurosci* 27, 7899–910. <https://doi.org/10.1523/JNEUROSCI.1396-07.2007>
- Teng, R., 2015. Ticagrelor: Pharmacokinetic, Pharmacodynamic and Pharmacogenetic Profile: An Update. *Clin. Pharmacokinet.* 54, 1125–1138. <https://doi.org/10.1007/s40262-015-0290-2>
- Thimm, D., Knospe, M., Abdelrahman, A., Moutinho, M., Alsdorf, B.B.A., von Kügelgen, I., Schiedel, A.C., Müller, C.E., 2013. Characterization of new G protein-coupled adenine receptors in mouse and hamster. *Purinergic Signal.* 9, 415–426. <https://doi.org/10.1007/s11302-013-9360-9>
- Tobrman, T., Dvořák, D., 2006. Selective Magnesiation of Chloro-iodopurines: An Efficient Approach to New Purine Derivatives. *Org. Lett.* 8, 1291–1294. <https://doi.org/10.1021/ol053013w>
- Tosh, D.K., Salmaso, V., Rao, H., Bitant, A., Fisher, C.L., Lieberman, D.I., Vorbrüggen, H., Reitman, M.L., Gavrilova, O., Gao, Z.-G., Auchampach, J.A., Jacobson, K.A., 2020. Truncated (N)-Methanocarpa Nucleosides as Partial Agonists at Mouse and Human A3 Adenosine Receptors: Affinity Enhancement by N6-(2-Phenylethyl) Substitution. *J. Med. Chem.* 63, 4334–4348. <https://doi.org/10.1021/acs.jmedchem.0c00235>
- Trott, O., Olson, A.J., 2010. AutoDock Vina: Improving the speed and accuracy of docking with a new scoring function, efficient optimization, and multithreading. *J. Comput. Chem.* 31, 455–461. <https://doi.org/10.1002/jcc.21334>
- Tsuda, M., Shigemoto-Mogami, Y., Koizumi, S., Mizokoshi, A., Kohsaka, S., Salter, M.W., Inoue, K., 2003. P2X4 receptors induced in spinal microglia gate tactile allodynia after nerve injury. *Nature* 424, 778–783. <https://doi.org/10.1038/nature01786>
- Tsunoda, I., Fujinami, R.S., 1996. Two models for multiple sclerosis: experimental allergic encephalomyelitis and Theiler's murine encephalomyelitis virus. *J Neuropathol Exp Neurol* 55, 673–86.
- Tumma, H., Nagaraju, N., Reddy, K.V., 2010. N-Alkylation of 2,6-Dichloropurine Hydrochloride with a Variety of Alcohols over Alumina Catalyst. *Synth. Commun.* 40, 1856–1866. <https://doi.org/10.1080/00397910903162791>
- Ulmann, L., Levavasseur, F., Avignone, E., Peyroutou, R., Hirbec, H., Audinat, E., Rassendren, F., 2013. Involvement of P2X4 receptors in hippocampal microglial activation after status epilepticus. *Glia* 61, 1306–1319. <https://doi.org/10.1002/glia.22516>

- Valdés, F.Z., Luna, V.Z., Arévalo, B.R., Brown, N.V., Gutiérrez, M.C., 2018. Adenosine: Synthetic Methods of Its Derivatives and Antitumor Activity. *Mini Rev. Med. Chem.* 18, 1684–1701. <https://doi.org/10.2174/1389557518666180516163539>
- Valera, S., Hussy, N., Evans, R.J., Adami, N., North, R.A., Surprenant, A., Buell, G., 1994. A new class of ligand-gated ion channel defined by P<sub>2</sub>X<sub>1</sub> receptor for extracellular ATP. *Nature* 371, 516–519. <https://doi.org/10.1038/371516a0>
- Varma, R., Chai, Y., Troncoso, J., Gu, J., Xing, H., Stojilkovic, S.S., Mattson, M.P., Haughey, N.J., 2009. Amyloid- $\beta$  Induces a Caspase-mediated Cleavage of P2X<sub>4</sub> to Promote Purinotoxicity. *NeuroMolecular Med.* 11, 63–75. <https://doi.org/10.1007/s12017-009-8073-2>
- Venkateswara Rao, P., Ravindhranath, K., Ravi, K.K., 2013. Synthesis of 9-Substituted Derivatives of tert-Butyl 6-(9h-Purin-6-Ylthio) Hexylcarbamate. *Med. Chem.* 03. <https://doi.org/10.4172/2161-0444.1000137>
- Volonté, C., Amadio, S., Liguori, F., Fabbrizio, P., 2020. Duality of P2X<sub>7</sub> Receptor in Amyotrophic Lateral Sclerosis. *Front. Pharmacol.* 11, 1148. <https://doi.org/10.3389/fphar.2020.01148>
- Webb, T.E., Simon, J., Krishek, B.J., Bateson, A.N., Smart, T.G., King, B.F., Burnstock, G., Barnard, E.A., 1993. Cloning and functional expression of a brain G-protein-coupled ATP receptor. *FEBS Lett.* 324, 219–225. [https://doi.org/10.1016/0014-5793\(93\)81397-I](https://doi.org/10.1016/0014-5793(93)81397-I)
- Wengert, M., Adão-Novaes, J., Assaife-Lopes, N., Leão-Ferreira, L.R., Caruso-Neves, C., 2007. Adenine-induced inhibition of Na<sup>+</sup>-ATPase activity: Evidence for involvement of the G<sub>i</sub> protein-coupled receptor in the cAMP signaling pathway. *Arch. Biochem. Biophys.* 467, 261–267. <https://doi.org/10.1016/j.abb.2007.08.018>
- Wilhelm, I., Nyúl-Tóth, Á., Suciú, M., Hermenean, A., Krizbai, I.A., 2016. Heterogeneity of the blood-brain barrier. *Tissue Barriers* 4, e1143544. <https://doi.org/10.1080/21688370.2016.1143544>
- Wilkinson, S.M., Barron, M.L., O'Brien-Brown, J., Janssen, B., Stokes, L., Werry, E.L., Chishty, M., Skarratt, K.K., Ong, J.A., Hibbs, D.E., Vugts, D.J., Fuller, S., Windhorst, A.D., Kassiou, M., 2017. Pharmacological Evaluation of Novel Bioisosteres of an Adamantanyl Benzamide P2X<sub>7</sub> Receptor Antagonist. *ACS Chem Neurosci* 8, 2374–2380. <https://doi.org/10.1021/acschemneuro.7b00272>
- Xiao, Y., Karra, S., Goutopoulos, A., Morse, N.T., Zhang, S., Dhanabal, M., Tian, H., Seenisamy, J., Jayadevan, J., Caldwell, R., Potnick, J., Bleich, M., Chekler, E., Sherer, B., Sriraman, V., 2019. Synthesis and SAR development of quinoline analogs as novel P2X<sub>7</sub> receptor antagonists. *Bioorg. Med. Chem. Lett.* 29, 1660–1664. <https://doi.org/10.1016/j.bmcl.2019.04.033>
- Yan, Z., Li, S., Liang, Z., Tomić, M., Stojilkovic, S.S., 2008. The P2X<sub>7</sub> Receptor Channel Pore Dilates under Physiological Ion Conditions. *J. Gen. Physiol.* 132, 563–573. <https://doi.org/10.1085/jgp.200810059>
- Yáñez, M., Matías-Guiu, J., Arranz-Tagarro, J.-A., Galán, L., Viña, D., Gómez-Pinedo, U., Vela, Á., Guerrero, A., Martínez-Vila, E., García, A.G., 2014. The Neuroprotection Exerted by Memantine, Minocycline and Lithium, against Neurotoxicity of CSF from Patients with Amyotrophic Lateral Sclerosis, Is Antagonized by Riluzole. *Neurodegener. Dis.* 13, 171–179. <https://doi.org/10.1159/000357281>

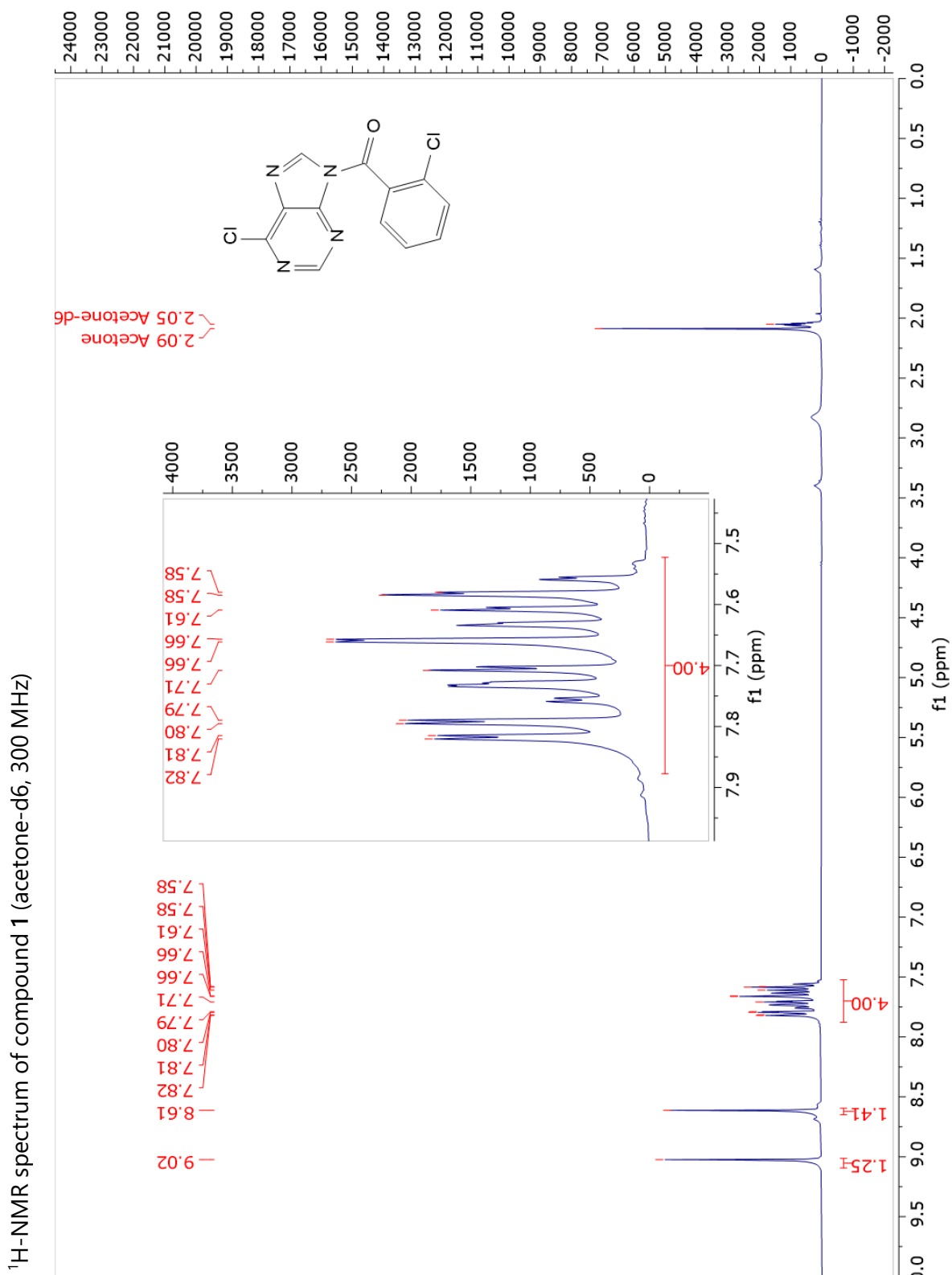
- Yang, D., He, Y., Muñoz-Planillo, R., Liu, Q., Núñez, G., 2015. Caspase-11 Requires the Pannexin-1 Channel and the Purinergic P2X7 Pore to Mediate Pyroptosis and Endotoxic Shock. *Immunity* 43, 923–932. <https://doi.org/10.1016/j.immuni.2015.10.009>
- Yang, Y., Wang, H., Kouadir, M., Song, H., Shi, F., 2019. Recent advances in the mechanisms of NLRP3 inflammasome activation and its inhibitors. *Cell Death Dis.* 10, 1–11. <https://doi.org/10.1038/s41419-019-1413-8>
- Yates, M.K., Seley-Radtke, K.L., 2019. The evolution of antiviral nucleoside analogues: A review for chemists and non-chemists. Part II: Complex modifications to the nucleoside scaffold. *Antiviral Res.* 162, 5–21. <https://doi.org/10.1016/j.antiviral.2018.11.016>
- Yiangou, Y., Facer, P., Durrenberger, P., Chessell, I.P., Naylor, A., Bountra, C., Banati, R.R., Anand, P., 2006. COX-2, CB2 and P2X7-immunoreactivities are increased in activated microglial cells/macrophages of multiple sclerosis and amyotrophic lateral sclerosis spinal cord. *BMC Neurol* 6, 12. <https://doi.org/10.1186/1471-2377-6-12>
- Young, M.T., Pelegrin, P., Surprenant, A., 2007. Amino Acid Residues in the P2X7 Receptor that Mediate Differential Sensitivity to ATP and BzATP. *Mol. Pharmacol.* 71, 92–100. <https://doi.org/10.1124/mol.106.030163>
- Zabala, A., Vazquez-Villoldo, N., Rissiek, B., Gejo, J., Martin, A., Palomino, A., Perez-Samartin, A., Pulagam, K.R., Lukowiak, M., Capetillo-Zarate, E., Llop, J., Magnus, T., Koch-Nolte, F., Rassendren, F., Matute, C., Domercq, M., 2018. P2X4 receptor controls microglia activation and favors remyelination in autoimmune encephalitis. *EMBO Mol Med* 10. <https://doi.org/10.15252/emmm.201708743>
- Zahid, A., Li, B., Kombe, A.J.K., Jin, T., Tao, J., 2019. Pharmacological Inhibitors of the NLRP3 Inflammasome. *Front. Immunol.* 10. <https://doi.org/10.3389/fimmu.2019.02538>
- Zajac, M.A., Zakrzewski, A.G., Kowal, M.G., Ph.D, S.N., 2003. A Novel Method of Caffeine Synthesis from Uracil. *Synth. Commun.* 33, 3291–3297. <https://doi.org/10.1081/SCC-120023986>
- Zhou, X., Ma, L.-M., Xiong, Y., Huang, H., Yuan, J.-X., Li, R.-H., Li, J.-N., Chen, Y.-M., 2016. Upregulated P2X3 Receptor Expression in Patients with Intractable Temporal Lobe Epilepsy and in a Rat Model of Epilepsy. *Neurochem. Res.* 41, 1263–1273. <https://doi.org/10.1007/s11064-015-1820-x>

A horizontal watercolor splash in shades of light blue and white, with a darker blue blotch on the right side. The word "Annexes" is centered within this splash.

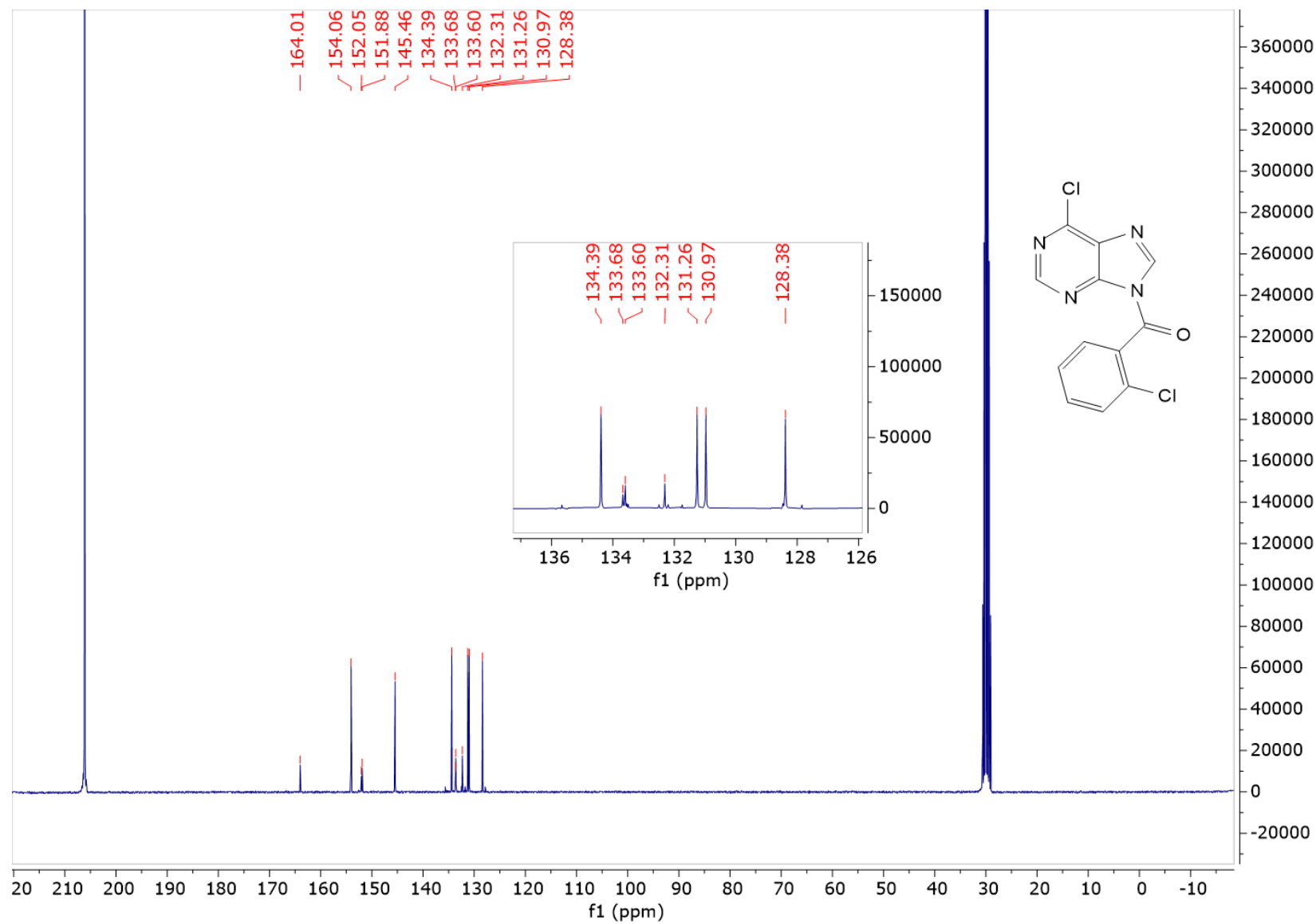
## Annexes

## 10. Annexes

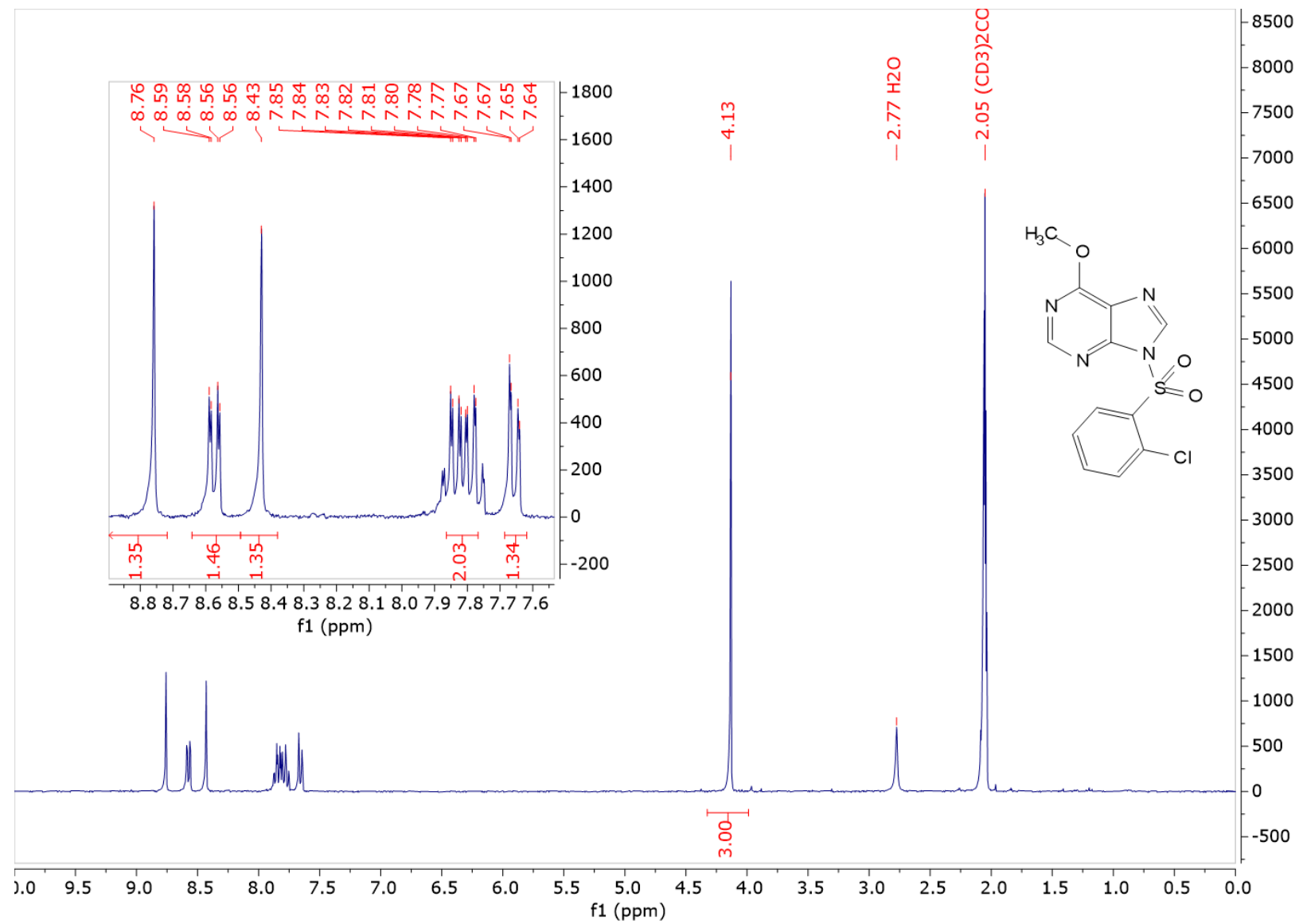
### 10.1. Nuclear magnetic resonance spectra of compounds **1**, **7**, **9**, **26**, **27** and **36**



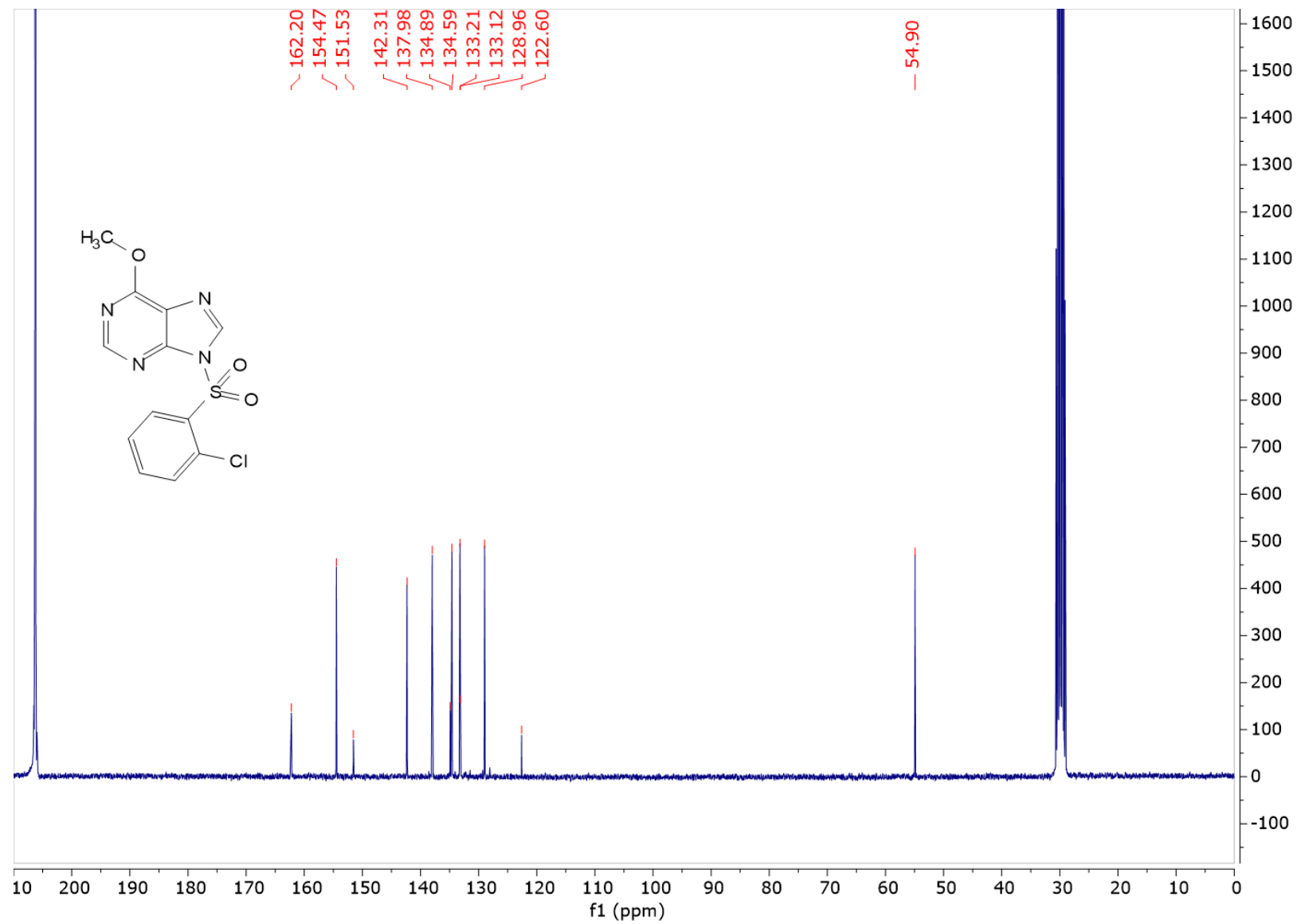
<sup>13</sup>C-NMR spectrum of compound 1 (acetone-d<sub>6</sub>, 75.4 MHz)



<sup>1</sup>H-NMR spectrum of compound 7 (acetone-d<sub>6</sub>, 300 MHz)

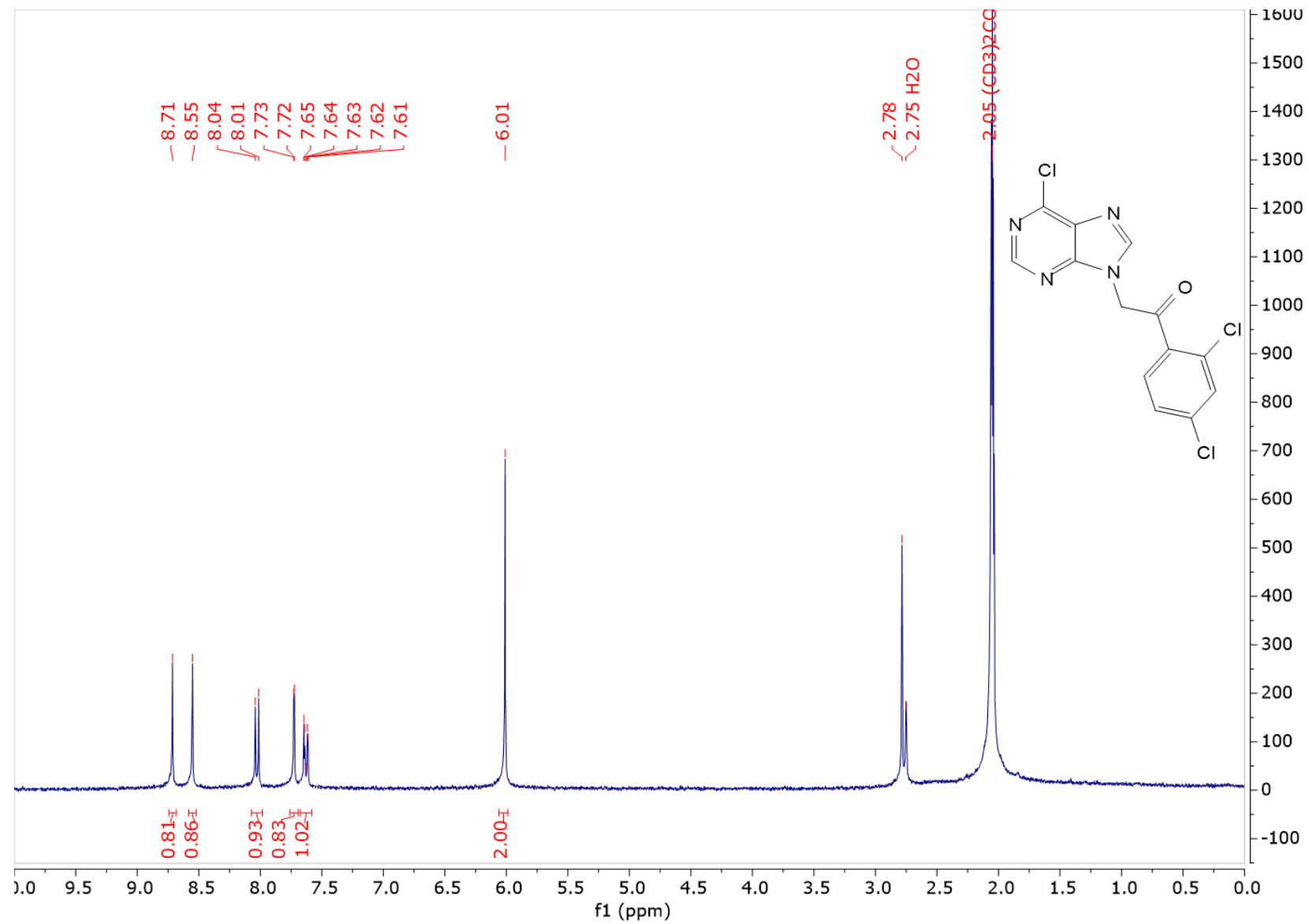


<sup>13</sup>C-NMR spectrum of compound 7 (acetone-d<sub>6</sub>, 75.4 MHz)

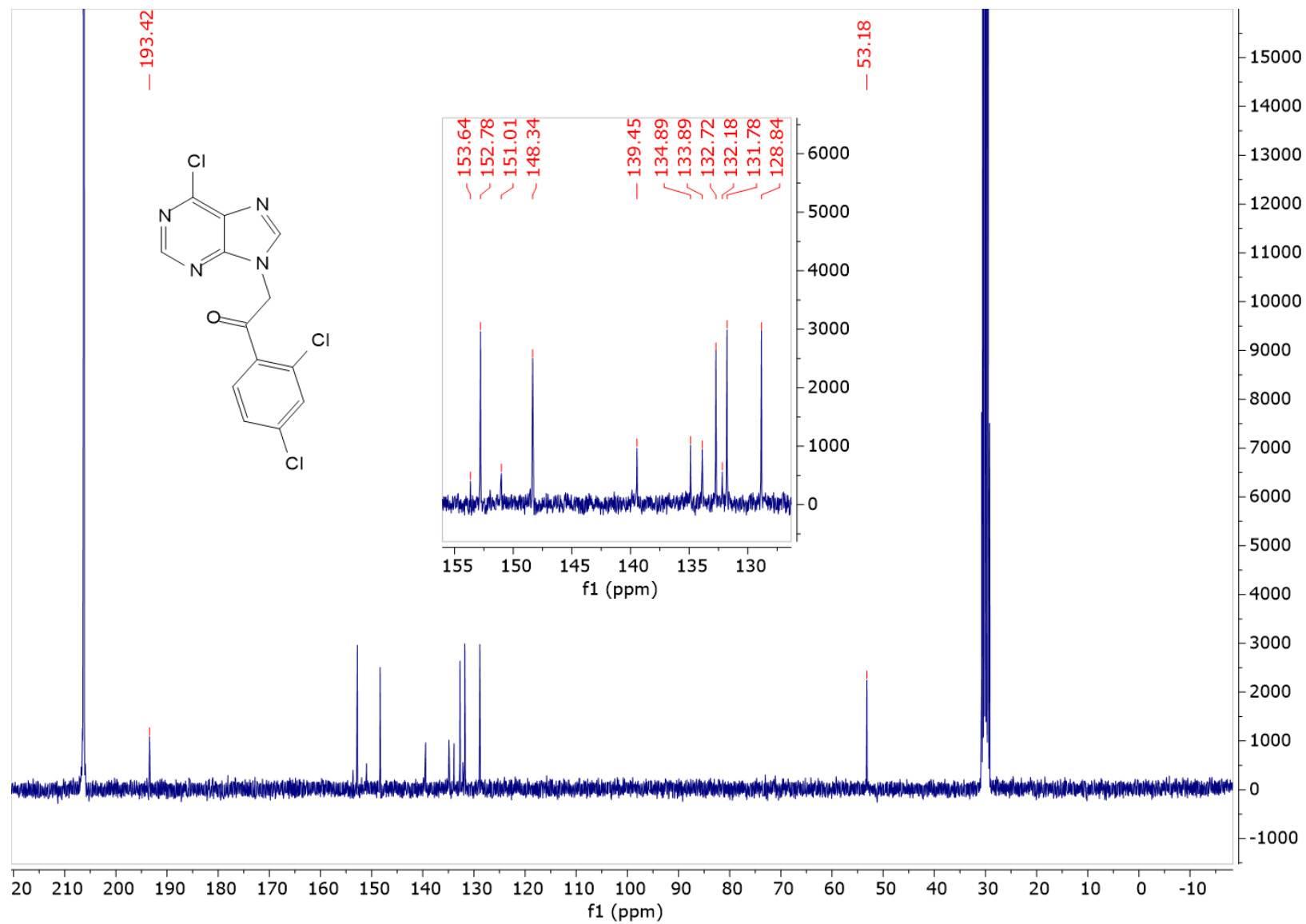




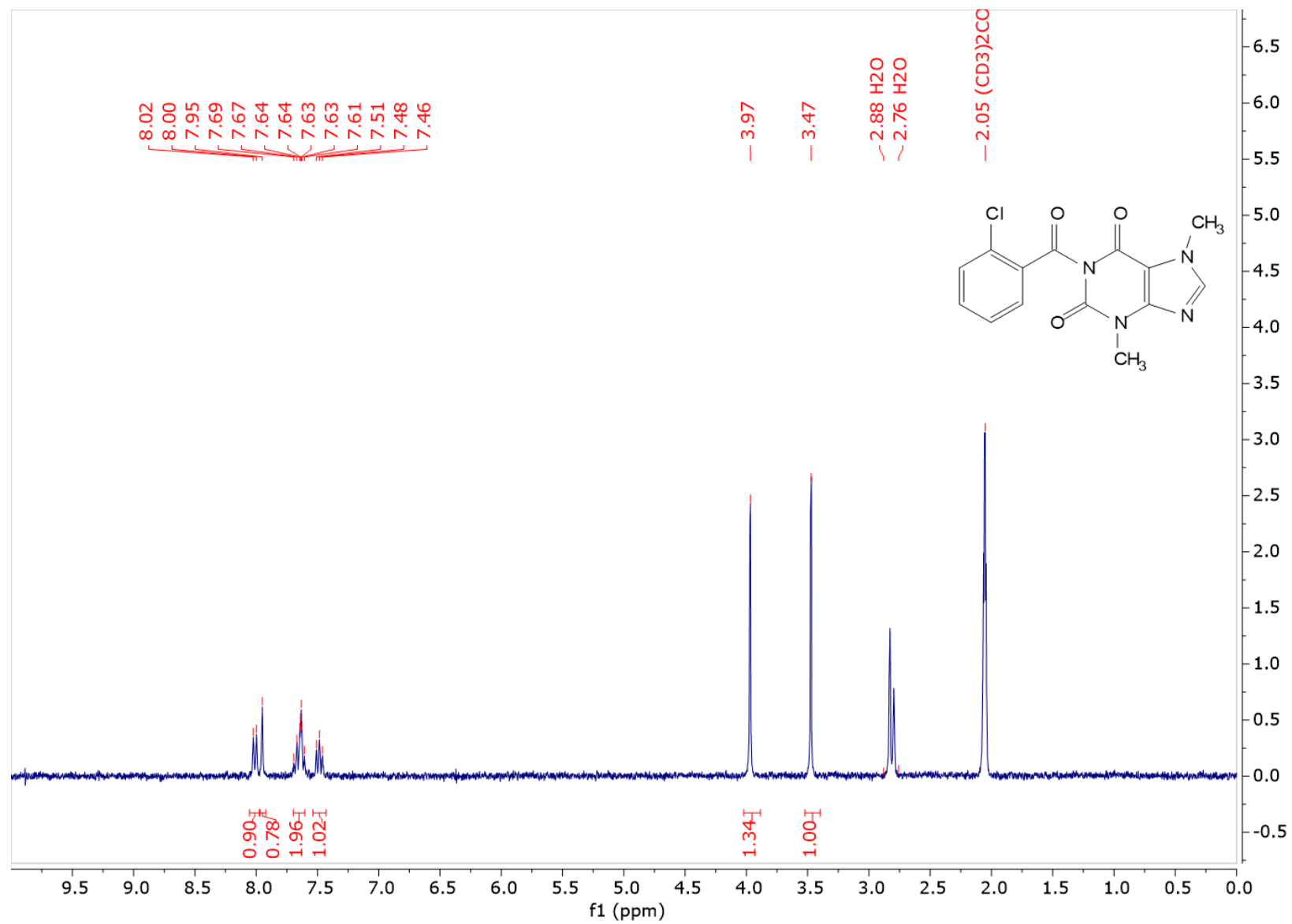
<sup>1</sup>H-NMR spectrum of compound **9** (acetone-d<sub>6</sub>, 300 MHz)



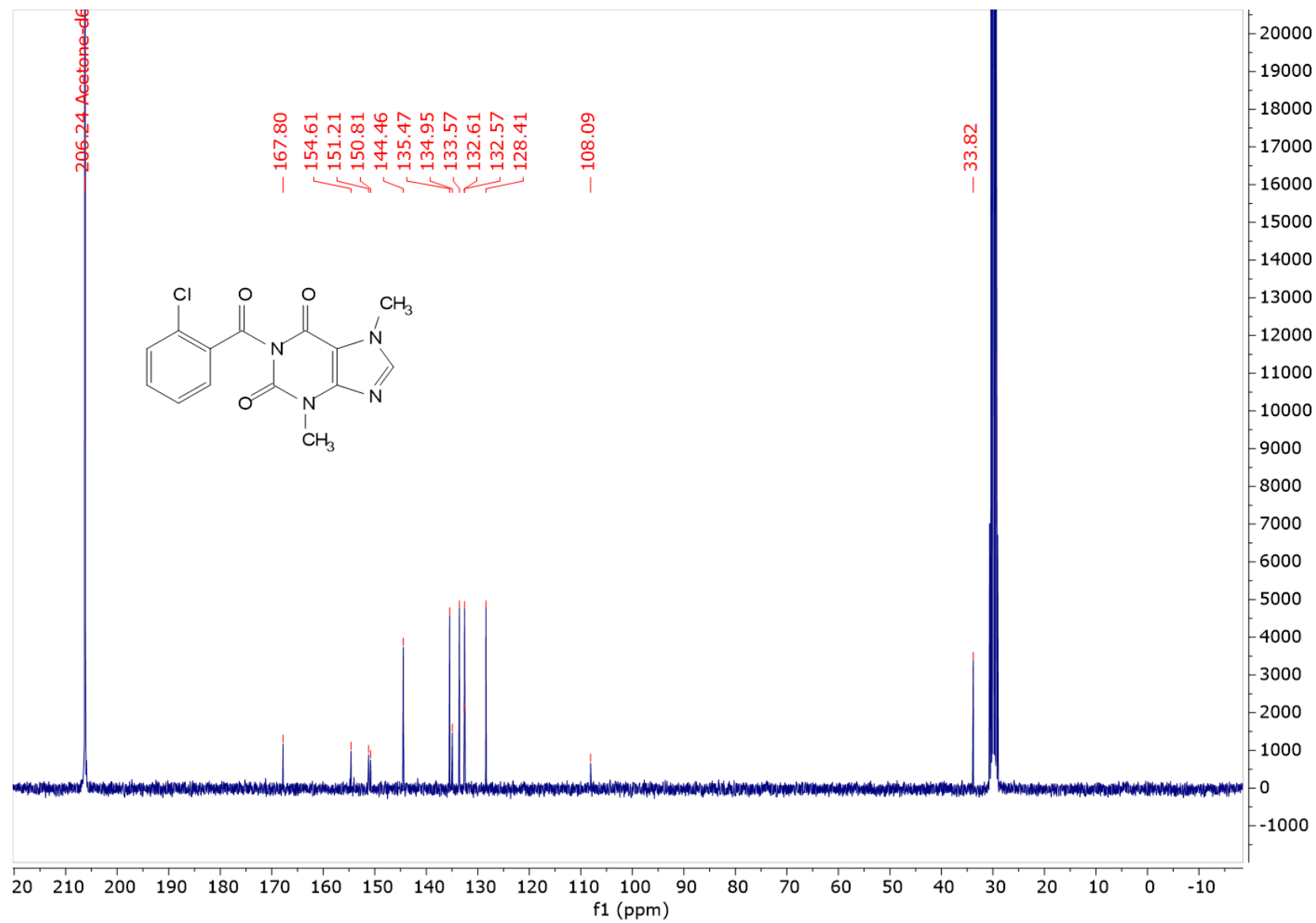
$^{13}\text{C}$ -NMR spectrum of compound **9** (acetone- $d_6$ , 75.4 MHz)



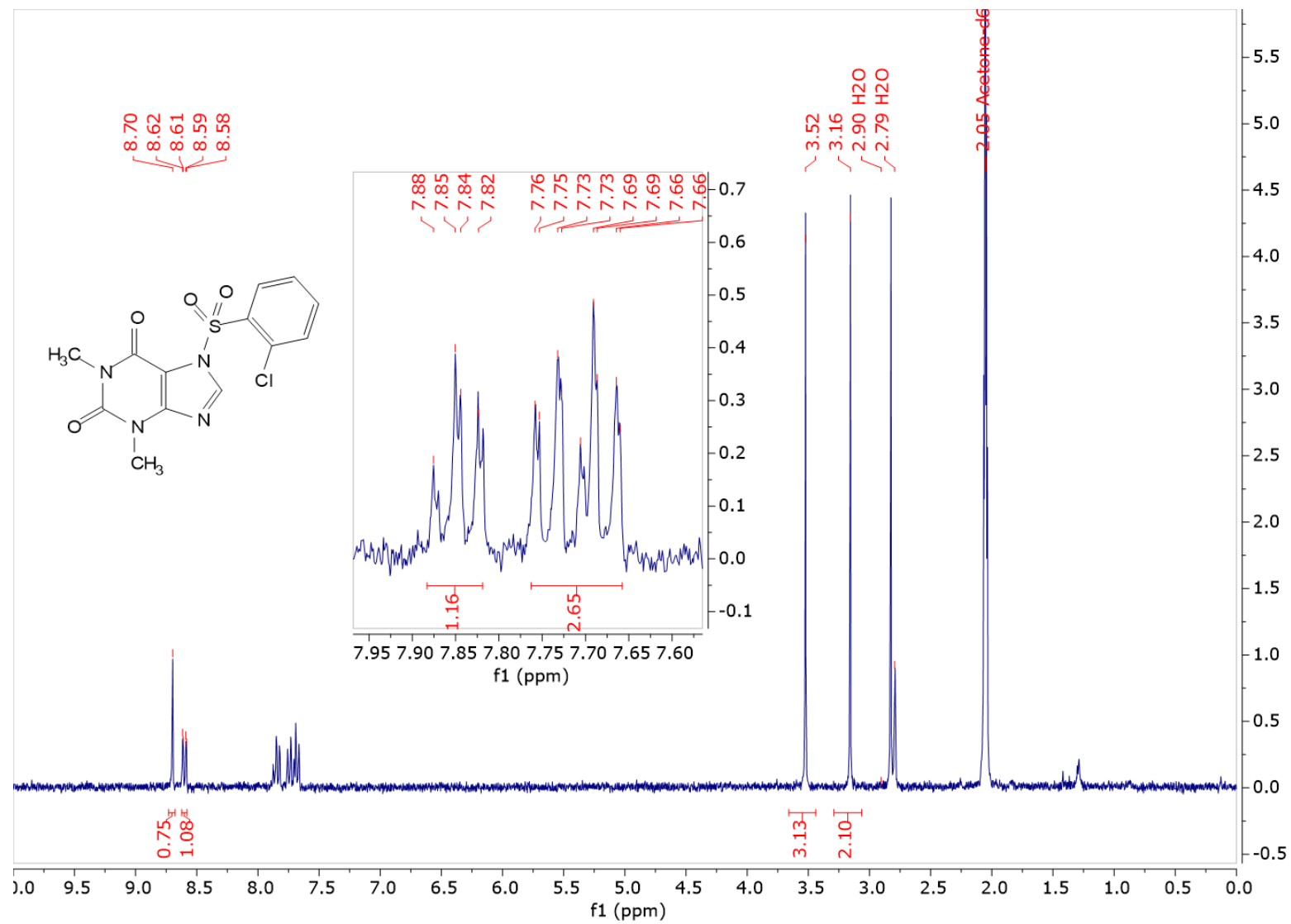
<sup>1</sup>H-NMR spectrum of compound **26** (acetone-d<sub>6</sub>, 300 MHz)



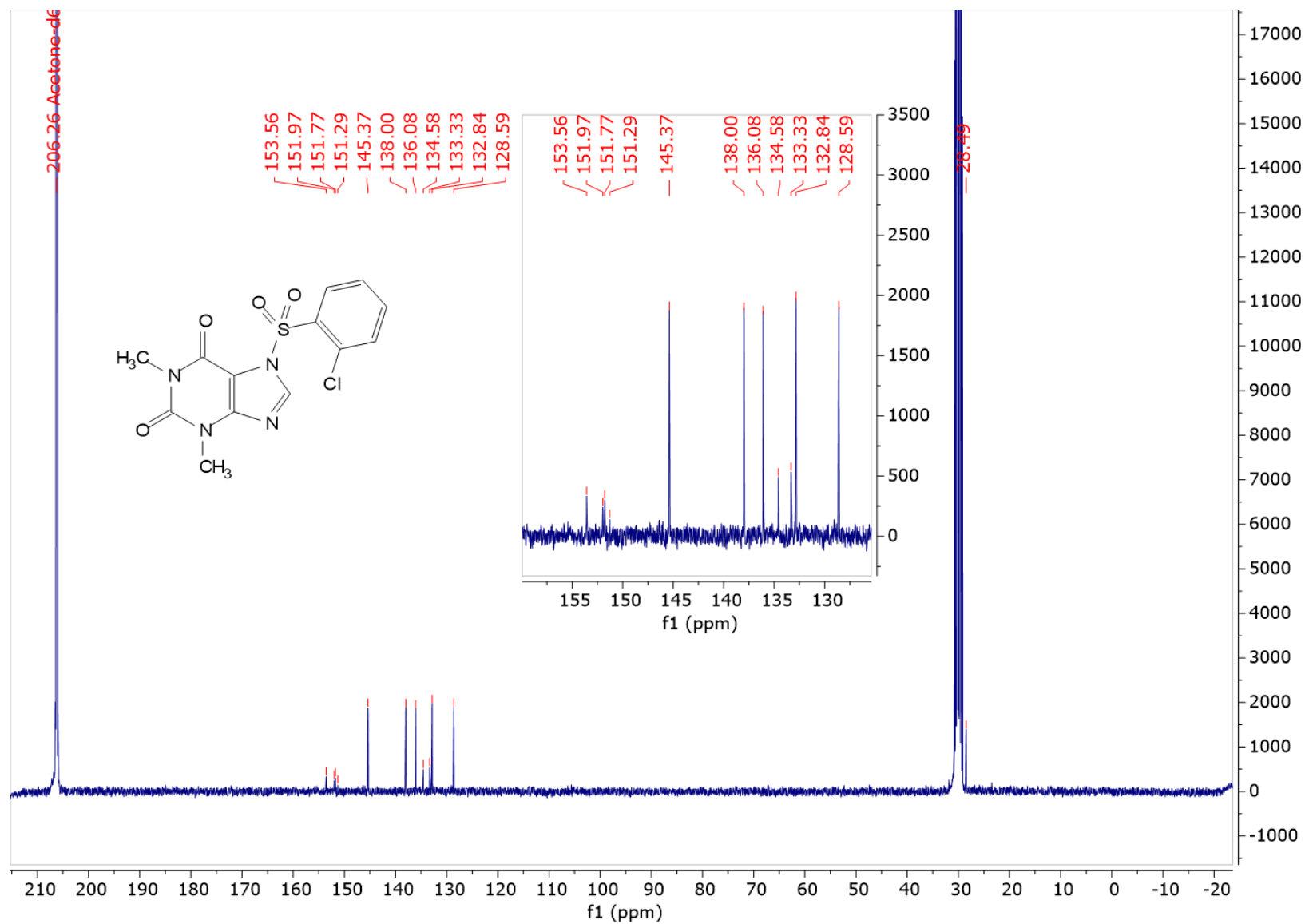
<sup>13</sup>C-NMR spectrum of compound **26** (acetone-d<sub>6</sub>, 75.4 MHz)



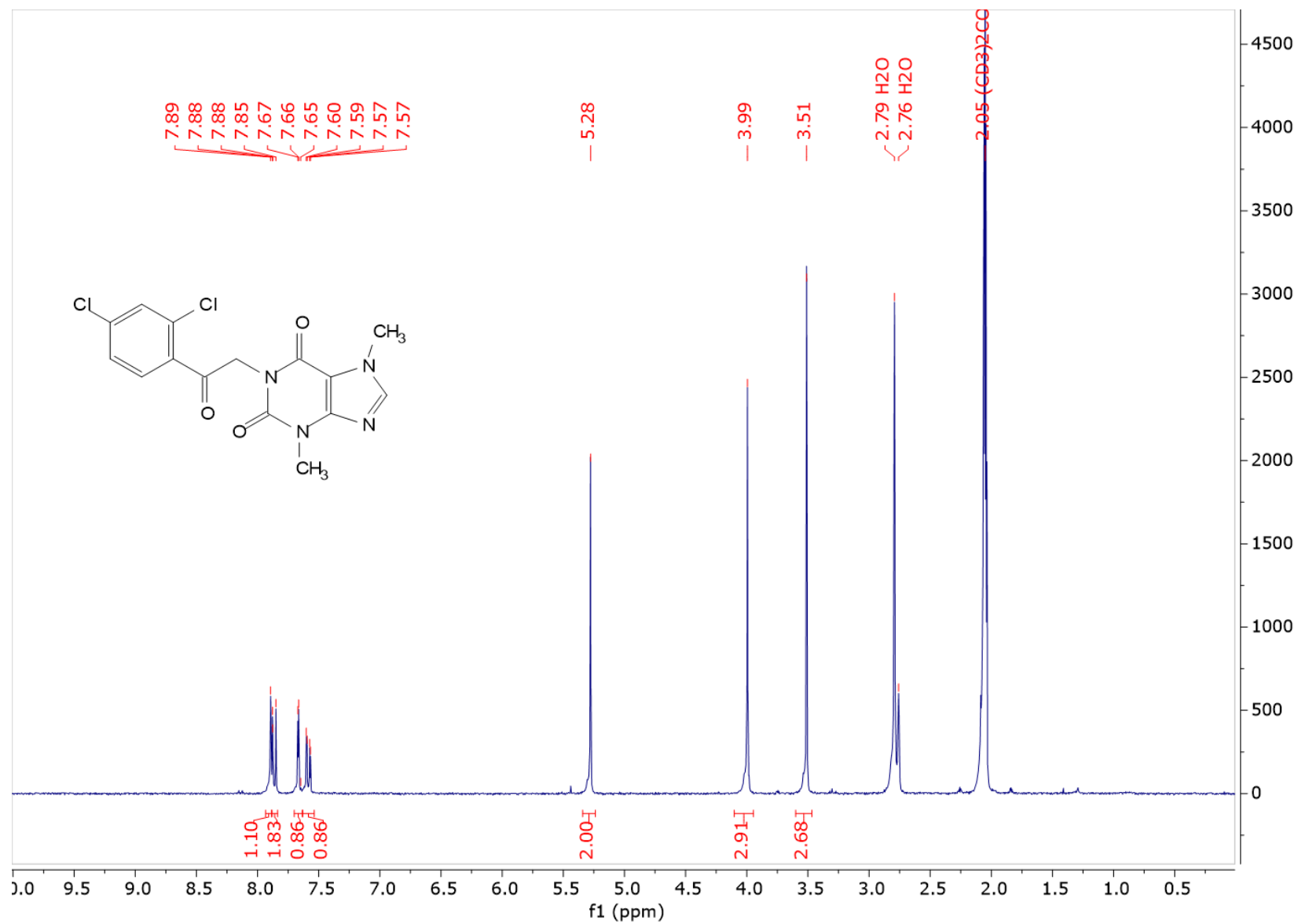
<sup>1</sup>H-NMR spectrum of compound **27** (acetone-d<sub>6</sub>, 300 MHz)



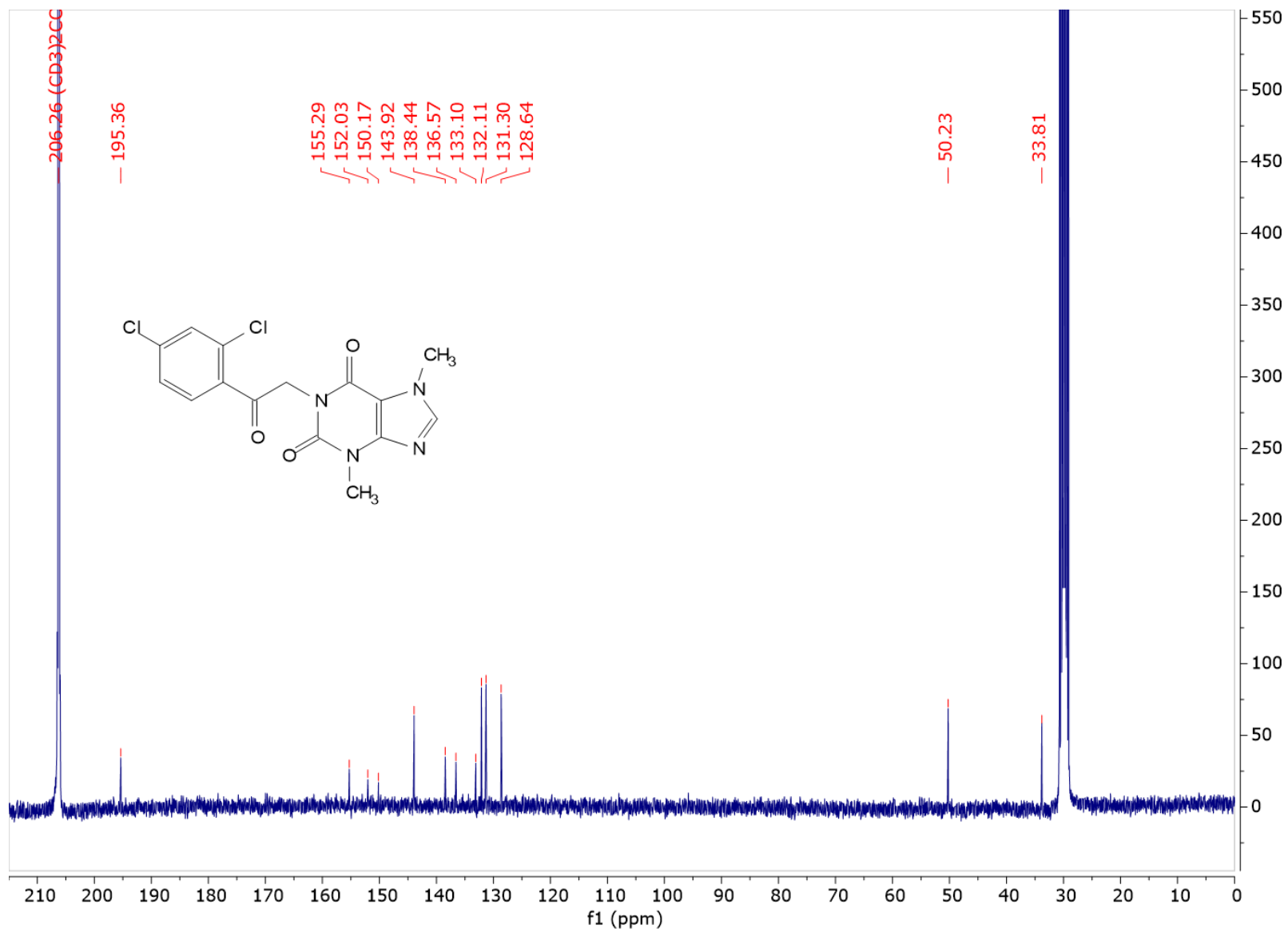
<sup>13</sup>C-NMR spectrum of compound 27 (acetone-d<sub>6</sub>, 75.4 MHz)



<sup>1</sup>H-NMR spectrum of compound **36** (acetone-d<sub>6</sub>, 300 MHz)



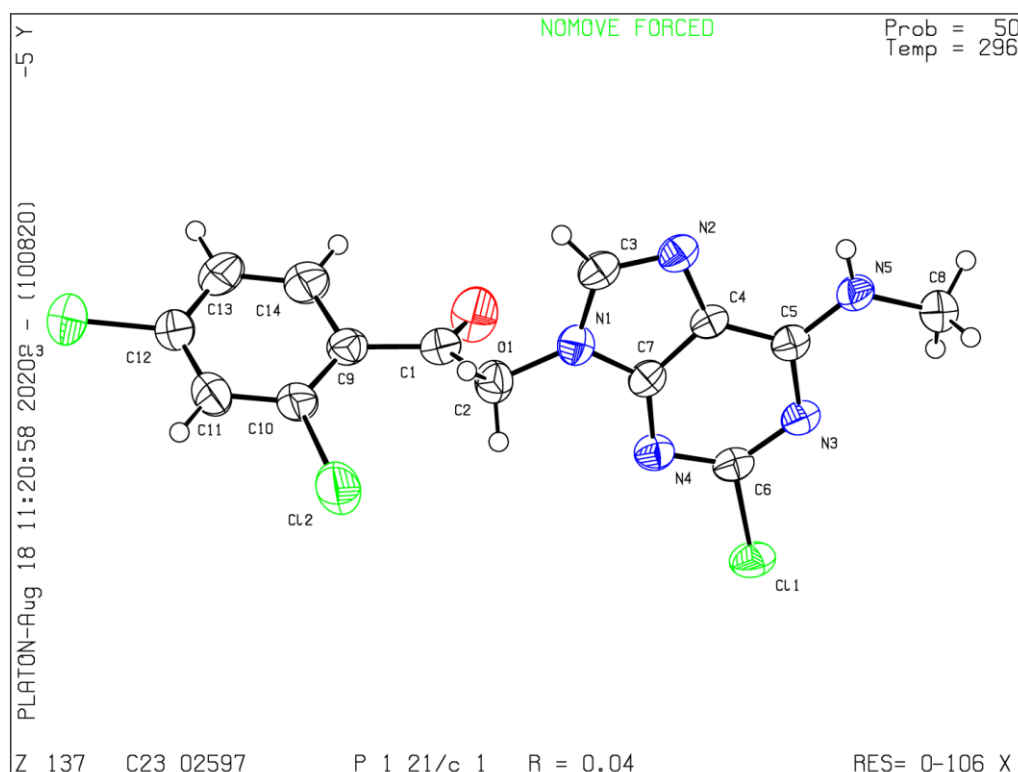
<sup>13</sup>C-NMR spectrum of compound **36** (acetone-d<sub>6</sub>, 75.4 MHz)





## 10.2. X-ray diffraction data of compounds **11** and **27**

### X-ray diffraction of compound **11**



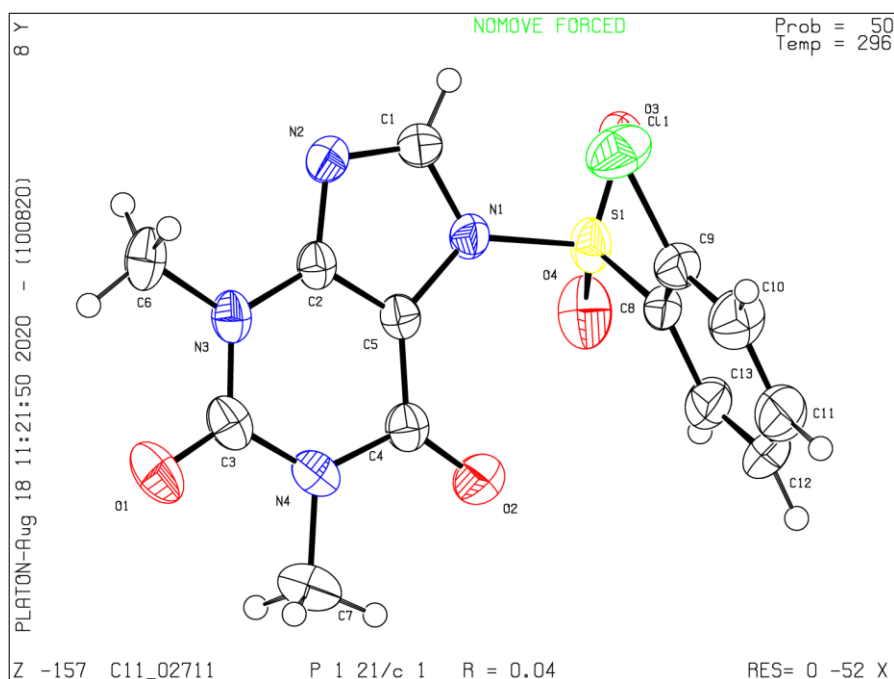
### Sample and crystal data for compound **11**

<i>Chemical formula</i>	C <sub>14</sub> H <sub>10</sub> Cl <sub>3</sub> N <sub>5</sub> O	
<i>Molecular weight</i>	370.62 g/mol	
<i>Temperature</i>	296(2) K	
<i>Wavelength</i>	0.71073 Å	
<i>Crystal size</i>	0.001 x 0.097 x 0.557 mm	
<i>Crystal habit</i>	clear colourless ribbon-like	
<i>Crystal system</i>	monoclinic	
<i>Space group</i>	P 1 21/c 1	
<i>Unit cell dimensions</i>	a = 22.2009(6) Å	α = 90°
	b = 4.55850(10) Å	β = 96.1095(14)°
	c = 15.5661(4) Å	γ = 90°
<i>Volume</i>	1566.39(7) Å <sup>3</sup>	
<i>Z</i>	4	
<i>Density (calculated)</i>	1.572 g/cm <sup>3</sup>	
<i>Absorption coefficient</i>	0.595 mm <sup>-1</sup>	
<i>F(000)</i>	752	

## Data collection and structure refinement for compound 11

<i>Diffractometer</i>	Bruker APEX-II CCD
<i>Theta range for data collection</i>	1.84 to 25.35°
<i>Index ranges</i>	-26<=h<=26, -5<=k<=5, -18<=l<=18
<i>Reflections collected</i>	54239
<i>Independent reflections</i>	2876 [R(int) = 0.0566]
<i>Coverage of independent reflections</i>	99.9%
<i>Absorption correction</i>	multi-scan
<i>Max. and min. transmission</i>	0.9990 and 0.7330
<i>Structure solution technique</i>	direct method
<i>Structure solution program</i>	SHELXS-97 (Sheldrick, 2008)
<i>Refinement method</i>	Full-matrix least-squares on F <sup>2</sup>
<i>Refinement program</i>	SHELXL-2014 (Sheldrick, 2014)
<i>Function minimised</i>	$\sum w(F_o^2 - F_c^2)^2$
<i>Data / restraints / parameters</i>	2876 / 0 / 213
<i>Goodness-of-fit on F<sup>2</sup></i>	1.070
<i><math>\Delta/\sigma_{max}</math></i>	0.001
<i>Final R indices</i>	2174 data;  >2 $\sigma$ (I)      R1 = 0.0397, wR2 = 0.0922 all data                              R1 = 0.0613, wR2 = 0.1103
<i>Weighting scheme</i>	w=1/[ $\sigma^2(F_o^2)+(0.0457P)^2+1.2715P$ ] where P=(F <sub>o</sub> <sup>2</sup> +2F <sub>c</sub> <sup>2</sup> )/3
<i>Largest diff. peak and hole</i>	0.309 and -0.314 eÅ <sup>-3</sup>
<i>R.M.S. deviation from mean</i>	0.049 eÅ <sup>-3</sup>

## X-ray diffraction of compound 27



## Sample and crystal data for compound 27

<i>Chemical formula</i>	C <sub>13</sub> H <sub>11</sub> ClN <sub>4</sub> O <sub>4</sub> S	
<i>Molecular weight</i>	354.77 g/mol	
<i>Temperature</i>	296(2) K	
<i>Wavelength</i>	0.71073 Å	
<i>Crystal size</i>	0.068 x 0.185 x 0.194 mm	
<i>Crystal habit</i>	clear colourless prismatic	
<i>Crystal system</i>	monoclinic	
<i>Space group</i>	P 1 21/c 1	
<i>Unit cell dimensions</i>	a = 12.0589(5) Å	α = 90°
	b = 13.5833(5) Å	β = 93.7825(15)°
	c = 8.9220(4) Å	γ = 90°
<i>Volume</i>	1458.24(10) Å <sup>3</sup>	
<i>Z</i>	4	
<i>Density (calculated)</i>	1.616 g/cm <sup>3</sup>	
<i>Absorption coefficient</i>	0.432 mm <sup>-1</sup>	
<i>F(000)</i>	728	

## Data collection and structure refinement for compound 27

<i>Diffractometer</i>	Bruker Kappa APEX II	
<i>Theta range for data collection</i>	1.69 to 25.35°	
<i>Index ranges</i>	-14<=h<=14, -16<=k<=16, -10<=l<=10	
<i>Reflections collected</i>	16487	
<i>Independent reflections</i>	2677 [R(int) = 0.0353]	
<i>Coverage of independent reflections</i>	100.0%	
<i>Absorption correction</i>	multi-scan	
<i>Max. and min. transmission</i>	0.9710 and 0.9210	
<i>Refinement method</i>	Full-matrix least-squares on F <sup>2</sup>	
<i>Refinement program</i>	SHELXL-2014 (Sheldrick, 2014)	
<i>Function minimised</i>	Σ w(F <sub>o</sub> <sup>2</sup> - F <sub>c</sub> <sup>2</sup> ) <sup>2</sup>	
<i>Data / restraints / parameters</i>	2677 / 0 / 210	
<i>Goodness-of-fit on F<sup>2</sup></i>	1.074	
<i>Final R indices</i>	2076 data; I>2σ(I)	R1 = 0.0364, wR2 = 0.0966
	all data	R1 = 0.0539, wR2 = 0.1211
<i>Weighting scheme</i>	w=1/[σ <sup>2</sup> (F <sub>o</sub> <sup>2</sup> )+( 0.0628P) <sup>2</sup> +0.7138P] where P=(F <sub>o</sub> <sup>2</sup> +2F <sub>c</sub> <sup>2</sup> )/3	
<i>Largest diff. peak and hole</i>	0.283 and -0.310 eÅ <sup>-3</sup>	
<i>R.M.S. deviation from mean</i>	0.062 eÅ <sup>-3</sup>	

A horizontal watercolor splash in shades of light blue and white, with a darker blue blotch on the right side, serving as a background for the text.

## Abbreviations

## 11. Abbreviations

<b>6-OHDA</b>	6-hydroxydopamine
<b>AD</b>	Alzheimer's disease
<b>ALS</b>	amyotrophic lateral sclerosis
<b>Anal.</b>	combustion elemental analysis
<b>BPI</b>	bactericidal permeability-increase protein
<b>BzATP</b>	2'(3')- <i>O</i> -(4-benzoylbenzoyl)ATP
<b>CC</b>	column chromatography
<b>[Ca<sup>2+</sup>]<sub>c</sub></b>	cytosolic calcium concentration
<b>CaM</b>	calmodulin
<b>cAMP</b>	3',5'-cyclic adenosine monophosphate
<b>dec</b>	decomposition
<b>DCM</b>	dichloromethane
<b>DF</b>	dorsal fin
<b>DMAP</b>	4-dimethylaminopyridine
<b>DMF</b>	dimethylformamide
<b>DMSO</b>	dimethylsulfoxide
<b>ENT1</b>	equilibrative nucleoside transporter 1
<b>equiv</b>	equivalent
<b>Et<sub>2</sub>O</b>	diethyl ether
<b>EtOAc</b>	ethyl acetate
<b>FL</b>	fluke
<b>GPCR</b>	G protein-coupled receptor
<b>HD</b>	Huntington's disease

<b>Hdom</b>	head domain
<b>HEK293</b>	human embryonic kidney
<b>HPB</b>	human tumour T-cells
<b>i.p.</b>	intraperitoneal
<b>IP<sub>3</sub></b>	inositol 1,4,5-triphosphate
<b>K<sub>i</sub></b>	inhibition constant
<b>LB</b>	lower body
<b>LBP</b>	LPS-binding protein
<b>LF</b>	left flipper
<b>LPS</b>	lipopolysaccharide
<b>MeCN</b>	acetonitrile
<b>MeOH</b>	methanol
<b>Mp</b>	melting point
<b>MPMs</b>	murine peritoneal macrophages
<b>MS</b>	multiple sclerosis
<b>NDD</b>	neurodegenerative disease
<b>NMDA</b>	<i>N</i> -methyl-D-aspartate
<b>NMR</b>	nuclear magnetic resonance
<b>NOE</b>	nuclear Overhauser effect
<b>NOESY</b>	nuclear Overhauser effect spectroscopy
<b>PD</b>	Parkinson's disease
<b>P<sub>e</sub></b>	effective permeability
<b>PK</b>	pharmacokinetic
<b>PL</b>	phospholipase

<b>R<sub>f</sub></b>	retention factor
<b>RF</b>	right flipper
<b>rt</b>	room temperature
<b>SEM</b>	standard error of the mean
<b>S<sub>N</sub>Ar</b>	nucleophilic aromatic substitution
<b>TBAHS</b>	tetrabutylammonium hydrogen sulfate
<b>TBN</b>	tert-butyl nitrite
<b>TCT</b>	cyanuric chloride
<b>TEA</b>	triethylamine
<b>TEVC</b>	two-electrode voltage clamp
<b>THF</b>	tetrahydrofuran
<b>TLC</b>	thin-layer chromatography
<b>TM</b>	transmembrane domain
<b>UB</b>	upper body